MULTIPLE SCATTERING OF WAVES IN ANISOTROPIC RANDOM MEDIA

Promotiecommissie

Promotoren	prof. dr. A. Lagendijk prof. dr. B. A. van Tiggelen
Overige leden	prof. dr. P. J. Kelly prof. dr. W. L. Vos prof. dr. W. van Saarloos prof. dr. C. A. Müller dr. R. Sprik

The work described in this thesis is part of the research program of the
'Stichting voor Fundamenteel Onderzoek der Materie (FOM)',
which is financially supported by the
'Nederlandse Organisatie voor Wetenschappelijk Onderzoek' (NWO)'.

This work was carried out at the
Complex Photonic Systems Group,
Faculty of Science and Technology and MESA$^+$ Research Institute for Nanotechnology,
University of Twente, P.O. Box 217, 7500AE Enschede, The Netherlands,
and at the
FOM Institute for Atomic and Molecular Physics
Kruislaan 407, 1098SJ Amsterdam, The Netherlands,
where a limited number of copies of this thesis is available.

This thesis can be downloaded from
http://www.wavesincomplexmedia.com.

ISBN:

MULTIPLE SCATTERING OF WAVES IN ANISOTROPIC RANDOM MEDIA

PROEFSCHRIFT

ter verkrijging van
de graad van doctor aan de Universiteit Twente,
op gezag van de rector magnificus,
prof. dr. W.H.M. Zijm,
volgens besluit van het College voor Promoties
in het openbaar te verdedigen
op donderdag 25 september 2008 om 15.00 uur

door

Bernard Christiaan Kaas

geboren op 25 april 1979
te Alkmaar

Dit proefschrift is goedgekeurd door:

prof. dr. A. Lagendijk en prof. dr. B. A. van Tiggelen

Table of Contents

List of Figures

Summary

In this thesis we develop a mathematical model that describes the propagation of waves through anisotropic disordered matter. There are many wave phenomena which can all be described by comparable mathematical equations, such as sound waves, water waves, and electromagnetic waves. The model we study is aimed at electromagnetic waves and classical scalar waves. Light is an example of an electromagnetic wave, and we often employ the word "light" instead of the much longer "classical scalar wave or electromagnetic wave".

Multiple scattered light for isotropic disordered media has been studied extensively, and it is well known that there are three energy transport regimes in multiple scattering. Which regime to expect in a material depends on the scattering strength of the material. Ballistic transport of energy occurs when there are hardly any scatterers, i.e. low scattering strength, and light propagates approximately undisturbed through a material. Diffuse transport of the radiative energy occurs at intermediate scattering strengths, and interference effects are negligible. Diffuse transport is most often observed, this is when the light scatters multiple times, such as in the clouds in the sky, milk or white paper. The light behaves as if it were milk diffusing through tea and the radiation energy is distributed smoothly through the medium. The third regime, Anderson localization of light, is hardly ever observed in three dimensional media, but is relatively easy to find in one and two dimensional media. The minimal scattering strength at which the transition should happen is predicted by the Ioffe-Regel criterion for Anderson localization. If the scattering cross section and the density of the atoms is high, the scattering strength is high and interference effects between the incident and the multiple scattered waves dominate transport in such a way that localized states appear inside the disordered material. Anderson localization of energy is described by a generalized Boltzmann equation containing all interference effects. This equation has never been solved analytically. It is usually approximated by the well known radiative transfer equation, but then all interference effects, and therefore Anderson localization, are neglected. The Ioffe-Regel criterion is obtained by correcting the diffusion equation with interference effects. The diffusion equation is an approximation to the radiative transfer equation, and

there are many analytic solutions known for the diffusion equation.

There exists no theory which is fully developed to encompass anisotropic multiple scattering of light. In the real world there are many media, such as teeth, muscle, bone and the white matter in the brain, in which propagation of light is governed by an anisotropic diffusion equation. Therefore we need to develop such a theory, e.g. to understand if the energy of the electromagnetic waves emanating from a mobile phone can cause brain damage, or if anisotropy influences the scattering strength at which Anderson localization takes place. Currently in biology and medicine often the radiative transfer equation is employed to describe anisotropic media and is supplied with incorrect anisotropy corrections. Sometimes numerical simulation of such an incorrect anisotropic radiative transfer equation even leads to the conclusion that anisotropic diffusion does not exist, a statement in conflict with observations in physical experiments.

The model we developed for multiple scattered waves in anisotropic disordered matter is based on the smallest scattering particles in the material, the atoms. These atoms are treated as classical scatterers, and are described by their scattering potential or by their (differential) scattering or extinction cross section. We present purely dielectric anisotropy, and show the changes required for a description of disordered materials with the anisotropy in the magnetic permeability.

After introductory chapter 1, we start in chapter 2 from a classical wave equation for the amplitude provided with scatterers. For anisotropic disordered media we derive a generalized Boltzmann transport equation which contains all interference effects. Since this equation has never been solved analytically, not even for isotropic media, we proceed by neglecting the interference effects, and derive an anisotropic radiative transfer equation. The radiative transfer equation is extremely hard, if not impossible, to solve analytically without additional approximations. Usually the isotropic radiative transfer equations is solved numerically, and therefore we provide a recipe for a Monte Carlo simulation of the anisotropic radiative transfer equation. In addition we provide some examples of the effects of anisotropy on the radiative transfer equation.

From the anisotropic radiative transfer equation we derive in chapter 3 an anisotropic diffusion equation. Examples of the effects of anisotropy on diffusion are provided, and we can take limits of extreme anisotropy and obtain either one or two dimensional diffusion. The anisotropic diffusion equation is supplied with interference corrections, and we obtain the Ioffe-Regel criterion for Anderson localization in anisotropic media. Our criterion is the first criterion indicating that anisotropy in a disordered material is favorable for

Anderson localization.

In chapter 4 the boundary conditions for our model are derived from the Maxwell equations, and applied to the anisotropic diffusion equation. We identify the transport mean free path and energy velocity in anisotropic media, and these quantities turn out to be vectors. Internal reflections are also in the model, and we express the reflectivity and transmissivity of anisotropic disordered media in Fresnel coefficients for anisotropic disordered media. The angular redistribution of light due to diffusion through an anisotropic material is calculated, and we find non-Lambertian behavior. For anisotropic disordered semi-infinite and slab geometries we calculate the bistatic coefficients. We partition the bistatic coefficient in three contributions, the contribution of single scattering, of diffuse multiple scattering, and of maximally crossed multiple scattering, i.e. the enhanced backscattering cone. In all of these bistatic coefficients we observe an effect of anisotropy.

Finally, in chapter 5, we present the key results of our model.

The work presented in this thesis is theory. The theory is often compared to results for isotropic media which are well known in the literature. Our theory is very well suited for predictions and descriptions of experiments. Our model allows us to predict the behavior of the energy density and flux requiring only little knowledge of the anisotropic multiple scattering material. The input parameters for the model are the typical scatterer, the average refractive index along the principal axes of the anisotropy, and the geometry of the sample. With only this information we can calculate every observable quantity described above. If we are only interested in anisotropic diffusion of the energy density, then the information is contained in the transport mean free path and in the energy velocity, which together determine the diffusion constant.

To conclude, we present a model which can straightforwardly be applied in all fields where anisotropic multiple scattering of classical or electromagnetic waves occurs.

Samenvatting

In dit proefschrift ontwikkelen we een wiskundig model dat het voortbewegen van golven door anisotrope wanordelijke materie beschrijft. Er zijn veel golfverschijnselen, die allemaal door vergelijkbare mathematische modellen te beschrijven zijn. Voorbeelden van golfverschijnselen zijn geluidsgolven, watergolven, en elektromagnetische golven. Het model dat wij bestuderen is gericht op elektromagnetische golven en klassieke golven. Licht is een voorbeeld van een elektromagnetische golf, en we zullen vaak het woord "licht" gebruiken in plaats van "klassieke golf of elektromagnetische golf".

Veelvuldig verstrooide golven in isotrope wanordelijke materialen zijn uitgebreid bestudeerd, en het is inmiddels goed bekend dat er drie manieren zijn waarop de energie van licht getransporteerd wordt door wanordelijke materialen. Welke manier we moeten verwachten hangt af van hoe sterk het materiaal verstrooid. Ballistisch transport van energie vindt plaats als er nauwelijks verstrooiers aanwezig zijn, dat wil zeggen wanneer de verstrooiingssterkte van het materiaal laag is, en het licht praktisch ongehinderd door het materiaal voortbeweegt. Diffuus transport van stralingsenergie vindt plaats wanneer het materiaal de verstrooiingssterkte van een materiaal niet heel erg zwak, maar ook niet heel er sterk is, en interferentieverschijnselen verwaarloosbaar zijn. Diffuus transport wordt het meest waargenomen, dit gebeurt als het licht veelvuldig verstrooit, zoals in de wolken in de lucht of in wit papier. Het licht gedraagt zich dan alsof het melk is die in de thee diffundeert, en de stralingsenergie is glad verdeeld over het medium. De derde manier waarop licht zich voortbeweegt, Anderson lokalisatie, wordt bijna nooit waargenomen in drie dimensionale materialen, maar is relatief eenvoudig waar te nemen in een en twee dimensionale media. De minimale verstrooiingssterkte waarop de overgang naar Anderson lokalisatie zou moeten plaatsvinden wordt voorspeld door het Ioffe-Regel criterium. Als de verstrooiings werkzame doorsnede en de dichtheid van atomen hoog is, dan zullen de inkomende en de veelvuldig verstrooide golven interfereren op een manier die er toe leidt dat er op willekeurige plaatsen in het wanordelijke materiaal energieophopingen ontstaan. Anderson lokalisatie van licht wordt beschreven door een gegeneraliseerde Boltzmann vergelijking, die alle interferentie effecten omvat. Deze vergelijking is nog nooit analytisch opgelost. Normaliter wordt deze

vergelijking benaderd door de bekende stralingstransportvergelijking, maar dan worden alle interferentie effecten verwaarloosd. Het Ioffe-Regel criterium wordt gevonden door middel van het toevoegen van interferentie effecten de diffusie vergelijking. De diffusie vergelijking zelf is een benadering van de stralingstransportvergelijking, en er zijn veel analytische oplossingen bekend voor de diffusievergelijking.

Er bestaat geen theorie die volledig ontwikkeld is en anisotrope veelvuldige verstrooiing van licht omvat. In de werkelijke wereld zijn er veel materialen, zoals tanden, spieren, bot, en de witte materie in de hersenen, waarin de voortbeweging van licht beschreven wordt door een anisotrope diffusievergelijking. Daarom moeten we deze theorie zelf ontwikkelen, bijvoorbeeld om te begrijpen of de elektromagnetische golven veroorzaakt door mobiele telefoons hersenschade kunnen veroorzaken, of misschien beïnvloed anisotropie de verstrooiingssterkte waarbij Anderson lokalisatie plaatsvindt. Momenteel wordt in biologie en geneeskunde vaak een stralingstransportvergelijking gebruikt waarin anisotropie incorrect wordt meegenomen. Soms leiden numerieke simulaties van deze incorrecte vergelijkingen zelfs tot de conclusie dat anisotrope diffusie niet bestaat, een stelling die strijdig is met waarnemingen in fysische experimenten.

Het model dat we ontwikkelen voor veelvuldige verstrooiing van golven in wanordelijke materie is gebaseerd op de kleinste verstrooiers in het materiaal, de atomen. Deze atomen worden behandeld als klassieke verstrooiers, en worden beschreven door hun verstrooiingspotentiaal of (differentiële) verstrooiings of extinctie werkzame doorsnede. We presenteren puur diëlektrische anisotropie, laten zien welke veranderingen nodig zijn om materie te beschrijven die anisotropie in de magnetische permeabiliteit bevat.

Na het inleidends hoofdstuk 1 beginnen we in hoofdstuk 2 met een klassieke golfvergelijking voor de amplitude, en we voegen verstrooiers toe aan de vergelijking. Voor anisotrope wanordelijke materialen leiden we een gegeneraliseerde Boltzmann transport vergelijking af, die alle interferentie effecten omvat. Aangezien deze vergelijking nog nooit analytisch is opgelost, ook niet voor isotrope materie, verwaarlozen we interferentie effecten en leiden een anisotropie stralingstransportvergelijking af. Het is ook zeer moeilijk, zo niet onmogelijk, om de stralingstransportvergelijking analytisch op te lossen zonder extra aannames te doen. Meestal wordt de isotrope stralingstransportvergelijking numeriek opgelost, en daarom presenteren we een recept voor een Monte Carlo simulatie van de anisotrope stralingstransportvergelijking. Daarbij geven we enkele voorbeelden van het effect van anisotropie op de stralingstransportvergelijking.

Van de anisotrope stralingstransportvergelijking leiden we een anisotrope

diffusievergelijking af in hoofdstuk 3. Er worden voorbeelden gegeven van het effect van anisotropie op diffusie. We nemen limieten met extreme anisotropie, en kunnen op die manier een of twee dimensionale diffusie verkrijgen. Aan de anisotrope diffusievergelijking voegen we interferentiecorrecties toe, en we vinden het Ioffe-Regel criterium voor Anderson lokalisatie. Ons criterium is het eerste criterium dat aangeeft dat anisotropie in een wanordelijk materiaal helpt om Anderson lokalisatie te vinden.

In hoofdstuk 4 leiden we randvoorwaarden voor ons model af van de Maxwell vergelijkingen, en passen deze toe op de anisotrope diffusie vergelijking. We identificeren de gemiddelde vrije weglengte voor energietransport, en de energiesnelheid, en beide blijken vectoren te zijn. Interne reflecties zitten ook in het model, en de reflectiviteit en transmissiviteit drukken we uit in termen van de Fresnel coëfficiënten voor anisotrope wanordelijke materialen. De herdistribuering van licht over hoeken wegens diffusie door een wanordelijk materiaal wordt uitgerekend, en we vinden niet-Lambertiaans gedrag. Voor anisotrope half oneindige media en plakken berekenen we de bistatische coëfficiënt. Deze coëfficiënt delen we op in drie bijdragen, enkelvoudige verstrooiing, diffuse veelvuldige verstrooiing, en voor maximaal gekruiste verstrooiing, ofwel de terugstrooikegel. In alle bistatische coëfficiënten zijn we het effect van anisotropie.

Uiteindelijk sluiten we af in hoofdstuk 5 met de belangrijkste resultaten die volgen uit ons model.

Het gepresenteerde werk in dit proefschrift is theorie. De theorie wordt vaak vergeleken met resultaten voor isotrope wanordelijke materialen, die welbekend zijn uit de literatuur. Onze theorie is zeer geschikt voor voorspellingen en beschrijvingen van experimenten. Ons model staat ons toe het gedrag te voorspellen van de energiedichtheid en de flux van de energiedichtheid, met slechts weinig kennis van het anisotrope wanordelijke materiaal. De parameters die nodig zijn voor het model zijn de typische verstrooier, de brekingsindex langs iedere hoofdas van de anisotropie, en de geometrie van het materiaal. Met deze parameters kunnen we alle hierboven beschreven fysische grootheden bepalen. Als we enkel geïnteresseerd zijn in de anisotrope diffusie van de energiedichtheid, dan de informatie is bevat in de gemiddelde vrije weglengte voor transport, en de energiesnelheid, die samen de diffusietensor vastleggen.

Tot slot, wij presenteren een model dat rechttoe rechtaan toegepast kan worden in ieder gebied waarin anisotrope veelvuldige verstrooiing van klassieke of elektromagnetische golven voorkomen.

Dankwoord, Remerciements, Acknowledgements

Chapter 1

General introduction

The relevant concepts in multiple scattering of waves through anisotropic disordered media are introduced through everyday life examples. The basic equations describing propagation of electromagnetic waves through matter are introduced and a short history of the scalar model which we use for light is presented. The general introduction concludes with an overview of this thesis.

1.1 Waves, disorder, and anisotropy

Exchange of information is an important part of everyday life. At the supermarket we talk about the price of the goods we wish to buy, with a colleague about our work, family life, the latest news or the heat wave in the weather report for your next holiday destination. This news we have either read in a newspaper or magazine, we heard it on the radio, saw it on television or on the internet. In all of these examples waves were used to transmit the information. Sound waves inform the ears, electromagnetic waves inform the eyes. Out in the open the waves travel in a straight line from a sender to a receiver. In buildings there is usually a large number of obstacles which can reflect, absorb, or produce waves, such as walls, people, desks, filing cabinets, doors, which open and close intermittently, etc. Many obstacles can be avoided when we want to exchange information, by shutting the door of our office, by using a wired connection, by moving closer to the sender or the receiver, or by moving both sender and receiver out of the building into the open.

Avoiding obstacles is very often impossible, and there is no choice but to deal with the effects of interference with the scattered waves. For example when we want to setup a wireless connection from our laptop to the internet in a building, it is not always possible to move closer to the wireless router, or move the wireless router into the open. It can very well happen that the signal from the wireless router is extinguished so much by the obstacles that only a

diffuse signal and a much smaller ballistic signal reaches our network card. The network card will tell us it has a bad reception, and is usually unable to recover enough information from the faint ballistic signal nor can it translate the diffuse signal into coherent information. Our internet browser will present us an error message informing us that the server is unavailable. It would be very nice if the network card could also recover information from the diffuse signal, as that would increase the range of wireless networks in buildings, especially if the obstacles predominantly scatter without absorbing the signal.

Many multistory office buildings look like huge concrete slabs, and inside these slabs the hallways are usually all aligned. The aligned hallways can waveguide signals, thus allowing signals to propagate longer distances along the hallways, and shorter distances sideways. In both directions obstacles are encountered. If we assume that the density and the strength of the scatterers is similar in all directions, then averaging over realizations of this disorder in our multistory office buildings will lead to anisotropic diffusion of both sound and electromagnetic waves. This wave diffusion is described by a diffusion tensor with the component along the hallways larger than the other components. The above example might seem two dimensional for sound, but everyone who has lived in such a building and has heard one of their neighbors drill a hole in the concrete wall knows otherwise. It also seems that the structure of the building is the sole cause of the anisotropy, but that is not necessarily true. The obstacles blocking the waves hardly ever have spherical symmetry, and give rise to a directionality in the scattered waves. In office buildings, walls, filing cabinets, and doors mainly reflect sound moving along a floor. For the other direction the floor, ceiling, desks and tables are the main scatterers, and we have to take into account the distribution of the orientation of the scattering cross sections to be able to tell what caused the anisotropy.

Most people will be familiar with the phenomena described above where the scatterers or reflecting surfaces are visible by eye. In fact such events can occur for any type of wave, only the length scales and obstacles differ for different waves. Water waves could scatter from a piece of wood, seismic waves can scatter from different types of rock embedded in Earth's crust. In a more abstract setting we can consider a probability density or Schrödinger wave for some elementary particle, which scatters from inhomogeneities in the energy density landscape. The picture of scatterers as inhomogeneities in the energy density landscape through which a wave propagates is best known from quantum mechanics, but it is very general and applies to classical waves as well. This thesis will focus on the theory of multiple scattering of classical electromagnetic waves of arbitrary wavelength in anisotropic disordered media. For these waves the scatterers discussed in this thesis are mainly much

smaller than the wavelength of the electromagnetic waves. The wavelengths visible by eye are in the range 350nm – 750nm, and typically these waves are scattered by the dipole moment of the electron clouds of atoms, which have diameters of the order of 0.1nm. Due to the difference in scale it is often correct to approximate the scattering dipoles by point scatterers. Although we do not limit ourselves to the visible wavelengths, we use the term light interchangeably with the term electromagnetic wave, and all results are valid at any wavelength, provided we identify the correct scatterers at these wavelengths.

At optical wavelengths we do not consider the disorder in multistory office buildings, as the size of the mentioned obstacles is orders of magnitude larger than the wavelength. Instead we can think of infrared light propagating through human tissue, such as teeth, bone, muscle and even the human brain, which all exhibit anisotropic diffusion of light, albeit sometimes obscured by boundary effects [1–5]. In this thesis we develop a model which has the potential to accurately describe the energy density and flux of multiple scattered waves in anisotropic disordered media.

From a theoretical viewpoint tissue samples are way too complicated as these consists of many layers all with different scattering properties and different anisotropy. If the sample is studied in vivo moving scatterers complicate matters even more. It is well known that homogeneous isotropic media are easiest to understand and easiest to describe mathematically. It is also feasible to analytically calculate simple scattering problems, but scattering from small clusters of particles already requires approximations, and calculations are usually performed numerically. It is no surprise that for materials which consists of 10^{23} scatterers nobody has succeeded nor tried to obtain exact analytic solutions for each particular realization of the medium.

If averages over all possible realizations of scatterers are considered, then we can obtain analytic solutions. For the radiance such a procedure eventually leads to the well known equation of radiative transfer, an equation which was first derived heuristically using arguments based on the physical properties of single scatterers and statistical mechanics [6, 7]. Media averaged over the disorder can be described by the density of the scatterers and their cross sections, provided the wavelength under consideration is much smaller than the transport mean free path. The radiative transfer equation is a Boltzmann transport equation for waves, and it does not contain interference effects.

The radiative transfer equation is very general, and in general impossible to solve analytically. Numerical simulations can be performed, but these cost a lot of time. The radiative transfer equation can be approximated by a diffusion equation up to very good agreement [6, 8]. The diffusion can often be solved analytically [9] and results are therefore obtained much quicker [8, 10–

12]. Only for media smaller than two mean free path the accuracy of the diffusion equation becomes less accurate [8], as single scattering and ballistic propagation start to dominate transport of light. The diffusion equation measures up so well to the radiative transfer equation due to the fact that both equations neglect all interference effects.

Photonic crystals are periodic structures which could change the optical density of states and localize light in certain frequency bands if they exhibit a full band gap [13, 14]. In these periodic structures it turns out that wave diffusion also occurs[15–18]. The reason for the disorder in photonic crystals is the second law of thermodynamics, which states that in a closed system the entropy increases over time. To reduce the entropy a such that all disorder is removed from a crystal takes a lot of energy, and the current state of the art crystals are not free from disorder. The band gap could be destroyed by the disorder thus hampering their wave guiding abilities used for photonic integrated circuits [19, 20]. However the disorder in the crystals was found to be useful for the determination of photonic crystal properties, such as the determination of the with of the stop-band through speckle measurements [21]. In this thesis a photonic crystal can be incorporated as the effective medium in our model for multiple scattering of light in anisotropic disordered media.

Although naively one might expect all interference effects to wash out when the waves are multiple scattered, it has been demonstrated through the enhanced backscattering phenomenon [22–26] that interference effects can survive scattering, and exhibit anisotropy [27–29]. There even exists a regime known as the Anderson localization regime [30], where interference effects dominate, and the waves form localized states inside the disordered medium.

The search for Anderson localization of classical scalar waves, used for descriptions of light and sound, picked up momentum in the 1980's [14, 31–33]. Direct observation of Anderson localization of light is very hard to achieve, but indirect methods can also be used to establish if a material Anderson localizes [34]. Moreover it possible to obtain a state in which only the directions transverse to to the propagation direction Anderson localize [33], which has recently been observed experimentally [35]. The search for Anderson localization, both theoretically and experimentally, is still going on for several wave phenomena [36–41] and also anisotropic media are studied [42, 43]. Currently many articles focus on Anderson localization of matter waves, i.e. cold atoms in one and two dimensional disordered optical lattices [44–49].

Especially in three dimensional media Anderson localization remains elusive for wave phenomena. One of our reasons for studying anisotropic three dimensional media is that strongly anisotropic media could resemble lower dimensional media, possible facilitating a transition to Anderson localization.

Classical waves in three dimensional media are the subject of this thesis, and we will explore the possibility of a transition to lower dimensional media. Our model predicts indeed that Anderson localization is facilitated by anisotropy [50]. Considering the journals in which recent publications on Anderson localization have appeared [35, 48, 49, 51, 52], we expect it will remain a hot topic in the foreseeable future.

1.2 Electromagnetic fields in matter

This thesis is about a model for electromagnetic radiation in disordered media. The Maxwell equations, are the key ingredient from which we will derive our results. In *SI* units the Maxwell equations in material media are [53]

$$\nabla \cdot \boldsymbol{D}(\boldsymbol{x},t) = \rho(\boldsymbol{x},t), \tag{1.1a}$$

$$\nabla \cdot \boldsymbol{B}(\boldsymbol{x},t) = 0, \tag{1.1b}$$

$$\nabla \times \boldsymbol{E}(\boldsymbol{x},t) = -\frac{\partial \boldsymbol{B}(\boldsymbol{x},t)}{\partial t}, \tag{1.1c}$$

$$\nabla \times \boldsymbol{H}(\boldsymbol{x},t) = \boldsymbol{J}(\boldsymbol{x},t) + \frac{\partial \boldsymbol{D}(\boldsymbol{x},t)}{\partial t}. \tag{1.1d}$$

Here $\boldsymbol{D}$ is the electric displacement, $\boldsymbol{B}$ is the magnetic flux, $\boldsymbol{E}$ the electric field, $\boldsymbol{H}$ is the magnetic field, ρ is the free charge density, and $\boldsymbol{J}$ is the electric current density [54]. The Maxwell equations have been combined and improved by Maxwell, but each individual equation also has a name, i.e. Eq. (1.1a) is Gauss's law of which (1.1b) can be considered a special case, Eq. (1.1c) is Faraday's law, and Eq. (1.1d) is Ampères law corrected by Maxwell with the additional term $\partial \boldsymbol{D}/\partial t$.

The divergence of equation (1.1d) and application of (1.1a) leads to a continuity equation for the free electric charge. In optics the electromagnetic waves scatter from electron clouds bound to atoms. Throughout this thesis we assume that there are neither free charges, nor free currents, i.e.

$$\rho(\boldsymbol{x},t) \equiv 0, \tag{1.2a}$$

$$\boldsymbol{J}(\boldsymbol{x},t) \equiv \boldsymbol{0}. \tag{1.2b}$$

To uniquely determine the electric and magnetic fields we supplement the Maxwell equations with constitutive relations. These relations are also known as material equations, and describe the behavior of the material under the influence of the electric and magnetic fields. We introduce the electric permittivity tensor $\varepsilon(\boldsymbol{x},\boldsymbol{x}_0) \equiv \varepsilon(\boldsymbol{x})\delta^3(\boldsymbol{x}-\boldsymbol{x}_0)$ and the magnetic permeability tensor

$\mu(\boldsymbol{x},\boldsymbol{x}_0) \equiv \mu(\boldsymbol{x})\delta^3(\boldsymbol{x}-\boldsymbol{x}_0)$, such that they are constant in time, and inhomogeneous and anisotropic in space. The constitutive relations we impose are

$$\boldsymbol{D}(\boldsymbol{x},t) \equiv \varepsilon(\boldsymbol{x})\cdot\boldsymbol{E}(\boldsymbol{x},t), \tag{1.3a}$$
$$\boldsymbol{B}(\boldsymbol{x},t) \equiv \mu(\boldsymbol{x})\cdot\boldsymbol{H}(\boldsymbol{x},t). \tag{1.3b}$$

Our permittivity and permeability are anisotropic, but there are more general constitutive relations in which the electric and magnetic fields are mixed by the material. Constitutive relations (1.3) are valid for media which do neither have temporal nor spatial memory. In such media it is not possible to extract a Dirac delta from $\varepsilon(\boldsymbol{x},\boldsymbol{x}_0)$ and $\mu(\boldsymbol{x},\boldsymbol{x}_0)$, and there is an additional convolution integral over all coordinates $\boldsymbol{x}_0$, and also a time integral if there is a time dependence.

The disorder is usually confined to some volume, and we consider the average of the permittivity and permeability over the volume as the host medium in which the disorder resides, and write

$$\varepsilon(\boldsymbol{x}) = \varepsilon + \delta\varepsilon(\boldsymbol{x}), \tag{1.4a}$$
$$\mu(\boldsymbol{x}) = \mu + \delta\mu(\boldsymbol{x}). \tag{1.4b}$$

Here ε and μ are the host permittivity and permeability tensors and $\delta\varepsilon(\boldsymbol{x})$ and $\delta\mu(\boldsymbol{x})$ are the electric and magnetic disorder respectively. In many optical experiments the magnetic disorder is negligible, but we keep track of it as it will be relevant for this thesis. The ensemble average of the permittivity and permeability over all realizations of the disorder restores homogeneity,

$$\langle\langle\varepsilon(\boldsymbol{x})\rangle\rangle = \varepsilon, \tag{1.5a}$$
$$\langle\langle\mu(\boldsymbol{x})\rangle\rangle = \mu. \tag{1.5b}$$

Isotropy is only restored when we also average over all possible orientations of the inhomogeneities, and then the average permittivity and permeability tensors of the host medium become proportional to the unit tensor. If we have an ensemble of slabs all with pores running from the front interface to the back interface, we can imagine that averaging over the realizations of the disorder will not remove the anisotropy created by the pores.

Obtaining exact solutions to the Maxwell equations in media with arbitrary anisotropy and disorder is a complicated matter. The components of the electromagnetic fields are not independent quantities, and several methods are available to reduce the number of field components. It is well known that equations (1.1b) and (1.1c) allow the introduction a magnetic vector potential

$\boldsymbol{A}$ and an electric scalar potential ϕ according to

$$\boldsymbol{B} \equiv \boldsymbol{\nabla} \times \boldsymbol{A}, \tag{1.6a}$$

$$\boldsymbol{E} \equiv -\frac{\partial \boldsymbol{A}}{\partial t} - \boldsymbol{\nabla}\phi. \tag{1.6b}$$

Together with the constitutive relations (1.3) the potentials (1.6) fully specify the four field vectors appearing in the Maxwell equations. The magnetic vector potential and electric scalar potential are not unique, and we can supply them with an equation of constraint such as the Lorentz gauge $\boldsymbol{\nabla}\cdot\boldsymbol{A}+\partial\phi/\partial t = 0$ or the Coulomb gauge $\boldsymbol{\nabla}\cdot\boldsymbol{A} = 0$ [54]. We observe that in media where there are no free charges and no free currents Eqs. (1.2) hold, and we can introduce an electric vector potential $\boldsymbol{W}$, and a magnetic scalar potential χ, by

$$\boldsymbol{D} \equiv \boldsymbol{\nabla} \times \boldsymbol{W}, \tag{1.7a}$$

$$\boldsymbol{H} \equiv \frac{\partial \boldsymbol{W}}{\partial t} + \boldsymbol{\nabla}\chi. \tag{1.7b}$$

Also by means of $\boldsymbol{W}$ and χ we can fully specify the four electromagnetic field vectors, and these potentials are not unique either. The potentials $\boldsymbol{W}$ and χ can only be used in the absence of free charges and currents, but for a description of scattering of light this is not a problem.

The Maxwell equations give rise to an energy balance equation. Using the absence of free charges and free currents (1.2) and constitutive relations (1.3), the continuity equation for the energy density follows from the inner product of $\boldsymbol{H}$ with (1.1c) subtracted from the inner product of $\boldsymbol{E}$ with (1.1d). The energy density $\mathscr{H}_{\text{em}}$ and energy density flux or Poynting vector $\boldsymbol{S}_{\text{em}}$ of the electromagnetic fields are identified by

$$\mathscr{H}_{\text{em}} \equiv \frac{1}{2}\left[\boldsymbol{E}^*\cdot\boldsymbol{D} + \boldsymbol{B}^*\cdot\boldsymbol{H} + \text{c.c.}\right], \tag{1.8a}$$

$$\boldsymbol{S}_{\text{em}} \equiv \boldsymbol{E}\times\boldsymbol{H}^* + \text{c.c.}. \tag{1.8b}$$

The energy density contains contributions of the permittivity and permeability of the disordered medium, and therefore consists of a radiative and a material contribution. The disorder term represents the interaction of the electromagnetic waves with the medium.

Very often we are not interested in the electric and magnetic fields themselves, but only in the conserved quantities in the problem at hand. For elastic scattering of light the energy is the conserved quantity. There are many polarization states of light which give rise to the same energy density and energy density flux, and we can wonder if instead of the magnetic potential vector and the electric scalar potential, there exists a single scalar wave field which correctly predicts the energy density and energy density flux, but does not necessarily predict the polarization.

1.3 A history of scalar models for light

The acceptance of light as a wave phenomenon has had a long history, and was refueled by the advent of quantum theory around 1900, with the introduction of the photon to explain the quantization of the electromagnetic energy emitted by an oscillating electric system. We discuss classical electromagnetism, and therefore in this thesis light is a wave. Here we present two key ideas in the development of the wave theory. Huygens advocated a wave model for light [55], and stated the principle that each element of a wave surface may be regarded as the center of a secondary disturbance which gives rise to spherical wavelets, and the position of the wave surface at any later time is the envelope of all such wavelets, which is now known as Huygens' principle or Huygens' construction [54]. More than a hundred years later Fresnel improved on Huygens' principle by allowing the wavelets to interfere, thus accounting for diffraction, which naturally became known as the Huygens-Fresnel principle.

The Huygens-Fresnel principle can be regarded as a special form of Kirchhoff's integral theorem [54], which is the basis of Kirchhoff's diffraction theory for scalar waves diffracting through a hole in a screen. As long as the diffracting objects are large compared to the wavelength, and the light is observed in the far field, Kirchhoff's diffraction theory works very well [54]. The simplest model, used by Kirchhoff, to describe freely propagating waves at velocity v is a scalar field which satisfies a wave equation

$$\Delta\psi(\boldsymbol{x},t) - \frac{1}{v^2}\frac{\partial^2\psi(\boldsymbol{x},t)}{\partial t^2} \quad = \quad 0. \tag{1.9}$$

It is very convenient to Fourier transform the time coordinate of the wave equation to frequency space, which yields the Helmholtz equation, which describes monochromatic waves of angular frequency ω

$$\Delta\psi_\omega(\boldsymbol{x}) + \frac{\omega^2}{v^2}\psi_\omega(\boldsymbol{x}) \quad = \quad 0. \tag{1.10}$$

The waves in Eq. (1.10) have wavelength $\lambda = k/(2\pi) = \omega/(2\pi v)$, and k is the wavenumber. The wavelength is the same for every propagation direction. Even though the scalar wave equation has been studied for such a long time, it is still actively studied, not only for light [56, 57].

The Helmholtz equation, Eq. (1.10), resembles the Schrödinger equation for electrons if we map $\omega^2/v^2 \to \hbar\omega/m_e$. In condensed matter theory the effect of disorder on the conductivity of electrons has been studied intensively in the 1980's [58–62] and this analogy has been used when it was found that interference effects survive for multiple scattered light in disordered media

[22–26]. In isotropic media each component of the electromagnetic wave vector satisfies the Helmholtz equation (1.10), and it is tempting to replace the electromagnetic field vector according to $\boldsymbol{E} \rightarrow \psi$ [63, 64], but this leads to a wrong energy density for the electromagnetic waves.

For homogeneous isotropic media a mapping of electromagnetic fields on a single complex scalar fields has been introduced in the 1950's and it was shown that both the time averaged energy density and energy density flux or Poynting vector of quasi monochromatic natural light can be represented by a single complex scalar field [65–67], and the scalar model describes diffraction phenomena very well. In the 1990's the model was reinvented and disorder has since been added [68], resulting in a generalized radiative transfer equation incorporating interference and the microscopic scatterers. One of the important contributions of the scalar model to the understanding of multiple scattering of light in disordered media is a scattering delay correction to the energy velocity of light due to frequency dependent scattering potentials. In this thesis we improve on that model by incorporating the effects of polarization anisotropy. The main limitation of the scalar model to be introduced lies in the fact that it does not predict the orientation of the electric and magnetic field vectors themselves.

1.4 Overview of this thesis

This thesis presents a scalar model for electromagnetic waves in anisotropic disordered media. We tried to keep each chapter as self-contained as possible, at the cost of occasional repetition of earlier results.

In chapter 2 we introduce the mapping of the electromagnetic fields on a scalar model, and study the amplitude of scalar waves in homogeneous and in disordered anisotropic infinite media. From the Bethe-Salpeter equation, which is related to the energy density, we derived a generalized Boltzmann transport equation, incorporating interference effects and anisotropy. An anisotropic radiative transfer equation is derived, and some ideas are presented to numerically model the radiative transfer equation. To get a grasp of the effect of anisotropy we present some explicit examples. Appendix A contains the derivation of the Ward identity in anisotropic media, used to establish energy conservation in this chapter.

In chapter 3 we derive an anisotropic diffusion equation for infinite media starting from the anisotropic radiative transfer equation. Some examples of anisotropic diffusion are presented and potential dimensional cross overs are studied. Interference corrections are added and we explore the location of the transition to Anderson localization in anisotropic media, and find that in

anisotropic media the transition occurs at larger mean free path. Appendix B presents a justification of the self consistent radiance expansion used in this chapter.

In chapter 4 we incorporate the effects of boundaries in the model, starting from the Maxwell equations. Snell's law and the Fresnel reflection and transmission coefficients for planar waves in the anisotropic scalar model are derived, and the Brewster angle is determined. For the energy density flux we derive the reflectivity and transmissivity. Also for the radiance and the diffuse energy density the conditions at the interface are established. The angle and polarization averaged reflectivity for the diffuse energy density is related to the reflectivity for the individual plane waves. The boundary conditions give rise to a transport mean free path and an energy velocity, and both turn out to be vector quantities. Green functions for the amplitude and the diffuse energy density are calculated. These Green functions are used to calculate the angular redistribution of light by anisotropic disordered semi-infinite media and slabs and also the bistatic coefficients, which describe angular resolved reflection and transmission for disordered samples, are calculated. The enhanced backscattering cone is affected by the anisotropy.

Finally in chapter 5 we discuss the collection of all the obtained results and implications for future experimental and theoretical studies of light in anisotropic disordered media.

Chapter 2

Anisotropic radiative transfer in infinite media

We set up a theory for multiple scattering of scalar waves in anisotropic disordered media, with anisotropy present in the scatterers or in the host medium. We analytically derive a radiative transfer equation valid in anisotropic host media, and we present a Monte Carlo method for modeling the anisotropic radiative transfer equation. Our radiative transfer equation is able to model either the radiance of ordinary or of extraordinary waves. In addition the well known relation between extinction mean free path and scattering cross section is generalized to anisotropic media. Finally some examples of disordered media illustrate the effect of anisotropy in the radiative transfer equation.

2.1 Introduction

When we send a wave into some arbitrary material, the wave encounters inhomogeneities from which it scatters. If there is not too much absorption in the material, we can use the wave intensity to probe the internal structure of the material by comparing it to the incident intensity. The potential applications of such a procedure are numerous. In biological tissue we could noninvasively image the brain, look for cancer cells, or the orientation and deformation of blood cells [5, 69–71]. We could use coda interferometry of seismic waves to detect temporal changes in Earth's crust or we can use electromagnetic waves to diagnose the organic content of oil shales [72–74]. Whether acoustic, electromagnetic, or seismic waves are used depends of course on the setting of the problem. Often the propagation of waves through scattering materials is described extremely well by the radiative transfer equation for an isotropic medium, supplied with some phase function of the scatterer

[75]. The radiative transfer equation describes everything from ballistic propagation to diffuse propagation, but can in general only be solved numerically. Anisotropic disordered media can not be treated by the standard isotropic radiative transfer equation. Statistically anisotropic media are encountered in many fields, such as in optics [27, 28, 76], in seismology [72, 73, 77], in quantum theory, [78], and in medicine and biology [2, 3, 5, 79–82].

In this chapter, we present a model for scalar waves in a random medium with anisotropy, and introduce two mappings of electromagnetic waves on scalar waves. New in our model as compared to other scalar wave models, see e.g. [68, 77] is the incorporation of an anisotropic host medium. We introduce scattering, extinction and momentum transfer cross sections for the wave amplitude and establish the optical theorem in an anisotropic host medium. We transform the exact Bethe-Salpeter equation for scalar waves in anisotropic media into a generalized Boltzmann transport equation. We obtain the Ward identity and a continuity equation for the wave energy density. Then we derive from the generalized Boltzmann transport equation an equation of radiative transfer with anisotropy, and we present some ideas that may help to create a Monte Carlo simulation of waves in anisotropic media.

We present the scalar wave theory in detail in sections 2.2 through 2.4, with a technical derivation of the Ward identity in appendix A. In section 2.5 we summarize the main results, and we present some examples of the effect of anisotropy in section 2.7.

2.2 Mapping vectors to scalars

In this section, we map the Maxwell equations to a scalar model in order to simplify future calculations for random multiple scattering media. In the absence of free electric charges and currents, the Maxwell equations, in an otherwise arbitrary medium, give rise to energy density $\mathscr{H}_{\text{em}}$ and flux $\boldsymbol{S}_{\text{em}}$,

$$\mathscr{H}_{\text{em}} = \frac{1}{2}\left[\boldsymbol{E}^* \cdot \boldsymbol{D} + \boldsymbol{B}^* \cdot \boldsymbol{H} + \text{c.c.}\right], \tag{2.1a}$$

$$\boldsymbol{S}_{\text{em}} = \boldsymbol{E} \times \boldsymbol{H}^* + \text{c.c.}. \tag{2.1b}$$

Employing the constitutive relations $\boldsymbol{D} = \varepsilon \cdot \boldsymbol{E}$ and $\boldsymbol{B} = \mu \cdot \boldsymbol{H}$, in media with dielectric permittivity tensor ε and permeability tensor μ, both constant in time, we find closed anisotropic wave equations for $\boldsymbol{E}$ and $\boldsymbol{H}$,

$$\boldsymbol{\nabla} \times \mu^{-1} \cdot (\boldsymbol{\nabla} \times \boldsymbol{E}) + \varepsilon \cdot \frac{\partial^2 \boldsymbol{E}}{\partial t^2} = \boldsymbol{0}, \tag{2.2a}$$

$$\boldsymbol{\nabla} \times \varepsilon^{-1} \cdot (\boldsymbol{\nabla} \times \boldsymbol{H}) + \mu \cdot \frac{\partial^2 \boldsymbol{H}}{\partial t^2} = \boldsymbol{0}. \tag{2.2b}$$

We identify (2.1a) and (2.1b) with the Hamiltonian $\mathscr{H}$ and flux $\boldsymbol{S}$ for a scalar field ψ in a homogeneous anisotropic medium,

$$\mathscr{H} = \frac{1}{2}\left[\frac{1}{{c_i}^2}\frac{\partial\psi^*}{\partial t}\frac{\partial\psi}{\partial t} + \boldsymbol{\nabla}\psi^*\cdot\mathsf{A}\cdot\boldsymbol{\nabla}\psi + \text{c.c.}\right], \tag{2.3a}$$

$$\boldsymbol{S} = -\frac{\partial\psi}{\partial t}\mathsf{A}\cdot\boldsymbol{\nabla}\psi^* + \text{c.c.}. \tag{2.3b}$$

Here A is a dimensionless tensor representing the anisotropy of the medium, and c_i is a velocity. The scalar field ψ satisfies an anisotropic wave equation

$$\boldsymbol{\nabla}\cdot\mathsf{A}\cdot\boldsymbol{\nabla}\psi - \frac{1}{{c_i}^2}\frac{\partial^2\psi}{\partial t^2} = 0. \tag{2.4}$$

Our mapping of the vector fields on a scalar field is neither bijective, nor unique. The disadvantage of having lost an exact description of polarization effects in multiple scattering of light is far outweighed by the numerous advantages. To solve for the electromagnetic fields we would require tensorial Green functions, which can have up to 6 independent components, whereas for ψ we need only one scalar Green function. For the average wave intensity, which is governed by the exact Bethe-Salpeter equation, we would need the product of two Green tensors, and, in the worst case, would have to solve up to 36 coupled equations. The actual number of independent equations could reduce to 4 in situations of high symmetry [83]. Interference effects in multiple scattering of light are often of greater importance than polarization. In isotropic media, polarization is washed out after less than 20 scattering events for Rayleigh scatterers [84], whereas interference effects could survive even after an infinite number of scattering events, such as in the cone of enhanced backscattering.

When we choose a mapping, we could follow [68] and interpret the scalar field ψ as a potential for the electromagnetic fields by mapping (2.1a) and (2.2a) to (2.3a) and (2.4) respectively, identifying in anisotropic media

$$\frac{\mu^{-1}}{\frac{1}{3}\text{Tr}\left(\mu^{-1}\right)} \rightarrow \mathsf{A}, \tag{2.5a}$$

$$\frac{\text{Tr}\left(\mu^{-1}\right)}{\text{Tr}\left(\varepsilon\right)} \rightarrow {c_i}^2, \tag{2.5b}$$

$$\sqrt{\frac{1}{3}\text{Tr}(\varepsilon)}\,|\boldsymbol{E}| \rightarrow \frac{1}{c_i}\frac{\partial\psi}{\partial t}, \tag{2.5c}$$

$$\sqrt{\frac{1}{3}\text{Tr}(\mu^{-1})}\,\boldsymbol{B} \rightarrow \boldsymbol{\nabla}\psi, \tag{2.5d}$$

where we see that only the trace of ε survives. In the scalar mapping we can take into account only the anisotropy in the permeability tensor μ. Anisotropic magnetic permeability tensors are not frequently encountered in optics. Rather than mapping (2.1a) and (2.2a) to (2.3a) and (2.4), we therefore map (2.1a) and (2.2b) to (2.3a) and (2.4) respectively, which leads to the identifications

$$\frac{\varepsilon^{-1}}{\frac{1}{3}\mathrm{Tr}\left(\varepsilon^{-1}\right)} \quad \rightarrow \quad \mathsf{A}, \tag{2.6a}$$

$$\frac{\mathrm{Tr}\left(\varepsilon^{-1}\right)}{\mathrm{Tr}\left(\mu\right)} \quad \rightarrow \quad \mathrm{c_i}^2, \tag{2.6b}$$

$$\sqrt{\frac{1}{3}\mathrm{Tr}(\mu)}\,|\boldsymbol{H}| \quad \rightarrow \quad \frac{1}{\mathrm{c_i}}\frac{\partial\psi}{\partial t}, \tag{2.6c}$$

$$\sqrt{\frac{1}{3}\mathrm{Tr}(\varepsilon^{-1})}\,\boldsymbol{D} \quad \rightarrow \quad \boldsymbol{\nabla}\psi. \tag{2.6d}$$

We use this model to calculate the effect of dielectric anisotropy on transport of waves through random media.

2.3 Scalar wave amplitude

To describe energy transport of waves exactly, we need to define a few quantities relating to the underlying ave amplitude. In this section we first present a homogeneous anisotropic media. We add a scatterer and determine cross sections. Finally we present the Dyson Green function for the ensemble averaged amplitude.

2.3.a Mean field quantities

In an anisotropic medium, rather than having an ordinary, extraordinary, and longitudinal dispersion relation, one has always only one dispersion relation for ψ, thus only one phase velocity v_p (a scalar), one group velocity $\boldsymbol{v}_\mathrm{g}$ (a vector), and one refractive index m. The dispersion relation in the homogeneous anisotropic medium reads

$$\frac{\omega^2}{\mathrm{c_i}^2} - \boldsymbol{k}\cdot\mathsf{A}\cdot\boldsymbol{k} \quad \equiv \quad 0. \tag{2.7}$$

We will use the notation $\boldsymbol{k}$ for wave vectors which satisfy (2.7), and $\boldsymbol{p}$ for wave vectors that do not.

Equation (2.7) implicitly defines the function $\omega(\boldsymbol{k})$, in terms of which the phase and group velocities and refractive index are defined by

$$v_\mathrm{p}(\boldsymbol{k}) \equiv \frac{\omega(\boldsymbol{k})}{|\boldsymbol{k}|} = \mathrm{c_i}\sqrt{\boldsymbol{e_k}\cdot\mathsf{A}\cdot\boldsymbol{e_k}}, \tag{2.8a}$$

$$\boldsymbol{v}_\mathrm{g}(\boldsymbol{k}) \equiv \frac{\partial\omega(\boldsymbol{k})}{\partial\boldsymbol{k}} = \frac{\mathrm{c_i}^2}{v_\mathrm{p}(\boldsymbol{e_k})}\mathsf{A}\cdot\boldsymbol{e_k}, \tag{2.8b}$$

$$m(\boldsymbol{e_k}) \equiv \frac{\mathrm{c_0}}{v_\mathrm{p}(\boldsymbol{e_k})} = \frac{\mathrm{c_0}}{\mathrm{c_i}}\frac{1}{\sqrt{\boldsymbol{e_k}\cdot\mathsf{A}\cdot\boldsymbol{e_k}}}, \tag{2.8c}$$

where $\mathrm{c_0}$ the velocity of light in vacuum. Along any principal axis $\boldsymbol{e}_\mathrm{a}$ of the anisotropy tensor A we have $\boldsymbol{v}_\mathrm{g}(\boldsymbol{e}_\mathrm{a}) = v_\mathrm{p}(\boldsymbol{e}_\mathrm{a})\,\boldsymbol{e}_\mathrm{a}$. In isotropic media $\mathsf{A}=1$, and the expressions above reduce to $v_\mathrm{g} = v_\mathrm{p} = \mathrm{c_i}$. We plot the frequency surface (2.7), the phase velocity (2.8a), and the group velocity (2.8b) in Fig. 2.1, 2.2, and 2.3 respectively.

When we obtain the solution for ψ for arbitrary A, we can model the ordinary and extraordinary polarizations by choosing the right values for A.

2.3.b Scatterers in an anisotropic medium

Instead of defining dielectric scatterers, with which our mapping would lead to unwanted nonlocal effects (a velocity dependent potential), we introduce inhomogeneities in the magnetic permeability μ. Then the frequency dependent scattering potential V is

$$V_\omega(\boldsymbol{x},\boldsymbol{x}_0) \equiv -\frac{\omega^2}{\mathrm{c_i}^2}\left[\frac{\mu(\boldsymbol{x})}{\mu}-1\right]\delta^3(\boldsymbol{x}-\boldsymbol{x}_0), \tag{2.9}$$

where both $\mu(\boldsymbol{x})$ and $\mu \equiv \mathrm{Tr}(\mu)/3$ are scalar quantities. The amplitude Green function G in the presence of scatterers satisfies

$$\left[\boldsymbol{\nabla}\cdot\mathsf{A}\cdot\boldsymbol{\nabla}+\frac{\omega^2}{\mathrm{c_i}^2}\right]G_\omega(\boldsymbol{x},\boldsymbol{x}_0) = \delta^3(\boldsymbol{x}-\boldsymbol{x}_0)+\int \mathrm{d}^3x_1\, V_\omega(\boldsymbol{x},\boldsymbol{x}_1)\,G_\omega(\boldsymbol{x}_1,\boldsymbol{x}_0). \tag{2.10}$$

In terms of the free space Green function g, which is the solution to Eq. (2.10) for $V=0$, the Green function for the inhomogeneous medium reads [6, 85]

$$G_\omega(\boldsymbol{x},\boldsymbol{x}_0) = g_\omega(\boldsymbol{x},\boldsymbol{x}_0)+\int \mathrm{d}^3x_2\int \mathrm{d}^3x_1\, g_\omega(\boldsymbol{x},\boldsymbol{x}_2)\,V_\omega(\boldsymbol{x}_2,\boldsymbol{x}_1)\,G_\omega(\boldsymbol{x}_1,\boldsymbol{x}_0). \tag{2.11}$$

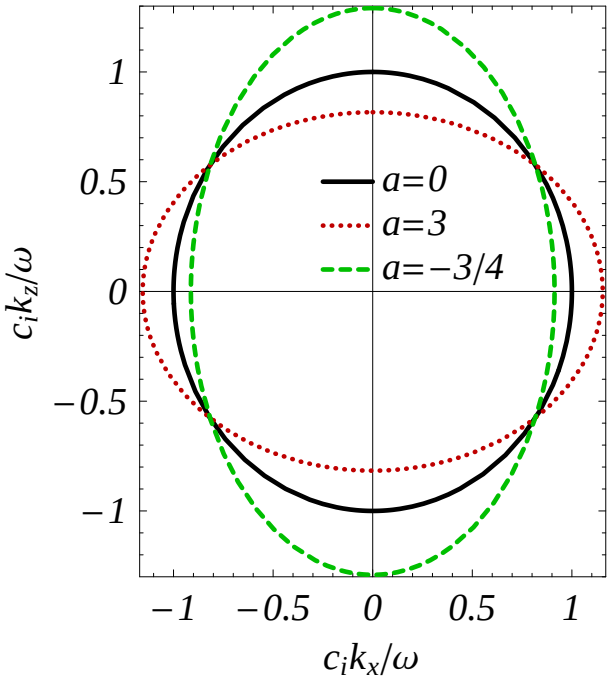

Figure 2.1 (color online).
Examples of the frequency surface defined by $1 \equiv \mathrm{c_i}^2 \boldsymbol{k}\cdot\varepsilon^{-1}\cdot\boldsymbol{k}/(\omega^2 \mathrm{Tr}[\varepsilon^{-1}]/3)$ *are plotted for a constant isotropic velocity* $\mathrm{c_i}$ *and constant frequency* ω*. The material is homogeneous with isotropic permeability* μ *and uniaxial dielectric permittivity* $\varepsilon = (3+a)[1+a\boldsymbol{e}_z\boldsymbol{e}_z/(1-a)]/(\mathrm{c_i}^2\mathrm{Tr}[\mu])$*, where* a *parameterizes the anisotropy. The solid line is for isotropic media,* $a = 0$*. The dotted line is for an anisotropic dielectric with* $a = 3$*, and the dashed line is for* $a = -3/4$*.*

The T matrix for potential V is defined by the recursion relation

$$T_\omega(\boldsymbol{x},\boldsymbol{x}_0) \equiv V_\omega(\boldsymbol{x},\boldsymbol{x}_0) + \int \mathrm{d}^3x_2 \int \mathrm{d}^3x_1\, V_\omega(\boldsymbol{x},\boldsymbol{x}_2)\, g_\omega(\boldsymbol{x}_2,\boldsymbol{x}_1)\, T_\omega(\boldsymbol{x}_1,\boldsymbol{x}_0)\,. \tag{2.12}$$

Free space is homogeneous, therefore momentum is conserved, and upon Fourier transforming our equations we extract a Dirac delta function, which leads to $g_\omega(\boldsymbol{p},\boldsymbol{p}_0) \equiv g_\omega(\boldsymbol{p})\,(2\pi)^3\,\delta^3(\boldsymbol{p}-\boldsymbol{p}_0)$, with the retarded solution

$$g_\omega(\boldsymbol{p}) \equiv \frac{1}{\frac{\omega^2}{\mathrm{c_i}^2} - \boldsymbol{p}\cdot\mathsf{A}\cdot\boldsymbol{p} + \mathrm{i}0^+}. \tag{2.13}$$

Any potential V of finite support we can interpret as a single scatterer, and

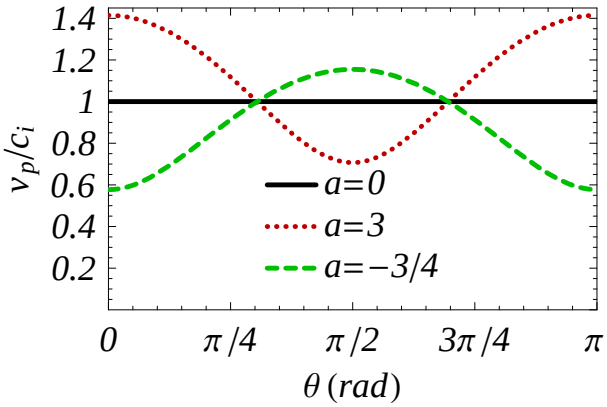

Figure 2.2 (color online).
The anisotropy in the phase velocity $v_\mathrm{p}(\boldsymbol{e_k})/\mathrm{c_i} = \sqrt{\boldsymbol{e_k}\cdot\varepsilon^{-1}\cdot\boldsymbol{e_k}/(\mathrm{Tr}[\varepsilon^{-1}]/3)}$ *is plotted for an arbitrary isotropic velocity* $\mathrm{c_i}$. *The material is homogeneous with isotropic permeability* μ *and uniaxial dielectric permittivity* $\varepsilon = (3+a)[1+ae_ze_z/(1-a)]/(\mathrm{c_i}^2\mathrm{Tr}[\mu])$, *where* a *parameterizes the strength of the anisotropy. The solid line is for isotropic media,* $a = 0$. *The dotted line is for an anisotropic medium with* $a = 3$, *and the dashed line is for* $a = -3/4$.

we can write down the optical theorem for the T matrices [85], with our free space Green function (2.13)

$$\mathrm{Im}\left[T_\omega\left(\boldsymbol{p},\boldsymbol{p}\right)\right] = \int\frac{\mathrm{d}^3p_0}{(2\pi)^3}\mathrm{Im}\left[g_\omega\left(\boldsymbol{p}_0\right)\right]\left|T_\omega\left(\boldsymbol{p},\boldsymbol{p}_0\right)\right|^2, \tag{2.14}$$

The imaginary part of g imposes the dispersion relation (2.7), thus fixing the wave vector magnitude as a function of frequency ω and direction $\boldsymbol{e_k}$. The optical theorem (2.14) gives rise to extinction and scattering cross sections σ_s and σ_e, which are found to be

$$\sigma_{\mathrm{s}\omega}\left(\boldsymbol{e_k}\right) \equiv \frac{\langle T_\omega\left(\boldsymbol{e_k},\boldsymbol{e_{k_1}}\right)T^*{}_\omega\left(\boldsymbol{e_k},\boldsymbol{e_{k_1}}\right)\rangle_{\boldsymbol{e_{k_1}}}}{4\pi\sqrt{\det\mathrm{A}}}, \tag{2.15a}$$

$$\sigma_{\mathrm{e}\omega}\left(\boldsymbol{e_k}\right) \equiv -\frac{\mathrm{c_i}\mathrm{Im}\left[T_\omega\left(\boldsymbol{e_k},\boldsymbol{e_k}\right)\right]}{\omega}. \tag{2.15b}$$

The scattering cross section (2.15a) is sensitive to the medium surrounding the scatterer. The effect of the medium is contained in the average $\langle\ldots\rangle$ over the anisotropic surface at constant frequency,

$$\langle\ldots\rangle_{\boldsymbol{e_k}} \equiv \int\frac{\mathrm{d}^2\boldsymbol{e_k}}{4\pi}\frac{\ldots}{\sqrt{\left(\boldsymbol{e_k}\cdot\mathrm{A}\cdot\boldsymbol{e_k}\right)^3\det\mathrm{A}^{-1}}}, \tag{2.16}$$

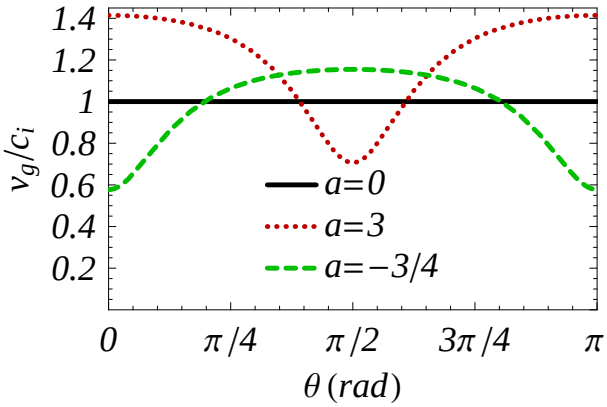

Figure 2.3 (color online).
The anisotropy in the group velocity $v_g(e_k) = c_i \varepsilon^{-1} \cdot e_k / \sqrt{e_k \cdot \varepsilon^{-1} \cdot e_k \mathrm{Tr}[\varepsilon^{-1}]/3}$ *is plotted for some constant velocity* c_i. *The material is homogeneous with isotropic permeability* μ *and uniaxial dielectric permittivity* $\varepsilon = (3+a)[1 + a e_z e_z/(1-a)]/(c_i{}^2 \mathrm{Tr}[\mu])$, *where* a *parameterizes the strength of the anisotropy. The solid line is for isotropic media,* $a = 0$. *The dotted line is for an anisotropic dielectric with* $a = 3$, *and the dashed line is for* $a = -3/4$.

such that $\langle 1 \rangle_{e_k} = 1$.

Apart from the scattering and extinction cross sections (2.15a) and (2.15b), we require the differential scattering cross section,

$$\frac{\mathrm{d}\sigma_{s\omega}(e_k, e_{k_1})}{\mathrm{d}^2 e_{k_1}} \equiv \frac{T_\omega(e_k, e_{k_1})\, T^*{}_\omega(e_k, e_{k_1})}{(4\pi)^2 (e_{k_1} \cdot \mathsf{A} \cdot e_{k_1})^{\frac{3}{2}}}. \tag{2.17}$$

The differential scattering cross section (2.17) is a measure for the amount of radiance send into solid angle $\mathrm{d}^2 e_{k_1}$ around e_{k_1}, after it is removed from an incoming beam with wave vector e_k.

Elastic point scatterer

As an example of a scatterer in an anisotropic medium we consider a point scatterer. The matrix elements of the scattering potential V_p of a point scatterer at x_p are

$$V_{p\omega}(x, x_0) \equiv V_{p\omega} \delta^3(x - x_p) \delta^3(x - x_0), \tag{2.18a}$$

$$V_{p\omega} \equiv -\frac{\omega^2}{c_i{}^2} \alpha_B. \tag{2.18b}$$

The strength of the potential is governed by α_B, which is the "bare" magnetic polarizability, which, for scalar waves, is equal to the static polarizability [86].

The T matrix of the isotropic point scatterer is

$$T_{\mathrm{p}_\omega}(\boldsymbol{x},\boldsymbol{x}_0) \equiv T_{\mathrm{p}_\omega}\delta^3(\boldsymbol{x}-\boldsymbol{x}_\mathrm{p})\delta^3(\boldsymbol{x}_0-\boldsymbol{x}_\mathrm{p}), \tag{2.19a}$$

$$T_{\mathrm{p}_\omega} \equiv \frac{V_{\mathrm{p}_\omega}}{1-\int\frac{\mathrm{d}^3p}{(2\pi)^3}g_\omega(\boldsymbol{p})V_{\mathrm{p}_\omega}}. \tag{2.19b}$$

The integral in the denominator of (2.19b) over the whole wave vector space diverges, but it can be regularized by using

$$\frac{1}{\frac{\omega^2}{{\mathrm{c_i}}^2}-\boldsymbol{p}\cdot\mathsf{A}\cdot\boldsymbol{p}} = \frac{1}{\frac{\omega^2}{{\mathrm{c_i}}^2}-\boldsymbol{p}\cdot\mathsf{A}\cdot\boldsymbol{p}}\frac{\omega^2}{{\mathrm{c_i}}^2\boldsymbol{p}\cdot\mathsf{A}\cdot\boldsymbol{p}}-\frac{1}{\boldsymbol{p}\cdot\mathsf{A}\cdot\boldsymbol{p}}. \tag{2.20}$$

A similar method has been employed in [68] in isotropic media. The divergence is now in the term $1/\boldsymbol{p}\cdot\mathsf{A}\cdot\boldsymbol{p}$. The integral over the regularized part is

$$\lim_{0^+\downarrow 0}\int\frac{\mathrm{d}^3p}{(2\pi)^3}\frac{1}{\frac{\omega^2}{{\mathrm{c_i}}^2}+\mathrm{i}0^+-\boldsymbol{p}\cdot\mathsf{A}\cdot\boldsymbol{p}}\frac{\omega^2}{{\mathrm{c_i}}^2\boldsymbol{p}\cdot\mathsf{A}\cdot\boldsymbol{p}} = -\frac{\mathrm{i}}{4\pi}\frac{\omega}{\mathrm{c_i}}\frac{1}{\sqrt{\det\mathsf{A}}}. \tag{2.21}$$

The integral over the diverging term is cut off at large wave vector, $|\mathsf{A}^{\frac{1}{2}}\cdot\boldsymbol{p}| = \Lambda\pi/2 \gg \omega/\mathrm{c_i}$,

$$\int\frac{\mathrm{d}^3p}{(2\pi)^3}\frac{1}{\boldsymbol{p}\cdot\mathsf{A}\cdot\boldsymbol{p}} = \frac{\Lambda}{4\pi\sqrt{\det\mathsf{A}}}. \tag{2.22}$$

The T matrix of the point scatterer has a Lorentzian-type of resonance, with resonance frequency ω_0 and linewidth Γ defined by

$${\omega_0}^2 \equiv \frac{4\pi{\mathrm{c_i}}^2\sqrt{\det\mathsf{A}}}{\alpha_\mathrm{B}\Lambda}, \tag{2.23a}$$

$$\Gamma \equiv \frac{{\omega_0}^2}{\mathrm{c_i}\Lambda}. \tag{2.23b}$$

Additionally the quality factor of the resonance is defined by $Q \equiv \omega_0/\Gamma$. We finally obtain the T matrix of an isotropic point scatterer in an anisotropic dielectric,

$$T_{\mathrm{p}_\omega} = -\frac{4\pi\mathrm{c_i}\sqrt{\det\mathsf{A}}\omega^2\Gamma/{\omega_0}^2}{{\omega_0}^2-\omega^2-\mathrm{i}\omega^3\Gamma/{\omega_0}^2}. \tag{2.24}$$

The ratio $\Gamma/{\omega_0}^2 = (\mathrm{c_i}\Lambda)^{-1}$ is independent of $\sqrt{\det\mathsf{A}}$. We require six independent quantities from the set $\{\mu,\varepsilon_{11},\varepsilon_{22},\varepsilon_{33},\omega_0,\alpha_\mathrm{B},\Gamma\}$ to determine the point scatterer. The dynamic polarizability is given by $\alpha_\omega = -T_{\mathrm{p}_\omega}/(\omega/\mathrm{c_i})^2$.

The T matrix of the point scatterer (2.24) satisfies the optical theorem, so its extinction and scattering cross sections are equal. The scattering cross section σ_{p} of the point scatterer is

$$\sigma_{\mathrm{p}_\omega} = \frac{4\pi {\mathrm{c_i}}^2 \sqrt{\det \mathsf{A}} (\omega^2 \Gamma / {\omega_0}^2)^2}{({\omega_0}^2 - \omega^2)^2 + (\omega^3 \Gamma / {\omega_0}^2)^2}. \tag{2.25}$$

If we take $\omega_0 = 0$, then the scattering cross section (2.25) divided by $(2\pi)^2 \Gamma / {\omega_0}^2$ exactly coincides with a Lorentzian function centered around 0. We plotted the frequency dependence of the scattering cross section in Fig 2.4.

The differential scattering cross is direction dependent, because the solid angle element is deformed by the anisotropy, it is

$$\frac{\mathrm{d}\sigma_{\mathrm{p}_\omega}(\boldsymbol{e_k}, \boldsymbol{e_{k_1}})}{\mathrm{d}^2 \boldsymbol{e_{k_1}}} \equiv \frac{\sigma_{\mathrm{p}_\omega}}{4\pi \left(\boldsymbol{e_{k_1}} \cdot \mathsf{A} \cdot \boldsymbol{e_{k_1}}\right)^{\frac{3}{2}}}. \tag{2.26}$$

2.3.c Ensemble averages and Dyson Green function

The Dyson Green function $\langle\langle G \rangle\rangle$ is the ensemble average of the amplitude Green function G, and defines the in general complex valued self energy Σ [87],

$$\begin{aligned} \langle\langle G_\omega(\boldsymbol{x}, \boldsymbol{x}_0)\rangle\rangle \equiv\ & g_\omega(\boldsymbol{x}, \boldsymbol{x}_0) \\ & + \int \mathrm{d}^3 x_2 \int \mathrm{d}^3 x_1 g_\omega(\boldsymbol{x}, \boldsymbol{x}_2) \Sigma_\omega(\boldsymbol{x}_2, \boldsymbol{x}_1) \langle\langle G_\omega(\boldsymbol{x}_1, \boldsymbol{x}_0)\rangle\rangle \\ & . \end{aligned} \tag{2.27}$$

The ensemble averaging restores homogeneity so that momentum is conserved

$$\langle\langle G_\omega(\boldsymbol{p}_-, \boldsymbol{p}_+)\rangle\rangle \equiv G_\omega(\boldsymbol{p}_-) (2\pi)^3 \delta^3(\boldsymbol{p}_+ - \boldsymbol{p}_-) \tag{2.28a}$$

$$\Sigma_\omega(\boldsymbol{p}_-, \boldsymbol{p}_+) \equiv \Sigma_\omega(\boldsymbol{p}_-) (2\pi)^3 \delta^3(\boldsymbol{p}_+ - \boldsymbol{p}_-). \tag{2.28b}$$

The Dyson Green function is

$$G_\omega(\boldsymbol{p}) = \frac{1}{\frac{\omega^2}{{\mathrm{c_i}}^2} - \boldsymbol{p} \cdot \mathsf{A} \cdot \boldsymbol{p} - \Sigma_\omega(\boldsymbol{p})}. \tag{2.29}$$

The poles of the Dyson Green function obey the complex dispersion relation

$$\frac{\omega^2}{{\mathrm{c_i}}^2} - \boldsymbol{\kappa} \cdot \mathsf{A} \cdot \boldsymbol{\kappa} - \Sigma_\omega(\boldsymbol{\kappa}) = 0 \tag{2.30}$$

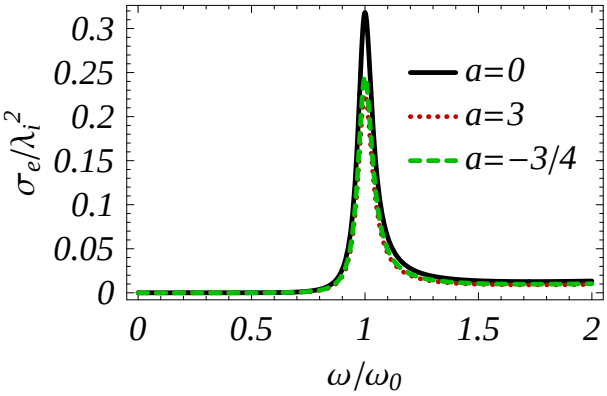

Figure 2.4 (color online).
The extinction cross section σ_e of point scatterers in anisotropic media is plotted as a function of frequency. $\lambda_i = 2\pi c_i/\omega$ is an isotropic wavelength. The anisotropic medium is given by $\varepsilon = (3+a)[1+ae_z e_z/(1-a)]/(c_i{}^2 \mathrm{Tr}[\mu])$. As large wave vector cutoff we set $\pi\Lambda/2 = 10\omega_{max}/c_i$. The solid line is for isotropic media, $a = 0$. The dotted line is for uniaxial media with $a = 3$, and the dashed line is for media which have $a = -3/4$. Waves at constant frequency ω inside the anisotropic material have a wavelength λ which is direction dependent, so for certain directions the dotted and the dashed curves will have different values. The differences between the cross sections shown in this plot are due to the volume element of the anisotropy tensor which is $\sqrt{(3/(3+a))^3(1+a)}$, which is smaller than unity for $a \neq 0$ and a must be larger than -1, otherwise the components of the dielectric tensor can become negative.

and we use notation $\boldsymbol{\kappa}$ for wave vectors satisfying dispersion relation (2.30). The real and imaginary parts of the wave vector magnitude $\kappa(\boldsymbol{e}_{\boldsymbol{\kappa}})$, defined such that $\boldsymbol{\kappa} = \kappa(\boldsymbol{e}_{\boldsymbol{\kappa}})\boldsymbol{e}_{\boldsymbol{\kappa}}$, as recursive functions of frequency ω and wave vector direction $\boldsymbol{e}_{\boldsymbol{\kappa}}$ are

$$\mathrm{Re}[\kappa(\boldsymbol{e}_{\boldsymbol{\kappa}})] \equiv \frac{\omega}{v_p(\boldsymbol{e}_{\boldsymbol{\kappa}})}\sqrt{\frac{\mathrm{Re}[\mu_\omega(\boldsymbol{\kappa})]+|\mu_\omega(\boldsymbol{\kappa})|}{2\mu}}, \tag{2.31a}$$

$$\mathrm{Im}[\kappa(\boldsymbol{e}_{\boldsymbol{\kappa}})] \equiv \frac{1}{2\mu}\frac{\omega^2}{v_p{}^2(\boldsymbol{e}_{\boldsymbol{\kappa}})}\frac{\mathrm{Im}[\mu_\omega(\boldsymbol{\kappa})]}{\mathrm{Re}[\kappa(\boldsymbol{e}_{\boldsymbol{\kappa}})]}, \tag{2.31b}$$

$$\frac{\mu_\omega(\boldsymbol{\kappa})}{\mu} \equiv 1-\frac{c_i{}^2}{\omega^2}\Sigma_\omega(\boldsymbol{\kappa}), \tag{2.31c}$$

with v_p defined in (2.8a), and $\mu_\omega(\boldsymbol{\kappa})$ an effective medium permeability incorporating scattering effects.

The real part of the wave vector defines a new phase velocity $\tilde{v}_{\rm p}$ "dressed" with scattering effects. The imaginary part of the wave vector defines an extinction mean free time $\tau_{\rm e}$, which is direction dependent. We find

$$\frac{1}{\tilde{v}_{{\rm p}\omega}(\boldsymbol{e}_{\boldsymbol{\kappa}})} \equiv \frac{{\rm Re}[\kappa(\boldsymbol{e}_{\boldsymbol{\kappa}})]}{\omega} \tag{2.32a}$$

$$\frac{1}{\tau_{{\rm e}\omega}(\boldsymbol{e}_{\boldsymbol{\kappa}})} \equiv 2v_{\rm p}(\boldsymbol{e}_{\boldsymbol{\kappa}}){\rm Im}[\kappa(\boldsymbol{e}_{\boldsymbol{\kappa}})], \tag{2.32b}$$

where in the latter indeed the "bare" phase velocity (2.8a) appears, because $\kappa(\boldsymbol{e}_{\boldsymbol{\kappa}})^2 = [\omega/v_{\rm p}(\boldsymbol{e}_{\boldsymbol{\kappa}})]^2\mu_\omega(\boldsymbol{\kappa})/\mu$. The group velocity associated with the effective medium is defined by

$$\tilde{\boldsymbol{v}}_{{\rm g}\omega}(\boldsymbol{e}_{\boldsymbol{\kappa}}) \equiv {\rm Re}\left[\frac{\partial\omega(\boldsymbol{\kappa})}{\partial\boldsymbol{\kappa}}\right] = \frac{{\rm c_i}^2{\rm A}\cdot\boldsymbol{e}_{\boldsymbol{\kappa}}}{\tilde{v}_{{\rm p}\omega}(\boldsymbol{e}_{\boldsymbol{\kappa}})}. \tag{2.33}$$

The second equality applies only when $\Sigma_\omega(\boldsymbol{\kappa})$ is isotropic.

The implicit equation for $\boldsymbol{\kappa}$ becomes explicit if we are given an explicit self energy Σ. In the independent scattering limit for scatterer density n and single scatterer T matrix T we approximate $\Sigma_\omega \approx nT_\omega$, and obtain for the real part of the wave vector and for the extinction mean free time

$$\frac{v_{\rm p}(\boldsymbol{e}_{\boldsymbol{\kappa}})}{\tilde{v}_{{\rm p}\omega}(\boldsymbol{e}_{\boldsymbol{\kappa}})} = 1 - \frac{n}{2}\frac{{\rm c_i}^2}{\omega^2}{\rm Re}[T_\omega(\boldsymbol{e}_{\boldsymbol{\kappa}},\boldsymbol{e}_{\boldsymbol{\kappa}})] + {\rm O}(n^2) \tag{2.34a}$$

$$\frac{1}{\tau_{{\rm e}\omega}(\boldsymbol{e}_{\boldsymbol{\kappa}})} = {\rm c_i}n\sigma_{\rm e}(\boldsymbol{e}_{\boldsymbol{\kappa}}) + {\rm O}(n^2), \tag{2.34b}$$

where we set $\boldsymbol{\kappa} = \boldsymbol{k}$ in the single scatterer T matrix $T_\omega(\boldsymbol{\kappa},\boldsymbol{\kappa})$ and $\sigma_{\rm e}(\boldsymbol{\kappa})$, with $\boldsymbol{k}$ satisfying the homogeneous dispersion relation of the homogeneous medium (2.7), which implies that the scatterers see each other in the far field. Likewise, in the low density regime, the scattering mean free time is introduced according to

$$\frac{1}{\tau_{{\rm s}\omega}(\boldsymbol{e}_{\boldsymbol{\kappa}})} = {\rm c_i}n\sigma_{\rm s}(\boldsymbol{e}_{\boldsymbol{\kappa}}) + {\rm O}(n^2), \tag{2.34c}$$

and in elastic media $\tau_{{\rm s}\omega}(\boldsymbol{e}_{\boldsymbol{\kappa}}) \equiv \tau_{{\rm e}\omega}(\boldsymbol{e}_{\boldsymbol{\kappa}})$, due to (2.14).

When we consider isotropic point scatterers in anisotropic media, then the self energy satisfies $\Sigma_\omega(\boldsymbol{p}) = \Sigma_\omega$, and we can solve the time dependent Dyson Green function in real space. Due to translational invariance the Green function depends only on the relative coordinate $\boldsymbol{X} = \boldsymbol{x} - \boldsymbol{x}_0$. The wave surface $\phi_\omega(\boldsymbol{X}) =$ constant and its unit normal vector $\boldsymbol{n}_\phi(\boldsymbol{X})$ are defined by

$$\phi_\omega(\boldsymbol{X}) \equiv |{\rm A}^{-\frac{1}{2}}\cdot\boldsymbol{X}|\sqrt{\frac{{\rm Re}[\mu_\omega]+|\mu_\omega|}{2\mu}} \tag{2.35a}$$

$$\boldsymbol{n}_\phi(\boldsymbol{X}) \equiv \frac{\boldsymbol{\nabla}\phi_\omega(\boldsymbol{X})}{|\boldsymbol{\nabla}\phi_\omega(\boldsymbol{X})|} = \frac{\boldsymbol{A^{-1}}\cdot\boldsymbol{X}}{|\boldsymbol{A^{-1}}\cdot\boldsymbol{X}|}, \tag{2.35b}$$

Upon closer inspection of the wave front we learn that it can be expressed in terms of group velocity (2.8b) and becomes

$$\phi_\omega(\boldsymbol{X}) \quad = \quad \sqrt{\frac{\mathrm{Re}[\mu_\omega]+|\mu_\omega|}{2\mu}}\,\frac{\mathrm{c_i}|\boldsymbol{X}|}{|\boldsymbol{v}_{\mathrm{g}\omega}(\boldsymbol{n}_\phi(\boldsymbol{X}))|}. \tag{2.35c}$$

We obtain a harmonic elliptical wave

$$G_\omega(\boldsymbol{X},t) \quad = \quad \frac{|\boldsymbol{v}_{\mathrm{g}}(\boldsymbol{n}_\phi(\boldsymbol{X}))|}{\mathrm{c_i}}\,\frac{\exp\left(\mathrm{i}\frac{\omega}{\mathrm{c_i}}[\phi_\omega(\boldsymbol{X})-\mathrm{c_i}\,t]-\frac{|\boldsymbol{X}|}{2|\boldsymbol{l}_{\mathrm{e}\omega}(\boldsymbol{n}_\phi(\boldsymbol{X}))|}\right)}{4\pi|\boldsymbol{X}|\sqrt{\det \mathsf{A}}}. \tag{2.36}$$

Eq. (2.35c) shows that the elliptical wave front (2.36) propagates along $\boldsymbol{e}_{\boldsymbol{X}}$ with a uniformly reduced group velocity (2.8b) due the effective permeability μ_ω. The elliptical wave (2.36) decays exponentially with the extinction mean free path vector $\boldsymbol{l}_{\mathrm{e}}$, or for elastic scatterers, when $\tau_{\mathrm{e}}=\tau_{\mathrm{s}}$, with the scattering mean free path vector $\boldsymbol{l}_{\mathrm{s}}$. These vectors are introduced by

$$\boldsymbol{l}_{\mathrm{e}\omega}(\boldsymbol{e}_{\boldsymbol{\kappa}}) \quad \equiv \quad \tau_{\mathrm{e}\omega}(\boldsymbol{e}_{\boldsymbol{\kappa}})\boldsymbol{v}_{\mathrm{g}}(\boldsymbol{e}_{\boldsymbol{\kappa}}), \tag{2.37a}$$

$$\boldsymbol{l}_{\mathrm{s}\omega}(\boldsymbol{e}_{\boldsymbol{\kappa}}) \quad \equiv \quad \tau_{\mathrm{s}\omega}(\boldsymbol{e}_{\boldsymbol{\kappa}})\boldsymbol{v}_{\mathrm{g}}(\boldsymbol{e}_{\boldsymbol{\kappa}}), \tag{2.37b}$$

such that both mean free path $\boldsymbol{l}_{\mathrm{e,s}}(\boldsymbol{n}_\phi(\boldsymbol{X}))\propto \boldsymbol{e}_{\boldsymbol{X}}$. In (2.36), and later on also in the radiative transfer equation, only the magnitudes $l_{\mathrm{e,s}}=|\boldsymbol{l}_{\mathrm{e,s}}|$ will appear. However only when we define the extinction mean free path as a vector we can write κ exclusively in terms of quantities which incorporate scattering effects, i.e. $\tilde{v}_{\mathrm{p}}$ and $\boldsymbol{l}_{\mathrm{e}}$. We obtain $\kappa(\boldsymbol{e}_{\boldsymbol{\kappa}})=\omega/\tilde{v}_{\mathrm{p}}(\boldsymbol{e}_{\boldsymbol{\kappa}})+\mathrm{i}/(2\boldsymbol{l}_{\mathrm{e}}(\boldsymbol{e}_{\boldsymbol{\kappa}})\cdot\boldsymbol{e}_{\boldsymbol{\kappa}})$. Here we made use of the fact that in the definition of the mean free time, Eq. (2.32b), we can write $v_{\mathrm{p}}(\boldsymbol{e}_{\boldsymbol{\kappa}})=\boldsymbol{v}_{\mathrm{g}}(\boldsymbol{e}_{\boldsymbol{\kappa}})\cdot\boldsymbol{e}_{\boldsymbol{\kappa}}$. Therefore, instead of the well known expression in isotropic media $l_{\mathrm{e}}=(n\sigma_{\mathrm{e}})^{-1}$, in anisotropic media we have the relation $l_{\mathrm{e}}(\boldsymbol{e}_{\boldsymbol{k}})=v_{\mathrm{g}}(\boldsymbol{e}_{\boldsymbol{k}})(\mathrm{c_i}n\sigma_{\mathrm{e}})^{-1}$. This relation expresses the fact that in between scattering events the amplitude propagates with the anisotropic group velocity (2.8b), and thus is sensitive not only to the scatterer, but also to the surrounding medium. We plotted the extinction mean free path for isotropic point scatterers in uniaxial media in Fig. 2.5.

When we compare in Fig 2.6 the frequency surface $\omega(\boldsymbol{k})=$ constant and the wave surface $\phi_\omega(\boldsymbol{x})=$ constant, we note that the group velocity is perpendicular to the frequency surface, but *not* to the wave surface. On the other hand, if we define the wave vector direction to be the direction of the phase velocity $v_{\mathrm{p}}(\boldsymbol{e}_{\boldsymbol{k}})$, then the direction of the phase velocity $v_{\mathrm{p}}(\boldsymbol{n}_\phi(\boldsymbol{X}))$ is normal to the wave surface as it should be [53].

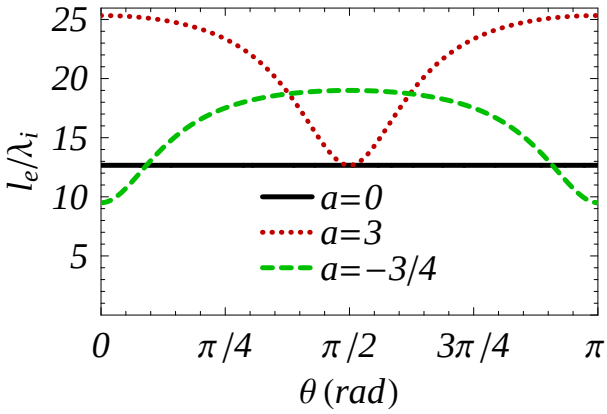

Figure 2.5 (color online).
The extinction mean free path for point scatterers on resonance, per wavelength $\lambda_i \equiv 2\pi c_i/\omega_0$. *The material is homogeneous with isotropic permeability* μ *and uniaxial dielectric permittivity* $\varepsilon = (3+a)[1+ae_z e_z/(1-a)]/(c_i{}^2 \mathrm{Tr}[\mu])$, *where* a *parameterizes the anisotropy. We set the scatterer density* $n = (2\pi)^3(10\lambda_i)^{-3}$. *The solid line is for isotropic media,* $a = 0$. *The dotted line is for an anisotropic dielectric with* $a = 3$, *and the dashed line is for* $a = -3/4$. *The anisotropy in the mean free path is due to the anisotropic medium in which the isotropic scatterers reside. Note that at a fixed frequency* ω *the wavelength inside the anisotropic material will be different in different directions.*

2.4 Wave Energy Transport

2.4.a Generalized Boltzmann Transport

In order to derive a transport equation for the ensemble averaged energy density, we start with the product of amplitude Green functions, which gives a first relation with the energy density, (2.3a). The Bethe-Salpeter equation is an exact equation for the ensemble averaged product of amplitude Green functions $\langle\langle G^* \otimes G\rangle\rangle$ and is schematically given by [88],

$$\langle\langle G^* \otimes G\rangle\rangle \quad = \quad \langle\langle G^*\rangle\rangle \otimes \langle\langle G\rangle\rangle + \langle\langle G^*\rangle\rangle \otimes \langle\langle G\rangle\rangle \, U \, \langle\langle G^* \otimes G\rangle\rangle \,. \quad (2.38)$$

Here U is known as the Bethe-Salpeter irreducible vertex, and similar to the Dyson self energy, which is an irreducible vertex for the wave amplitude.

Ensemble averaging restores homogeneity of space. As a result both from

$\langle\langle G^* \otimes G \rangle\rangle$ and U a momentum conserving delta function can be extracted,

$$\begin{aligned} \langle\langle G^*_{\omega_+}(\boldsymbol{p}_+, \tilde{\boldsymbol{p}}_+) G_{\omega_-}(\boldsymbol{p}_-, \tilde{\boldsymbol{p}}_-)\rangle\rangle &\equiv \Phi_\omega(\boldsymbol{p}, \tilde{\boldsymbol{p}}, \boldsymbol{P}, \Omega) \\ &\quad \times (2\pi)^3 \delta^3(\boldsymbol{p}_+ - \tilde{\boldsymbol{p}}_+ - \boldsymbol{p}_- + \tilde{\boldsymbol{p}}_-), \quad (2.39a) \\ U_{\omega_+\omega_-}(\boldsymbol{p}_+, \tilde{\boldsymbol{p}}_+, \boldsymbol{p}_-, \tilde{\boldsymbol{p}}_-) &\equiv U_\omega(\boldsymbol{p}, \tilde{\boldsymbol{p}}, \boldsymbol{P}, \Omega) \\ &\quad \times (2\pi)^3 \delta^3(\boldsymbol{p}_+ - \tilde{\boldsymbol{p}}_+ - \boldsymbol{p}_- + \tilde{\boldsymbol{p}}_-), \quad (2.39b) \end{aligned}$$

where we defined

$$\begin{aligned} \boldsymbol{p}_\pm &\equiv \boldsymbol{p} \pm \frac{\boldsymbol{P}}{2} && (2.40a) \\ \tilde{\boldsymbol{p}}_\pm &\equiv \tilde{\boldsymbol{p}} \pm \frac{\tilde{\boldsymbol{P}}}{2} && (2.40b) \\ \omega_\pm &\equiv \omega \pm \frac{\Omega}{2} + \mathrm{i}0^+, && (2.40c) \end{aligned}$$

with 0^+ an infinitesimal positive quantity to obtain the retarded solution; $\boldsymbol{p}$ and ω represent the internal oscillations of a wave packet in space and time, $\boldsymbol{P}$ and Ω represent the oscillations of the wave packet envelope. Furthermore we define the response Ψ to an arbitrary source S by

$$\Psi_\omega(\boldsymbol{p}, \boldsymbol{P}, \Omega) \equiv \int \frac{\mathrm{d}^3\tilde{p}}{(2\pi)^3} \Phi_\omega(\boldsymbol{p}, \tilde{\boldsymbol{p}}, \boldsymbol{P}, \Omega) S_\omega(\tilde{\boldsymbol{p}}, \boldsymbol{P}, \Omega). \quad (2.41)$$

When we integrate Eq. (2.38) over $\int \mathrm{d}^3\tilde{p} \int \mathrm{d}^3\tilde{P} S_\omega(\tilde{\boldsymbol{p}}, \tilde{\boldsymbol{P}}, \Omega) / (2\pi)^6$, using the Eqs. (2.39a), (2.39b), and (2.41), we obtain an equation for Ψ

$$\begin{aligned} \Psi_\omega(\boldsymbol{p}, \boldsymbol{P}, \Omega) &= G^*_{\omega_+}(\boldsymbol{p}_+) G_{\omega_-}(\boldsymbol{p}_-) \\ &\quad \times \left[S_\omega(\boldsymbol{p}, \boldsymbol{P}, \Omega) + \int \frac{\mathrm{d}^3 p_0}{(2\pi)^3} U_\omega(\boldsymbol{p}, \boldsymbol{p}_0, \boldsymbol{P}, \Omega) \Psi_\omega(\boldsymbol{p}_0, \boldsymbol{P}, \Omega) \right]. \end{aligned} \quad (2.42)$$

We can transform (2.42) into a generalized transport equation by rewriting the product $G^* G$ using $ab = (a^{-1} - b^{-1})^{-1}(b - a)$, supplied with (2.29), (2.40a), and the definitions

$$\begin{aligned} \Delta G_\omega(\boldsymbol{p}, \boldsymbol{P}, \Omega) &\equiv \frac{G_{\omega_-}(\boldsymbol{p}_-) - G^*_{\omega_+}(\boldsymbol{p}_+)}{2\mathrm{i}}, && (2.43a) \\ \Delta\Sigma_\omega(\boldsymbol{p}, \boldsymbol{P}, \Omega) &\equiv \frac{\Sigma_{\omega_-}(\boldsymbol{p}_-) - \Sigma^*_{\omega_+}(\boldsymbol{p}_+)}{2\mathrm{i}}, && (2.43b) \\ s_\omega(\boldsymbol{p}, \boldsymbol{P}, \Omega) &\equiv -\frac{{c_i}^2}{\omega} \Delta G_\omega(\boldsymbol{p}, \boldsymbol{P}, \Omega) S_\omega(\boldsymbol{p}, \boldsymbol{P}, \Omega), && (2.43c) \\ \gamma_\omega(\boldsymbol{p}, \boldsymbol{p}_0, \boldsymbol{P}, \Omega) &\equiv \frac{{c_i}^2}{\omega} \Delta\Sigma_\omega(\boldsymbol{p}, \boldsymbol{P}, \Omega) (2\pi)^3 \delta^3(\boldsymbol{p} - \boldsymbol{p}_0) \\ &\quad - \frac{{c_i}^2}{\omega} \Delta G_\omega(\boldsymbol{p}, \boldsymbol{P}, \Omega) U_\omega(\boldsymbol{p}, \boldsymbol{p}_0, \boldsymbol{P}, \Omega). && (2.43d) \end{aligned}$$

The quantity γ, defined in (2.43d), represents extinction of the direct beam through the self energy term with $\Delta\Sigma$, and a collision term containing U. Here U may be interpreted as a generalized differential scattering cross section. The result is a generalized Boltzmann transport equation for Ψ containing all interference effects,

$$\left[\mathrm{i}\Omega - \frac{\mathrm{c_i}^2}{\omega}\boldsymbol{p}\cdot\mathsf{A}\cdot\mathrm{i}\boldsymbol{P}\right]\Psi_\omega\left(\boldsymbol{p},\boldsymbol{P},\Omega\right) = s_\omega\left(\boldsymbol{p},\boldsymbol{P},\Omega\right) + \int\frac{\mathrm{d}^3p_0}{(2\pi)^3}\gamma_\omega\left(\boldsymbol{p},\boldsymbol{p}_0,\boldsymbol{P},\Omega\right)\Psi_\omega\left(\boldsymbol{p}_0,\boldsymbol{P},\Omega\right), \tag{2.44}$$

in which we recognize $\mathrm{i}\Omega$ as the Fourier transform of a time derivative, $-\mathrm{i}\boldsymbol{P}$ as the Fourier transform of the gradient, s as a source, and the integral over γ falls apart into a $\Delta\Sigma$ term, related to extinction, and into a scattering integral over U and Ψ, which represents the contribution of all the light scattering into the path. Specific for anisotropic media in (2.44) is the quantity $\mathrm{c_i}^2\boldsymbol{p}\cdot\mathsf{A}/\omega$, which reduces to the group velocity(2.8b) if $\boldsymbol{p}$ satisfies the dispersion relation without scattering effects. Generalized Boltzmann transport equations of the type (2.44) have never been solved exactly, not even for $\mathsf{A} = 1$. In the next sections we will present approximate solutions for anisotropic host media for which $\mathsf{A} \neq 1$.

2.4.b Energy Conservation

In section 2.4.a we derived a generalized Boltzmann transport equation (2.44) for the ensemble averaged product of wave functions Ψ in anisotropic media. The conserved quantity related to Ψ is the total energy. From the expression for the energy density (2.3a) in anisotropic media we know that the energy density must be an integral of Ψ over all internal wave vectors $\boldsymbol{p}$. In Eq. (2.3a) for the energy density the scattering potential can be incorporated by modifying $\mathrm{c_i}$, and thus also contributes to the total energy density. The scalar waves we describe scatter from an ensemble averaged frequency dependent potential (2.9).

In order to determine the amount of energy density in the scattering process, we need the Ward identity for classical scalar waves in anisotropic media. The Ward identity is a relation between the Dyson self energy and the Bethe-Salpeter irreducible vertex, and we establish the identity for classical scalar waves in anisotropic media in appendix A. The result is,

$$\int\frac{\mathrm{d}^3p_0}{(2\pi)^3}\gamma_\omega\left(\boldsymbol{p}_0,\boldsymbol{p},\boldsymbol{P},\Omega\right) = -\mathrm{i}\Omega\delta_\omega\left(\boldsymbol{p},\boldsymbol{P},\Omega\right), \tag{2.45a}$$

where the dimensionless function δ is

$$\frac{\delta_\omega(\boldsymbol{p},\boldsymbol{P},\Omega)}{{c_i}^2} \equiv -\frac{\Sigma^*_{\omega_+}(\boldsymbol{p}_+)+\Sigma_{\omega_-}(\boldsymbol{p}_-)}{{\omega_+}^2+{\omega_-}^2} - \int \frac{\mathrm{d}^3\tilde{p}}{(2\pi)^3} U_\omega\left(\boldsymbol{p},\tilde{\boldsymbol{p}},\boldsymbol{P},\Omega\right) \frac{G^*_{\omega_+}\left(\tilde{\boldsymbol{p}}_+\right)+G_{\omega_-}\left(\tilde{\boldsymbol{p}}_-\right)}{{\omega_+}^2+{\omega_-}^2}. \quad (2.45b)$$

The Ward identity (2.45a) is similar to results found in the literature [68, 89, 90]. The fact that $\delta_\omega \neq 0$ informs us that the total energy density $\mathscr{H}$ is the sum of a radiative energy density $\mathscr{H}_\mathrm{r}$ and material energy density $\mathscr{H}_\mathrm{m}$. We define these two parts of the energy density and their ratio $\delta_\omega(\boldsymbol{P},\Omega)$ by

$$\mathscr{H}_{\mathrm{r}\omega}(\boldsymbol{P},\Omega) \equiv \frac{\omega^2}{{c_i}^2}\int\frac{\mathrm{d}^3p}{(2\pi)^3}\Psi_\omega\left(\boldsymbol{p},\boldsymbol{P},\Omega\right) \quad (2.46a)$$

$$\mathscr{H}_{\mathrm{m}\omega}(\boldsymbol{P},\Omega) \equiv \frac{\omega^2}{{c_i}^2}\int\frac{\mathrm{d}^3p}{(2\pi)^3}\delta_\omega(\boldsymbol{p},\boldsymbol{P},\Omega)\Psi_\Omega\left(\boldsymbol{p},\boldsymbol{P},\Omega\right) \quad (2.46b)$$

$$\delta_\omega(\boldsymbol{P},\Omega) \equiv \frac{\mathscr{H}_\mathrm{m}(\boldsymbol{P},\Omega)}{\mathscr{H}_\mathrm{r}(\boldsymbol{P},\Omega)}, \quad (2.46c)$$

where the ratio of energy densities satisfies $\delta_\omega(\boldsymbol{P},\Omega) \geq -1$ for the total energy density to be positive, even when we take either $\Omega \to 0$ or $\boldsymbol{P} \to \boldsymbol{0}$.

The quantities relevant for conservation of energy are the total energy density $\mathscr{H} = \mathscr{H}_\mathrm{r} + \mathscr{H}_\mathrm{m}$, which follows from equations (2.46), the energy density flux $\boldsymbol{S}$ defined in equation (2.3b), which in our case does not achieve a material contribution, and a source $s_\omega(\boldsymbol{P},\Omega)$ for the energy density, obtained by integrating the source $s_\omega(\boldsymbol{p},\boldsymbol{P},\Omega)$ over the internal wave vector $\boldsymbol{p}$. Thus the total energy density, energy density flux and energy density source related to the generalized Boltzmann equation (2.44) are defined by

$$\mathscr{H}_\omega(\boldsymbol{P},\Omega) \equiv \frac{\omega^2}{{c_i}^2}\int\frac{\mathrm{d}^3p}{(2\pi)^3}[1+\delta_\omega(\boldsymbol{p},\boldsymbol{P},\Omega)]\Psi_\omega\left(\boldsymbol{p},\boldsymbol{P},\Omega\right) \quad (2.47a)$$

$$\boldsymbol{S}_\omega(\boldsymbol{P},\Omega) \equiv \frac{\omega^2}{{c_i}^2}\int\frac{\mathrm{d}^3p}{(2\pi)^3}\frac{{c_i}^2}{\omega}\mathsf{A}\cdot\boldsymbol{p}\Psi_\omega\left(\boldsymbol{p},\boldsymbol{P},\Omega\right) \quad (2.47b)$$

$$s_\omega(\boldsymbol{P},\Omega) \equiv \frac{\omega^2}{{c_i}^2}\int\frac{\mathrm{d}^3p}{(2\pi)^3}s_\omega\left(\boldsymbol{p},\boldsymbol{P},\Omega\right). \quad (2.47c)$$

In the definition of the flux (2.47b) we recognize the group velocity ${c_i}^2\mathsf{A}\cdot\boldsymbol{p}/\omega$ of the host medium, were we to use dispersion relation (2.7) and set $\boldsymbol{p}=\boldsymbol{k}$.

If we apply $\omega^2/{c_i}^2\int\mathrm{d}^3p/(2\pi)^3$ to (2.44), then, with the help of equations (2.47) for total energy density $\mathscr{H}$, flux $\boldsymbol{S}$, and source s, we establish the conservation of the total energy,

$$\mathrm{i}\Omega\mathscr{H}_\omega(\boldsymbol{P},\Omega) - \mathrm{i}\boldsymbol{P}\cdot\boldsymbol{S}_\omega(\boldsymbol{P},\Omega) = s_\omega(\boldsymbol{P},\Omega). \quad (2.48)$$

We recall that $\mathrm{i}\Omega$ and $-\mathrm{i}\boldsymbol{P}$ are the Fourier representations of the time and space derivatives.

2.4.c Radiative Transfer

The radiance per frequency band, $I_\omega\left(\boldsymbol{e_p}, \boldsymbol{x}, t\right)$, in the astrophysical literature better known as specific intensity, is closely related to the energy density flux (2.47b). In Fourier space it is

$$I_\omega\left(\boldsymbol{e_p}, \boldsymbol{P}, \Omega\right) \equiv \frac{\omega^2}{{c_i}^2} \int \frac{\mathrm{d}p}{(2\pi)^3} p^2 \frac{|{c_i}^2 \mathsf{A} \cdot \boldsymbol{p}|}{\omega} \Psi_\omega\left(\boldsymbol{p}, \boldsymbol{P}, \Omega\right), \tag{2.49}$$

where $p \equiv |\boldsymbol{p}|$. In order to acquire a radiative transfer equation for the radiance I, we will adopt the dispersion relation (2.7), which comes down to making the following replacements in the generalized Boltzmann transport equation (2.44),

$$-\frac{{c_i}^2}{\omega} \Delta G_\omega(\boldsymbol{p}, \boldsymbol{P}, \Omega) \rightarrow \frac{\pi}{2} \frac{{c_i}^4}{\omega^2} \frac{\delta\left(\frac{\omega}{v_p(\boldsymbol{e_p})} - p\right)}{v_p(\boldsymbol{e_p})}, \tag{2.50a}$$

$$\frac{\omega^2}{{c_i}^2} \Psi_\omega(\boldsymbol{p}, \boldsymbol{P}, \Omega) \rightarrow \frac{(2\pi)^3 v_p^2(\boldsymbol{e_p})}{|\boldsymbol{v}_g(\boldsymbol{e_p})| \omega^2} \delta\left(\frac{\omega}{v_p(\boldsymbol{e_p})} - p\right) I_\omega(\boldsymbol{e_p}, \boldsymbol{P}, \Omega). \tag{2.50b}$$

In order to obtain a radiative transfer equation for the radiance per frequency band in wave vector space, we integrate the generalized Boltzmann transport equation (2.44) over $\omega^2/{c_i}^2 \int \mathrm{d}p/(2\pi)^3 p^2 \left|\boldsymbol{v}_g\left(\boldsymbol{p}\right)\right|$, and insert (2.50). We identify the group velocity (2.8b) and obtain a Boltzmann transport transport equation for the radiance I,

$$\begin{aligned}\left[\mathrm{i}\Omega - \boldsymbol{v}_g\left(\boldsymbol{e_k}\right) \cdot \mathrm{i}\boldsymbol{P}\right] I_\omega\left(\boldsymbol{e_k}, \boldsymbol{P}, \Omega\right) &= \xi_\omega\left(\boldsymbol{e_k}, \boldsymbol{P}, \Omega\right) \\ &\quad + \int \mathrm{d}^2 e_{k_0} \zeta_\omega\left(\boldsymbol{e_k}, \boldsymbol{e}_{k_0}, \boldsymbol{P}, \Omega\right) I_\omega\left(\boldsymbol{e}_{k_0}, \boldsymbol{P}, \Omega\right),\end{aligned} \tag{2.51}$$

where we have defined the source for the radiance, ξ, and the scattering and extinction term ζ by

$$\xi_\omega\left(\boldsymbol{e_p}, \boldsymbol{P}, \Omega\right) \equiv \frac{\omega^2}{{c_i}^2} \int \frac{\mathrm{d}p}{(2\pi)^3} p^2 \left|\boldsymbol{v}_g\left(\boldsymbol{p}\right)\right| s_\omega\left(\boldsymbol{p}, \boldsymbol{P}, \Omega\right), \tag{2.52a}$$

$$\zeta_\omega\left(\boldsymbol{e_p}, \boldsymbol{e_k}, \boldsymbol{P}, \Omega\right) \equiv \int \frac{\mathrm{d}p}{(2\pi)^3} \frac{p^2 \left|\boldsymbol{v}_g\left(\boldsymbol{e_p}\right)\right| \gamma_\omega\left(\boldsymbol{p}, \boldsymbol{e_k}, \boldsymbol{P}, \Omega\right)}{\left|\boldsymbol{v}_g\left(\boldsymbol{e_k}\right)\right|}. \tag{2.52b}$$

We approximate ζ in lowest order in the scatterer density n, i.e. approximate the Dyson Self energy in the independent scattering approximation and at the

same time the Bethe-Salpeter irreducible vertex in the Boltzmann approximation,

$$\Sigma_\omega(\boldsymbol{p}) = nT_\omega(\boldsymbol{p},\boldsymbol{p}) + \mathrm{O}(n^2), \tag{2.53a}$$

$$U_\omega(\boldsymbol{p},\tilde{\boldsymbol{p}},\boldsymbol{P},\Omega) = nT^*_{\omega_+}(\boldsymbol{p}_+,\tilde{\boldsymbol{p}}_+)\,T_{\omega_-}(\tilde{\boldsymbol{p}}_-,\boldsymbol{p}_-) + \mathrm{O}(n^2). \tag{2.53b}$$

Here we used definitions (2.40) with $\tilde{\boldsymbol{P}} = \boldsymbol{P}$. Approximations (2.53) preserve energy conservation. The phase function $\mathfrak{p}_\omega\left(\boldsymbol{e}_{\boldsymbol{k}},\boldsymbol{e}_{\boldsymbol{k}_0}\right)$ is defined by

$$\mathfrak{p}_\omega\left(\boldsymbol{e}_{\boldsymbol{k}},\boldsymbol{e}_{\boldsymbol{k}_0}\right) \equiv \frac{1}{\sigma_{\mathrm{s}\omega}\left(\boldsymbol{e}_{\boldsymbol{k}_0}\right)}\frac{\mathrm{d}\sigma_{\mathrm{s}\omega}\left(\boldsymbol{e}_{\boldsymbol{k}},\boldsymbol{e}_{\boldsymbol{k}_0}\right)}{\mathrm{d}^2\boldsymbol{e}_{\boldsymbol{k}}}. \tag{2.54}$$

For the final term in Eq. (2.51) we find, using (A.13), the length scales (2.37a), and (2.37b) in the low density approximations (2.34b) and Eq. (2.34c), the relation

$$\begin{aligned}\frac{I_\omega\left(\boldsymbol{e}_{\boldsymbol{k}},\boldsymbol{P},\Omega\right)}{\left|\boldsymbol{l}_{\mathrm{e}\omega}\left(\boldsymbol{e}_{\boldsymbol{k}}\right)\right|} &= \frac{1}{\left|\boldsymbol{v}_{\mathrm{g}}\left(\boldsymbol{e}_{\boldsymbol{k}}\right)\right|}\int \mathrm{d}^2\boldsymbol{e}_{\boldsymbol{k}_0}\zeta\left(\boldsymbol{e}_{\boldsymbol{k}},\boldsymbol{e}_{\boldsymbol{k}_0},\boldsymbol{P},\Omega\right)I_\omega\left(\boldsymbol{e}_{\boldsymbol{k}_0},\boldsymbol{P},\Omega\right)\\ &\quad -\mathrm{i}\Omega\int \mathrm{d}^2\boldsymbol{e}_{\boldsymbol{k}_0}\frac{\mathrm{d}\delta_\omega\left(\boldsymbol{e}_{\boldsymbol{k}},\boldsymbol{e}_{\boldsymbol{k}_0},\boldsymbol{0},0\right)}{\mathrm{d}^2\boldsymbol{e}_{\boldsymbol{k}}}\frac{I_\omega\left(\boldsymbol{e}_{\boldsymbol{k}_0},\boldsymbol{P},\Omega\right)}{\left|\boldsymbol{v}_{\mathrm{g}}\left(\boldsymbol{e}_{\boldsymbol{k}_0}\right)\right|}\\ &\quad +\int \mathrm{d}^2\boldsymbol{e}_{\boldsymbol{k}_0}\frac{\mathfrak{p}_\omega\left(\boldsymbol{e}_{\boldsymbol{k}},\boldsymbol{e}_{\boldsymbol{k}_0}\right)I_\omega\left(\boldsymbol{e}_{\boldsymbol{k}_0},\boldsymbol{P},\Omega\right)}{\left|\boldsymbol{l}_{\mathrm{s}\omega}\left(\boldsymbol{e}_{\boldsymbol{k}_0}\right)\right|}.\end{aligned} \tag{2.55}$$

Due to the general symmetry

$$\gamma(\boldsymbol{p},\boldsymbol{p}_0,\boldsymbol{P})\frac{\delta(\frac{\omega}{v_{\mathrm{p}}(\boldsymbol{e}_{\boldsymbol{p}_0})}-p_0)}{v_{\mathrm{p}}(\boldsymbol{e}_{\boldsymbol{p}_0})} = \gamma(\boldsymbol{p}_0,\boldsymbol{p},\boldsymbol{P})\frac{\delta(\frac{\omega}{v_{\mathrm{p}}(\boldsymbol{e}_{\boldsymbol{p}})}-p)}{v_{\mathrm{p}}(\boldsymbol{e}_{\boldsymbol{p}})} \tag{2.56}$$

we have in particular

$$\int \mathrm{d}^2\boldsymbol{e}_{\boldsymbol{k}_0}\frac{\mathrm{d}\delta_\omega\left(\boldsymbol{e}_{\boldsymbol{k}},\boldsymbol{e}_{\boldsymbol{k}_0},\boldsymbol{0},0\right)}{\mathrm{d}^2\boldsymbol{e}_{\boldsymbol{k}}}\frac{I_\omega(\boldsymbol{e}_{\boldsymbol{k}_0},\boldsymbol{P},\Omega)}{\left|\boldsymbol{v}_{\mathrm{g}}\left(\boldsymbol{e}_{\boldsymbol{k}_0}\right)\right|} = \frac{\delta_\omega(\boldsymbol{e}_{\boldsymbol{k}},\boldsymbol{0},0)\,I_\omega(\boldsymbol{e}_{\boldsymbol{k}},\boldsymbol{P},\Omega)}{\left|\boldsymbol{v}_{\mathrm{g}}\left(\boldsymbol{e}_{\boldsymbol{k}}\right)\right|}. \tag{2.57}$$

We will now introduce the derivative along a curve. At any point $(t,\boldsymbol{x})$ we can consider an infinitesimal cylindrical volume element $\mathrm{d}V = \mathrm{d}A\mathrm{d}s$ with $\mathrm{d}A$ the cross section of the cylinder and $\mathrm{d}s$ the length. The cylinder is oriented along the group or energy velocity direction, i.e. $\boldsymbol{e}_s \equiv \boldsymbol{v}_{\mathrm{g}}\left(\boldsymbol{e}_{\boldsymbol{k}}\right)/\left|\boldsymbol{v}_{\mathrm{g}}\left(\boldsymbol{e}_{\boldsymbol{k}}\right)\right|$, while keeping $\boldsymbol{e}_{\boldsymbol{k}}$ fixed, see Fig. 2.8. Given an $\boldsymbol{e}_{\boldsymbol{k}}$ at $(t,\boldsymbol{x})$, then the irradiance $\mathrm{d}I$, traveling a distance $\mathrm{d}s$ along $\boldsymbol{e}_s$ at velocity $\mathrm{d}s/\mathrm{d}t = \boldsymbol{v}_{\mathrm{g}}(\boldsymbol{e}_{\boldsymbol{k}})/[1+\delta_\omega(\boldsymbol{e}_{\boldsymbol{k}},\boldsymbol{0},0)]$, is

$$\frac{\mathrm{d}I_\omega\left(\boldsymbol{e}_{\boldsymbol{k}},\boldsymbol{x},t\right)}{\mathrm{d}s} = \left[\frac{1+\delta_\omega(\boldsymbol{e}_{\boldsymbol{k}},\boldsymbol{0},0)}{|\boldsymbol{v}_{\mathrm{g}}(\boldsymbol{e}_{\boldsymbol{k}})|}\frac{\partial}{\partial t}+\boldsymbol{e}_{\boldsymbol{s}}(\boldsymbol{e}_{\boldsymbol{k}})\cdot\boldsymbol{\nabla}\right]I_\omega\left(\boldsymbol{e}_{\boldsymbol{k}},\boldsymbol{x},t\right). \tag{2.58}$$

Inserting (2.55) into (2.51), Fourier transforming $\boldsymbol{P}$ to $\boldsymbol{x}$ and Ω to t, dividing by $|\boldsymbol{v}_\mathrm{g}|$, and using (2.58) we finally find the radiative transfer equation,

$$\begin{aligned}\frac{\mathrm{d}I_\omega(\boldsymbol{e_k},\boldsymbol{x},t)}{\mathrm{d}s} &= \frac{\xi_\omega(\boldsymbol{e_k},\boldsymbol{x},t)}{|\boldsymbol{v}_\mathrm{g}(\boldsymbol{e_k})|} - \frac{I_\omega(\boldsymbol{e_k},\boldsymbol{x},t)}{|\boldsymbol{l}_{\mathrm{e}\omega}(\boldsymbol{e_k})|} \\ &\quad + \int \mathrm{d}^2 e_{\boldsymbol{k}_0} \frac{\mathfrak{p}_\omega(\boldsymbol{e_k},\boldsymbol{e}_{\boldsymbol{k}_0})\, I_\omega(\boldsymbol{e}_{\boldsymbol{k}_0},\boldsymbol{x},t)}{|\boldsymbol{l}_{\mathrm{s}\omega}(\boldsymbol{e}_{\boldsymbol{k}_0})|}. \end{aligned} \tag{2.59}$$

We refer to Fig. 2.8 for a phenomenological picture. The source term of the radiative transfer equation can be related to the source term S for the Bethe-Salpeter equation according to

$$\frac{\xi_\omega(\boldsymbol{e_k},\boldsymbol{x},t)}{|\boldsymbol{v}_\mathrm{g}(\boldsymbol{e_k})|} = \frac{\omega^2 {\mathrm{c_i}}^2}{(4\pi)^2 v_\mathrm{p}^3(\boldsymbol{e_k})} S_\omega(\boldsymbol{e_k},\boldsymbol{x},t), \tag{2.60}$$

where the prefactor results from the radiative density of states. For an incoming unit plane wave $S_\omega(\boldsymbol{e_k},\boldsymbol{x},t)=1$.

When we compare Eq. (2.59) with Ref. [68] we see some differences. Firstly, we see the appearance of a group velocity in the denominator of the source term, which represents the anisotropy in the available local radiative density of propagating states. Secondly, we see the appearance of mean free paths as function of $\boldsymbol{e_k}$, and $\boldsymbol{l}_{\mathrm{s,e}}(\boldsymbol{e_k}) \propto \boldsymbol{e}_s$.

Note that there is a scattering delay contained in $\mathrm{d}/\mathrm{d}s$, and that integrating (2.59) over $\int \mathrm{d}^2 \boldsymbol{e_k}$ will cancel the extinction and scattering term against each other. This results in a continuity equation for the energy density $\mathscr{H}$, see Eq. (2.48).

In Eq. (2.59) we may introduce the albedo a by

$$a_\omega(\boldsymbol{e_k}) \equiv \frac{\sigma_{\mathrm{s}\omega}(\boldsymbol{e_k})}{\sigma_{\mathrm{e}\omega}(\boldsymbol{e_k})} = \frac{|\boldsymbol{l}_{\mathrm{e}\omega}(\boldsymbol{e_k})|}{|\boldsymbol{l}_{\mathrm{s}\omega}(\boldsymbol{e_k})|}, \tag{2.61}$$

which is just the ratio of extinction and scattering mean free path vector components along the direction of propagation $\boldsymbol{e}_s$. We replace the distance $\mathrm{d}s$ by the optical depth $\mathrm{d}o$ defined by

$$\mathrm{d}o_\omega(\boldsymbol{e_k}) \equiv \frac{\mathrm{d}s}{|\boldsymbol{l}_{\mathrm{e}\omega}(\boldsymbol{e_k})|}, \tag{2.62}$$

such that we obtain the radiative transfer equation in terms of optical depth and albedo as

$$\begin{aligned}\frac{\mathrm{d}I_\omega(\boldsymbol{e_k},\boldsymbol{x},t)}{\mathrm{d}o_\omega(\boldsymbol{e_k})} &= \frac{|\boldsymbol{l}_{\mathrm{e}\omega}(\boldsymbol{e_k})|}{|\boldsymbol{v}_\mathrm{g}(\boldsymbol{e_k})|}\xi_\omega(\boldsymbol{e_k},\boldsymbol{x},t) - I_\omega(\boldsymbol{e_k},\boldsymbol{x},t) \\ &\quad + \int \mathrm{d}^2 e_{\boldsymbol{k}_0}\, \mathfrak{p}_\omega(\boldsymbol{e_k},\boldsymbol{e}_{\boldsymbol{k}_0}) \frac{\mathrm{d}o_\omega(\boldsymbol{e}_{\boldsymbol{k}_0})}{\mathrm{d}o_\omega(\boldsymbol{e_k})} a_\omega(\boldsymbol{e}_{\boldsymbol{k}_0})\, I_\omega(\boldsymbol{e}_{\boldsymbol{k}_0},\boldsymbol{x},t). \end{aligned} \tag{2.63}$$

We infer that the radiance scattering into direction $\boldsymbol{e}_s$ is reduced by the albedo factor due to extinction along the traveled optical depth towards the scatterer at $\boldsymbol{x}$. We recognize a ratio of optical path lengths, which expresses the fact that in anisotropic media the optical depth is different in different directions.

The radiance travels along the propagation direction $\boldsymbol{e}_s$, and the observed phase function in anisotropic media is

$$\mathfrak{p}_\omega\left(\boldsymbol{e}_s, \boldsymbol{e}_{s_0}\right) \equiv \frac{1}{\sigma_{s\omega}\left(\boldsymbol{e}_{s_0}\right)} \frac{\mathrm{d}\sigma_{s\omega}\left(\boldsymbol{e}_s, \boldsymbol{e}_{s_0}\right)}{\mathrm{d}^2 \boldsymbol{e}_s}, \tag{2.64}$$

We recall that the propagation direction of the radiance equals the direction $\boldsymbol{e}_s$ of the group velocity (2.8b), which is in anisotropic media is not equal to $\boldsymbol{e}_{\boldsymbol{k}}$. In section 2.7 we present some examples of the (an)isotropic quantities appearing in the radiative transfer equation (2.59).

2.5 Summary of radiative transfer

In the previous sections we presented a long derivation of the radiative transfer equation for anisotropic media starting from basic building blocks. These building blocks were a scalar wave amplitude and a scattering potential. In this section we give a brief summary of the ingredients of the model and the resulting radiative transfer equation.

In the absence of scattering potentials the scalar wave satisfied an anisotropic scalar wave equation

$$\boldsymbol{\nabla} \cdot \mathsf{A} \cdot \boldsymbol{\nabla} \psi - \frac{1}{\mathrm{c_i}^2} \frac{\partial^2 \psi}{\partial t^2} = 0. \tag{2.65}$$

We mapped the physical quantities in the Maxwell equations on the scalar wave ψ, the anisotropy tensor A, and the isotropic velocity of light $\mathrm{c_i}$ according to

$$\frac{\varepsilon^{-1}}{\frac{1}{3}\mathrm{Tr}\left(\varepsilon^{-1}\right)} \rightarrow \mathsf{A}, \tag{2.66a}$$

$$\frac{\mathrm{Tr}\left(\varepsilon^{-1}\right)}{\mathrm{Tr}\left(\mu\right)} \rightarrow \mathrm{c_i}^2, \tag{2.66b}$$

$$\sqrt{\frac{1}{3}\mathrm{Tr}(\mu)}\,|\boldsymbol{H}| \rightarrow \frac{1}{\mathrm{c_i}} \frac{\partial \psi}{\partial t}, \tag{2.66c}$$

$$\sqrt{\frac{1}{3}\mathrm{Tr}(\varepsilon^{-1})}\,\boldsymbol{D} \rightarrow \boldsymbol{\nabla}\psi. \tag{2.66d}$$

In contrast with other scalar wave models for light we can use this mapping to incorporate an anisotropic permittivity tensor ε in a scalar wave model.

Because we put a locality requirement on the scattering potential, we must incorporate (anisotropic) scatterers as inhomogeneities in the permeability, which in the scalar model must be a scalar quantity. Our mapping forces us to incorporate scatterers, which may be anisotropic. Mapping (2.66a) is not unique, an alternative mapping incorporating a tensorial permeability and dielectric scatterers is presented in section 2.2.

In section 2.3 we discussed the propagation of the scalar wave amplitude. The dispersion relation in the absence of scatterers defines the real valued wave vector $\boldsymbol{k}$,

$$\frac{\omega^2}{\mathrm{c_i}^2} - \boldsymbol{k}\cdot\mathsf{A}\cdot\boldsymbol{k} \quad \equiv \quad 0, \tag{2.67}$$

and determines the phase and group velocity v_p and $\boldsymbol{v}_\mathrm{g}$. When scatterers are added to the problem we have to deal with the complex wave vector $\boldsymbol{\kappa}$. We derived the radiative transfer equation in the independent scattering and Boltzmann approximations, thus the scatterers see each other in the far field. The complex wave vector consistent with this limit is

$$\boldsymbol{\kappa} \quad = \quad \boldsymbol{k} + \frac{\mathrm{i}}{\boldsymbol{l}_\mathrm{e}(\boldsymbol{e}_{\boldsymbol{k}})\cdot\boldsymbol{e}_{\boldsymbol{k}}}\boldsymbol{e}_{\boldsymbol{k}}. \tag{2.68}$$

In isotropic media $\boldsymbol{l}_\mathrm{e}(\boldsymbol{e}_{\boldsymbol{k}})\cdot\boldsymbol{e}_{\boldsymbol{k}} = l_\mathrm{e}(\boldsymbol{e}_{\boldsymbol{k}})$. However in anisotropic media (2.68) $\boldsymbol{l}_\mathrm{e}(\boldsymbol{e}_{\boldsymbol{k}}) \not\propto \boldsymbol{e}_{\boldsymbol{k}}$, but it is still $l_\mathrm{e}(\boldsymbol{e}_{\boldsymbol{k}}) = |\boldsymbol{l}_\mathrm{e}(\boldsymbol{e}_{\boldsymbol{k}})|$ which turns up in the radiative transfer equation.

Given a scatterer density n, the extinction mean free path vector $\boldsymbol{l}_\mathrm{e}$ in (2.68), and the scattering mean free path vector $\boldsymbol{l}_\mathrm{s}$ are related to the extinction and scattering cross sections σ_e and σ_s by

$$\boldsymbol{l}_{\mathrm{s}\omega}(\boldsymbol{e}_{\boldsymbol{k}}) \quad = \quad \frac{\boldsymbol{v}_\mathrm{g}(\boldsymbol{e}_{\boldsymbol{k}})}{\mathrm{c_i} n\sigma_{\mathrm{s}\omega}(\boldsymbol{e}_{\boldsymbol{k}})}, \tag{2.69a}$$

$$\boldsymbol{l}_{\mathrm{e}\omega}(\boldsymbol{e}_{\boldsymbol{k}}) \quad = \quad \frac{\boldsymbol{v}_\mathrm{g}(\boldsymbol{e}_{\boldsymbol{k}})}{\mathrm{c_i} n\sigma_{\mathrm{e}\omega}(\boldsymbol{e}_{\boldsymbol{k}})}. \tag{2.69b}$$

If the scattering is elastic, then $\boldsymbol{l}_\mathrm{e} = \boldsymbol{l}_\mathrm{s}$ as expected.

In section 2.4 we proceeded with a derivation of the radiative transfer equation for anisotropic media starting from the exact Bethe-Salpeter equation. In order to write down the resulting radiative transfer equation for anisotropic media in a familiar form we now only need to introduce derivative of the radiance along the path given by

$$\frac{\mathrm{d}I(\boldsymbol{e}_{\boldsymbol{k}},\boldsymbol{x},t)}{\mathrm{d}s} \quad = \quad \frac{1+\delta_\omega(\boldsymbol{e}_{\boldsymbol{k}},\boldsymbol{0},0)}{|\boldsymbol{v}_\mathrm{g}(\boldsymbol{e}_{\boldsymbol{k}})|}\frac{\partial I(\boldsymbol{e}_{\boldsymbol{k}},\boldsymbol{x},t)}{\partial t} + \frac{\boldsymbol{v}_\mathrm{g}(\boldsymbol{e}_{\boldsymbol{k}})}{|\boldsymbol{v}_\mathrm{g}(\boldsymbol{e}_{\boldsymbol{k}})|}\cdot\boldsymbol{\nabla} I(\boldsymbol{e}_{\boldsymbol{k}},\boldsymbol{x},t). \tag{2.70}$$

The quantity δ is a scattering delay due to the fact that the scatterers are frequency dependent, and is derived in appendix A. When there is no scattering, the radiance propagates at velocity $\boldsymbol{v}_{\mathrm{g}}$. The scatterers along the path of the radiance are inhomogeneities in the refractive index, and therefore the radiance is delayed due to internal reflections inside the scatterers.

The radiative transfer equation in anisotropic media, for the radiance per frequency band I_ω is given by

$$\begin{aligned}\frac{\mathrm{d}I_\omega(\boldsymbol{e}_{\boldsymbol{k}},\boldsymbol{x},t)}{\mathrm{d}s} &= \frac{\xi_\omega(\boldsymbol{e}_{\boldsymbol{k}},\boldsymbol{x},t)}{\left|\boldsymbol{v}_{\mathrm{g}}(\boldsymbol{e}_{\boldsymbol{k}})\right|}-\frac{I_\omega(\boldsymbol{e}_{\boldsymbol{k}},\boldsymbol{x},t)}{|\boldsymbol{l}_{\mathrm{e}\omega}(\boldsymbol{e}_{\boldsymbol{k}})|}\\ &\quad+\int \mathrm{d}^2 e_{\boldsymbol{k}_0}\frac{\mathrm{p}_\omega\left(\boldsymbol{e}_{\boldsymbol{k}},\boldsymbol{e}_{\boldsymbol{k}_0}\right)I_\omega\left(\boldsymbol{e}_{\boldsymbol{k}_0},\boldsymbol{x},t\right)}{|\boldsymbol{l}_{\mathrm{s}\omega}\left(\boldsymbol{e}_{\boldsymbol{k}_0}\right)|}.\end{aligned} \tag{2.71}$$

Equation (2.71) describes transport of radiance. When the radiance I propagates along a a path parameterized by s, then it the amount of radiance increases due to a source of incoming radiance per unit time ξ, it decreases because of extinction due to scattering and absorption, and it can increase because radiance is scattered into its propagation direction, see also Fig. 2.8 for this phenomenological picture. The derivation of the anisotropic radiative transfer equation was presented in section 2.4.c.

Indeed equation (2.71) appears to have the same structure as the radiative transfer equation for isotropic media. There are a few differences however. In our equation there is not only anisotropy in the phase function, but there is also anisotropy in the mean free path. Furthermore, because in our equation the wave vector has a different direction as the group velocity, and can therefore be used for either the ordinary, or the extraordinary radiance (not at the same time however). Finally hidden in the derivative along a path $\mathrm{d}I/\mathrm{d}s$ is an anisotropic scattering delay.

Radiative transfer equation (2.71) gives rise to a continuity equation for the total energy density. The energy density per frequency band $\mathscr{H}_\omega$ and energy density flux per frequency band $\boldsymbol{S}_\omega$, are related to the radiance per frequency band I_ω by

$$\mathscr{H}_\omega(\boldsymbol{x},t) = \int \mathrm{d}^2 e_{\boldsymbol{k}}\frac{1+\delta_\omega(\boldsymbol{e}_{\boldsymbol{k}},\boldsymbol{0},0)}{\left|\boldsymbol{v}_{\mathrm{g}}(\boldsymbol{e}_{\boldsymbol{k}})\right|}I_\omega(\boldsymbol{e}_{\boldsymbol{k}},\boldsymbol{x},t), \tag{2.72a}$$

$$\boldsymbol{S}_\omega(\boldsymbol{x},t) = \int \mathrm{d}^2 e_{\boldsymbol{k}} I_\omega(\boldsymbol{e}_{\boldsymbol{k}},\boldsymbol{x},t)\frac{\boldsymbol{v}_{\mathrm{g}}(\boldsymbol{e}_{\boldsymbol{k}})}{\left|\boldsymbol{v}_{\mathrm{g}}(\boldsymbol{e}_{\boldsymbol{k}})\right|}. \tag{2.72b}$$

In the total energy density we observe again both a radiative part and a material part due to the scattering delay represented by δ.

2.6 Monte Carlo Method for Radiative Transfer

In this section we will provide a recipe for a Monte Carlo simulation [10, 11] of the radiative transfer equation (2.59) in an unbounded homogeneous anisotropic random medium [83]. We recall that

$$\begin{aligned}\frac{\mathrm{d}I_\omega(\boldsymbol{e}_{\boldsymbol{k}},\boldsymbol{x},t)}{\mathrm{d}s} &= \frac{\xi_\omega(\boldsymbol{e}_{\boldsymbol{k}},\boldsymbol{x},t)}{\left|\boldsymbol{v}_{\mathrm{g}}(\boldsymbol{e}_{\boldsymbol{k}})\right|} - \frac{I_\omega(\boldsymbol{e}_{\boldsymbol{k}},\boldsymbol{x},t)}{|\boldsymbol{l}_{\mathrm{e}\omega}(\boldsymbol{e}_{\boldsymbol{k}})|} \\ &\quad + \int \mathrm{d}^2 e_{\boldsymbol{k}_0} \frac{\mathfrak{p}_\omega(\boldsymbol{e}_{\boldsymbol{k}},\boldsymbol{e}_{\boldsymbol{k}_0})\, I_\omega(\boldsymbol{e}_{\boldsymbol{k}_0},\boldsymbol{x},t)}{|\boldsymbol{l}_{\mathrm{s}\omega}(\boldsymbol{e}_{\boldsymbol{k}_0})|}. \end{aligned} \tag{2.73}$$

In order to solve the radiative transfer equation for the radiance $I_\omega \mathrm{d}\omega$ per frequency band $\mathrm{d}\omega$ we require

- a tensor host permittivity ε and a scalar host permeability μ which, using the dispersion relation (2.7), determine the group and phase velocity,
- the absorption and scattering properties of the microscopic scatterers, i.e. their differential scattering cross section, and their absorption cross section, which then yield the extinction and scattering mean free path, albedo, phase function, and scattering delay.
- a source function for the radiance,

$$\frac{\xi_\omega(\boldsymbol{e}_{\boldsymbol{k}},\boldsymbol{x},t)}{\left|\boldsymbol{v}_{\mathrm{g}}(\boldsymbol{e}_{\boldsymbol{k}})\right|} = \frac{\omega^2 {\mathrm{c_i}}^2}{(4\pi)^2 v_{\mathrm{p}}^3(\boldsymbol{e}_{\boldsymbol{k}})} S_\omega(\boldsymbol{e}_{\boldsymbol{k}},\boldsymbol{x},t), \tag{2.74}$$

  which is normalized such that for plane waves of unit amplitude we have $S_\omega(\boldsymbol{e}_{\boldsymbol{k}},\boldsymbol{x},t)=1$.

We consider an infinite medium with homogeneous anisotropic disorder, and follow the evolution of an initial state of the radiance for some time $t_{\mathrm{f}}-t$. The initial radiance I_0, which for simplicity we take to be a unit impulse function located at phase space coordinate $(\boldsymbol{e}_{\boldsymbol{k}},\boldsymbol{x})$ is divided in N finite radiance elements I_i. The size of N is chosen such that the desired accuracy is met. Our initial state has only a single wave vector coordinate and a single spatial coordinate. In the procedure we present below new coordinates are generated from these initial coordinates, and these we may store. Thus we can run our Monte Carlo simulation without discretizing the phase space in advance. Afterwards we can evaluate the stored coordinates, and we can determine if and how we want to discretize the phase space. As an example we may want to have a snapshot of where each radiance element was each femtosecond.

Provided the mean free path is much longer than the wavelength, in the first few femtoseconds almost all radiance elements will still have their initial wave vector, and all radiance elements are still close to their original spatial coordinate. In order to see the small deviations from the initial coordinate, we need to make the spatial bins very small. On the other hand, at much longer time scales radiance elements will have spread thinly over a large part of the phase space, and the bin size should be increased.

For more complicated initial states of the radiance we discretize the phase space in advance in elements $(\mathrm{d}\boldsymbol{e_k}, \mathrm{d}\boldsymbol{x})$ where in each element the amount of radiance is approximately constant. In each phase space element we can assign the radiance again a single wave vector and a single spatial coordinate. For each of these initial coordinates we can follow the procedure prescribed in the above paragraph, and make the discretization of phase space consistent with the accuracy requirements at each time step.

We will follow the trajectory of each discrete radiance element I_i of an initial unit impulse function, so we require the initial wave vector direction, space and time coordinates, $\boldsymbol{e_k}$, $\boldsymbol{x}$ and t respectively, and we can start the simulation. The radiative transfer equation (2.59) tells us that for each discrete element two random quantities exist. First, radiance with a given wave vector $\boldsymbol{e_k}$ has a (conditional) probability P to travel some (positive valued) distance $\delta x_\omega(\boldsymbol{e_k})$ without scattering,

$$P_\omega[\delta x_\omega(\boldsymbol{e_k})|\boldsymbol{e_k}] \quad = \quad \mathrm{e}^{-\frac{\delta x_\omega(\boldsymbol{e_k})}{|l_{\mathrm{e}\omega}(\boldsymbol{e_k})|}}. \tag{2.75}$$

Next, the radiance has, again given the wave vector $\boldsymbol{e_k}$, a (conditional) probability $\mathfrak{p}_\omega\left(\boldsymbol{e}_{\boldsymbol{k}_\mathrm{n}}|\boldsymbol{e_k}\right)\mathrm{d}^2\boldsymbol{e}_{\boldsymbol{k}_\mathrm{n}}$ to scatter with another wave vector $\boldsymbol{e}_{\boldsymbol{k}_\mathrm{n}}$,

$$\mathfrak{p}_\omega\left(\boldsymbol{e}_{\boldsymbol{k}_\mathrm{n}}|\boldsymbol{e_k}\right) \quad \equiv \quad \frac{1}{\sigma_{\mathrm{s}\omega}(\boldsymbol{e_k})}\frac{\mathrm{d}\sigma_{\mathrm{s}\omega}\left(\boldsymbol{e}_{\boldsymbol{k}_\mathrm{n}}, \boldsymbol{e_k}\right)}{\mathrm{d}^2\boldsymbol{e}_{\boldsymbol{k}_\mathrm{n}}}. \tag{2.76}$$

These two steps are taken, until the addition of time increments δt has reached the final time t_f:

1. I_i travels some space and time distance,

$$\begin{aligned}
\delta x_\omega(\boldsymbol{e_k}) &= -|\boldsymbol{l}_{\mathrm{e}\omega}(\boldsymbol{e_k})|\ln P_\omega[\delta x_\omega(\boldsymbol{e_k})|\boldsymbol{e_k}], && \text{(2.77a)}\\
\boldsymbol{x}_\mathrm{n} &= \boldsymbol{x} + \delta x_\omega(\boldsymbol{e_k})\boldsymbol{e}_\mathrm{s}(\boldsymbol{e_k}), && \text{(2.77b)}\\
\delta t_\omega(\boldsymbol{e_k}) &= \frac{1}{|\boldsymbol{v}_\mathrm{g}(\boldsymbol{e_k})|}\delta x_\omega(\boldsymbol{e_k}), && \text{(2.77c)}\\
\tilde{t} &= t + \delta t_\omega(\boldsymbol{e_k}), && \text{(2.77d)}
\end{aligned}$$

2. I_i undergoes absorbtion and scattering and obtains a scattering delay time,

$$\begin{aligned}
\delta \boldsymbol{e}_{\boldsymbol{k}} &= \boldsymbol{f}[\boldsymbol{e}_{\boldsymbol{k}}, p_\omega\left(\boldsymbol{e}_{\boldsymbol{k}_\mathrm{n}}|\boldsymbol{e}_{\boldsymbol{k}}\right)], && \text{(2.77e)}\\
\boldsymbol{e}_{\boldsymbol{k}_\mathrm{n}} &= \boldsymbol{e}_{\boldsymbol{k}} + \delta \boldsymbol{e}_{\boldsymbol{k}}, && \text{(2.77f)}\\
\delta t_{\mathrm{m}\omega}(\boldsymbol{e}_{\boldsymbol{k}}) &= \frac{\delta_\omega(\boldsymbol{e}_{\boldsymbol{k}}, \boldsymbol{0}, 0)}{|\boldsymbol{v}_\mathrm{g}(\boldsymbol{e}_{\boldsymbol{k}})|}\delta x_\omega(\boldsymbol{e}_{\boldsymbol{k}}), && \text{(2.77g)}\\
t_\mathrm{n} &= \tilde{t} + \delta \tilde{t}_\omega(\boldsymbol{e}_{\boldsymbol{k}}), && \text{(2.77h)}\\
I_{\mathrm{n}i\omega}(\boldsymbol{e}_{\boldsymbol{k}_\mathrm{n}}, \boldsymbol{x}_\mathrm{n}, t_\mathrm{n}) &= a_\omega(\boldsymbol{e}_{\boldsymbol{k}}) I_{i\omega}(\boldsymbol{e}_{\boldsymbol{k}_\mathrm{n}}, \boldsymbol{x}_\mathrm{n}, t_\mathrm{n}), && \text{(2.77i)}
\end{aligned}$$

where a is the albedo of the scatterers, which is unity in elastic media (2.61), and $\boldsymbol{f}$ some complicated vector function which can only be made explicit given a phase function.

When this iterative procedure has been carried out for all N radiance elements, we end up with a distribution of radiance over phase space. During the procedure we can also make snapshots, but there is a caveat, because in any snapshot different I_i have traveled trajectories with different times. However, each radiance element travels in a straight line before it undergoes scattering or absorption, and we can calculate where the radiance was at any time. It is straightforward to account for the number of scattering events along the trajectory of radiance element I_i, because it is just the number of iterations used to produce the trajectory. In our two step procedure we incremented the time twice in order to focus attention to the physics in the energy velocity, which consists of a radiative and a material part. In a real simulation one could add both time increments in the first step.

The Monte Carlo method for unbounded media can be extended to incorporate bounded media. In bounded media the iteration is to be stopped as well when the radiance element leaves the scattering material, as there will be no scattering or absorption events anymore. Note that the attenuation for the distance traveled inside the scattering material and possible (internal) reflections have to be accounted for.

In contrast with other Monte Carlo recipes for anisotropic media, our procedure has three key differences. Firstly, we incorporate an anisotropic host medium. Thus in our model the direction of propagation of the radiance is different from the wave vector direction, and can not only model the radiance of ordinary waves, but can also model the radiance of extraordinary waves. Secondly, we incorporate the effect of scattering delay, a quantity which is anisotropic for anisotropic scatterers. Thus in media with anisotropic scatterers, it is not sufficient to incorporate scattering delay by a rescaling the velocity of light by a constant multiplicative factor. Thirdly the scattering and extinction

mean free path can be different for different propagation directions, not only for the principal axes of the anisotropy, but for all directions.

2.7 Special host media

In this section we consider some special cases of scatterers and host media. The magnetic permeability tensor of the host medium is assumed to be isotropic, $\mu = \frac{1}{3}\mathrm{Tr}[\mu]1$, whereas the dielectric tensor can be anisotropic. In these examples we take the anisotropic host dielectric permittivity tensor on principal axes. In a convenient Cartesian coordinate system we have

$$\varepsilon = \varepsilon_{xx}\boldsymbol{e}_x\boldsymbol{e}_x + \varepsilon_{yy}\boldsymbol{e}_y\boldsymbol{e}_y + \varepsilon_{zz}\boldsymbol{e}_z\boldsymbol{e}_z, \tag{2.78}$$

and the anisotropy tensor A is

$$\mathsf{A} = 3\frac{\varepsilon_{yy}\varepsilon_{zz}\boldsymbol{e}_x\boldsymbol{e}_x + \varepsilon_{xx}\varepsilon_{zz}\boldsymbol{e}_y\boldsymbol{e}_y + \varepsilon_{xx}\varepsilon_{yy}\boldsymbol{e}_z\boldsymbol{e}_z}{\varepsilon_{yy}\varepsilon_{zz} + \varepsilon_{xx}\varepsilon_{zz} + \varepsilon_{xx}\varepsilon_{yy}}. \tag{2.79}$$

We include elastic isotropic point scatterers, with some scattering cross section, that is constant with respect to wave vector, but dependent on frequency,

$$\sigma_{\mathrm{e}\omega} = \sigma_{\mathrm{s}\omega}. \tag{2.80}$$

The source for the radiative transfer equation is a plane wave of unit amplitude, i.e $S = 1\,\mathrm{J\,s\,m^{-2}\,sr^{-1}}$, and

$$\frac{\xi_\omega(\boldsymbol{e}_{\boldsymbol{k}}, \boldsymbol{x}, t)}{\left|\boldsymbol{v}_{\mathrm{g}}(\boldsymbol{e}_{\boldsymbol{k}})\right|} = \frac{\omega^2 {\mathrm{c_i}}^2}{(4\pi)^2 v_{\mathrm{p}}^3(\boldsymbol{e}_{\boldsymbol{k}})}. \tag{2.81}$$

2.7.a Isotropic media

The simplest medium has isotropic permittivity $\varepsilon_{xx} = \varepsilon_{yy} = \varepsilon_{zz}$ and therefore

$$\mathsf{A} = 1. \tag{2.82}$$

All physical quantities in the radiative transfer equation simplify, here we present them in spherical polar coordinates,

$$\frac{v_{\mathrm{p}}(\theta,\varphi)}{\mathrm{c_i}} = 1, \tag{2.83a}$$

$$\frac{\boldsymbol{v}_{\mathrm{g}}(\theta,\varphi)}{\mathrm{c_i}} = \sin\theta(\cos\varphi\boldsymbol{e}_x+\sin\varphi\boldsymbol{e}_y)+\cos\theta\boldsymbol{e}_z, \tag{2.83b}$$

$$l_{\mathrm{s}}(\theta,\varphi) = l_{\mathrm{e}}(\theta,\varphi) = \frac{1}{n\sigma_{\mathrm{p}}}, \tag{2.83c}$$

$$\sigma_{\mathrm{p}_\omega} = \frac{4\pi{\mathrm{c_i}}^2(\omega^2\Gamma/{\omega_0}^2)^2}{({\omega_0}^2-\omega^2)^2+(\omega^3\Gamma/{\omega_0}^2)^2}, \tag{2.83d}$$

$$\mathfrak{p}_\omega(\theta,\varphi,\theta_0,\varphi_0) = \frac{1}{4\pi}, \tag{2.83e}$$

$$\delta_\omega = \frac{2n{\mathrm{c_i}}^3(4\pi-1)\Gamma/{\omega_0}^2({\omega_0}^2-\omega^2)}{({\omega_0}^2-\omega^2)^2+(\omega^3\Gamma/{\omega_0}^2)^2}. \tag{2.83f}$$

Here n is the scatterer density, σ_{p} is the scattering cross section of the point scatterer, which is in isotropic media fully determined by its resonance frequency ω_0 and its linewidth Γ.

The equation of radiative transfer reduces to its familiar form

$$\frac{\mathrm{d}I_\omega(\theta,\varphi,\boldsymbol{x},t)}{\mathrm{d}s} = \frac{\omega^2}{(4\pi)^2\mathrm{c_i}} - \frac{I_\omega(\theta,\varphi,\boldsymbol{x},t)}{l_{\mathrm{e}\omega}} + \iint\frac{\mathrm{d}\varphi_0\mathrm{d}\theta_0\sin\theta_0}{4\pi}\frac{I_\omega(\theta_0,\varphi_0,\boldsymbol{x},t)}{l_{\mathrm{s}\omega}}. \tag{2.84}$$

2.7.b Uniaxial media

Uniaxial media are characterized by a dimensionless anisotropy parameter $a>-1$. As we will only consider elastic scatterers in this section, which have albedo $a_\omega(\boldsymbol{e_k})=1$, no confusion with anisotropy parameter a can arise. If the optical axis is along $\boldsymbol{e}_z$, the uniaxial permittivity is given by

$$\varepsilon = \frac{3+a}{{\mathrm{c_i}}^2\mathrm{Tr}[\mu]}\left[1-\frac{a}{1+a}\boldsymbol{e}_z\boldsymbol{e}_z\right], \tag{2.85}$$

and the anisotropy tensor reduces to

$$\mathsf{A} = \frac{3}{3+a}\left[1+a\boldsymbol{e}_z\boldsymbol{e}_z\right]. \tag{2.86}$$

The radiative transfer equation with source (2.81) reads

$$\frac{\mathrm{d}I_\omega(\theta,\varphi,\boldsymbol{x},t)}{\mathrm{d}s} = \frac{\omega^2 {c_\mathrm{i}}^2}{(4\pi)^2 v_\mathrm{p}^3(\theta,\varphi)} - \frac{I_\omega(\theta,\varphi,\boldsymbol{x},t)}{l_{\mathrm{e}\omega}(\theta,\varphi)} + \iint \mathrm{d}\varphi_0 \mathrm{d}\theta_0 \sin\theta_0 \frac{\mathfrak{p}_\omega(\theta,\varphi,\theta_0,\varphi_0)\, I_\omega(\theta_0,\varphi_0,\boldsymbol{x},t)}{l_{\mathrm{s}\omega}(\theta_0,\varphi_0)}. \quad (2.87)$$

with mean free paths $l_{\mathrm{s,e}} = |\boldsymbol{l}_{\mathrm{s,e}}|$. The three situations we should discuss are isotropic, $a = 0$, positive anisotropy, $a > 0$, and negative anisotropy $-1 < a < 0$.

In isotropic media the length scales, velocities and phase function, Eqs. (2.83) in the radiative transfer equation are independent of the wave vector direction. In anisotropic media with anisotropy tensor (2.86) these physical quantities become direction dependent. In terms of spherical polar coordinates

$$\frac{v_\mathrm{p}(\theta,\varphi)}{c_\mathrm{i}} = \sqrt{\frac{3}{3+a}}\sqrt{1+a\cos^2\theta}, \quad (2.88a)$$

$$\frac{\boldsymbol{v}_\mathrm{g}(\theta,\varphi)}{c_\mathrm{i}} = \sqrt{\frac{3}{3+a}}\frac{\sin\theta(\cos\varphi\boldsymbol{e}_x+\sin\varphi\boldsymbol{e}_y)+(1+a)\cos\theta\boldsymbol{e}_z}{\sqrt{1+a\cos^2\theta}}, \quad (2.88b)$$

$$l_\mathrm{s}(\theta,\varphi) = l_\mathrm{e}(\theta,\varphi) = \sqrt{\frac{3}{3+a}}\sqrt{\frac{1+a(2+a)\cos^2\theta}{1+a\cos^2\theta}}\frac{1}{n\sigma_\mathrm{s}}, \quad (2.88c)$$

$$\mathfrak{p}(\theta,\varphi,\theta_0,\varphi_0) = \frac{1}{4\pi}\sqrt{\frac{1+a}{(1+a\cos^2\theta)^3}}, \quad (2.88d)$$

$$\sigma_{\mathrm{p}\omega} = \frac{4\pi {c_\mathrm{i}}^2(\omega^2\Gamma/{\omega_0}^2)^2}{({\omega_0}^2-\omega^2)^2+(\omega^3\Gamma/{\omega_0}^2)^2}\sqrt{\left(\frac{3}{3+a}\right)^3(1+a)}, \quad (2.88e)$$

$$\delta_\omega = \frac{2n{c_\mathrm{i}}^3\Gamma/{\omega_0}^2({\omega_0}^2-\omega^2)}{({\omega_0}^2-\omega^2)^2+(\omega^3\Gamma/{\omega_0}^2)^2}\left[4\pi\sqrt{\left(\frac{3}{3+a}\right)^3(1+a)}-1\right]. \quad (2.88f)$$

Here n is the scatterer density, σ_p is the cross section of the point scatterer, which is fully determined by its resonance frequency ω_0, its linewidth Γ, and the value of the anisotropy parameter a. The value of a depends on the anisotropy of the uniaxial medium to be studied. In this kind of disordered material the scattering delay δ and the scattering cross section do depend on the anisotropy parameter a, but are independent of the propagation direction.

If $a > 0$, then all length scales and all velocities, except c_i which is constant, are a factor $\sqrt{1+a}$ larger in the $\boldsymbol{e}_z$ direction, as compared to the $\boldsymbol{e}_x$ and $\boldsymbol{e}_y$ directions. We note that the phase function has become anisotropic even though the scatterers themselves are isotropic, because the element of solid

angle is deformed by the anisotropy in the host medium. The phase function is a factor $\sqrt{(1+a)^3}$ larger in the e_x or e_y direction as compared to the e_z direction. So although the scattering strength of the medium, as measured by the mean free path, is for $a > 0$ stronger in the xy planes, the anisotropy of the host medium also restrains more of the scattered radiance in the xy plane. We conclude that anisotropy of the host medium confines radiation in the xy plane when $a > 0$. If on the other hand $a < 0$, then we may follow a similar argument to conclude that for $a < 0$ the radiation is confined along the z axis.

2.8 Conclusion

In this section we present an overview of the results of this chapter, and what we want to use it for.

We have presented a derivation of the radiative transfer equation for radiance in anisotropic media in terms of basic building blocks. The building blocks were a scalar wave and some scattering potential. Anisotropy in the random medium in- or decreases the phase and group velocity in certain directions and has an impact on the extinction and scattering cross sections of the inhomogeneities in the refractive index. We illustrated this for point scatterers. Instead of scattered spherical waves we encountered elliptical waves, in which the group velocity governs the shape of the wave surface. In anisotropic media the group velocity also turns up in the expressions for the extinction and scattering mean free path. In an anisotropic multiple scattering medium, the waves do decay due to extinction or scattering, but this decay does not satisfy the well known relation $l_{\mathrm{e,s}} = (n\sigma_{\mathrm{e,s}})^{-1}$ valid in isotropic disordered media. Instead we found a direction dependent length scale $l_{\mathrm{e,s}}(\boldsymbol{e_k}) = v_{\mathrm{g}}(\boldsymbol{e_k})/(\mathrm{c_i} n\sigma_{\mathrm{e,s}})$. Here $v_{\mathrm{g}}(\boldsymbol{e_k})$ contains the anisotropy of the surrounding medium. Apart from the surrounding medium the scatterers themselves can also contribute to the anisotropy. Moreover the $l_{\mathrm{e,s}}(\boldsymbol{e_k})$ are the magnitude of an extinction or scattering mean free path vector.

From the Bethe-Salpeter equation for the ensemble averaged product of amplitudes we derived a radiative transfer equation. In this transport equation again the aforementioned anisotropic scattering and extinction mean free paths show up. In an appendix we derived the Ward identity for anisotropic media, and, as is well known in the literature, we found a scattering delay due to the energy dependence of the scattering potentials. In anisotropic media this scattering delay can also contain anisotropy. In the radiative transfer equation it shows up as a correction to the propagation velocity along a radiance trajectory through a multiple scattering medium. However, the scattering delay can not be absorbed as a scaling factor in the group velocity due

to fact that the anisotropy in these two quantities do not necessarily coincide. Finally, because in our model the wave vector direction is in general different from that of the group velocity, we can not only use it to describe the transport of the radiance of ordinary waves, but we can also use it for transport of the radiance of extraordinary waves.

It is well known that radiative transfer equation for isotropic multiple scattering media is in general impossible to solve analytically, and the usual way to obtain solutions is through Monte Carlo simulations. Our radiative transfer equation for anisotropic disordered media is even more difficult to solve analytically. For this reason we presented a scheme to numerically solve our radiative transfer equation through Monte Carlo simulation. Our ideas can serve as a starting point for those who in practice have to deal with complicated anisotropic media and wish to obtain accurate numerical solutions for their anisotropic radiative transfer problems.

To facilitate the understanding of the anisotropic radiative transfer equation we gave two examples of the two least complicated disordered media. The least complicated is of course the isotropic medium which we presented as reference material in order to compare our anisotropic example. Our anisotropic example is a uniaxial medium in which the anisotropy is fully determined by a single anisotropy parameter. In both of these examples the scatterers are point scatterers such that there are only three additional parameters which characterize the scattering strength of the uniaxial disordered medium. These three parameters are the number density of the point scatterers, the resonance frequency, and the linewidth of the point scatterers. We expressed the the velocities and length scales explicitly in terms of spherical polar coordinates and the anisotropy parameter. In the uniaxial medium only the polar angle is relevant. In these examples the scattering delay and the scattering cross section depend only on the anisotropy parameter and the three scattering strength parameters, not on the angles. The isotropic example is recovered as a limit of the uniaxial medium.

The radiative transfer equation for anisotropic disordered media has firm foundations, and it describes a broad range of transport phenomena, both isotropic and anisotropic. The radiative transfer equation describes ballistic transport in the limit $l_{\mathrm{e},s} \to \infty$. When the extinction and scattering mean free path are finite we can determine the anisotropic diffusion tensor. The anisotropic diffusion equation is an accurate description of transport of waves through most disordered media. However neither the radiative transfer equation, nor the diffusion equation incorporate interference effects, not even for isotropic disordered media. It is well known that it is extremely difficult to directly add interference corrections to the radiative transfer equation. On

the other, it is also well known that through a renormalization of the diffusion constant interference effects such as the enhanced backscattering cone can be accounted for. Doing this renormalization procedure for anisotropic media is expected to give an accurate description of the anisotropy which is observed in the enhanced backscattering cone of anisotropic media. Through such a renormalization procedure we can also generalize the Ioffe-Regel criterion, which predicts the onset of Anderson localization in isotropic media, to anisotropic media. However all thing mentioned in this paragraph are outside the scope of this chapter.

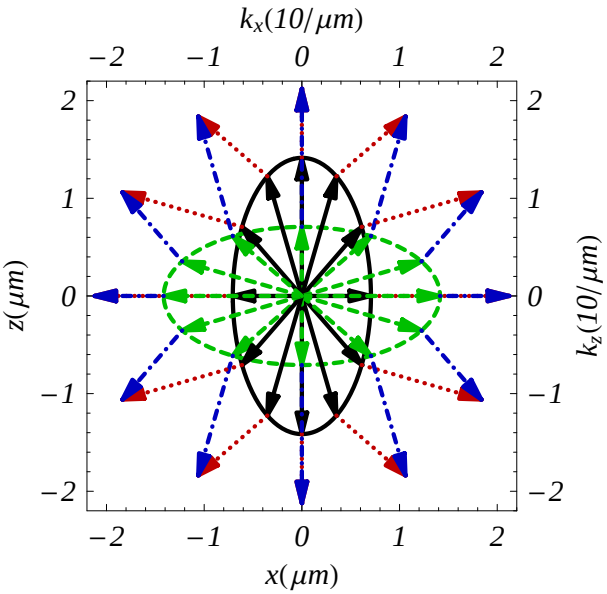

Figure 2.6 (color online).
In this plot the units left and below refer to the solid and dotted lines, whereas the units right and above refer to the dashed and dot-dashed lines. The solid ellipse is a phase surface $\phi(\boldsymbol{X})$ = constant *of an elliptical wave emerging from an isotropic scatterer located at* $\boldsymbol{X} = \boldsymbol{0}$ *in a uniaxial medium with dispersion relation* $\omega^2/{c_i}^2 = \boldsymbol{k}\cdot(1+3\boldsymbol{e}_z\boldsymbol{e}_z)/2\cdot\boldsymbol{k}$. *Each black arrow points to a coordinate* $\boldsymbol{X}$ *on the phase surface. For each of these coordinates* $\boldsymbol{X}$ *we plotted the unit normal* $\boldsymbol{n}_\phi(\boldsymbol{X})$ *scaled such that the dotted and the dashed arrows running parallel have the same length. The dashed ellipse is a frequency surface* $\omega(\boldsymbol{k})/c_i$ = constant. *The dashed arrows are wave vectors* $\boldsymbol{k}$ *on the frequency surface. For each of these* $\boldsymbol{k}$ *we have drawn a dot-dashed arrow which is proportional to the group velocity* $\boldsymbol{v}_g(\boldsymbol{k})$ *and therefore normal to the frequency surface. Each dot-dashed arrow is scaled such that it has the same length as the parallel solid arrow. For each* $\boldsymbol{X}$ *we can identify* $\boldsymbol{n}_\phi(\boldsymbol{X})$ *with a unit wave vector* $\boldsymbol{e}_{\boldsymbol{k}}$. *Using the identification we find* $\boldsymbol{v}_g(\boldsymbol{k}) = \boldsymbol{v}_g(\boldsymbol{n}_\phi(\boldsymbol{X})) \propto \boldsymbol{X}$. *We define the wave vector direction to be the direction of the phase velocity, and we see that the phase velocity is normal to the wave surface, as it should be.*

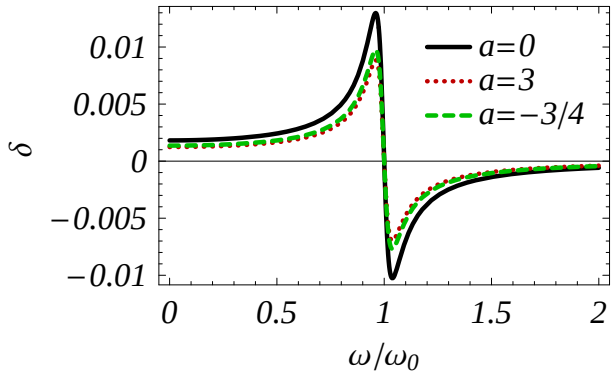

Figure 2.7 (color online).
We plotted the scattering delay factor δ for point scatterers in a uniaxial dielectric $\varepsilon = (3+a)[1+ae_z e_z/(1-a)]/(c_i{}^2 \mathrm{Tr}[\mu])$, where a parameterizes the anisotropy. We set the scatterer density $n = (2\pi)^3(10\lambda_i)^{-3}$. The solid line is for isotropic media, $a = 0$. The dotted line is for an anisotropic dielectric with $a = 3$, and the dashed line is for $a = -3/4$. The magnitude of the delay depends on the linewidth of the scatterer. For real atoms the size of the delay is orders magnitude larger, as the delay is inversely proportional to the linewidth.

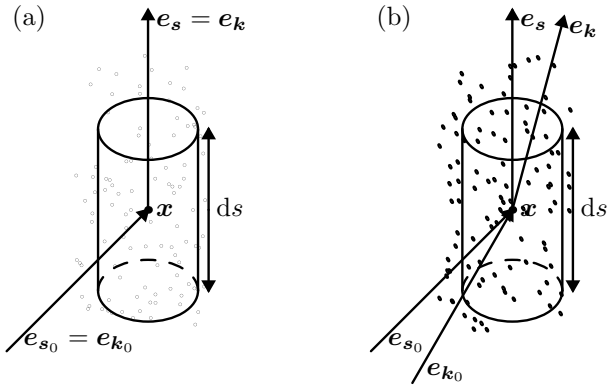

Figure 2.8.
The phenomenology behind radiative transfer. In a multiple scattering medium the radiance element $\mathrm{d}I(e_p, x, t)$ *at time* t*, spatial coordinate* x*, and wave vector* e_p*, travels along a path element* $\mathrm{d}s$ *in the propagation direction* e_s *inside a comoving cylindrical volume element oriented along the propagation direction* e_s*. Along* $\mathrm{d}s$ *the radiance reduces if sinks and (possibly absorbing) scatterers are encountered. Scattering into direction* e_s *from all directions* e_{s_0}*, and possible sources along the path can increase the radiance. (a) In isotropic media the wave vector* e_p *coincides with the direction of propagation* e_s*. (b) In anisotropic media the direction of propagation* e_s *and wave vector* e_p *in general do not coincide. We find a bijective mapping between* e_s *and* e_p*, and that* e_s *coincides with the direction of the group velocity.*

Chapter 3

Diffusion and Anderson localization in infinite media

We derive anisotropic diffusion from the equation of radiative transfer in infinite anisotropic media. We add interference corrections to find the location of the transition to Anderson localization in anisotropic media. In anisotropic media we find that the transition to Anderson localization occurs at lower values of the scattering strength parameter.

3.1 Introduction

Every material contains a certain amount of disorder. Therefore, when we send a wave into some non-absorbing material, the way of transport of the wave energy is governed by the disorder. If the disorder is small, most energy passes ballistically through the material. However, most materials have a significant amount of disorder, and waves inside will scatter many times. Multiple scattering of waves gives rise to diffusion or, for extreme amounts of disorder, to Anderson localization of the wave energy. When light diffuses through the material most interference effects are washed out. Anderson localization [30], on the other hand, is a situation in which interference conquers, and gives rise to localized states in the disordered material, rather than extended states.

The scattering strength of statistically isotropic disordered matter is characterized by the transport mean free path l and the wave vector k. It is intuitively clear that a large transport mean free path implies a weaker disorder. Diffuse propagation of wave energy is governed by the diffusion constant D, which can be expressed in terms of the transport mean free path. For three dimensional statistically isotropic disordered media it is common to write $D = vl/3$, with energy velocity v. The shorter the transport mean free path, the stronger the diffusion, until finally the transition to Anderson localization sets in when

the transport mean free path becomes kl = constant, with the constant of order 1 but model-dependent [32, 88]. This is known as the Ioffe-Regel criterion for Anderson localization. Alternatively, the Ioffe-Regel criterion is sometimes expressed in terms of a transport mean free time τ and a frequency ω, so that the transition occurs at $kl = \omega\tau \approx 1$.

The equation of radiative transfer is more general than the diffusion equation, but it does not contain interference effects [6]. It turns out to be extremely complicated to add interference corrections to the radiative transfer equation, unless when it is first approximated by a diffusion equation.

In statistically isotropic disordered infinite media of dimension lower than three the that the diffusive solution is actually not believed to exist. In those dimensions there is either ballistic transport or Anderson localization, without diffusion. We may imagine lower dimensional media to be three dimensional media whose frequency surfaces are strongly anisotropic. Thus we may conjecture that anisotropy in materials with strong disorder is favorable for Anderson localization, but this idea has never been confirmed [62, 91]. In Ref. [91] three cases were considered, with one of them a quasi two dimensional metal with a cylindrical frequency surface, and the, perhaps counterintuitive, result was obtained that it was harder to localize along the directions parallel to the axis of the cylinder, than in the plane perpendicular to it. This was explained by the consideration that the conductivity across the planes, i.e. the direction parallel to the cylinder, did not constitute a quasi one dimensional medium and therefore required a three dimensional treatment.

In this chapter we study the effect of anisotropy on diffusion and on the transition to Anderson localization. We start from the equation of radiative transfer in anisotropic media, which we derived from first principles in chapter 2 in a low scatterer density approximation. We derive a self-consistent diffusion equation for the energy density. Next we consider the effect of reciprocity for wave amplitude on transport. We then use that information to add an interference correction to the anisotropic diffusion solution. The interference correction is a set of higher order terms in a scatterer density expansion. With this correction we derive a Ioffe-Regel criterion for anisotropic media, which is the main result of this article. There are two appendices. In appendix B we present some linear response theory, and some background on the self consistent approach to the equation of radiative transfer. Finally, in appendix 3.4 we present some explicit special cases of the effect of anisotropy on diffusion and the Ioffe-Regel criterion.

3.2 Anisotropic Radiative Transfer

The radiative transfer equation describes transport specific intensity [6, 7, 92], or in *SI* units, the radiance per frequency band I_ω [75]. In general the radiance depends 6 coordinates, a unit wave vector $\boldsymbol{e_k}$, a space coordinate $\boldsymbol{x}$, and time t. The transport mean free path l does not explicitly appear in the radiative transfer equation. In chapter 2, we derived the radiative transfer equation for anisotropic media for radiance per frequency band $I_\omega(\boldsymbol{e_k}, \boldsymbol{x}, t)$. In that equation we encountered anisotropy in both the scattering and extinction mean free path, $\boldsymbol{l}_\mathrm{s}$ and $\boldsymbol{l}_\mathrm{e}$. These turn into vector quantities, and are functions of the wave vector direction $\boldsymbol{e_k}$. The magnitude of the wave vector, k, is also anisotropic, and is is fixed by the dispersion relation $k(\boldsymbol{e_k}) = \omega / v_\mathrm{p}(\boldsymbol{e_k})$, with phase velocity v_p. When we follow the radiance $\mathrm{d}I_\omega(\boldsymbol{e_k}, \boldsymbol{x}, t)$ along an infinitesimal path $\mathrm{d}s$ in an anisotropic medium, then hydrodynamic derivative becomes

$$\frac{\mathrm{d}I_\omega(\boldsymbol{e_k}, \boldsymbol{x}, t)}{\mathrm{d}s} = \frac{1+\delta_\omega(\boldsymbol{e_k})}{|\boldsymbol{v}_\mathrm{g}(\boldsymbol{e_k})|}\frac{\partial I_\omega(\boldsymbol{e_k}, \boldsymbol{x}, t)}{\partial t} + \frac{\boldsymbol{v}_\mathrm{g}(\boldsymbol{e_k})}{|\boldsymbol{v}_\mathrm{g}(\boldsymbol{e_k})|}\cdot\boldsymbol{\nabla} I_\omega(\boldsymbol{e_k}, \boldsymbol{x}, t)\,. \tag{3.1}$$

Here $\boldsymbol{v}_\mathrm{g}$ is the group velocity vector, and $\delta_\omega(\boldsymbol{e_k})$ is the well known scattering delay [68], generalized to anisotropic media.

The anisotropic radiative transfer equation (2.71) for the radiance per frequency band I_ω is, for an isotropic point source of strength $\mathfrak{s}_\omega$ located at $\boldsymbol{x} = 0$ and $t = 0$,

$$\begin{aligned}\frac{\mathrm{d}I_\omega(\boldsymbol{e_k}, \boldsymbol{x}, t)}{\mathrm{d}s} &= \frac{\omega^2 \mathrm{c_i}^2 \mathfrak{s}_\omega \delta^3(\boldsymbol{x})\delta(t)}{(4\pi)^2 v_\mathrm{p}^3(\boldsymbol{e_k})} - \frac{I_\omega(\boldsymbol{e_k}, \boldsymbol{x}, t)}{|\boldsymbol{l}_{\mathrm{e}\omega}(\boldsymbol{e_k})|} \\ &\quad + \int \mathrm{d}^2 e_{\boldsymbol{k}_0} \frac{\mathfrak{p}_\omega(\boldsymbol{e_k}, \boldsymbol{e_{k_0}})\, I_\omega(\boldsymbol{e_{k_0}}, \boldsymbol{x}, t)}{|\boldsymbol{l}_{\mathrm{s}\omega}(\boldsymbol{e_{k_0}})|}.\end{aligned} \tag{3.2}$$

The left-hand side of Eq. (3.2) describes transport of radiance along a path. The first term on the right-hand side, which contains an isotropic velocity $\mathrm{c_i}^2 = \mathrm{Tr}[\varepsilon^{-1}]/\mathrm{Tr}[\mu]$ is the point source, the second term is extinction and a the third term stands for a scattering integral, featuring the phase function $\mathfrak{p}$. The source strength $\mathfrak{s}_\omega$ has *SI* units of $\mathrm{J\,m\,s^2}$. The strength of the isotropic point source is weighted by a direction dependent product of phase velocities, deforming the isotropic output energy density into an anisotropic radiation pattern. This deformation is caused by the density of states in an anisotropic medium, which is proportional to $\delta(\omega^2 - v_\mathrm{p}^2(\boldsymbol{e_k})k^2)$.

The radiative transfer equation describes redistribution of radiation over angles, and in elastically scattering media, the energy is conserved in this process. The total energy density $\mathscr{H}$ in a multiple scattering medium, has two components, a radiative component $\mathscr{H}_\mathrm{r}$ and a material component $\mathscr{H}_\mathrm{m}$ described by $\delta_\omega(\boldsymbol{e_k})$. The energy density per frequency band $\mathscr{H}_\omega$ and the energy

density flux per frequency band, $\boldsymbol{S}_\omega$ are related to the radiance per frequency band I_ω by

$$\mathscr{H}_\omega(\boldsymbol{x},t) = \int \frac{\mathrm{d}^2 e_{\boldsymbol{k}}}{\left|\boldsymbol{v}_\mathrm{g}(\boldsymbol{e}_{\boldsymbol{k}})\right|}\left[1+\delta_\omega(\boldsymbol{e}_{\boldsymbol{k}})\right] I_\omega(\boldsymbol{e}_{\boldsymbol{k}},\boldsymbol{x},t) = \mathscr{H}_\mathrm{r}+\mathscr{H}_\mathrm{m}, \tag{3.3a}$$

$$\boldsymbol{S}_\omega(\boldsymbol{x},t) = \int \frac{\mathrm{d}^2 e_{\boldsymbol{k}}}{\left|\boldsymbol{v}_\mathrm{g}(\boldsymbol{e}_{\boldsymbol{k}})\right|}\boldsymbol{v}_\mathrm{g}(\boldsymbol{e}_{\boldsymbol{k}})\, I_\omega(\boldsymbol{e}_{\boldsymbol{k}},\boldsymbol{x},t). \tag{3.3b}$$

The material energy density in the process of scattering is

$$\delta_\omega = \frac{\mathscr{H}_{\mathrm{m}\omega}(\boldsymbol{x},t)}{\mathscr{H}_{\mathrm{r}\omega}(\boldsymbol{x},t)} = \int \frac{\mathrm{d}^2 e_{\boldsymbol{k}}}{\left|\boldsymbol{v}_\mathrm{g}(\boldsymbol{e}_{\boldsymbol{k}})\right|}\delta_\omega(\boldsymbol{e}_{\boldsymbol{k}})\frac{I_\omega(\boldsymbol{e}_{\boldsymbol{k}},\boldsymbol{x},t)}{\mathscr{H}_{\mathrm{r}\omega}(\boldsymbol{x},t)}. \tag{3.3c}$$

The radiative transfer equation (3.2) gives rise to a continuity equation for the total energy density when we integrate over $\int \mathrm{d}^2 e_{\boldsymbol{k}}$, which yields for our point source

$$\frac{\partial \mathscr{H}_\omega(\boldsymbol{x},t)}{\partial t} + \boldsymbol{\nabla}\cdot\boldsymbol{S}_\omega(\boldsymbol{x},t) = \frac{\omega^2 \mathrm{c_i}^2 \mathfrak{s}_\omega \delta^3(\boldsymbol{x})\delta(t)}{4\pi v_\mathrm{p}(\boldsymbol{e}_1)v_\mathrm{p}(\boldsymbol{e}_2)v_\mathrm{p}(\boldsymbol{e}_3)}, \tag{3.4}$$

with $\{\boldsymbol{e}_i\}$ unit vectors along the principal axes of the anisotropy. In continuity equation (3.4) for the energy density we can not see the anisotropy of the radiance anymore, because we integrated over all angles. The only explicit remnant of the anisotropy is the product of the phase velocities along the different principal axes. This product is related to the deformation of the volume element by the anisotropy of the medium. The appearance of the total energy density instead of only the radiative energy density in continuity equation (3.4) expresses the fact that frequency dependent scatterers can cause an energy density increase near or in the scatterers. Continuity equation (3.4) indicates that transport in the diffusive regime is governed by a diffusion constant which relates the sum of the radiative and material energy density to the energy density flux $\boldsymbol{S}$ [68]. In the next section we derive the diffusion constant, which in anisotropic media will be a diffusion tensor.

3.3 Diffusion

The anisotropic radiative transfer equation describes a whole range of transport phenomena without interference effects, including ballistic and diffusive transport. We have two reasons to approximate the anisotropic radiative transfer equation by an anisotropic diffusion equation. The first reason is that the radiative transfer equation is, exactly because it is such a general equation, hard to solve without resorting to numerical methods such as Monte

Carlo simulations. The anisotropic diffusion equation on the other hand, is much less complex, and can often be solve analytically. The second reason for approximating the anisotropic radiative transfer equation by an anisotropic diffusion equation is to be able to cope with interference corrections. In the literature it is well known how to add interference corrections to a diffusion equation [32, 62, 88]. In this section we approximate the anisotropic radiative transfer equation by an anisotropic diffusion equation, and determine the diffusion tensor.

The radiative transfer equation gives rise to a continuity equation (3.4) for the total energy density. Therefore, to obtain an anisotropic diffusion equation we seek for a Fick law relating the total energy density to the energy density flux, $\boldsymbol{S} = -\mathsf{D}\cdot\boldsymbol{\nabla}\mathscr{H}$, to identify the diffusion tensor. It is easiest to derive the Fick law in Fourier space where it reads $\boldsymbol{S} = \mathsf{D}\cdot \mathrm{i}\boldsymbol{P}\mathscr{H}$. In Fourier space the diffusion equation, for an isotropic point source of strength $\mathfrak{s}_\omega$, reads

$$\mathrm{i}\Omega\mathscr{H}_\omega(\boldsymbol{P},\Omega) - \mathrm{i}\boldsymbol{P}\cdot\mathsf{D}_\omega\cdot\mathrm{i}\boldsymbol{P}\mathscr{H}_\omega(\boldsymbol{P},\Omega) \quad = \quad \frac{\omega^2 \mathrm{c_i}^2 \mathfrak{s}_\omega}{4\pi v_\mathrm{p}(\boldsymbol{e}_1) v_\mathrm{p}(\boldsymbol{e}_2) v_\mathrm{p}(\boldsymbol{e}_3)}. \tag{3.5}$$

In order to identify the diffusion tensor D in (3.5) we self-consistently expand the radiance I in terms of the radiative energy density $\mathscr{H}_\mathrm{r}$ and the energy density flux $\boldsymbol{S}$,

$$\begin{aligned} I_\omega(\boldsymbol{e}_{\boldsymbol{k}},\boldsymbol{P},\Omega) \quad = \quad & \frac{|\boldsymbol{v}_\mathrm{g}(\boldsymbol{e}_{\boldsymbol{k}})|}{4\pi}\frac{v_\mathrm{p}(\boldsymbol{e}_1)v_\mathrm{p}(\boldsymbol{e}_2)v_\mathrm{p}(\boldsymbol{e}_3)}{v_\mathrm{p}^3(\boldsymbol{e}_{\boldsymbol{k}})} \\ & \times\left[\mathscr{H}_{\mathrm{r}\omega}(\boldsymbol{P},\Omega) + 3\frac{\boldsymbol{e}_{\boldsymbol{k}}\cdot\boldsymbol{S}_\omega(\boldsymbol{P},\Omega)}{\boldsymbol{e}_{\boldsymbol{k}}\cdot\boldsymbol{v}_\mathrm{g}(\boldsymbol{e}_{\boldsymbol{k}})}\right]. \end{aligned} \tag{3.6}$$

Expansion (3.6) closely resembles the often encountered ordinary multipole expansion of radiance in isotropic media [68]. It is weighted by the magnitude of the group velocity, and a ratio of phase velocities v_p, to assure Eqs. (3.3). Since we anticipate a Fick law relating the energy density and flux, the small parameter in this expansion is $\boldsymbol{P}$ multiplied by some length scale. In appendix B we derive (3.6).

Before proceeding with the derivation of the Fick law, we introduce some useful notation and a useful transport quantity. For notational convenience, we write for the average over the frequency surface,

$$\langle\ldots\rangle_{\boldsymbol{e}_{\boldsymbol{p}}} \quad \equiv \quad \frac{\int \mathrm{d}^3p\,\delta(\omega^2 - v_\mathrm{p}^2(\boldsymbol{e}_{\boldsymbol{p}})p^2)\ldots}{\int \mathrm{d}^3p\,\delta(\omega^2 - v_\mathrm{p}^2(\boldsymbol{e}_{\boldsymbol{p}})p^2)} \quad = \quad \int \frac{\mathrm{d}^2\boldsymbol{e}_{\boldsymbol{p}}}{4\pi}\frac{v_\mathrm{p}(\boldsymbol{e}_1)v_\mathrm{p}(\boldsymbol{e}_2)v_\mathrm{p}(\boldsymbol{e}_3)}{v_\mathrm{p}^3(\boldsymbol{e}_{\boldsymbol{p}})}\ldots. \tag{3.7}$$

Using (3.7), the differential scattering cross section $\mathrm{d}\sigma_{\mathrm{s}\omega}\left(\boldsymbol{e}_{\boldsymbol{k}},\boldsymbol{e}_{\boldsymbol{k}_0}\right)/\mathrm{d}^2\boldsymbol{e}_{\boldsymbol{k}_0}$ and scatterer density n, we define a tensor quantity t, with the dimension of time,

by

$$\begin{aligned} c_i t_\omega \quad &\equiv \quad 3\langle \boldsymbol{v}_g(\boldsymbol{e_k})\boldsymbol{v}_g(\boldsymbol{e_k})\rangle_{\boldsymbol{e_k}} \\ &\cdot \Big\langle \int d^2\boldsymbol{e}_{\boldsymbol{k}_0}\, n \frac{d\sigma_{s\omega}\left(\boldsymbol{e_k},\boldsymbol{e}_{\boldsymbol{k}_0}\right)}{d^2\boldsymbol{e}_{\boldsymbol{k}_0}} [\boldsymbol{v}_g(\boldsymbol{e_k}) - \boldsymbol{v}_g(\boldsymbol{e}_{\boldsymbol{k}_0})]\boldsymbol{v}_g(\boldsymbol{e_k})\Big\rangle_{\boldsymbol{e_k}}^{-1}, \end{aligned} \tag{3.8}$$

with $c_i^2 = \mathrm{Tr}[\varepsilon^{-1}]/\mathrm{Tr}[\mu]$ the isotropic part of the phase velocity v_p^2. We recognize that the trace of $c_i t$ is the transport cross section $\sigma_\omega(\boldsymbol{e_k})$ multiplied by the scatterer density n, [50], averaged over the frequency surface. Hence we can define a scalar transport time scale τ by

$$\frac{1}{c_i \tau_\omega} \quad \equiv \quad \frac{1}{3}\mathrm{Tr}[(c_i t)_\omega^{-1}] \quad = \quad \langle n\sigma_\omega(\boldsymbol{e_k})\rangle_{\boldsymbol{e_k}}\,. \tag{3.9}$$

For isotropic scatterers in an anisotropic medium the tensor t always reduces to $\tau 1$.

The Fick law for diffusion of waves in anisotropic media is obtained when we multiply equation (3.2) by the group velocity $\boldsymbol{v}_g$ and integrate over all directions $\boldsymbol{e_k}$. We drop the term $i\Omega\boldsymbol{S}$, which is of order $\Omega\boldsymbol{P}$ and is therefore beyond the diffusion approximation. Using (3.8), and $v_p^{-3}(\boldsymbol{e_k})d\sigma_{s\omega}\left(\boldsymbol{e_k},\boldsymbol{e}_{\boldsymbol{k}_0}\right)/d^2\boldsymbol{e}_{\boldsymbol{k}_0} = v_p^{-3}(\boldsymbol{e}_{\boldsymbol{k}_0})d\sigma_{s\omega}\left(\boldsymbol{e_k},\boldsymbol{e}_{\boldsymbol{k}_0}\right)/d^2\boldsymbol{e_k}$ we find a relation between the radiative energy density and the flux

$$\langle \boldsymbol{v}_g(\boldsymbol{e_k})\boldsymbol{v}_g(\boldsymbol{e_k})\rangle_{\boldsymbol{e_k}} \cdot i\boldsymbol{P}\mathscr{H}_{r\omega}(\boldsymbol{P},\Omega) \quad = \quad t_\omega^{-1}\cdot\boldsymbol{S}_\omega(\boldsymbol{P},\Omega), \tag{3.10}$$

which is of the form $\boldsymbol{S} = D\cdot i\boldsymbol{P}\mathscr{H}$. We can replace the radiative energy density $\mathscr{H}_r$ by the total energy density $\mathscr{H}$ through the relation $\mathscr{H} = [1+\delta]\mathscr{H}_r$, which follows from Eqs. (3.3a) and (3.3c). The diffusion tensor, relating total energy density $\mathscr{H}$ and flux $\boldsymbol{S}$ becomes,

$$D_\omega \quad \equiv \quad \frac{t_\omega\cdot\langle \boldsymbol{v}_g(\boldsymbol{e_k})\boldsymbol{v}_g(\boldsymbol{e_k})\rangle_{\boldsymbol{e_k}}}{1+\delta_\omega}, \tag{3.11a}$$

$$= \quad \frac{\langle \boldsymbol{v}_g(\boldsymbol{e_k})\boldsymbol{v}_g(\boldsymbol{e_k})\rangle_{\boldsymbol{e_k}}\cdot t_\omega^{T}}{1+\delta_\omega} \quad = \quad D_\omega{}^{T}, \tag{3.11b}$$

which is the result we announced at the beginning of this section. To obtain Eq. (3.11b)we use $\langle\int d^2\boldsymbol{e}_{\boldsymbol{k}_0} n d\sigma_{s\omega}\left(\boldsymbol{e_k},\boldsymbol{e}_{\boldsymbol{k}_0}\right)/d^2\boldsymbol{e}_{\boldsymbol{k}_0}[\boldsymbol{v}_g(\boldsymbol{e_k}) - \boldsymbol{v}_g(\boldsymbol{e}_{\boldsymbol{k}_0})]\boldsymbol{v}_g(\boldsymbol{e_k})\rangle_{\boldsymbol{e_k}}$, which is sandwiched between two identical symmetric tensors $\langle \boldsymbol{v}_g\boldsymbol{v}_g\rangle$, is itself also symmetric under transposition, because $v_p^{-3}(\boldsymbol{e_k})d\sigma_{s\omega}\left(\boldsymbol{e_k},\boldsymbol{e}_{\boldsymbol{k}_0}\right)/d^2\boldsymbol{e}_{\boldsymbol{k}_0}$ is symmetric with respect to switching $\boldsymbol{e_k}$ and $\boldsymbol{e}_{\boldsymbol{k}_0}$. We do not obtain an expression in terms of a transport mean free path and a transport velocity, because such a partitioning can only be defined unambiguously in the presence of a boundary, which is beyond the scope of this paper [50]. For isotropic scatterers in anisotropic media, the diffusion tensor (3.11) reduces to

$\mathsf{D}_\omega = \tau_\omega \langle \boldsymbol{v}_\mathrm{g} \boldsymbol{v}_\mathrm{g} \rangle / (1+\delta_\omega)$, whereas for anisotropic scatterers in an isotropic medium we end up with anisotropy in t alone, $\mathsf{D}_\omega = \mathsf{t}_\omega {\mathrm{c_i}}^2 / [3(1+\delta_\omega)]$. In fully isotropic media we recover the familiar result $\mathsf{D}_\omega = \tau_\omega {\mathrm{c_i}}^2 / [3(1+\delta_\omega)]$, [68]. In section 3.4 we present the solution to diffusion equation (3.5) in space and time coordinates $\boldsymbol{x}$ and t, and we compare certain results for anisotropic media with isotropic media.

3.4 Examples of anisotropic diffusion and its extremities

In this section we take an instantaneous point source and solve the diffusion equation. We treat the solution of the diffusion equation for some special cases of scatterers and host media, and discuss the limits of extreme anisotropy.

The magnetic permeability tensor of the host medium is assumed to be isotropic, $\mu = \frac{1}{3}\mathrm{Tr}[\mu]1$, whereas the dielectric tensor can be anisotropic. In these examples we take the anisotropic host dielectric permittivity tensor on principal axes. In a convenient Cartesian coordinate system we have

$$\varepsilon \quad = \quad \varepsilon_{xx}\boldsymbol{e}_x\boldsymbol{e}_x + \varepsilon_{yy}\boldsymbol{e}_y\boldsymbol{e}_y + \varepsilon_{zz}\boldsymbol{e}_z\boldsymbol{e}_z, \tag{3.12}$$

and the anisotropy tensor A is

$$\mathsf{A} \quad = \quad 3\frac{\varepsilon_{yy}\varepsilon_{zz}\boldsymbol{e}_x\boldsymbol{e}_x + \varepsilon_{xx}\varepsilon_{zz}\boldsymbol{e}_y\boldsymbol{e}_y + \varepsilon_{xx}\varepsilon_{yy}\boldsymbol{e}_z\boldsymbol{e}_z}{\varepsilon_{yy}\varepsilon_{zz} + \varepsilon_{xx}\varepsilon_{zz} + \varepsilon_{xx}\varepsilon_{yy}}. \tag{3.13}$$

We include elastic isotropic point scatterers, with some scattering cross section, that is constant with respect to wave vector, but dependent on frequency,

$$\sigma_{\mathrm{e}\omega} \quad = \quad \sigma_{\mathrm{s}\omega}. \tag{3.14}$$

For isotropic point scatterers in an anisotropic medium we obtain for the diffusion tensor

$$\mathsf{D}_\omega \quad = \quad \frac{1}{3}\frac{\tau_\omega {\mathrm{c_i}}^2}{1+\delta_\omega}\mathsf{A}. \tag{3.15}$$

The instantaneous isotropic point source for the diffusion equation is

$$\mathfrak{s}_\omega \delta^3(\boldsymbol{x})\delta(t) \tag{3.16}$$

The source strength $\mathfrak{s}_\omega$ has *SI* units of $\mathrm{J\,m\,s^2}$.

3.4.a Isotropic media

In isotropic media we have $\varepsilon_{xx} = \varepsilon_{yy} = \varepsilon_{zz}$ and therefore

$$\mathsf{A} \quad = \quad 1, \tag{3.17}$$

The diffusion tensor becomes proportional to the unit tensor

$$\mathsf{D}_\omega \quad = \quad \frac{1}{3}\frac{\tau_\omega {\mathrm{c_i}}^2}{1+\delta_\omega}1 \quad = \quad D_\omega 1. \tag{3.18}$$

Here D is the trace of the isotropic diffusion tensor, and is the diffusion constant for the isotropic medium.

In space and time coordinates diffusion equation (3.5) for a point source of strength $\mathfrak{s}_\omega$ has the familiar form

$$\frac{\partial \mathscr{H}_\omega(\boldsymbol{x},t)}{\partial t} - D_\omega \boldsymbol{\nabla}\cdot\boldsymbol{\nabla}\mathscr{H}_\omega(\boldsymbol{x},t) \quad = \quad \frac{\omega^2 \mathfrak{s}_\omega \delta^3(\boldsymbol{x})\delta(t)}{4\pi \mathrm{c_i}}. \tag{3.19}$$

In disordered infinite media the energy density from the instantaneous point source is spread thinly, and at infinity the energy density is negligible,

$$\lim_{|\boldsymbol{x}|\to\infty} \mathscr{H}_\omega(t,\boldsymbol{x}) \quad = \quad 0. \tag{3.20}$$

The solution for isotropic diffuse energy density $\mathscr{H}_\omega(\boldsymbol{x},t)$ in a infinite medium is well known, it is

$$\mathscr{H}_\omega(\boldsymbol{x},t) \quad = \quad \frac{\omega^2\mathfrak{s}_\omega}{4\pi \mathrm{c_i}} \frac{\exp\left[-\frac{|\boldsymbol{x}|^2}{4D_\omega t}\right]}{(4\pi D_\omega t)^{\frac{3}{2}}}. \tag{3.21}$$

In isotropic media the energy density distribution is an isotropic Gaussian with variance $2D_\omega t$. We can ask the question if we can define a mean free path for diffusion in unbounded media. The answer is no, because mean free paths are defined as the length scale after which something has decayed exponentially. So maybe we should look for exponential decay in the stationary limit. When we integrate (3.21) from $t = 0$ to infinity, then we obtain the stationary solution

$$\mathscr{H}_\omega(\boldsymbol{x}) \quad = \quad \frac{\omega^2\mathfrak{s}_\omega}{4\pi \mathrm{c_i}} \frac{1}{4\pi D_\omega |\boldsymbol{x}|}. \tag{3.22}$$

The stationary solution (3.22) does not decay exponentially either. We conclude again that in unbounded media it is impossible to define an exponential decay length for the energy density. In bounded media the boundary conditions define the partitioning of the diffusion constant in an energy velocity and a transport mean free path according to $D = vl/3$, but bounded media are beyond the scope of this chapter. We see that the amount of energy density at each location is governed by the diffusion constant

3.4.b Anisotropic media

In space and time coordinates the diffusion equation given a point source of strength $\mathfrak{s}_\omega$ reads,

$$\frac{\partial \mathscr{H}_\omega(\boldsymbol{x},t)}{\partial t} - \boldsymbol{\nabla}\cdot \mathsf{D}_\omega \cdot \boldsymbol{\nabla}\mathscr{H}_\omega(\boldsymbol{x},t) \quad = \quad \frac{\omega^2 \mathrm{c_i}^2 \mathfrak{s}_\omega \delta^3(\boldsymbol{x})\delta(t)}{4\pi v_\mathrm{p}(\boldsymbol{e}_1) v_\mathrm{p}(\boldsymbol{e}_2) v_\mathrm{p}(\boldsymbol{e}_3)}. \tag{3.23}$$

Also in anisotropic disordered infinite media the energy density from the instantaneous point source is spread thinly, and at infinity the energy density is negligible,

$$\lim_{|\boldsymbol{x}|\to\infty} \mathscr{H}_\omega(t,\boldsymbol{x}) \quad = \quad 0. \tag{3.24}$$

The solution for the diffuse energy density $\mathscr{H}_\omega(\boldsymbol{x},t)$ is in anisotropic media

$$\mathscr{H}_\omega(\boldsymbol{x},t) \quad = \quad \frac{\omega^2 \mathrm{c_i}^2 \mathfrak{s}_\omega}{4\pi v_\mathrm{p}(\boldsymbol{e}_1) v_\mathrm{p}(\boldsymbol{e}_2) v_\mathrm{p}(\boldsymbol{e}_3)} \frac{\exp\left[-\frac{\boldsymbol{x}\cdot \mathsf{D}^{-1}\cdot \boldsymbol{x}}{4t}\right]}{(4\pi t)^{\frac{3}{2}}\sqrt{\det \mathsf{D}}}. \tag{3.25}$$

The energy density distribution is a three dimensional anisotropic Gaussian with variance $2t/\boldsymbol{e}_{\boldsymbol{x}}\cdot \mathsf{D}^{-1}\cdot \boldsymbol{e}_{\boldsymbol{x}}$. When we integrate (3.25) from $t=0$ to infinity, then we obtain the anisotropic stationary solution

$$\mathscr{H}_\omega(\boldsymbol{x}) \quad = \quad \frac{\omega^2 \mathrm{c_i}^2 \mathfrak{s}_\omega}{4\pi v_\mathrm{p}(\boldsymbol{e}_1) v_\mathrm{p}(\boldsymbol{e}_2) v_\mathrm{p}(\boldsymbol{e}_3)} \frac{1}{4\pi\sqrt{\det \mathsf{D}}\sqrt{\boldsymbol{x}\cdot \mathsf{D}^{-1}\cdot \boldsymbol{x}}}. \tag{3.26}$$

Compared with the isotropic solutions (3.21) and (3.22) are clearly anisotropic, as each direction is weighted differently by the diffusion tensor.

In order to clarify the effects we consider a uniaxial dielectric. Uniaxial media are characterized by a dimensionless anisotropy parameter $a > -1$ and an optical axes. If the optical axis is along $\boldsymbol{e}_z$, the uniaxial permittivity is given by

$$\varepsilon \quad = \quad \frac{3+a}{\mathrm{c_i}^2 \mathrm{Tr}[\mu]}\left[1 - \frac{a}{1+a}\boldsymbol{e}_z\boldsymbol{e}_z\right], \tag{3.27}$$

and the anisotropy tensor reduces to

$$\mathsf{A} \quad = \quad \frac{3}{3+a}\left[1 + a\boldsymbol{e}_z\boldsymbol{e}_z\right]. \tag{3.28}$$

The diffusion tensor becomes

$$\mathsf{D}_\omega \quad = \quad \frac{1}{3}\frac{\tau_\omega \mathrm{c_i}^2}{1+\delta_\omega}\mathsf{A} \quad = \quad \frac{1}{3+a}\frac{\tau_\omega \mathrm{c_i}^2}{1+\delta_\omega}\left[1 + a\boldsymbol{e}_z\boldsymbol{e}_z\right]. \tag{3.29}$$

For all a the trace of the diffusion tensor is given by

$$\mathrm{Tr}[\mathsf{D}_\omega] \quad = \quad \frac{\tau_\omega {c_i}^2}{1+\delta_\omega}. \tag{3.30}$$

Our diffusion tensor was obtained using a mapping of the energy of electromagnetic waves onto scalar waves. There are two types of propagating electromagnetic waves in uniaxial media, the ordinary waves, which are subject to an isotropic dispersion relation, and the extraordinary waves, which are subject to an anisotropic dispersion relation. It is well known that in uniaxial dielectrics with one principal axis longer than the other axes, the extraordinary wave dominates [93]. In our mapping of electromagnetic waves to scalar waves, the parameter range $-1 < a < 0$ is therefore of most interest, because in this range light is most sensitive to the anisotropy. For $a = 0$ we recover isotropic media, whereas for $a > 0$, the anisotropy of the dielectric has a smaller effect on the transport of electromagnetic waves as more of the wave energy will be transported by the ordinary waves than by the extraordinary waves.

In porous materials such as the etched semiconductor Gallium Phosphide [76], the aligned air cylinders have a low permittivity compared to the GaP. In this material the ordinary waves carry more energy than the extraordinary waves. Still,in GaP exists strong optical anisotropy, leading even to a ratio of four between principal diffusion constants. Equation (3.29) can be used for a description of the anisotropic diffusion light in porous GaP. We let the total energy density of both ordinary and extraordinary waves diffuse anisotropically, and we set anisotropy parameter $a = 3$. Alternatively we could construct the diffusion of energy in GaP out of a weighed sum of an isotropically diffusing ordinary and an anisotropically diffusing extraordinary contribution. Such a sum may yield better results, but we must note that the scattering delay and the mean free time need to be evaluated for both the isotropic and the anisotropic waves.

Stronger anisotropic diffusion is to be expected if we have disordered samples of aligned GaP cylinders (e.g. nanowires [94]) in air instead of porous Gap, because the contribution of the anisotropically diffusing extraordinary waves to the diffusion outweighs the contribution of the isotropically diffusing ordinary waves. The expected anisotropy parameter to use for the description of anisotropic diffusion of the total radiance is at worst $a = -3/4$, but probably $a < -3/4$ due to the domination of extraordinary waves.

3.4.c Dimensionality in anisotropic diffusion

In our result for the uniaxial diffusion constant, Eq. (3.29), it is clear that the anisotropy alters the factor 3 by an amount a. The factor three is always ob-

tained in isotropic media. The fact that we find $3+a$ suggests the possibility of a dimensional cross over, because in three dimensional we can write down a single diffusion constant by $D = \mathrm{Tr}[\mathsf{D}]/3$ where the factor 3 is the dimensionality of the medium. We can compare this to the expression for the diffusion constant in terms of mean free path l and energy velocity v, which is $D = vl/3$ [68], and we observe that $\mathrm{Tr}[\mathsf{D}]$ plays the role of vl. We can explore the limits of (3.29), in the hope to find $D = \mathrm{Tr}[\mathsf{D}]/2$ or even $D = \mathrm{Tr}[\mathsf{D}]$ for two and one dimensional media respectively. Below we discussion of these limits assuming that $\mathrm{Tr}[\mathsf{D}]$ is nonzero and finite in the limits $a \to -1$ and $a \to \infty$. Afterwards we will discuss the behavior of $\mathrm{Tr}[\mathsf{D}]$.

When we take $a \to \infty$ we obtain the limit of one dimensional diffusion. Even though at first sight it may seem that for $a > 0$ we can increase the factor three to any desired value, this observation is incorrect. Actually two of the three principal diffusion constants vanish, because the limit for both the D_{xx} and D_{yy} components is

$$\lim_{a\to\infty} \frac{\mathrm{Tr}[\mathsf{D}_\omega]}{3+a} = 0. \tag{3.31a}$$

For the D_{zz} component the limit is nonzero and finite, it is

$$\lim_{a\to\infty} \frac{\mathrm{Tr}[\mathsf{D}_\omega](1+a)}{3+a} = \mathrm{Tr}[\mathsf{D}]. \tag{3.31b}$$

For the dielectric tensor the limit $a \to \infty$ implies that both ε_{xx} and ε_{yy} go to infinity, while ε_{zz} remains finite. Also the width of the energy distributions (3.25) and (3.26) vanishes in both the x and y directions, and thus we have typical one dimensional diffusion.

The limit $a \to -1$ leads to two dimensional diffusion. In this limit ε_{zz} becomes infinite, while ε_{xx} and ε_{yy} remain finite. For the principal diffusion constants we have

$$\lim_{a\to-1} \frac{\mathrm{Tr}[\mathsf{D}_\omega]}{3+a} = \frac{\mathrm{Tr}[\mathsf{D}]}{2}, \tag{3.32a}$$

$$\lim_{a\to-1} \frac{\mathrm{Tr}[\mathsf{D}_\omega](1+a)}{3+a} = 0. \tag{3.32b}$$

The width of the energy distributions (3.25) and (3.26) vanishes in the z direction, and thus the dimensionality of our problem becomes two instead of three.

There are caveats while taking the limits $a \to \infty$ and $a \to -1$, the first is that many workers in the field obtained diverging diffusion solutions in one and two dimensions [88, 89], and concluded that in infinite media lower than three dimensions the diffusion asymptotics do not exist. The basis for this

conclusion is the contribution of interference effects to wave transport. Our starting point for the derivation of diffusion was the radiative transfer equation, so there are no interference effects to cause this divergence. The second caveat is that also the determinant of A vanishes in the limit $a \to -1$, which can cause divergences for us. The determinant is present in the transport time $\tau = 1/(c_i n\sigma)$, because from the optical theorem it follows that $\sigma \propto \sqrt{\det \mathsf{A}}$, and thus we seem to create a division by zero. However, to make the cross section satisfy the dispersion relation, already an integration over the magnitude of wave vector $\boldsymbol{p}$ has been carried out. In that integration we should also take $a \to -1$, and here the zero in A_{zz} naturally cancels the integration in the z direction, and we are saved. On top of that in Eq. (3.7) we could also run into trouble when $a \to -1$, but here as well we have vanishing A_{zz} which naturally cancel diverging integrations along the z direction.

Sometimes we encounter biaxial media, and for completeness we treat the possible dimensional crossovers. Biaxial media have two anisotropy parameters a_{yy} and a_{zz} which range from -1 to ∞. We generalize our uniaxial medium to a biaxial medium according to

$$\varepsilon = \frac{3 + a_{yy} + a_{zz}}{{c_i}^2 \mathrm{Tr}[\mu]} \left[1 - \frac{a_{yy}}{1 + a_{yy}} \boldsymbol{e}_y \boldsymbol{e}_y - \frac{a_{zz}}{1 + a_{zz}} \boldsymbol{e}_z \boldsymbol{e}_z \right], \tag{3.33}$$

and the anisotropy tensor reduces to

$$\mathsf{A} = \frac{3}{3 + a_{yy} + a_{zz}} \left[1 + a_{yy} \boldsymbol{e}_y \boldsymbol{e}_y + a_{zz} \boldsymbol{e}_z \boldsymbol{e}_z \right]. \tag{3.34}$$

The biaxial diffusion tensor reads

$$\mathsf{D}_\omega = \frac{1}{3} \frac{\tau_\omega {c_i}^2}{1 + \delta_\omega} \mathsf{A} = \frac{1}{3 + a_{yy} + a_{zz}} \frac{\tau_\omega {c_i}^2}{1 + \delta_\omega} \left[1 + a_{yy} \boldsymbol{e}_y \boldsymbol{e}_y + a_{zz} \boldsymbol{e}_z \boldsymbol{e}_z \right]. \tag{3.35}$$

and again for all values of the anisotropy parameters the trace is given by (3.30). We can obtain a factor of two instead of 3 for all values such that $a_{yy} + a_{zz} = -1$, but for these values there is no vanishing of diffusion constants, and no cross over to a lower dimensional medium. There are three limits that were not possible for uniaxial media, both a_{yy} and a_{zz} to infinity or -1, and one of the two to infinity, while the other goes to -1. When both parameters are taken to infinity independently all principal diffusion constants vanish. We only obtain a nonzero result for the some of the principal diffusion constants when $a_{yy} = a_{zz}$, which reduces the biaxial medium to a uniaxial medium, but with a parametrization different from (3.28). Instead of diffusion in the xy planes, we obtain diffusion in the xz plane. For a_{yy} and

a_{zz} to -1 independently also all principal diffusion constants vanish. When $a_{yy} = a_{zz}$ we again have a uniaxial medium, but with one dimensional diffusion is along the x axis. when we take $a_{yy} \to -1$ and $a_{zz} \to \infty$ we obtain one dimensional diffusion along the z axis, and the other principal diffusion constants vanish. Finally, when these limits are switched, we find one dimensional diffusion along the y axis.

Vector waves in uniaxial media can be separated in ordinary and extraordinary waves. In uniaxial media with two principal permittivities larger than the third the ordinary waves dominate ($a > 0$). Hence the contribution of the anisotropic diffusion of the energy of the ordinary waves to the total energy density is outweighed by the isotropic diffusing ordinary wavesBased on the argument that extraordinary waves transport the larger part of the energy in media with $a < 0$, provided we can overcome the difficulty of creating the required anisotropy, it is much more likely that a cross over to two dimensional diffusion occurs than a cross over to one dimensional diffusion.

3.5 Reciprocity and Transport

Neither the anisotropic diffusion equation (3.5), nor the more general anisotropic radiative transfer equation (3.2) contain interference effects or satisfy reciprocity. Had the radiative transfer equation satisfied reciprocity, then the survival of the interference effect for multiple scattered waves known as enhanced backscattering would not have been such a big surprise some twenty three years ago. In this section we explain the effect of reciprocity and relate it to interference corrections.

Reciprocity is satisfied by the Green function for the wave amplitude, and is in coordinate space or wave vector space given by [6],

$$G_\omega(\boldsymbol{x}_1, \boldsymbol{x}_2) = G_\omega(\boldsymbol{x}_2, \boldsymbol{x}_1), \tag{3.36a}$$

$$G_\omega(\boldsymbol{p}_1, \boldsymbol{p}_2) = G_\omega(-\boldsymbol{p}_2, -\boldsymbol{p}_1). \tag{3.36b}$$

Eq. (3.36a) expresses the principle that a cause at $\boldsymbol{x}_2$ has the same effect at $\boldsymbol{x}_1$, as when the cause were at $\boldsymbol{x}_1$ and the effect were at $\boldsymbol{x}_2$. In the wave vector terminology of Eq. (3.36b) we have extra minus signs, because the direction of propagation reverses in a reciprocity operation. In anisotropic media the direction of the wave vector is not the same as the propagation direction, but for scalar waves there is a unique relation between them.

The microscopic quantity that underlies the radiance is a product of the amplitude Green function with its complex conjugate, and depends on four wave vectors. We will consider the quantity $\Phi_\omega(\boldsymbol{p}, \tilde{\boldsymbol{p}}, \boldsymbol{P}, \Omega)$, as the product of amplitude Green functions obtained in phase space after extraction of a

momentum conserving Dirac delta function. This quantity must have certain symmetries due to reciprocity, expressed by the equalities

$$\Phi_\omega(\boldsymbol{p},\tilde{\boldsymbol{p}},\boldsymbol{P},\Omega) = \Phi_\omega(-\tilde{\boldsymbol{p}},-\boldsymbol{p},-\boldsymbol{P},\Omega), \tag{3.37a}$$

$$\Phi_\omega(\boldsymbol{p},\tilde{\boldsymbol{p}},\boldsymbol{P},\Omega) = \Phi_\omega(\frac{\boldsymbol{P}+\boldsymbol{p}-\tilde{\boldsymbol{p}}}{2},\frac{\boldsymbol{P}-\boldsymbol{p}+\tilde{\boldsymbol{p}}}{2},\boldsymbol{p}+\tilde{\boldsymbol{p}},\Omega), \tag{3.37b}$$

$$\Phi_\omega(\boldsymbol{p},\tilde{\boldsymbol{p}},\boldsymbol{P},\Omega) = \Phi_\omega(\frac{\tilde{\boldsymbol{p}}-\boldsymbol{p}-\boldsymbol{P}}{2},\frac{\boldsymbol{p}-\tilde{\boldsymbol{p}}-\boldsymbol{P}}{2},-\boldsymbol{p}-\tilde{\boldsymbol{p}},\Omega). \tag{3.37c}$$

In Eq. (3.37a) we interchanged cause and effect in both amplitude Green functions, which is a reciprocity symmetry in energy transport that is also satisfied by the radiative transfer equation. In Eq. (3.37b) however, we interchange cause and effect in only one amplitude, whereas in (3.37c) we change cause and effect only in the conjugate amplitude, which is just application of symmetry (3.36b).

Neither the radiative transfer equation nor the diffusion equation satisfy Eq. (3.37b) or Eq. (3.37c). If we define Φ_B to be the solution in the Boltzmann limit, i.e. the solution to either the anisotropic radiative transfer equation or the anisotropic diffusion equation, then we can write

$$\Phi_\omega(\boldsymbol{p},\tilde{\boldsymbol{p}},\boldsymbol{P},\Omega) = \Phi_{\mathrm{B}\omega}(\boldsymbol{p},\tilde{\boldsymbol{p}},\boldsymbol{P},\Omega)+\Phi_{\mathrm{c}\omega}(\boldsymbol{p},\tilde{\boldsymbol{p}},\boldsymbol{P},\Omega). \tag{3.38}$$

Here Φ_c contains all terms neglected by the Boltzmann approximation Φ_B, and Φ satisfies energy conservation.

A first attempt to add interference corrections to the radiative transfer equation whilst keeping the energy conserved has been presented by Stephen [95]. We temporarily disregard the energy conservation law for Φ, because then we can take Φ_c to be the reciprocal conjugate to Φ_B. In this way it is easiest to restore the full reciprocity symmetry for the diffusive solution, because that solution depends only on wave vector $\boldsymbol{P}$ describing the envelope of the energy density packet, but not on the wave vector $\boldsymbol{p}$ of the internal oscillation. The diffusion solution for Φ_B is, in terms of eigenfunctions Ψ_0 in the diffusive regime, given by

$$\Phi_{\mathrm{B}\omega}(\boldsymbol{p},\tilde{\boldsymbol{p}},\boldsymbol{P},\Omega) \equiv \frac{\Psi^*_{0\omega}(\boldsymbol{p},\boldsymbol{P},\Omega)\Psi_{0\omega}(\tilde{\boldsymbol{p}},\boldsymbol{P},\Omega)}{\mathrm{i}\Omega-\mathrm{i}\boldsymbol{P}\cdot\mathsf{D}_{\mathrm{B}\omega}\cdot\mathrm{i}\boldsymbol{P}}, \tag{3.39}$$

where D_B is the diffusion tensor in the Boltzmann limit (3.11). The interference correction to the diffusion solution follows from reciprocity symmetry (3.37b) and is found to be

$$\Phi_{\mathrm{c}\omega}(\boldsymbol{p},\tilde{\boldsymbol{p}},\boldsymbol{P},\Omega) \equiv \frac{\Psi^*_{0\omega}(\frac{\boldsymbol{P}}{2}-\frac{\boldsymbol{p}-\tilde{\boldsymbol{p}}}{2},\boldsymbol{p}+\tilde{\boldsymbol{p}},\Omega)\Psi_{0\omega}(\frac{\boldsymbol{P}}{2}+\frac{\boldsymbol{p}-\tilde{\boldsymbol{p}}}{2},\boldsymbol{p}+\tilde{\boldsymbol{p}},\Omega)}{\mathrm{i}\Omega-\mathrm{i}(\boldsymbol{p}+\tilde{\boldsymbol{p}})\cdot\mathsf{D}_{\mathrm{B}\omega}\cdot\mathrm{i}(\boldsymbol{p}+\tilde{\boldsymbol{p}})}. \tag{3.40}$$

Equations (3.39) and (3.40) break energy conservation. In the Boltzmann limit we approximated the eigenfunctions $\mathrm{Im}[G]$ by the independent scattering approximation and set $\mathrm{Im}[G] \to \mathrm{Im}[g]$, with g the Green function for the homogeneous medium. Using these approximations we obtained diffusion constant (3.11), here denoted by D_B. The rigorous eigenfunction with long range diffusion is $\mathrm{Im}[G]$, and D is the diffusion tensor related to the eigenfunction $\mathrm{Im}[G]$. To restore energy conservation for Φ we should replace D_B by the renormalized diffusion tensor D, and the eigenfunctions Ψ_0^* and Ψ_0 in (3.39) and (3.40) by the eigenfunctions $\mathrm{Im}[G]$, which are valid beyond the Boltzmann limit. In practice it is very hard to work with eigenfunctions $\mathrm{Im}[G]$ and directly obtain the renormalized diffusion tensor D. Instead, interference corrections to the derivation of D_B are added, and an equation for D is obtained in terms of D_B.

For stationary solutions we have $\Omega = 0$, and the main contribution from the reciprocity symmetry (3.37b) occurs when the denominator vanishes, i.e. at $\tilde{\boldsymbol{p}} = -\boldsymbol{p}$, which is exactly where the tip of the enhanced backscattering cone is. Just like the diffusion equation, which can be seen as an expansion of the exact solution to the radiative transfer equation up to and including $\mathrm{O}[(\mathrm{c_i}\tau P)^2]$, the interference correction to diffusion is also an approximation to the exact interference correction.

3.6 Ioffe-Regel criterion

In this section we calculate the strength of the disorder in anisotropic media required to induce the transition to Anderson localization, and compare it to the known result for isotropic media. Starting from the anisotropic equation of radiative transfer (3.2), we have identified the diffusion tensor (3.11) in the anisotropic diffusion equation (3.5). The anisotropic diffusion solution was derived in the limit of low scatterer density n. We have shown that we can add an interference correction to solution (3.40).

We consider an anisotropic host medium with elastic isotropic point scatterers. Following Vollhardt and Wölfle and others [32, 62, 88, 96], we improve the Boltzmann approximation of the irreducible Bethe-Salpeter vertex by adding the terms correcting reciprocity symmetry, and by replacing the Boltzmann diffusion tensor (3.11) by the renormalized diffusion tensor D,

$$U_\omega(\boldsymbol{p},\boldsymbol{p}_0,\boldsymbol{0},0) = n\,|T_\omega|^2 + \frac{4\pi}{\mathrm{c_i}\tau_\omega{}^2}\,\frac{\sqrt{\det \mathsf{A}}}{1+\delta_\omega}\,\frac{1}{(\boldsymbol{p}+\boldsymbol{p}_0)\cdot \mathsf{D}_\omega \cdot (\boldsymbol{p}+\boldsymbol{p}_0)}. \tag{3.41}$$

The density of states factor $\sqrt{\det \mathsf{A}}/(1+\delta_\omega)$ was accidentally omitted in [50], but this does not alter the conclusions of that paper.

To obtain the interference correction to the diffusion tensor, then according to Eq. (B.19), we need to calculate the object Γ, determined by equation (B.18),

$$\Gamma_\omega(\boldsymbol{p},\boldsymbol{P}) \quad = \quad \boldsymbol{P}\cdot\frac{{c_i}^2}{\omega}\mathsf{A}\cdot\boldsymbol{p}+\int\frac{\mathrm{d}^3p_0}{(2\pi)^3}U_\omega(\boldsymbol{p},\boldsymbol{p}_0,\boldsymbol{0},0)|G_\omega(\boldsymbol{p}_0)|^2\Gamma(\boldsymbol{p}_0,\boldsymbol{P}). \tag{3.42}$$

When we consider the Boltzmann limit for isotropic scatterers $U_\mathrm{B} = n|T|^2$, then $\Gamma_\omega(\boldsymbol{p},\boldsymbol{P}) = {c_i}^2\boldsymbol{P}\cdot\mathsf{A}\cdot\boldsymbol{p}/\omega$ due the fact that the integrand is odd in $\boldsymbol{p}_0$ and vanishes. This automatically leads to our previous result for the diffusion tensor (3.11).

The correction to the Boltzmann limit is most relevant when $\boldsymbol{p}\approx-\boldsymbol{p}_0$. $[(\boldsymbol{p}+\boldsymbol{p}_0)\cdot\mathsf{D}\cdot(\boldsymbol{p}+\boldsymbol{p}_0)]^{-1} = \delta^3(\boldsymbol{p}+\boldsymbol{p}_0)/\det\mathsf{A}\int\mathrm{d}^3p_1[\boldsymbol{p}_1\cdot\mathsf{D}\cdot\boldsymbol{p}_1]^{-1}$. where the integral is carried out over a subset of wave vectors with upper bound $k_\mathrm{max}(\boldsymbol{e_k}) = \beta/(\boldsymbol{e_k}\cdot\tau_\omega\boldsymbol{v}_\mathrm{g}(\boldsymbol{e_k}))$, with β some dimensionless numerical constant. The cutoff k_max regularizes the divergence that occurs in the Green function $G_{\mathscr{H}}(\boldsymbol{x},\boldsymbol{x}_0)$ for diffuse energy density when $\boldsymbol{x}\to\boldsymbol{x}_0$. The product $\tau_\omega\boldsymbol{v}_\mathrm{g}(\boldsymbol{e_k}))$ is the extinction or scattering mean free path in an elastic anisotropic medium, because we consider elastic isotropic point scatterers it also coincides with the transport mean free path in anisotropic media [50].

The function $\Gamma_\omega(\boldsymbol{p},\boldsymbol{P})$ is odd in $\boldsymbol{p}$ also after adding the correction to the Boltzmann limit, i.e. $\Gamma_\omega(\boldsymbol{p},\boldsymbol{P}) = -\Gamma_\omega(-\boldsymbol{p},\boldsymbol{P})$. Using the equality $|G_\omega(\boldsymbol{p})|^2 = \mathrm{Im}[G_\omega(\boldsymbol{p})]/\mathrm{Im}[\Sigma_\omega] = -\mathrm{Im}[G_\omega(\boldsymbol{p})]{c_i}^2\tau_\omega/\omega$, together with the on-shell equality $\mathrm{Im}[G_\omega(\boldsymbol{p})] = -{c_i}^2\tau_\omega/\omega$, we obtain

$$\frac{\omega\Gamma_\omega(\boldsymbol{p},\boldsymbol{P})}{{c_i}^2\boldsymbol{P}\cdot\mathsf{A}\cdot\boldsymbol{p}} \quad = \quad \left[1+\frac{4\pi{c_i}^3}{\omega^2\sqrt{\det\mathsf{A}}}\int\frac{\mathrm{d}^3p_1}{(2\pi)^3}\frac{1}{\boldsymbol{p}_1\cdot\mathsf{D}\cdot\boldsymbol{p}_1}\right]^{-1} \quad = \quad \text{const.} \tag{3.43}$$

Using result (3.43) in Eq. (B.19) yields

$$\boldsymbol{P}\cdot\mathsf{D}\cdot\boldsymbol{P} \quad = \quad \boldsymbol{P}\cdot\mathsf{D}_\mathrm{B}\cdot\boldsymbol{P}\left[1+\frac{4\pi{c_i}^3}{\omega^2\sqrt{\det\mathsf{A}}}\int\frac{\mathrm{d}^3p_1}{(2\pi)^3}\frac{1}{\boldsymbol{p}_1\cdot\mathsf{D}\cdot\boldsymbol{p}_1}\right]^{-1}. \tag{3.44}$$

The Boltzmann diffusion tensor D_B is renormalized by the multiplicative constant (3.43). The anisotropy of the diffusion tensor is not altered, and therefore we can exchange the D in the integral with the D_B outside the integral. Eq. (B.19) holds for any direction of $\boldsymbol{P}$, and $\mathsf{D} = \mathsf{D}^\mathrm{T}$, so we can remove the $\boldsymbol{P}$ from the equation.

We choose parameter $\beta = \pi/6$ to set the isotropic Ioffe-Regel criterion at $\omega\tau_\omega = 1$ for an isotropic medium. This leads to

$$\mathsf{D}^{-1} \quad = \quad {\mathsf{D}_\mathrm{B}}^{-1}+\left[\frac{1}{\sqrt{\det\mathsf{A}}\omega\tau_\omega}\right]^2\mathsf{D}^{-1}, \tag{3.45}$$

where D_B is given by (3.11). The transition to Anderson localization occurs when

$$\omega\tau_{c\omega} = \frac{1}{\sqrt{\det A}} \geq 1. \tag{3.46}$$

The transition is affected by the anisotropy in the dielectric tensor the determinant of anisotropy tensor A. We can check that both $\omega\tau_c$ and $1/\sqrt{\det A}$ scale in the same way when we alter the anisotropy, (2.15). This means that given a mean free time near the transition to Anderson localization in an isotropic medium, and consider an identical a mean free time in an anisotropic medium, then the anisotropic medium could already be beyond the transition to Anderson localization.

Our result can be compared with the potential well analogy [61]. The potential well analogy predicts the mobility edge to occur at $Sl^2 \approx 9$, with S the Fermi surface, and l the magnitude of the mean free path averaged over the Fermi surface. For our classical waves describing light the Fermi surface is the surface of constant frequency $S = \omega^2/(c_i{}^2\sqrt{\det A})$. The mean free path averaged over the surface of constant frequency is $l = \langle|\boldsymbol{l}(\boldsymbol{e_k})|\rangle_{\boldsymbol{e_k}} = c_i\tau_\omega\sqrt{\det A}$. Inserting this result in $Sl^2 = 9$ yields $\omega\tau_{c\omega} \approx 3$. Had we taken our parameter $\beta = \det A\pi/(2)$ instead of $\pi/6$ we would have had the same result, but the cut-off should not depend on $\det A$.

In anisotropic dielectric media $\sqrt{\det A}$ is always smaller than one, therefore Anderson localization should be easier to find in statistically anisotropic media. This result is quantitatively worked out in Fig 3.1 for a uniaxial host medium.

Vector waves in uniaxial media can be separated in ordinary and extraordinary waves, and we can apply an isotropic scalar model to the ordinary waves and an anisotropic scalar model to the extraordinary waves. A realistic example of a medium for which we know the anisotropy tensor is porous Gallium Phosphide (GaP) [76]. In the uniaxial porous GaP, the principal diffusion constants have been measured to be a factor of four different, i.e. if the pores are along the z direction, the principal components of the diffusion tensor for GaP are related by $D_{xx} = D_{yy} = D_{zz}/4$. When we calculate the mobility edge for uniaxial media with such a ratio we must insert $a = 3$ in the anisotropy matrix (3.28) and we obtain

$$\omega\tau_{c\omega} = \sqrt{2} \approx 1.4 > 1. \tag{3.47}$$

The value $a = 3$ can be used for a description of porous GaP, but we do note that for $a = 3$ the ordinary waves dominate, and these diffuse isotropically. If we invert porous GaP, we get aligned GaP cylinders in air, and in this material

the extraordinary waves prevail. Therefore we can expect that a disordered material of GaP cylinders will give rise to at least a factor of four difference in the principal diffusion constants, but with the relation $D_{xx} = D_{yy} = 4D_{zz}$. Anisotropy parameter $a = -3/4$ realizes this ratio, and the Ioffe-Regel criterion yields

$$\omega\tau_{c\omega} \quad = \quad \frac{3\sqrt{3}}{4} \quad \approx \quad 1.3 \quad > \quad 1. \tag{3.48}$$

The location of the transition to Anderson localization is not the same for porous GaP and the aligned GaP nanowires in air.In Fig. 3.2 we observe that the locations of the transition to Anderson localization for a ratio of $fD_{xx} = D_{zz}$ or $D_{xx} = fD_{zz}$ are only equal for $f = 1$. In uniaxial media where anisotropy has more effect on the light traveling through it, i.e. for $a < 0$, the transition to Anderson localization occurs for shorter mean free times. This may sound as bad news for those searching for Anderson localization, but it fits nicely with the results from section 3.4. In that section we observed that for $a \to \infty$ two of the three principal components of the diffusion tensor vanished, and for $a \to -1$ only one principal component vanished. We thus conclude that the lower the effective dimension of the medium, the quicker the onset of Anderson localization.

The above criterion for Anderson localization (3.46) has been derived for stationary situations. We conjecture that in non stationary experiments even in uniaxial media with $a > 0$ Anderson localization is more likely to occur as compared to isotropic media. The reason is that when we have a disordered uniaxial medium, in which the ordinary waves already scatter very strongly, every now and then there will be a scattering event through which they become extraordinary waves. The extraordinary waves are sensitive to the anisotropy, and could be subject to a mean free time τ which is already lower than the critical value. Thus in non stationary experiments, the possibility exists that for some time even for $a > 0$ more energy is transported by the Anderson localized extraordinary waves than by the non localized ordinary waves.

3.7 Conclusions

In unbounded media we derived anisotropic diffusion starting from the radiative transfer equation in anisotropic media. The diffusion tensor we obtained consisted of a mean free time and a product of group velocities averaged over the surface of constant frequency, divided by a scattering delay term. In unbounded media we showed that it is impossible to identify a mean free path or an energy velocity. We presented solutions to the anisotropic diffusion equa-

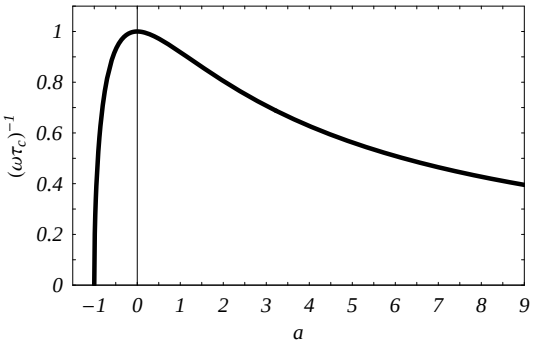

Figure 3.1.
The critical strength of the disorder $(\omega\tau_c)^{-1}$ *required for the transition to Anderson localization is plotted for a uniaxial medium with anisotropy* a*. The transition to Anderson localization is at scattering strength* $(\omega\tau_c)^{-1} = \sqrt{\det \mathsf{A}}$*, with* $\sqrt{\det \mathsf{A}}$ *volume element of the anisotropy of the host medium. The uniaxial dielectric with director* $\boldsymbol{n}$ *is* $\varepsilon = (3+a)[1-a\boldsymbol{nn}/(1+a)]/(c_i{}^2\mathrm{Tr}[\mu])$*, and the anisotropy of this medium is* $\mathsf{A} = 3\varepsilon^{-1}/\mathrm{Tr}[\varepsilon^{-1}]$*. For* $a = 0$*, i.e. isotropic media we have an absolute maximum. The anisotropy lowers the required scattering strength for Anderson localization. The critical value* $\omega\tau_c$ *drops rapidly for* $a < 0$*, i.e. two axes of the permittivity smaller than the third axis. In this regime in vector models for light in uniaxial media the extraordinary wave dominates, which is the wave sensitive to the anisotropy. For* $a > 0$ *the ordinary wave dominates, and the anisotropy has much less influence on wave transport.*

tion given a point source in an infinite medium. In the limit of extreme anisotropy, the dimension of the diffusion tensor is reduced, such that it projects on a two or even one dimensional subspace in which isotropic diffusion occurs. Interference effects were incorporated into the anisotropic diffusion equation by restoring reciprocity. We found that anisotropy lowers the required scattering strength for a transition to Anderson localization. For uniaxial media the results for the transition to Anderson localization coincide with the reduction of the dimension in anisotropic diffusion for strong anisotropy.

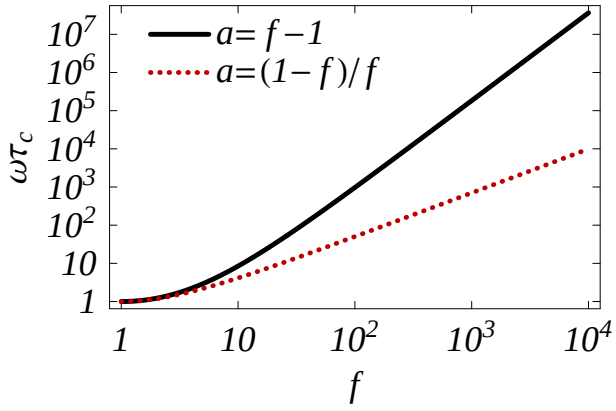

Figure 3.2 (color online).
The transition to Anderson localization occurs at the critical strength of the disorder $\omega\tau_c = \sqrt{\frac{(1+a/3)^2}{1+a}}$, *and is plotted for anisotropy ratio* f. *The solid line is for a uniaxial medium with* $\varepsilon_{zz} < \varepsilon_{yy} = \varepsilon_{xx}$, *and for this material* $f \equiv \varepsilon_{xx}/\varepsilon_{zz}$ *such that* $a > 0$. *In this type of medium more energy is transported by ordinary waves, which are not sensitive to the anisotropic medium, than by extraordinary waves The dotted line is for media with* $\varepsilon_{zz} > \varepsilon_{yy} = \varepsilon_{xx}$, *and here* $f \equiv \varepsilon_{zz}/\varepsilon_{xx}$, *such that* $-1 < a < 0$. *Here the extraordinary waves transport most energy. We note that for extreme anisotropy the curves are linear on this double logarithmic scale. The factor* 2 *difference is related to the fact that for* $\varepsilon_{zz} \to 0$ *only* D_{zz} *remains finite and* D_{xx}*and* D_{yy} *both vanish, whereas for both* $\varepsilon_{xx} = \varepsilon_{yy} \to 0$, *both* $D_{xx} = D_{yy}$ *remain finite, and* D_{zz} *vanishes.*

Chapter 4

Wave transport in the presence of boundaries

In this chapter we study transport of light in bounded anisotropic media. Boundaries have an effect on both the wave amplitude and radiance. We calculate anisotropic diffuse reflection and transmission. The energy density is redistributed over angles in a non-Lambertian way. The enhanced backscattering cone becomes anisotropic.

4.1 Introduction

The propagation of waves through any material is almost always hampered by a certain amount of disorder. This disorder could stem from some local inhomogeneities in the refractive index, or it could be a discontinuous jump, i.e. an interface between two materials.

Currently the effect of anisotropy on transport of radiance through disordered media is extensively investigated. Some examples of anisotropic media under study are semiconductors [27, 76], liquid crystals [28, 97], multilayer films [43], blood cells [5], and the brain [4]. Radiative transfer in these anisotropic media is usually either numerically modeled by Monte Carlo simulation, or, to very good agreement, approximated by an anisotropic diffusion equation. The key advantage of the diffusion equation over the radiative transfer equation is the fact that it can much more often be solved analytically.

In disordered media the waves can only travel a certain distance without losing all directionality. Stationary diffusion of waves in some disordered material is fully governed by the transport mean free path, a quantity which can only be determined through boundary conditions on the diffusion equation. Once the transport mean free path is known, we can measure the diffusion constant, and obtain the energy velocity. In an experiment the transport mean free path may be obtained by total transmission or enhanced backscattering

measurements. The diffusion constant may be extracted from a time resolved transmission experiment.

In this chapter, we study the boundary conditions at a planar interface between a homogeneous medium and an anisotropic disordered material. We use a scalar wave model to describe the propagation of the amplitude of light. In chapter 2 we related our model to the Maxwell equations and derived anisotropic radiative transfer and in chapter 3 we studied anisotropic diffusion in infinite media. Using boundary conditions we establish the transport mean free path and the energy velocity. For semi-infinite media we present the escape function and the enhanced backscattering cone, for slab like geometries we present angle resolved transmission, and also the enhanced backscattering cone.

4.2 Conditions at an interface

When we want to describe a multiple scattering experiment it is crucial to know what happens at the interface between a homogeneous medium and a multiple scattering medium. In an illumination experiment we would send some radiance into a disordered medium. This radiance will then scatter a number of times due to the disorder, and, if it is not absorbed, eventually exit the medium in some direction with a certain probability. Outside the disordered material the radiance is governed by the wave equation for the wave amplitude, whereas inside the disordered medium, once it scatters, it will be governed by the radiative transfer or the diffusion equation. To give an accurate description of such an experiment, we also need to determine what happens at the interface for the wave amplitude, its radiance, or its diffuse energy density.

In this section we consider a planar interface between a homogeneous and an elastic inhomogeneous medium, either of which is allowed to be anisotropic. We will study the wave amplitude near the interface, the energy density flux, the radiance, and the diffuse energy density. Before we proceed, we will first revisit the mapping of vector waves to scalar waves, and see if there are significant differences.

4.2.a Boundary conditions for electromagnetic fields

In this chapter we will study the boundary conditions for a scalar model for light. The scalar model was obtained by mapping the electromagnetic energy density onto the energy density of a scalar wave. In this section we determine the boundary conditions on the scalar wave, the energy density and flux.

These results are used in section 4.2.b to generalize Snell's law to anisotropic media, in section 4.2.c to obtain the Fresnel coefficients for anisotropic media, and in section 4.2.e we determine the reflection and transmission coefficients for the energy density flux.

We have a planar surface at $z = 0$ with unit normal $\boldsymbol{n}_\perp \equiv \boldsymbol{e}_z$. There are no free charges. The fields at an infinitesimal distance $z = 0^- < 0$ are denoted by the superscript $^<$, the fields at infinitesimal distance $z = 0^+ > 0$ are denoted by the superscript $^>$. The components parallel to the boundary have subscript $\parallel$, whereas the perpendicular components have the subscript $\perp$. The four boundary conditions on the electromagnetic fields which follow from the integral form of the Maxwell equations in matter are [53]

$$\boldsymbol{D}_\perp^< = \boldsymbol{D}_\perp^>, \tag{4.1a}$$
$$\boldsymbol{B}_\perp^< = \boldsymbol{B}_\perp^>, \tag{4.1b}$$
$$\boldsymbol{E}_\parallel^< = \boldsymbol{E}_\parallel^>, \tag{4.1c}$$
$$\boldsymbol{H}_\parallel^< = \boldsymbol{H}_\parallel^>. \tag{4.1d}$$

For convenience we suppose here that the fields are all plane waves of frequency ω, and we suppress the $(\boldsymbol{x}, t)$ dependence. The media are linear and we use the constitutive relations $\boldsymbol{D} = \varepsilon \cdot \boldsymbol{E}$ and $\boldsymbol{B} = \mu \cdot \boldsymbol{H}$.

Instead of the Maxwell equations we consider a mapping of the energy density of the electromagnetic fields on the energy density of a scalar field. In our scalar model the displacement $\boldsymbol{D}$ is related to $\boldsymbol{\nabla}\psi$, whereas $|\boldsymbol{H}|$ is related to $\partial\psi/\partial t$. Since we can not incorporate magnetic anisotropy in our mapping, we take μ to be a scalar permeability, which can be inhomogeneous. The Maxwell equations are not satisfied by our identifications of electric and magnetic fields, and boundary conditions (4.1) should not be applied directly to the electromagnetic fields derived from ψ. To arrive at boundary conditions for the scalar field we need to consider the effect of Eqs. (4.1) on the energy density and flux of the electromagnetic fields.

The electromagnetic fields which appear in the Maxwell equations can be partitioned in fields polarized parallel or perpendicular to the plane of incidence. For vector waves the plane of incidence is defined by normal vector $\boldsymbol{e}_{\boldsymbol{k}} \times \boldsymbol{n}_\perp$. Following [53] we say an electromagnetic wave is polarized parallel to the plane of incidence if $\boldsymbol{B}_\perp = \boldsymbol{0}$, and polarized perpendicular to the plane of incidence when $\boldsymbol{E}_\perp = \boldsymbol{0}$. These polarizations are indeed orthogonal as Faraday's law transformed to Fourier space yields $\boldsymbol{p} \times \boldsymbol{E} = \omega \boldsymbol{B}$. We can not apply this terminology to the fields derived from ψ, because $\boldsymbol{E} \propto \varepsilon^{-1} \cdot \boldsymbol{k}\psi$ and $\boldsymbol{B} \propto \psi$, but we can consider the energy density of parallel or perpendicular polarized vector waves separately.

The energy density per frequency band $\mathscr{H}_\omega$ is equally distributed over the electric and magnetic fields. The parallel polarized ($\boldsymbol{B}_\perp = \boldsymbol{0}$) waves give rise to a discontinuity of the energy density at the interface, given by

$$\frac{3\mu_0}{\mathrm{Tr}[\mu^<]}\mathscr{H}_\omega^< = \frac{3\mu_0}{\mathrm{Tr}[\mu^>]}\mathscr{H}_\omega^>. \tag{4.2a}$$

Here we introduced the permeability of the vacuum μ_0 in order to make the proportionality factors dimensionless. Introducing the permittivity of vacuum ε_0 we have for perpendicularly polarized waves ($\boldsymbol{E}_\perp = \boldsymbol{0}$) for the two orthogonal orientations of $\boldsymbol{E}$ along $\boldsymbol{e}_x$ and $\boldsymbol{e}_y$,

$$\frac{\varepsilon_0}{\varepsilon_{xx}^<}\mathscr{H}_\omega^< = \frac{\varepsilon_0}{\varepsilon_{xx}^>}\mathscr{H}_\omega^>, \tag{4.2b}$$

$$\frac{\varepsilon_0}{\varepsilon_{yy}^<}\mathscr{H}_\omega^< = \frac{\varepsilon_0}{\varepsilon_{yy}^>}\mathscr{H}_\omega^>. \tag{4.2c}$$

In general we require a superposition of Eqs. (4.2). We introduce the dimensionless weights w_i which satisfy $0 \le w_i \le 1$ and $w_1 + w_2 + w_3 + w_4 = 1$. The weight w_1 represents the amount of perpendicular polarized light oriented with $\boldsymbol{E} \propto \boldsymbol{e}_x$, weight w_2 the amount of perpendicular polarized light oriented with $\boldsymbol{E} \propto \boldsymbol{e}_y$, w_3 is the amount of parallel polarized light with $\boldsymbol{B} \propto \boldsymbol{e}_x$ and w_4 is the amount of parallel polarized light with $\boldsymbol{B} \propto \boldsymbol{e}_y$. Equations (4.2) can be combined in a single equation by defining a dimensionless quantity B, which can not be confused with $B = |\boldsymbol{B}|$, since the magnitude of the electric flux is not used, representing the distribution of polarizations by

$$\left(\frac{\mathrm{c_i}}{\mathrm{c_0 B}}\right)^2 \mathscr{H}_\omega \equiv \frac{\varepsilon_0}{\varepsilon_{xx}} w_1 \mathscr{H}_\omega + \frac{\varepsilon_0}{\varepsilon_{yy}} w_2 \mathscr{H}_\omega + \frac{3\mu_0}{\mathrm{Tr}[\mu]}\left[w_3 + w_4\right]\mathscr{H}_\omega. \tag{4.3}$$

Here we used $\mathrm{c_i}^2 = \mathrm{Tr}[\varepsilon^{-1}]/\mathrm{Tr}[\mu]$. In isotropic media we find for parallel polarized ($w_3 + w_4 = 1$) light $\mathrm{B}^2 = \varepsilon_0/\varepsilon$, whereas for perpendicular polarized ($w_1 + w_2 = 1$) light $\mathrm{B}^2 = \mu_0/\mu$, which reflect the discontinuity in $\boldsymbol{E}_\perp$ and $\boldsymbol{H}_\perp$ for parallel and perpendicular polarized light respectively. Equation (4.3) is closely connected to the Stokes parameters, which describe $\boldsymbol{E}_\omega \cdot \boldsymbol{E}_\omega$. The four Stokes parameters $\{s_i\}$ for plane waves satisfy ${s_0}^2 = {s_1}^2 + {s_2}^2 + {s_3}^2$. Here ${s_0}^2$ represents $\boldsymbol{E}_\omega \cdot \boldsymbol{E}_\omega$, and the other s_i form a coordinate $\boldsymbol{s}$ on the surface of a sphere with radius s_0. This sphere is known as the Poincaré sphere [54]. The total energy density of the electric field and the medium is $\boldsymbol{E}_\omega \cdot \varepsilon \cdot \boldsymbol{E}_\omega$, not $\boldsymbol{E}_\omega \cdot \boldsymbol{E}_\omega$, which explains the ratios. Using B we can write a single boundary condition on the energy density which guarantees that boundary conditions (4.1) are satisfied,

$$\left(\frac{\mathrm{c_i}^<}{\mathrm{c_0 B}^<}\right)^2 \mathscr{H}_\omega^< \equiv \left(\frac{\mathrm{c_i}^>}{\mathrm{c_0 B}^>}\right)^2 \mathscr{H}_\omega^>. \tag{4.4}$$

In real situations even monochromatic light is not truly monochromatic, but consists of a sum of a large number of plane waves, and ${s_0}^2 \geq {s_1}^2 + {s_2}^2 + {s_3}^2$ [53, 54, 98]. To obtain that result we must integrate (4.3) over frequency band $\mathrm{d}\omega$.

For the energy density flux we do not need to consider each polarization separately. From Eqs. (4.1c) and (4.1d) we immediately obtain continuity of

$$\boldsymbol{n}_\perp \cdot \boldsymbol{S}_\omega^< \quad = \quad \boldsymbol{n}_\perp \cdot \boldsymbol{S}_\omega^>. \tag{4.5}$$

The parallel components of the energy density flux have a discontinuity, but do not provide new information.

Equations (4.4) and (4.5) have implications on the scalar field ψ. In the limit of vanishing index mismatch the transmitted wave must be in phase with the incident wave, and for ψ boundary condition (4.4) reads

$$\frac{\psi^<}{\mathrm{B}^<} \quad = \quad \frac{\psi^>}{\mathrm{B}^>}. \tag{4.6a}$$

The continuity of the perpendicular flux component, Eq. (4.5), implies a discontinuity in $\boldsymbol{n}_\perp \cdot \boldsymbol{\nabla}\psi = \partial\psi/\partial z$ at the interface,

$$\frac{\partial\psi^<}{\partial z} \quad = \quad \frac{\mathrm{B}^>}{\mathrm{B}^<} \frac{\boldsymbol{n}_\perp \cdot \mathrm{A}^> \cdot \boldsymbol{\kappa} \mathrm{B}^{>2} - \boldsymbol{n}_\perp \cdot \mathrm{A}^< \cdot \boldsymbol{k}_\parallel \mathrm{B}^{<2}}{\boldsymbol{n}_\perp \cdot \mathrm{A}^< \cdot \boldsymbol{\kappa}_\perp \mathrm{B}^{>2}} \frac{\partial\psi^>}{\partial z}. \tag{4.6b}$$

Here A_{zz} is a component of the anisotropy tensor $\mathrm{A} = 3\varepsilon^{-1}/\mathrm{Tr}[\varepsilon^{-1}]$. For isotropic media $A_{zz} = 1$. If the incident light is polarized parallel to the plane of incidence, then $\mathrm{B} = \sqrt{\varepsilon_0 \mathrm{Tr}[\varepsilon^{-1}]/3}$.

In the past, the analogy of classical waves with Schrödinger waves or probability amplitudes has been used extensively, and often continuity of both ψ and $\partial\psi/\partial z$ has been imposed. These latter boundary conditions are obviously correct in the absence of index mismatch as $\mathrm{B}^< = \mathrm{B}^>$ and $\mathrm{A}^< = \mathrm{A}^>$. They are approximately correct if the index mismatch is due to a low density of scatterers on one side of the interface. We will come back to the difference between these boundary conditions in more detail in sections 4.2.c and 4.2.e. In order to follow the analogy with Schrödinger waves we could absorb the B's in the ψ's by redefining the field according to $\tilde{\psi} \equiv \psi/\mathrm{B}$. The resulting boundary conditions for $\tilde{\psi}$ are $\tilde{\psi}^< = \tilde{\psi}^>$ and $\partial\tilde{\psi}^</\partial z = (\boldsymbol{n}_\perp \cdot \mathrm{A}^> \cdot \boldsymbol{\kappa} \mathrm{B}^{>2} - \boldsymbol{n}_\perp \cdot \mathrm{A}^< \cdot \boldsymbol{k}_\parallel \mathrm{B}^{<2})/(\boldsymbol{n}_\perp \cdot \mathrm{A}^< \cdot \boldsymbol{\kappa}_\perp \mathrm{B}^{<2}) \partial\tilde{\psi}^>/\partial z$. The new field $\tilde{\psi}$ behaves as a Schrödinger wave, and the boundary as a scattering potential $V(z) \propto \delta(z)$. This scattering potential is not a potential well, but a potential barrier, and does not give rise to bound states. Our main interest is the effect of anisotropy on transport of light through disordered media, not the analogy with Schrödinger waves, and for this reason we proceed to work with the field ψ.

The presence of a boundary with an index mismatch causes an impinging, a reflected, and a transmitted plane wave, so all fields have the structure $\mathscr{A}_\mathrm{i} e^{\mathrm{i}(\boldsymbol{k}_\mathrm{i}\cdot\boldsymbol{x}-\omega t)} + \mathscr{A}_\mathrm{r} e^{\mathrm{i}(\boldsymbol{k}_\mathrm{r}\cdot\boldsymbol{x}-\omega t)} = \mathscr{A}_\mathrm{t} e^{\mathrm{i}(\boldsymbol{k}_\mathrm{t}\cdot\boldsymbol{x}-\omega t)}$ on the interface at $z = 0$, and therefore also in anisotropic media

$$\boldsymbol{k}_{\mathrm{i}\parallel} \quad = \quad \boldsymbol{k}_{\mathrm{r}\parallel} \quad = \quad \boldsymbol{k}_{\mathrm{t}\parallel}. \tag{4.7}$$

Equation (4.7) indicates that the incident, reflected and transmitted (or refracted) wave vectors all lie in the plane of incidence. For the incident and reflected waves Eq. (4.7) also shows that the angle with $\boldsymbol{n}_\perp$ is identical, which is known as the law of reflection. These two implications of Eq. (4.7) are both well known results in isotropic media [53, 54].

Had we switched the interpretation of the electromagnetic fields according to $\boldsymbol{B} \leftrightarrow \boldsymbol{D}$ and $\boldsymbol{E} \leftrightarrow \boldsymbol{H}$, and used the relevant identifications of the anisotropy matrix with the anisotropy in μ^{-1}, we had recovered identical boundary conditions on ψ. The model with these switches is a generalization of the scalar model employed in [68] to anisotropic magnetic permeability. Since ψ is indifferent to switching the interpretation, our results are equally applicable to problems with anisotropic permeability and isotropic permittivity instead of anisotropic permittivity and isotropic permeability.

4.2.b Snell's law for anisotropic disordered media

In this section we study the discontinuity in the wave vector at the interface, and generalize Snell's law, also known as the law of refraction, to disordered anisotropic media.

In the homogeneous medium the scalar wave amplitude is governed by a possibly anisotropic wave equation (2.4), which gives rise to a wave vector $\boldsymbol{k}$. In section 4.2.a we found the wave vector components parallel to the interface to be continuous at the interface,

$$\boldsymbol{k}_\parallel \quad = \quad \boldsymbol{\kappa}_\parallel, \tag{4.8}$$

where $\boldsymbol{\kappa}$ is the complex wave vector in the disordered medium. Propagation in the ensemble averaged inhomogeneous medium is governed by the Dyson equation (2.27)[87, 99].

As warming up we present the well known conditions at interfaces between an isotropic homogeneous medium and an isotropic disordered medium. In an isotropic host medium with arbitrary scatterers the Dyson equation implies the dispersion relation

$$0 \quad = \quad \frac{\omega^2}{{c_\mathrm{i}}^2} - \boldsymbol{\kappa}\cdot\boldsymbol{\kappa} - \Sigma_\omega(\boldsymbol{\kappa}). \tag{4.9}$$

Here c_i is the (phase) velocity of light in the homogeneous isotropic medium where $\Sigma = 0$. From dispersion relation (4.9) and wave vector requirement (4.8) it is well known that the implicit equation for the perpendicular component of the wave vector inside the multiple scattering medium is

$$\mathrm{Re}[\kappa_\perp(\boldsymbol{e}_{\boldsymbol{\kappa}})] \equiv \frac{\omega}{c_i}\sqrt{\frac{\mathrm{Re}[\tilde{\varepsilon}_\omega(\boldsymbol{\kappa})]+|\tilde{\varepsilon}_\omega(\boldsymbol{\kappa})|}{2\varepsilon}}, \tag{4.10a}$$

$$\mathrm{Im}[\kappa_\perp(\boldsymbol{e}_{\boldsymbol{\kappa}})] \equiv \frac{\omega}{c_i}\frac{\mathrm{Im}[\tilde{\varepsilon}_\omega(\boldsymbol{\kappa})]}{2\mu}\sqrt{\frac{2\varepsilon}{\mathrm{Re}[\tilde{\varepsilon}_\omega(\boldsymbol{\kappa})]+|\tilde{\varepsilon}_\omega(\boldsymbol{\kappa})|}}, \tag{4.10b}$$

$$\frac{\tilde{\varepsilon}_\omega(\boldsymbol{\kappa})}{\varepsilon} \equiv 1-\frac{{c_i}^2}{\omega^2}\Sigma_\omega(\boldsymbol{\kappa})-\frac{{c_i}^2}{\omega^2}\boldsymbol{\kappa}_\parallel\cdot\boldsymbol{\kappa}_\parallel. \tag{4.10c}$$

The quantity $\tilde{\varepsilon}_\omega$ is introduced for notational convenience, because the dielectric constant modified by scattering effects is actually given by $\tilde{\varepsilon}_\omega(\boldsymbol{\kappa})+\varepsilon {c_i}^2\boldsymbol{\kappa}_\parallel\cdot\boldsymbol{\kappa}_\parallel/\omega^2$. Equations (4.10) describe refraction of light at the interface with a multiple scattering medium. When there are no extinction effects due to the disorder, i.e. when $\mathrm{Im}[\Sigma] = 0$, then for the refracted wave the phase velocity is $v_r(\boldsymbol{\kappa}) = c_i/\sqrt{1-c_i^2\mathrm{Re}[\Sigma(\boldsymbol{\kappa})]/\omega^2}$, and we recover Snell's law for incident light with phase velocity v_i,

$$\frac{\sin\theta_i}{\sin\theta_r} = \sqrt{\frac{\mathrm{Re}[\kappa_\perp]^2+\boldsymbol{\kappa}_\parallel\cdot\boldsymbol{\kappa}_\parallel}{\boldsymbol{k}\cdot\boldsymbol{k}}} = \frac{v_i}{v_r(\boldsymbol{\kappa})}. \tag{4.11}$$

We want to generalize the above treatment for isotropic media to anisotropic media with a tensorial dielectric. However such a dielectric can not be incorporated it in the above model 2.2. Therefore, instead of dielectric scatterers, we consider magnetic scatterers. Then we can introduce an anisotropic permittivity tensor ε and anisotropy tensor $\mathsf{A} = 3\varepsilon^{-1}/\mathrm{Tr}[\varepsilon^{-1}]$. The dispersion relation (4.9) becomes

$$0 = \frac{\omega^2}{{c_i}^2}-\boldsymbol{\kappa}\cdot\mathsf{A}\cdot\boldsymbol{\kappa}-\Sigma_\omega(\boldsymbol{\kappa}). \tag{4.12}$$

Again the discontinuity in the wave vector at the interface can be determined. Using the anisotropic dispersion relation (4.12) together with wave

vector requirement (4.8), we obtain for anisotropic media the result

$$\mathrm{Re}[\kappa_\perp(\boldsymbol{e}_\kappa)] \equiv \frac{\omega}{v_\mathrm{p}(\boldsymbol{n}_\perp)}\left[\sqrt{\frac{\mathrm{Re}[\tilde{\mu}_\omega(\boldsymbol{\kappa})]+|\tilde{\mu}_\omega(\boldsymbol{\kappa})|}{2\mu}}-\frac{\boldsymbol{v}_\mathrm{g}(\boldsymbol{n}_\perp)\cdot\boldsymbol{e}_{\boldsymbol{\kappa}_\parallel}}{v_\mathrm{i}(\boldsymbol{e}_\kappa)}\boldsymbol{e}_{\boldsymbol{\kappa}_\parallel}\cdot\boldsymbol{e}_\kappa\right], \tag{4.13a}$$

$$\mathrm{Im}[\kappa_\perp(\boldsymbol{e}_\kappa)] \equiv \frac{\omega}{v_\mathrm{p}(\boldsymbol{n}_\perp)}\frac{\mathrm{Im}[\tilde{\mu}_\omega(\boldsymbol{\kappa})]}{2\mu}\sqrt{\frac{2\mu}{\mathrm{Re}[\tilde{\mu}_\omega(\boldsymbol{\kappa})]+|\tilde{\mu}_\omega(\boldsymbol{\kappa})|}}, \tag{4.13b}$$

$$\frac{\tilde{\mu}_\omega(\boldsymbol{\kappa})}{\mu} \equiv 1-\frac{{c_\mathrm{i}}^2}{\omega^2}\Sigma_\omega(\boldsymbol{\kappa})-\left[\left(\frac{v_\mathrm{p}(\boldsymbol{e}_{\boldsymbol{\kappa}_\parallel})}{v_\mathrm{i}(\boldsymbol{e}_\kappa)}\right)^2-\left(\frac{\boldsymbol{v}_\mathrm{g}(\boldsymbol{n}_\perp)\cdot\boldsymbol{e}_{\boldsymbol{\kappa}_\parallel}}{v_\mathrm{i}(\boldsymbol{e}_\kappa)}\right)^2\right](\boldsymbol{e}_{\boldsymbol{\kappa}_\parallel}\cdot\boldsymbol{e}_\kappa)^2. \tag{4.13c}$$

Here v_p is the phase velocity in the disordered anisotropic medium without the scattering effects Σ, v_i is the phase velocity of the incident wave, $\boldsymbol{n}_\perp$ is the unit normal to the interface and pointing towards the inhomogeneous medium, and $\mu_\perp(\boldsymbol{\kappa})$ is an effective permeability related to $\boldsymbol{\kappa}_\perp$. Given an explicit self energy Σ, Eqs. (4.13) can be solved for $\kappa_\perp$. We can not guarantee that the square root in Eqs. (4.13) remains real valued for all wave vector directions for any possible combination of neighboring media. When this happens, it means that there exists no wave vector, hence no propagation in those directions. If there is no propagation into the medium, it means the incoming wave vector is totally reflected.

In the independent scattering approximation, the disorder term Σ and the related vectorial extinction mean free path are, using Eq. (2.37a),

$$\Sigma_\omega(\boldsymbol{\kappa}) = nT_\omega(\boldsymbol{e}_\kappa,\boldsymbol{e}_\kappa), \tag{4.14a}$$

$$\boldsymbol{l}_{\mathrm{e}\omega}(\boldsymbol{e}_\kappa) = \frac{\boldsymbol{v}_\mathrm{g}(\boldsymbol{e}_\kappa)}{{c_\mathrm{i}}n\sigma_{\mathrm{e}\omega}(\boldsymbol{e}_\kappa)} = -\frac{\omega\boldsymbol{v}_\mathrm{g}(\boldsymbol{e}_\kappa)}{{c_\mathrm{i}}^2 n\mathrm{Im}[T_\omega(\boldsymbol{e}_\kappa,\boldsymbol{e}_\kappa)]}. \tag{4.14b}$$

The velocity $\boldsymbol{v}_\mathrm{g}$ is the group velocity in the homogeneous anisotropic medium and σ_e is the extinction cross section. In the limit (4.14a) we have the simplification $\mathrm{Re}[\tilde{\mu}_\omega(\boldsymbol{\kappa})]+|\tilde{\mu}_\omega(\boldsymbol{\kappa})| = 2\mathrm{Re}[\tilde{\mu}_\omega(\boldsymbol{\kappa})]+\mathrm{O}(n^2)$. From now on we adopt the independent scattering approximation (4.14a).

Due to the appearance of $\boldsymbol{n}_\perp\cdot\mathsf{A}\cdot\boldsymbol{\kappa}_\parallel$, in (4.13a) and (4.13c) there is no simple expression for Snell's law for media with arbitrary anisotropy. When we have a material in which $\boldsymbol{n}_\perp\cdot\mathsf{A}\cdot\boldsymbol{\kappa}_\parallel = 0$, then, for an incident wave with phase velocity v_i and identifying the "dressed" phase velocity (2.34a) of the refracted wave by $\tilde{v}_\mathrm{p}(\boldsymbol{\kappa}) = v_\mathrm{p}(\boldsymbol{\kappa})/\sqrt{1-{c_\mathrm{i}}^2 n\mathrm{Re}[T(\boldsymbol{e}_\kappa,\boldsymbol{e}_\kappa)]/\omega^2}$, Snell's law is the relatively simple expression

$$\frac{\sin\theta_\mathrm{i}}{\sin\theta_\mathrm{r}} = \sqrt{\frac{{v_\mathrm{i}}^2}{\tilde{v}_\mathrm{p}(\boldsymbol{\kappa})^2}+\frac{{v_\mathrm{i}}^2}{\omega^2}\boldsymbol{\kappa}_\parallel\cdot\left[1-\frac{\mathsf{A}}{\boldsymbol{n}_\perp\cdot\mathsf{A}\cdot\boldsymbol{n}_\perp}\right]\cdot\boldsymbol{\kappa}_\parallel}. \tag{4.15}$$

For isotropic media we have A = 1, and only then (4.15) reduces to (4.10). The possibility exists that a negative value is obtained on the right hand side, which means that there is total reflection. Incident waves coming in from an anisotropic homogeneous medium will cause an additional dependence on direction in $\nu_{\rm i}$.

4.2.c Fresnel's equations for anisotropic disordered media

In a homogeneous medium the wave amplitude propagates without any hindrance. When it reaches an interface with an inhomogeneous medium, a part of it may reflect due to a possible index mismatch, and the other part of the wave is refracted (or transmitted). The wave vector component perpendicular to the interface has a well defined discontinuity, which gives rise to the three fundamental laws of geometrical optics. We use these three fundamental laws of geometrical optics, which we established for disordered anisotropic media in sections 4.2.a and 4.2.b, to determine the Fresnel coefficients for reflection and transmission of the scalar wave ψ. We also determine the far field amplitude propagator for amplitude crossing an interface between a disordered anisotropic medium to a homogeneous medium. We will need both of these results when we calculate reflection and transmission properties such as the enhanced backscattering cone.

In illumination experiments the light usually enters the disordered anisotropic medium from air. Thus, in general there will be an index mismatch at the interface. When there is an index mismatch at the boundary, then there will be a reflected and a refracted wave, the amplitude of which is governed by Fresnel coefficients [53]. We consider a plane wave $\psi(\boldsymbol{k}_\parallel, z)$ of amplitude ψ_0 originating from a possibly anisotropic, but homogeneous medium, impinging on an anisotropic material with low scatterer density. The interface is located at $z = 0$ with unit normal $\boldsymbol{n}_\perp = \boldsymbol{e}_z$, and we write the spatial coordinate as $\boldsymbol{x} = \boldsymbol{x}_\parallel + z\boldsymbol{n}_\perp$. We write the plane wave solution in terms of Fresnel reflection and transmission coefficients $r_{\rm F}$ and $t_{\rm F}$, which are determined by the boundary conditions. Outside the disordered medium ($z < 0$) we have the incident and reflected wave amplitudes,

$$\begin{aligned}\psi^{<}_{\boldsymbol{k}}(\boldsymbol{x}, t) &= \psi_0 \exp\left[-\mathrm{i}\left(\omega t - \boldsymbol{k}_\parallel \cdot \boldsymbol{x}_\parallel\right)\right] \\ &\quad \times \left[\exp\left[\mathrm{i}k_\perp(\boldsymbol{e}_{\boldsymbol{k}})z\right] - r_{\rm F}(\boldsymbol{k}) \exp\left[-\mathrm{i}k_\perp(\boldsymbol{e}_{\boldsymbol{k}})z\right]\right]. \qquad (4.16a)\end{aligned}$$

Inside the disordered medium ($z > 0$) we have the refracted or transmitted wave,

$$\psi^{>}_{\boldsymbol{k}}(\boldsymbol{x}, t) = t_{\rm F}(\boldsymbol{k})\psi_0 \exp\left[-\mathrm{i}\left(\omega t - \boldsymbol{k}_\parallel \cdot \boldsymbol{x}_\parallel\right)\right] \exp\left[\mathrm{i}\kappa_\perp(\boldsymbol{e}_{\boldsymbol{k}})z\right]. \qquad (4.16b)$$

These equations look familiar, their appearance is identical to those for isotropic media, but we need to realize that the wave vectors and Fresnel coefficients are different for anisotropic media.

In section 4.2.a we established that the boundary conditions on the scalar wave are $\psi^</\mathrm{B}^< = \psi^>/\mathrm{B}^>$ and $\boldsymbol{n}_\perp \cdot \mathsf{A}^< \cdot \boldsymbol{\kappa}_\perp \mathrm{B}^> \mathrm{B}^< \partial\psi^</\partial z = (\boldsymbol{n}_\perp \cdot \mathsf{A}^> \cdot \boldsymbol{\kappa} \mathrm{B}^{>2} - \boldsymbol{n}_\perp \cdot \mathsf{A}^< \cdot \boldsymbol{k}_\parallel \mathrm{B}^{<2}) \partial\psi^>/\partial z$. The constants B are determined by the polarization distribution incident on the interface, and $\mathsf{A}^<$ and $\mathsf{A}^>$, the anisotropy matrices of the media. $\mathsf{A} = 3\varepsilon^{-1}/\mathrm{Tr}[\varepsilon^{-1}]$. If the impinging wave is polarized parallel to the plane of incidence, $\mathrm{B} = \sqrt{\varepsilon_0 \mathrm{Tr}[\varepsilon^{-1}]/3}$. We also noted that these boundary conditions with discontinuities can be approximated by $\psi^< = \psi^>$ and $\partial\psi^</\partial z = \partial\psi^>/\partial z$ when the media are almost perfectly index matched, and the density of the disorder is very low, that is when we are in the independent scattering limit (4.14a). For both boundary conditions we will establish the Fresnel coefficients.

The approximated boundary conditions $\psi^< = \psi^>$ and $\partial\psi^</\partial z = \partial\psi^>/\partial z$ for vanishing index mismatch, lead to the approximated Fresnel reflection and transmission coefficients r_{aF} and t_{aF}

$$r_{\mathrm{F}}(\boldsymbol{k}) \approx r_{\mathrm{aF}}(\boldsymbol{e}_{\boldsymbol{k}}) \equiv \frac{\kappa_\perp(\boldsymbol{e}_{\boldsymbol{k}}) - k_\perp(\boldsymbol{e}_{\boldsymbol{k}})}{\kappa_\perp(\boldsymbol{e}_{\boldsymbol{k}}) + k_\perp(\boldsymbol{e}_{\boldsymbol{k}})}, \tag{4.17a}$$

$$t_{\mathrm{F}}(\boldsymbol{k}) \approx t_{\mathrm{aF}}(\boldsymbol{e}_{\boldsymbol{k}}) \equiv \frac{2k_\perp(\boldsymbol{e}_{\boldsymbol{k}})}{\kappa_\perp(\boldsymbol{e}_{\boldsymbol{k}}) + k_\perp(\boldsymbol{e}_{\boldsymbol{k}})} = 1 - r_{\mathrm{aF}}(\boldsymbol{e}_{\boldsymbol{k}}). \tag{4.17b}$$

If the anisotropy $\mathsf{A}^> \approx \mathsf{A}^<$ and $\mathrm{B}^< \approx \mathrm{B}^>$, then Eqs. (4.17) hold by definition. Fresnel reflection and transmission coefficients (4.17) are valid in other anisotropic media, provided for all unit vectors $\boldsymbol{e}_\parallel$ in the plane defined by $\boldsymbol{n}_\perp$ the media satisfy

$$\boldsymbol{n}_\perp \cdot \mathsf{A}^< \cdot \boldsymbol{e}_\parallel \approx 0, \tag{4.18a}$$

$$\boldsymbol{n}_\perp \cdot \mathsf{A}^> \cdot \boldsymbol{e}_\parallel \approx 0, \tag{4.18b}$$

$$\boldsymbol{n}_\perp \cdot \mathsf{A}^< \cdot \boldsymbol{n}_\perp \approx \boldsymbol{n}_\perp \cdot \mathsf{A}^> \cdot \boldsymbol{n}_\perp, \tag{4.18c}$$

$$\mathrm{B}^< \approx \mathrm{B}^>. \tag{4.18d}$$

With the four requirements (4.18) it seems that the approximated Fresnel coefficients (4.17) are not very useful. However, when $\mathrm{B}^< \approx \mathrm{B}^>$ and one of the principal axes of the anisotropy is perpendicular to the interface on both sides of the boundary, such that $\boldsymbol{A}^<_{zz} \approx \boldsymbol{A}^>_{zz}$, we can have arbitrary anisotropy in the plane parallel to the interface, and Fresnel coefficients (4.17) remain valid.

The exact Fresnel coefficients can also be determined. Using $\boldsymbol{k} = \boldsymbol{k}_\parallel + \boldsymbol{k}_\perp$, $\boldsymbol{k}_\mathrm{r} = \boldsymbol{k}_\parallel - \boldsymbol{k}_\perp$, and $\boldsymbol{\kappa} = \boldsymbol{k}_\parallel + \boldsymbol{\kappa}_\perp(\boldsymbol{e}_{\boldsymbol{k}})$, the Fresnel reflection and transmission coefficients for anisotropic disordered media derived from boundary conditions

(4.6) are

$$r_{\mathrm{F}}(\boldsymbol{k}) \equiv \frac{\boldsymbol{n}_\perp \cdot \mathsf{A}^> \cdot \boldsymbol{\kappa} \mathsf{B}^{>2} - \boldsymbol{n}_\perp \cdot \mathsf{A}^< \cdot \boldsymbol{k} \mathsf{B}^{<2}}{\boldsymbol{n}_\perp \cdot \mathsf{A}^> \cdot \boldsymbol{\kappa} \mathsf{B}^{>2} - \boldsymbol{n}_\perp \cdot \mathsf{A}^< \cdot \boldsymbol{k}_{\mathrm{r}} \mathsf{B}^{<2}}, \tag{4.19a}$$

$$t_{\mathrm{F}}(\boldsymbol{k}) \equiv \frac{\mathsf{B}^>}{\mathsf{B}^<} \frac{2\boldsymbol{n}_\perp \cdot \mathsf{A}^< \cdot \boldsymbol{k}_\perp \mathsf{B}^{<2}}{\boldsymbol{n}_\perp \cdot \mathsf{A}^> \cdot \boldsymbol{\kappa} \mathsf{B}^{>2} - \boldsymbol{n}_\perp \cdot \mathsf{A}^< \cdot \boldsymbol{k}_{\mathrm{r}} \mathsf{B}^{<2}} = \frac{\mathsf{B}^>}{\mathsf{B}^<} [1 - r_{\mathrm{F}}(\boldsymbol{e}_{\boldsymbol{k}})]. \tag{4.19b}$$

Taking $\mathsf{B}^< \to \mathsf{B}^>$ and $\mathsf{A}^> \to \mathsf{A}^<$, or imposing requirements Eqs. (4.18), we recover Eqs. (4.17). The Fresnel coefficients depend implicitly on frequency ω, through the definitions of $\boldsymbol{k}$ and $\boldsymbol{\kappa}$. Moreover, not only the perpendicular component of the wave vectors is relevant, but also the parallel components play a role in anisotropic media with optical axes at an angle with the interface.

In many experiments the medium from which the incident light originates is isotropic, and $\mathsf{A}^< = 1$. If the disordered medium is also isotropic, then $\mathsf{A}^> = 1$, and these Fresnel coefficients become almost identical to those for $\boldsymbol{E}$ had we used the Maxwell equations [53], including the Brewster angle for parallel polarization, see Fig 4.1. In the transmission coefficient we observe a difference which depends on the incoming polarization. For parallel polarized waves the difference is given by the factor $\sqrt{\mu^</\mu^>}$. We can understand this factor when we recall that in isotropic media for plane waves $|\boldsymbol{E}| = \mathrm{c_i}|\boldsymbol{B}| = \mathrm{i}\omega\sqrt{\mu}\psi$, which is why the discontinuity in ψ differs by the factor $\sqrt{\mu^</\mu^>}$ from the discontinuity in $\boldsymbol{E}$ for parallel polarized waves. For perpendicular polarizations a similar argument holds, leading to differences like $\sqrt{\varepsilon^<_{xx}/\varepsilon^>_{xx}}$.

The Brewster angle θ_{B} is defined by $\boldsymbol{n}_\perp \cdot \mathsf{A}^> \cdot \boldsymbol{\kappa} \mathsf{B}^{>2} \equiv \boldsymbol{n}_\perp \cdot \mathsf{A}^< \cdot \boldsymbol{k} \mathsf{B}^{<2}$, where $B = \sqrt{\mathrm{Tr}[\varepsilon^{-1}]}$ because the incident wave is parallel polarized. In experiments usually the medium from which the waves impinge on the sample is homogeneous and isotropic, being air or vacuum. Isotropic media have $A^<_{zz} = 1$, and the incident phase velocity is v_{i}. If we neglect the angular dependence of the disorder and assume one of the optical axes is along $\boldsymbol{n}_\perp = \boldsymbol{e}_z$, then we have an explicit and relatively simple expression for the Brewster angle θ_{B}

$$\sin^2\theta_{\mathrm{B}} = \frac{1 - \frac{\mathrm{c_i}^2}{\omega^2}\mathrm{Re}[\Sigma_\omega] - \left(\frac{v_{\mathrm{i}}\mu^<}{v_{\mathrm{p}}(\boldsymbol{n}_\perp)\mu^>}\right)^2}{\left(\frac{v_{\mathrm{p}}(\boldsymbol{e}_{\boldsymbol{\kappa}_\parallel})}{v_{\mathrm{i}}}\right)^2 - \left(\frac{v_{\mathrm{i}}\mu^<}{v_{\mathrm{p}}(\boldsymbol{n}_\perp)\mu^>}\right)^2}. \tag{4.20}$$

In the absence of disorder ($\Sigma = 0$) and anisotropy ($v_{\mathrm{p}}(\boldsymbol{e}_{\boldsymbol{\kappa}_\parallel}) = v_{\mathrm{p}}(\boldsymbol{n}_\perp) = v_{\mathrm{p}}$), the Brewster angle (4.20) for the scalar field ψ is identical to the Brewster angle for the electric field [53, 54].

4.2.d Amplitude scattering out of anisotropic disordered media

Inside the disordered material the wave will scatter many times and is governed by the radiative transfer equation or the diffusion equation, until finally it scatters out of the disordered medium and escapes to infinity. For this final scattering event we need the propagator from some point $\boldsymbol{x}_0$ inside the inhomogeneous medium to some point $\boldsymbol{x}$ in the homogeneous medium, far away from the interface. Again the coordinates are such that the the homogeneous medium is at $z<0$, and the disordered medium at $z>0$.

We calculated the real space Dyson Green function G for an infinite multiple scattering medium in chapter 2. Under the assumption that $|\boldsymbol{x}| \gg |\boldsymbol{x}_0|$, we make a far field expansion of G for the amplitude escaping the multiple scattering medium. Using $|\mathsf{A}^{-\frac{1}{2}}\cdot(\boldsymbol{x}-\boldsymbol{x}_0)| = |\mathsf{A}^{-\frac{1}{2}}\cdot\boldsymbol{x}| - \boldsymbol{x}_0\cdot\boldsymbol{n}_\phi(\boldsymbol{x})/\sqrt{\boldsymbol{n}_\phi(\boldsymbol{x})\cdot\mathsf{A}\cdot\boldsymbol{n}_\phi(\boldsymbol{x})}$, where $\boldsymbol{n}_\phi$ is the unit normal of the wave surface $\phi_\omega(\boldsymbol{x})$ of the elliptical wave, the asymptotic behavior of the amplitude (2.36) is

$$G(\boldsymbol{x},\boldsymbol{x}_0,t) \overset{|\boldsymbol{x}|\gg|\boldsymbol{x}_0|}{\longrightarrow} \frac{\left|\boldsymbol{v}_\mathrm{g}(\boldsymbol{n}_\phi(\boldsymbol{x}))\right|}{\mathrm{c_i}\sqrt{\det\mathsf{A}}} \frac{\exp\left\{\mathrm{i}\frac{\omega}{\mathrm{c_i}}[\phi_\omega(\boldsymbol{x})-\mathrm{c_i}t] - \frac{|\boldsymbol{x}|}{2|\boldsymbol{l}_{\mathrm{e}\omega}(\boldsymbol{n}_\phi(\boldsymbol{x}))|}\right\}}{4\pi|\boldsymbol{x}|} \times\exp\left\{-\frac{\mathrm{i}\omega\boldsymbol{n}_\phi(\boldsymbol{x})\cdot\boldsymbol{x}_0}{\tilde{v}_\mathrm{p}(\boldsymbol{n}_\phi(\boldsymbol{x}))} + \frac{\boldsymbol{n}_\phi(\boldsymbol{x})\cdot\boldsymbol{x}_0}{2\boldsymbol{l}_{\mathrm{e}\omega}(\boldsymbol{n}_\varphi(\boldsymbol{x}))\cdot\boldsymbol{n}_\phi(\boldsymbol{x})}\right\}. \quad (4.21)$$

Here $\tilde{v}_\mathrm{p}(\boldsymbol{n}_\varphi)$ is the phase velocity dressed with scattering effects (2.34a). Coordinate $\boldsymbol{x}$ is outside the disordered medium, and in the first exponential we must take $\boldsymbol{l}_\mathrm{e}$ to infinity, because there are no scatterers outside the inhomogeneous medium. On the other hand, $\boldsymbol{x}_0$ is inside the medium, so in the second exponential we have $\boldsymbol{n}_\phi(\boldsymbol{x})\cdot\boldsymbol{x}_0 \le 0$ and therefore a the emerging amplitude decays more when the last scattering event is deeper inside the disordered medium. In the second exponential we can identify the complex wave vector of the infinite medium (2.68) by

$$\boldsymbol{\kappa}(\boldsymbol{n}_\varphi(\boldsymbol{x})) = \frac{\omega\boldsymbol{n}_\phi(\boldsymbol{x})}{\tilde{v}_\mathrm{p}(\boldsymbol{n}_\phi(\boldsymbol{x}))} + \mathrm{i}\frac{\boldsymbol{n}_\phi(\boldsymbol{x})}{2\boldsymbol{l}_{\mathrm{e}\omega}(\boldsymbol{n}_\varphi(\boldsymbol{x}))\cdot\boldsymbol{n}_\phi(\boldsymbol{x})}. \quad (4.22)$$

The normal to the wave surface $\boldsymbol{n}_\varphi(\boldsymbol{x})$ acts as wave vector, and we write $\boldsymbol{e}_{\boldsymbol{k}} = \boldsymbol{n}_\varphi(\boldsymbol{x})$. In the presence of a boundary we must express wave vector (4.22) in terms of the wave vector outside the disordered medium. For this we use continuity requirement (4.8) for the parallel wave vector components, and Eqs. (4.13) for the perpendicular component.

For notational convenience, we introduce two generalizations of $\cos\theta =$

$-\boldsymbol{e}_{\boldsymbol{\kappa}}\cdot\boldsymbol{n}_\perp$ by

$$u_\omega(\boldsymbol{e}_{\boldsymbol{\kappa}},\boldsymbol{n}_\perp) \equiv \sqrt{\frac{\mathrm{Re}[\tilde{\mu}_\omega(\boldsymbol{\kappa})]+|\tilde{\mu}_\omega(\boldsymbol{\kappa})|}{2\mu}}, \tag{4.23}$$

$$\tilde{u}_\omega(\boldsymbol{e}_{\boldsymbol{\kappa}},\boldsymbol{n}_\perp) \equiv u_\omega(\boldsymbol{e}_{\boldsymbol{\kappa}},\boldsymbol{n}_\perp) - \frac{\boldsymbol{v}_{\mathrm{g}}(\boldsymbol{n}_\perp)\cdot\boldsymbol{e}_{\boldsymbol{\kappa}_\parallel}}{v_{\mathrm{i}}(\boldsymbol{e}_{\boldsymbol{\kappa}})}\boldsymbol{e}_{\boldsymbol{\kappa}_\parallel}\cdot\boldsymbol{e}_{\boldsymbol{\kappa}}. \tag{4.24}$$

For scatterer density $n=0$ and isotropic media $\mathsf{A}=1$ both of these quantities reduce to $(1-(\boldsymbol{e}_{\boldsymbol{\kappa}}\cdot\boldsymbol{e}_{\boldsymbol{\kappa}_\parallel})^2)^{1/2}=\sqrt{(-\boldsymbol{e}_{\boldsymbol{\kappa}}\cdot\boldsymbol{n}_\perp)^2}=\cos\theta$.

Using the asymptotic Green function (4.21), and boundary condition (4.6a) for ψ, we finally obtain the Green function describing propagation across a boundary,

$$\begin{aligned} G_{\mathrm{b}\omega}(\boldsymbol{x},\boldsymbol{x}_0,t) \equiv{}& \frac{\mathrm{B}^>}{\mathrm{B}^<}\frac{|\boldsymbol{v}_{\mathrm{g}}(\boldsymbol{e}_{\boldsymbol{k}})|}{\mathrm{c_i}\sqrt{\det\mathsf{A}}}\frac{\exp\left\{\mathrm{i}\frac{\omega}{\mathrm{c_i}}[\phi_\omega(\boldsymbol{x})-\mathrm{c_i}t]\right\}}{4\pi|\boldsymbol{x}|} \\ &\times\exp\left\{\mathrm{i}\boldsymbol{k}_\parallel\cdot\boldsymbol{x}_0+\mathrm{i}\frac{\omega\tilde{u}_\omega(\boldsymbol{e}_{\boldsymbol{\kappa}},\boldsymbol{n}_\perp)z_0}{|\boldsymbol{v}_{\mathrm{g}}(\boldsymbol{n}_\perp)|}-\frac{z_0}{2|\boldsymbol{l}_{\mathrm{e}\omega}(\boldsymbol{n}_\perp)|u_\omega(\boldsymbol{e}_{\boldsymbol{\kappa}},\boldsymbol{n}_\perp)}\right\}. \end{aligned} \tag{4.25}$$

In the second exponent we used $v_{\mathrm{p}}(\boldsymbol{n}_\perp)/|\boldsymbol{v}_{\mathrm{g}}(\boldsymbol{n}_\perp)|=\boldsymbol{n}_\phi(z_0\boldsymbol{n}_\perp)\cdot\boldsymbol{n}_\perp$.

We will use the results of this section for calculations on reflection, enhanced backscattering and total transmission of multiple scattered light. We disregard the reflections at the interface for the waves escaping the disordered medium, because these internal reflections will be accounted for in the boundary conditions on the (diffuse) radiance.

4.2.e Reflectivity and transmissivity

Not only the amplitude is reflected and refracted when crossing an interface, but also the energy density flux (per frequency band) is partitioned in a reflected and a transmitted part. In this section we will determine the transmissivity and reflectivity which quantify how much of the energy density actually traverses the boundary and how much is reflected. We will also introduce reflection and transmission tensors, which are related to the reflectivity and transmissivity.

We could call the energy flux density the intensity as it has units $\mathrm{W\,m^{-2}}$, which is an intensity according to the *SI*. However the term intensity is in the literature used for many different quantities, which do not always represent power per area. To prevent confusion with specific intensity $\mathrm{W\,m^{-2}\,sr^{-1}}$, which appears a lot in the literature on radiative transfer, and which is radiance according to the *SI*, we prefer to avoid the term intensity.

The reflectivity and transmissivity are, for an incident harmonic plane wave at frequency ω and wave vector $\boldsymbol{k}(\omega)$ at each point $\boldsymbol{x}$ on the interface at $z = 0$, defined by

$$R_{\boldsymbol{k}}(\boldsymbol{x}) \equiv -\frac{\boldsymbol{n}_\perp \cdot \boldsymbol{S}_{\mathrm{r}\boldsymbol{k}}(\boldsymbol{x})}{\boldsymbol{n}_\perp \cdot \boldsymbol{S}_{\mathrm{i}\boldsymbol{k}}(\boldsymbol{x})}, \tag{4.26a}$$

$$T_{\boldsymbol{k}}(\boldsymbol{x}) \equiv \frac{\boldsymbol{n}_\perp \cdot \boldsymbol{S}_{\mathrm{t}\boldsymbol{k}}(\boldsymbol{x})}{\boldsymbol{n}_\perp \cdot \boldsymbol{S}_{\mathrm{i}\boldsymbol{k}}(\boldsymbol{x})} = 1 - R_{\boldsymbol{k}}. \tag{4.26b}$$

Here $\boldsymbol{S}_{\mathrm{i}}$, $\boldsymbol{S}_{\mathrm{r}}$, and $\boldsymbol{S}_{\mathrm{t}}$ are the energy density flux of the incident, reflected and transmitted harmonic plane respectively, which we will identify below. The time dependence of the harmonic plane wave drops out of the equation, but its direction does not.

In section 4.2.a we established flux conservation for the component perpendicular to the boundary in Eq. (4.5), which we repeat here for the energy density flux of the harmonic plane wave,

$$\lim_{z\uparrow 0} \boldsymbol{n}_\perp \cdot \boldsymbol{S}^{<}_{\boldsymbol{k}}(\boldsymbol{x}) = \lim_{z\downarrow 0} \boldsymbol{n}_\perp \cdot \boldsymbol{S}^{>}_{\boldsymbol{k}}(\boldsymbol{x}). \tag{4.27}$$

The energy density flux of a scalar wave in an anisotropic medium is $\boldsymbol{S} = -\partial\psi/\partial t \mathsf{A}\cdot\boldsymbol{\nabla}\psi^* + \text{c.c.}$, where c.c. means complex conjugate. We send in a harmonic plane wave originating from $z \to -\infty$, and traveling through a (possibly anisotropic) homogeneous medium. A part of the incident wave amplitude is reflected and another part is refracted, which is described by wave amplitude (4.16). The wave vectors of the incident, reflected, and transmitted waves are $\boldsymbol{k} = \boldsymbol{k}_\parallel + \boldsymbol{k}_\perp$, $\boldsymbol{k}_{\mathrm{r}} = \boldsymbol{k}_\parallel - \boldsymbol{k}_\perp$, and $\boldsymbol{\kappa} = \boldsymbol{k}_\parallel + \boldsymbol{\kappa}_\perp(\boldsymbol{e}_{\boldsymbol{k}})$, with $\kappa_\perp$ given by (4.13). We obtain for the energy density fluxes on each side of the boundary

$$\lim_{z\uparrow 0} \boldsymbol{S}^{<}_{\boldsymbol{k}}(\boldsymbol{x}) = 2\omega|\psi_0|^2 \mathsf{A}^{<}\cdot\left[\boldsymbol{k} + \boldsymbol{k}_{\mathrm{r}}|r_{\mathrm{F}}(\boldsymbol{k})|^2 - (\boldsymbol{k}+\boldsymbol{k}_{\mathrm{r}})\mathrm{Re}[r_{\mathrm{F}}(\boldsymbol{k})]\right], \tag{4.28a}$$

$$\lim_{z\downarrow 0} \boldsymbol{S}^{>}_{\boldsymbol{k}}(\boldsymbol{x}) = 2\omega|\psi_0|^2 \mathsf{A}^{>}\cdot\mathrm{Re}[\boldsymbol{\kappa}]|t_{\mathrm{F}}(\boldsymbol{k})|^2. \tag{4.28b}$$

It turns out that the flux does not depend on $\boldsymbol{x}$, unless we were to make the anisotropy A coordinate dependent, but this would at the same time destroy the harmonic plane wave. At the boundary it makes sense that only the real part of the complex wave vector $\boldsymbol{\kappa}$ appears, as infinitesimally close to the boundary the transmitted energy has not had the chance to scatter.

In Eq. (4.28a) we identify three terms, an incident flux, a reflected flux proportional to $|r_{\mathrm{F}}(\boldsymbol{k})|^2$, and a term proportional to $\mathrm{Re}[r_{\mathrm{F}}]$ which represents interference of the incident and reflected wave. Note that $\boldsymbol{k} + \boldsymbol{k}_{\mathrm{r}} = 2\boldsymbol{k}_\parallel$, and in isotropic media this is a flux parallel to the interface. The interference term does not vanish when we average over surface area, nor when we cycle average. In

the absence of an interface, the interference term is also absent, and therefore we count it as a contribution to the reflected flux, using $\boldsymbol{k}_\parallel = (1-\boldsymbol{n}_\perp\boldsymbol{n}_\perp)\cdot\boldsymbol{k}_\mathrm{r}$. There is an ambiguity in counting the term containing $\mathrm{Re}[r_\mathrm{F}(\boldsymbol{k})]$ as a reflection, because that term can be expressed as

$$\mathrm{Re}[r_\mathrm{F}(\boldsymbol{k})] = 1 + |r_\mathrm{F}(\boldsymbol{k})|^2 - \frac{\mathrm{B}^{<2}}{\mathrm{B}^{>2}}|t_\mathrm{F}(\boldsymbol{k})|^2. \tag{4.29}$$

Inserting Eq. (4.29) in (4.28a) together with $\boldsymbol{k}+\boldsymbol{k}_\mathrm{r} = 2\boldsymbol{k}_\parallel$ shows that the parallel components of the wave vector are not reflected, provided we enlist the term $2\omega|\psi_0|^2(\mathrm{B}^</\mathrm{B}^>)^2|t_\mathrm{F}(\boldsymbol{k})|^2\mathsf{A}^<\cdot\boldsymbol{k}_\parallel$ as contribution to the transmitted flux. Nonetheless, we identify the incident, reflected, and transmitted flux, $\boldsymbol{S}_\mathrm{i}$, $\boldsymbol{S}_\mathrm{r}$, and $\boldsymbol{S}_\mathrm{t}$ respectively, by

$$\boldsymbol{S}_{\mathrm{i}\boldsymbol{k}} \equiv 2\omega|\psi_0|^2\mathsf{A}^<\cdot\boldsymbol{k}, \tag{4.30a}$$

$$\boldsymbol{S}_{\mathrm{r}\boldsymbol{k}} \equiv 2\omega|\psi_0|^2\mathsf{A}^<\cdot\left[|r_\mathrm{F}(\boldsymbol{k})|^2\mathsf{1} - 2\mathrm{Re}[r_\mathrm{F}(\boldsymbol{k})](1-\boldsymbol{n}_\perp\boldsymbol{n}_\perp)\right]\cdot\boldsymbol{k}_\mathrm{r} \equiv -\mathsf{R}_{\boldsymbol{k}}\cdot\boldsymbol{S}_{\mathrm{i}\boldsymbol{k}}, \tag{4.30b}$$

$$\boldsymbol{S}_{\mathrm{t}\boldsymbol{k}} \equiv 2\omega|\psi_0|^2\mathsf{A}^>\cdot\mathrm{Re}[\boldsymbol{\kappa}]|t_\mathrm{F}(\boldsymbol{k})|^2 \equiv \mathsf{T}_{\boldsymbol{k}}\cdot\boldsymbol{S}_{\mathrm{i}\boldsymbol{k}}. \tag{4.30c}$$

The reflection and transmission tensors R and T are

$$\mathsf{R}_{\boldsymbol{k}} = \mathsf{A}^<\cdot\left[|r_\mathrm{F}(\boldsymbol{k})|^2\boldsymbol{n}_\perp\boldsymbol{n}_\perp - \left(|r_\mathrm{F}(\boldsymbol{k})|^2 - 2\mathrm{Re}[r_\mathrm{F}(\boldsymbol{k})]\right)(1-\boldsymbol{n}_\perp\boldsymbol{n}_\perp)\right]\cdot\mathsf{A}^{<-1}, \tag{4.31a}$$

$$\mathsf{T}_{\boldsymbol{k}} = \mathsf{A}^>\cdot\left[\frac{\mathrm{Re}[\kappa_\perp(\boldsymbol{e}_{\boldsymbol{k}})]}{k_\perp(\boldsymbol{e}_{\boldsymbol{k}})}|t_\mathrm{F}(\boldsymbol{k})|^2\boldsymbol{n}_\perp\boldsymbol{n}_\perp + |t_\mathrm{F}(\boldsymbol{k})|^2(1-\boldsymbol{n}_\perp\boldsymbol{n}_\perp)\right]\cdot\mathsf{A}^{<-1}. \tag{4.31b}$$

We start by considering boundary condition (4.27) for media which satisfy requirements (4.18), i.e. $\boldsymbol{n}_\perp\cdot\mathsf{A}^<\cdot\boldsymbol{n}_\perp \approx \boldsymbol{n}_\perp\cdot\mathsf{A}^>\cdot\boldsymbol{n}_\perp$, $\boldsymbol{n}_\perp\cdot\mathsf{A}^<\cdot\boldsymbol{e}_\parallel \approx \boldsymbol{n}_\perp\cdot\mathsf{A}^>\cdot\boldsymbol{e}_\parallel$ and $\mathrm{B}^< \approx \mathrm{B}^>$. The Fresnel coefficients r_F and t_F are approximated by r_aF and t_aF respectively. The definitions (4.26) of reflectivity and transmissivity definitions applied in these media lead to

$$R_{\boldsymbol{k}} \approx R_{\mathrm{a}\boldsymbol{k}} \equiv |r_\mathrm{aF}(\boldsymbol{k})|^2, \tag{4.32a}$$

$$T_{\boldsymbol{k}} \approx T_{\mathrm{a}\boldsymbol{k}} \equiv \frac{\boldsymbol{n}_\perp\cdot\mathrm{Re}[\boldsymbol{\kappa}]}{\boldsymbol{n}_\perp\cdot\boldsymbol{k}}|t_\mathrm{aF}(\boldsymbol{k})|^2 = 1 - R_{\mathrm{a}\boldsymbol{k}}. \tag{4.32b}$$

The final equality is established using Eqs. (4.17) for the Fresnel coefficients. We have total transmission $T_{\boldsymbol{k}} = 1$ for all $\boldsymbol{k}$ only in the absence of both index mismatch and scatterers. We can use the approximation $T_{\boldsymbol{k}} \approx 1$ if $\mathrm{Re}[\boldsymbol{\kappa}] \approx \boldsymbol{k}$, which happens when we either are in the independent scattering approximation (4.14a), or when the scatterers are on resonance. In isotropic media

$\boldsymbol{n}_\perp \cdot \mathsf{A}^< \cdot \boldsymbol{n}_\perp = 1 = \boldsymbol{n}_\perp \cdot \mathsf{A}^> \cdot \boldsymbol{n}_\perp$, and reflectivity and transmissivity (4.26) reduce to the well known result [53, 54, 100]. We note that the reflection and transmission tensor R and T in these media become

$$\mathsf{R}_{\boldsymbol{k}} \approx \mathsf{R}_{\mathrm{a}\boldsymbol{k}} \equiv R_{\mathrm{a}\boldsymbol{k}} \boldsymbol{n}_\perp \boldsymbol{n}_\perp + \left(1 - |t_{\mathrm{aF}}(\boldsymbol{k})|^2\right)[1 - \boldsymbol{n}_\perp \boldsymbol{n}_\perp], \tag{4.33a}$$

$$\mathsf{T}_{\boldsymbol{k}} \approx \mathsf{T}_{\mathrm{a}\boldsymbol{k}} \equiv T_{\mathrm{a}\boldsymbol{k}} \boldsymbol{n}_\perp \boldsymbol{n}_\perp + |t_{\mathrm{aF}}(\boldsymbol{k})|^2 [1 - \boldsymbol{n}_\perp \boldsymbol{n}_\perp] = 1 - \mathsf{R}_{\mathrm{a}\boldsymbol{k}}, \tag{4.33b}$$

All components of the flux are continuous in media which satisfy requirements (4.18), so for every harmonic plane wave we have

$$\boldsymbol{S}_{\mathrm{i}\boldsymbol{k}} = \mathsf{R}_{\mathrm{a}\boldsymbol{k}} \cdot \boldsymbol{S}_{\mathrm{i}\boldsymbol{k}} + \mathsf{T}_{\mathrm{a}\boldsymbol{k}} \cdot \boldsymbol{S}_{\mathrm{i}\boldsymbol{k}} \approx -\boldsymbol{S}_{\mathrm{r}\boldsymbol{k}} + \boldsymbol{S}_{\mathrm{t}\boldsymbol{k}}. \tag{4.34}$$

We continue with the treatment for general anisotropic dielectrics. The reflectivity and transmissivity follow from definitions (4.26) using fluxes (4.30) without any approximations, and are

$$R_{\boldsymbol{k}} = -\frac{\boldsymbol{n}_\perp \cdot \mathsf{A}^< \cdot \left\{|r_{\mathrm{F}}(\boldsymbol{k})|^2 1 - 2\mathrm{Re}[r_{\mathrm{F}}(\boldsymbol{k})](1 - \boldsymbol{n}_\perp \boldsymbol{n}_\perp)\right\} \cdot \boldsymbol{k}_{\mathrm{r}}}{\boldsymbol{n}_\perp \cdot \mathsf{A}^< \cdot \boldsymbol{k}}, \tag{4.35a}$$

$$T_{\boldsymbol{k}} = \frac{\boldsymbol{n}_\perp \cdot \mathsf{A}^> \cdot \mathrm{Re}[\boldsymbol{\kappa}] |t_{\mathrm{F}}(\boldsymbol{k})|^2}{\boldsymbol{n}_\perp \cdot \mathsf{A}^< \cdot \boldsymbol{k}} = 1 - R_{\boldsymbol{k}}. \tag{4.35b}$$

In contrast with the approximated reflectivity and transmissivity (4.32), the exact reflectivity and transmissivity depend on the polarization of the harmonic plane wave through the ratio $B^{>2}/B^{<2}$ present in Fresnel coefficients (4.19). Thus, by taking the appropriate values for this ratio, as discussed in section 4.2.a, we obtain separate expressions for the reflectivity and transmissivity as well as for the reflection and transmission tensors for waves polarized parallel and perpendicular to the plane of incidence. In Fig. 4.2 we plotted the reflectivity and transmissivity for parallel polarized waves in isotropic and anisotropic media.

The reflection and transmission tensors R and T do not add up for all components as only the flux component perpendicular to the interface is continuous. However, we can write for all unit vectors $\boldsymbol{e}_\parallel$ in the planes defined by normal $\boldsymbol{n}_\perp$

$$\boldsymbol{n}_\perp \cdot \boldsymbol{S}_{\mathrm{i}\boldsymbol{k}} = -\boldsymbol{n}_\perp \cdot \boldsymbol{S}_{\mathrm{r}\boldsymbol{k}} + \boldsymbol{n}_\perp \cdot \boldsymbol{S}_{\mathrm{t}\boldsymbol{k}} = \boldsymbol{n}_\perp \cdot \mathsf{R}_{\boldsymbol{k}} \cdot \boldsymbol{S}_{\mathrm{i}\boldsymbol{k}} + \boldsymbol{n}_\perp \cdot \mathsf{T}_{\boldsymbol{k}} \cdot \boldsymbol{S}_{\mathrm{i}\boldsymbol{k}}. \tag{4.36}$$

In the derivation of the reflectivity, transmissivity, and the reflection and transmission tensors presented in this section, so far there is only a single wave vector for a harmonic plane wave of some polarization. Often waves consist of many wave vectors and many polarizations. If all these wave vectors belong to the same frequency and the same polarization, we can integrate

Eqs. (4.36) over the distribution of wave vectors, and extract angle averaged reflectivity and transmissivity tensors and the angle averaged reflected and transmitted flux. If there is also a certain distribution of polarizations, then we can write it as a superposition of the orthogonal polarizations discussed in section 4.2.a, which we can send into the medium with certain weights w_i, and add these up. The angle and polarization averaged fluxes are

$$\boldsymbol{S}_{\mathrm{i}\omega} \equiv \sum_{i=1}^{4} w_i \int \mathrm{d}^2 e_{\boldsymbol{k}} \boldsymbol{S}_{\mathrm{i}\boldsymbol{k}}^{i}, \tag{4.37a}$$

$$\boldsymbol{S}_{\mathrm{r}\omega} \equiv \sum_{i=1}^{4} w_i \int \mathrm{d}^2 e_{\boldsymbol{k}} \boldsymbol{S}_{\mathrm{r}\boldsymbol{k}}^{i} \equiv -\mathsf{R}_\omega \cdot \boldsymbol{S}_{\mathrm{i}\omega}, \tag{4.37b}$$

$$\boldsymbol{S}_{\mathrm{t}\omega} \equiv \sum_{i=1}^{4} w_i \int \mathrm{d}^2 e_{\boldsymbol{k}} \boldsymbol{S}_{\mathrm{t}\boldsymbol{k}}^{i} \equiv \mathsf{T}_\omega \cdot \boldsymbol{S}_{\mathrm{i}\omega}. \tag{4.37c}$$

Here $\boldsymbol{k}$ is the wave vector of the incident harmonic plane wave of frequency ω and the index i identifies the polarization of the weights and fluxes.

The angle and polarization averaged fluxes (4.37) are also subject to boundary condition (4.27) or (4.5), and therefore

$$\boldsymbol{n}_\perp \cdot \boldsymbol{S}_{\mathrm{i}\omega} = -\boldsymbol{n}_\perp \cdot \boldsymbol{S}_{\mathrm{r}\omega} + \boldsymbol{n}_\perp \cdot \boldsymbol{S}_{\mathrm{t}\omega} = \boldsymbol{n}_\perp \cdot \mathsf{R}_\omega \cdot \boldsymbol{S}_{\mathrm{i}\omega} + \boldsymbol{n}_\perp \cdot \mathsf{T}_\omega \cdot \boldsymbol{S}_{\mathrm{i}\omega}. \tag{4.38}$$

The continuity of the perpendicular flux component (4.38) gives rise to angle and polarization averaged reflectivity and transmissivity, which are by definition

$$R_\omega \equiv -\frac{\boldsymbol{n}_\perp \cdot \boldsymbol{S}_{\mathrm{r}\omega}}{\boldsymbol{n}_\perp \cdot \boldsymbol{S}_{\mathrm{i}\omega}} = \frac{\boldsymbol{n}_\perp \cdot \mathsf{R}_\omega \cdot \boldsymbol{S}_{\mathrm{i}\omega}}{\boldsymbol{n}_\perp \cdot \boldsymbol{S}_{\mathrm{i}\omega}}, \tag{4.39a}$$

$$T_\omega \equiv \frac{\boldsymbol{n}_\perp \cdot \boldsymbol{S}_{\mathrm{t}\omega}}{\boldsymbol{n}_\perp \cdot \boldsymbol{S}_{\mathrm{i}\omega}} = \frac{\boldsymbol{n}_\perp \cdot \mathsf{T}_\omega \cdot \boldsymbol{S}_{\mathrm{t}\omega}}{\boldsymbol{n}_\perp \cdot \boldsymbol{S}_{\mathrm{i}\omega}} = 1 - R_\omega. \tag{4.39b}$$

We have only formally related the angle and polarization averaged reflectivity and transmissivity to the reflectivity for plane waves through equations (4.37) and (4.39). Explicit relations are only obtained when we are provided with additional information about the angle and polarization distributions of the plane waves which constitute the angle and polarization averaged fluxes.

Although the reflection and transmission tensors have the drawback that they do not add up to yield the unit tensor, they do have one advantage over the reflectivity and transmissivity. If we want to incorporate surface roughness which is anisotropic on average, then adding anisotropy to the reflectivity or transmissivity necessarily implies that all components of the energy density flux are affected equally, but by adding it to the reflection or transmission tensor we can independently influence each component of the energy

density flux. Angle and polarization averaged reflectivity, transmissivity and reflection and transmission tensors are used in sections 4.2.f and 4.2.g in the boundary conditions on the radiance and diffuse energy density, and in all other sections on multiple scattered light.

4.2.f Radiance per frequency band

To determine the what happens at an interface between a homogeneous and a disordered medium for the multiple scattered radiance, we suppose an initial situation in which there is radiance in the disordered medium only. Such an initial situation is achieved by switching on a light somewhere deep inside the sample as in Fig. 4.3 We again choose coordinates such that the homogeneous medium is at $z < 0$, and the inhomogeneous medium is at $z > 0$. There are no scatterers in the homogeneous medium to change the propagation direction of the energy density, so we know that at the interface there is no energy density flux coming in from the homogeneous medium. The energy density flux $\boldsymbol{S}^{\pm}$ crossing the interface in the $\pm\boldsymbol{n}_{\perp}$ direction is

$$\boldsymbol{S}_{\omega}^{\pm}(\boldsymbol{x},t) \quad \equiv \quad \int_{B_{\pm}} \mathrm{d}^2 \boldsymbol{e}_{\boldsymbol{k}} I_{\omega}(\boldsymbol{e}_{\boldsymbol{k}},\boldsymbol{x},t) \frac{\boldsymbol{v}_{\mathrm{g}}(\boldsymbol{e}_{\boldsymbol{k}})}{|\boldsymbol{v}_{\mathrm{g}}(\boldsymbol{e}_{\boldsymbol{k}})|}, \tag{4.40}$$

where the integration domain $B_{\pm}$ is the set of all wave vectors $\boldsymbol{e}_{\boldsymbol{k}}$ such that $\pm\boldsymbol{n}_{\perp}\cdot\boldsymbol{v}_{\mathrm{g}}(\boldsymbol{p}) \geq 0$. The boundary condition which expresses that there is no flux moving towards the inhomogeneous medium is [6]

$$0 \quad = \quad \boldsymbol{n}_{\perp}\cdot\boldsymbol{S}_{\omega}^{+}(\boldsymbol{x}) \quad = \quad \frac{\omega^2}{\mathrm{c_i}^2}\int_{B_{+}} \frac{\mathrm{d}^2\boldsymbol{e}_{\boldsymbol{k}}}{(2\pi)^3} \frac{\boldsymbol{n}_{\perp}\cdot\boldsymbol{v}_{\mathrm{g}}(\boldsymbol{e}_{\boldsymbol{k}})}{|\boldsymbol{v}_{\mathrm{g}}(\boldsymbol{e}_{\boldsymbol{k}})|} I_{\omega}(\boldsymbol{e}_{\boldsymbol{k}},\boldsymbol{x},t), \tag{4.41}$$

where the integration domain B_{+} is the set of all wave vectors $\boldsymbol{e}_{\boldsymbol{k}}$ such that $\boldsymbol{n}_{\perp}\cdot\boldsymbol{v}_{\mathrm{g}}(\boldsymbol{e}_{\boldsymbol{k}}) \geq 0$. However, there may be an index mismatch at the interface, and then part of the flux moving towards the homogeneous medium will reflect. As explained in section 4.2.f we can introduce angle and polarization averaged reflection and transmission tensors R and T defined as (4.37). The boundary condition becomes

$$\boldsymbol{n}_{\perp}\cdot\boldsymbol{S}_{\omega}^{+}(\boldsymbol{x}) \quad = \quad -\boldsymbol{n}_{\perp}\cdot\mathsf{R}_{\omega}\cdot\boldsymbol{S}_{\omega}^{-}(\boldsymbol{x}). \tag{4.42}$$

We illustrate boundary condition (4.42) in Fig 4.3. Note that in contrast to the situation described in section 4.2.f here the waves originate from the disordered medium instead of the homogeneous medium. When $\mathsf{R} \to 0$, then (4.42) reduces to (4.40). In Eq. (4.42) we could use the identity $-\boldsymbol{n}_{\perp}\cdot\mathsf{R}_{\omega}\cdot\boldsymbol{S}_{\omega}^{-}(\boldsymbol{x}) = -R_{\omega}\boldsymbol{n}_{\perp}\cdot\boldsymbol{S}_{\omega}^{-}(\boldsymbol{x})$ with R_{ω} an average reflectivity. The advantage of using an average reflection tensor R over an average reflectivity R is that a reflection tensor makes it possible to incorporate anisotropic surface roughness, which can

affect each component of $\boldsymbol{S}^-$ in a different way if the anisotropy of the roughness does not average out. Both boundary conditions, (4.41) and (4.42), will be applied to the diffuse radiance in section 4.2.g.

4.2.g Diffuse energy density

The diffusion equation for the energy density of the waves is an approximation on the radiative transfer equation, and yields very accurate results for a description of transport of light through most disordered media if (homogeneous) Dirichlet-Neumann boundary conditions are used [6, 101, 102]. The Dirichlet-Neumann boundary conditions are also known under the names impedance, Robin, or mixed boundary conditions. These boundary conditions are direct consequence of the condition for the radiance (4.41).

Not only are Dirichlet-Neumann boundary conditions relevant for an accurate description of the distribution of diffuse energy density, but they are also essential for the definition of the transport mean free path, even in isotropic media. The reason is that a stationary isotropic diffusion equation, for energy density $\mathscr{H}$, which reads $D\boldsymbol{\nabla}\cdot\boldsymbol{\nabla}\mathscr{H} = 0$, can be scaled by an arbitrary multiplicative constant, without altering the diffusive behavior. A boundary condition can fix this ambiguity. In isotropic media, in the absence of internal reflections, the boundary condition looks like $\mathscr{H} = 2l\boldsymbol{n}_\perp\cdot\boldsymbol{\nabla}\mathscr{H}/3$, with l the transport mean free path and $\boldsymbol{n}_\perp$ the normal to the surface [101]. The stationary diffusion equation then becomes $l\boldsymbol{\nabla}\cdot\boldsymbol{\nabla}\mathscr{H}/3 = 0$. Once we know the transport mean free path, and we consider only stationary diffusion, we still can not define the diffusion constant. For a proper definition of the diffusion constant we must start with a dynamic diffusion equation $\partial\mathscr{H}/\partial t - D\boldsymbol{\nabla}\cdot\boldsymbol{\nabla}\mathscr{H} = 0$, and use boundary condition (4.41). Boundary condition (4.41) applied to dynamic diffuse radiance results, for isotropic diffusion, in $v\mathscr{H}/4 + D\boldsymbol{n}_\perp\cdot\boldsymbol{\nabla}\mathscr{H}/2 = 0$, where v is the energy velocity of the waves, and $\mathscr{H}$ is the energy density [102]. The energy velocity v is the quantity that is not present in stationary diffusion. Stationary diffusion is a special case of dynamic diffusion, so we identify $D = vl/3$, and recover the stationary boundary condition $\mathscr{H} = 2l\boldsymbol{n}_\perp\cdot\boldsymbol{\nabla}\mathscr{H}/3$. We will use a similar approach to determine the transport mean free path and energy velocity in anisotropic media.

We again start with the assumption that at first there is radiance only inside the multiple scattering medium. If we calculate the right hand side using (4.41) and the self consistent expansion of the radiance in anisotropic media, which we derived in chapter 2, we find for the total diffuse energy density $\mathscr{H}$ the boundary condition

$$0 \quad \equiv \quad \frac{1}{4}\frac{\boldsymbol{n}_\perp\cdot\boldsymbol{v}_{\mathrm{g}}(\boldsymbol{n}_\perp)}{1+\delta_\omega}\mathscr{H}_\omega(\boldsymbol{x},t) - \frac{1}{2}\boldsymbol{n}_\perp\cdot\mathsf{D}_\omega\cdot\boldsymbol{\nabla}\mathscr{H}_\omega(\boldsymbol{x},t)\,. \tag{4.43}$$

The factors 1/4 and 1/2 are always obtained in three dimensions for isotropic media [68, 102]. We can write down (4.43) for boundaries of arbitrary orientation $\boldsymbol{n}_\perp$ with respect to the principal axes of the anisotropy $\{\boldsymbol{e}_i\}$. Therefore we identify an energy velocity vector $\boldsymbol{v}$ and a transport mean free path vector $\boldsymbol{l}$ by

$$\boldsymbol{v}_\omega(\boldsymbol{e_k}) \equiv \frac{\boldsymbol{v}_g(\boldsymbol{e_k})}{1+\delta_\omega} \tag{4.44}$$

$$\boldsymbol{l}_\omega(\boldsymbol{e_k}) \equiv \frac{3\boldsymbol{e_k}\cdot \mathsf{D}_\omega}{\boldsymbol{e_k}\cdot\boldsymbol{v}_\omega(\boldsymbol{e_k})} = \mathsf{t}_\omega\cdot\boldsymbol{v}_g(\boldsymbol{e_k}). \tag{4.45}$$

Had we not had boundary condition (4.43), we would not have been able to unambiguously define a transport velocity and transport mean free path. For example, the scattering delay could erroneously be absorbed in the transport mean free path. The transport mean free path reduces to the extinction mean free path when the scatterers scatter isotropic.

Transport mean free path (4.45) gives rise to the equivalent boundary condition which has a completely stationary appearance

$$\mathscr{H}_\omega(\boldsymbol{x},t) = \frac{2}{3}\boldsymbol{l}_\omega(\boldsymbol{n}_\perp)\cdot\boldsymbol{\nabla}\mathscr{H}_\omega(\boldsymbol{x},t). \tag{4.46}$$

In chapter 3 we derived diffusion tensor $\mathsf{D} = \mathsf{t}\cdot\langle \boldsymbol{v}_g\boldsymbol{v}_g\rangle/(1+\delta)$, were we introduced the angular average over the surface of constant frequency by,

$$\langle\ldots\rangle_{\boldsymbol{e_k}} = \int \frac{\mathrm{d}^2\boldsymbol{e_k}}{4\pi}\frac{\ldots}{\sqrt{(\boldsymbol{e_k}\cdot\mathsf{A}\cdot\boldsymbol{e_k})^3\det\mathsf{A}^{-1}}}. \tag{4.47}$$

Using Eqs. (4.44), (4.45), and (4.47), we express the diffusion tensor in terms of the transport mean free path and transport velocity, and a few interesting variants,

$$\mathsf{D}_\omega = \langle \boldsymbol{v}_\omega(\boldsymbol{e_k})\boldsymbol{l}_\omega(\boldsymbol{e_k})\rangle_{\boldsymbol{e_k}} \tag{4.48a}$$

$$= \frac{\mathsf{t}_\omega^{-1}}{1+\delta_\omega}\cdot\langle \boldsymbol{l}_\omega(\boldsymbol{e_k})\boldsymbol{l}_\omega(\boldsymbol{e_k})\rangle_{\boldsymbol{e_k}} \tag{4.48b}$$

$$= \langle (1+\delta_\omega)\boldsymbol{v}_\omega(\boldsymbol{e_k})\mathsf{t}_\omega\cdot\boldsymbol{v}_\omega(\boldsymbol{e_k})\rangle_{\boldsymbol{e_k}} \tag{4.48c}$$

$$= \frac{1}{3}\sum_{i=1}^{3}\left[\boldsymbol{e}_i\cdot\boldsymbol{v}_\omega(\boldsymbol{e}_i)\boldsymbol{e}_i\boldsymbol{l}_\omega(\boldsymbol{e}_i)\right]. \tag{4.48d}$$

The second option (4.48b) explicitly separates a dynamic transport time tensor from the stationary transport mean free path. In stationary experiments it is only possible to measure the stationary mean free path. The dynamic time scales are inaccessible in stationary measurements. Therefore it is impossible to measure the complete diffusion tensor in a stationary measurement.

For a full characterization of the diffusion tensor dynamic measurements are necessary to discover the anisotropy in the dynamic time scale.

The mean free path vector and the energy velocity vector are physically well defined, but sometimes difficult to work with. We might also define a scalar or tensorial mean free path and energy velocity, although these are much less well defined as physical quantities. To obtain either of these we strip boundary condition (4.41) from the normal vector $\boldsymbol{n}_\perp$. There is no reason why there should the flux components along the boundary should vanish, which is why the tensor mean free path is ill defined. We know that $\boldsymbol{v}_g(\boldsymbol{n}_\perp)/(1+\delta_\omega) = c_i^2 A \cdot \boldsymbol{n}_\perp / [v_p(\boldsymbol{n}_\perp)(1+\delta_\omega)]$. Another normal vector $\boldsymbol{n}_\perp$ can be stripped from the energy velocity, and we end up with an energy velocity tensor defined by $v_\omega \equiv c_i^2 A / [v_p(\boldsymbol{n}_\perp)(1+\delta_\omega)]$. The transport mean free path tensor is then defined by $l_\omega \equiv 3 v_\omega^{-1} \cdot D_\omega$. Obviously, instead of stripping $\boldsymbol{n}_\perp$ from the energy velocity vector, we could also have stripped another vector, e.g. the unit direction of the energy velocity $A \cdot \boldsymbol{n}_\perp / |A \cdot \boldsymbol{n}_\perp|$. Had we done the latter, the energy velocity had been scalar, and the anisotropy in the diffusion tensor had been identical to the anisotropy in the mean free path tensor. By separating still another vector we could even create a scalar mean free path and a tensor energy velocity. Although not well defined physically, tensorial or scalar transport mean free path and energy velocity might sometimes be more practical to work with, because they can be inverted.

For boundary condition (4.43) we assumed that the media we perfectly index matched, which is very often not true. If the media are not perfectly index matched we expect internal reflection. Thus, when we consider the flux infinitesimally close to the boundary inside the scattering medium, we apply boundary condition (4.41) The resulting boundary condition for the energy density is

$$\mathscr{H}_\omega(\boldsymbol{x},t) = \frac{2}{3}\frac{\boldsymbol{n}_\perp \cdot (1+R_\omega) \cdot \boldsymbol{v}_\omega(\boldsymbol{n}_\perp)}{\boldsymbol{n}_\perp \cdot (1-R_\omega) \cdot \boldsymbol{v}_\omega(\boldsymbol{n}_\perp)} \boldsymbol{l}_\omega(\boldsymbol{n}_\perp) \cdot \boldsymbol{\nabla} \mathscr{H}_\omega(\boldsymbol{x},t). \tag{4.49}$$

If there is no internal reflection, $R = 0$, and we recover (4.46). We preferred to use the angle and polarization averaged reflection tensor in boundary condition (4.49) in order to be able to model disordered materials with anisotropic surface roughness. As explained in section 4.2.f, if we do not want to consider anisotropic surface roughness we could equally well have expressed (4.49) in terms of an angle and polarization averaged reflectivity R_ω, which leads to $\mathscr{H}_\omega(\boldsymbol{x},t) = (2/3)(1+R_\omega)/(1-R_\omega)\boldsymbol{l}_\omega(\boldsymbol{n}_\perp) \cdot \boldsymbol{\nabla}\mathscr{H}_\omega(\boldsymbol{x},t)$. In isotropic media the transport mean free path becomes a scalar quantity, and we recover the well known factor $(2/3)(1+R)/(1-R)\,l$ [102]. At perfectly reflecting boundaries the total diffuse energy density flux $\boldsymbol{S} = \boldsymbol{0}$ and the reflectivity $R_\omega = 1$, or

equivalently $\boldsymbol{\nabla}\mathscr{H} = \mathbf{0}$, and the vanishing denominator of (4.49) has no consequences.

In isotropic media the angle and polarization averaged reflectivity (4.39a) and transmissivity (4.39b) have been expressed as integrals over the diffuse radiance [102, 103]. We can follow a similar procedure, for which we introduce the angular averages over two halves of the frequency surface, by

$$\langle \ldots \rangle^{\pm}_{\boldsymbol{e_k}} \equiv \int_{B_\pm} \frac{\mathrm{d}^2 \boldsymbol{e_k}}{2\pi} \frac{v_\mathrm{p}(\boldsymbol{e}_1) v_\mathrm{p}(\boldsymbol{e}_2) v_\mathrm{p}(\boldsymbol{e}_3)}{v_\mathrm{p}^3(\boldsymbol{e_k})} \ldots . \tag{4.50}$$

Here Here $B_\pm$ represents again the set of all wave vectors $\boldsymbol{e_k}$ such that $\pm \boldsymbol{n}_\perp \cdot \boldsymbol{v}_\mathrm{g}(\boldsymbol{p}) \geq 0$. Recalling Eqs. (4.37) and (4.26) which relate the reflectivity and transmissivity of a single plane wave to the angle averaged reflectivity and transmissivity, we define two auxiliary dimensionless quantities Q_1, Q_2 and Q_2 by

$$Q_{1\omega} \equiv \frac{\boldsymbol{n}_\perp \cdot \mathsf{Q}_{1\omega} \cdot \boldsymbol{v}_\mathrm{g}(\boldsymbol{n}_\perp)}{\boldsymbol{n}_\perp \cdot \boldsymbol{v}_\mathrm{g}(\boldsymbol{n}_\perp)}, \tag{4.51a}$$

$$Q_{2\omega} \equiv \frac{\boldsymbol{n}_\perp \cdot \mathsf{Q}_{2\omega} \cdot \boldsymbol{v}_\mathrm{g}(\boldsymbol{n}_\perp)}{\boldsymbol{n}_\perp \cdot \boldsymbol{v}_\mathrm{g}(\boldsymbol{n}_\perp)}, \tag{4.51b}$$

$$\mathsf{Q}_{1\omega} \cdot \boldsymbol{v}_\mathrm{g}(\boldsymbol{n}_\perp) \equiv \langle \mathsf{R}_{\boldsymbol{k}} \cdot \boldsymbol{v}_\mathrm{g}(\boldsymbol{e_k}) \rangle^{-}_{\boldsymbol{e_k}}, \tag{4.51c}$$

$$\mathsf{Q}_{2\omega} \equiv \left\langle \frac{\mathsf{R}_{\boldsymbol{k}} \cdot \boldsymbol{v}_\mathrm{g}(\boldsymbol{e_k})\, \boldsymbol{e_k}}{\boldsymbol{e_k} \cdot \boldsymbol{v}_\mathrm{g}(\boldsymbol{e_k})} \right\rangle^{-}_{\boldsymbol{e_k}}. \tag{4.51d}$$

In the isotropic limit the auxiliary quantities Q_1 and Q_2 become identical to the quantities C_1 and C_2 as used in [102]. We recall that $\boldsymbol{n}_\perp \cdot \mathsf{R}_{\boldsymbol{k}} \cdot \boldsymbol{v}_\mathrm{g}(\boldsymbol{e_k}) = R_{\boldsymbol{k}}$. The angle and polarization averaged reflection tensor for anisotropic diffusing light can be expressed in terms of the auxiliary quantities by

$$R_\omega = \frac{3Q_{\omega 2} + 2Q_{\omega 1}}{3Q_{\omega 2} - 2Q_{\omega 1} + 2}. \tag{4.52}$$

The angle and polarization averaged reflectivity appears to identical to the result found in isotropic media, except for the generalization of Q_1 and Q_2 to anisotropic media.

Instead of the reflectivity we can also consider the reflection tensor. As both $\boldsymbol{S}^+$ and $\boldsymbol{S}^-$ are on the same side of the boundary, also the parallel components of the flux are continuous. Therefore we can remove the projection on $\boldsymbol{n}_\perp$ and

obtain at the boundary these equations,

$$\left[1-2\mathsf{Q}_{1\omega}\right]\cdot\boldsymbol{v}(\boldsymbol{n}_\perp)\mathscr{H}_\omega(\boldsymbol{x},t) = \frac{2}{3}\left[1+3\mathsf{Q}_{2\omega}\right]\cdot\boldsymbol{v}(\boldsymbol{n}_\perp)\boldsymbol{l}(\boldsymbol{n}_\perp)\cdot\boldsymbol{\nabla}\mathscr{H}_\omega(\boldsymbol{x},t), \tag{4.53a}$$

$$\left[1-\mathsf{R}_\omega\right]\cdot\boldsymbol{v}(\boldsymbol{n}_\perp)\mathscr{H}_\omega(\boldsymbol{x},t) = \frac{2}{3}\left[1+\mathsf{R}_\omega\right]\cdot\boldsymbol{v}(\boldsymbol{n}_\perp)\boldsymbol{l}(\boldsymbol{n}_\perp)\cdot\boldsymbol{\nabla}\mathscr{H}_\omega(\boldsymbol{x},t). \tag{4.53b}$$

Equations (4.53a) and (4.53b) can differ at most by an overall scaling factor. Provided the inverse of $3\mathsf{Q}_{2\omega}/2-\mathsf{Q}_{1\omega}+1$ exists, it is easy to check that the angle and polarization averaged reflection tensor can be expressed in terms the reflection tensor for harmonic plane waves $\mathsf{R}_{\boldsymbol{k}}$ with the help the auxiliary tensors Q_1 and Q_2 by

$$\mathsf{R}_\omega = \left[\frac{3}{2}\mathsf{Q}_{2\omega}-\mathsf{Q}_{1\omega}+1\right]^{-1}\cdot\left[\frac{3}{2}\mathsf{Q}_{2\omega}+\mathsf{Q}_{1\omega}\right]. \tag{4.54}$$

The advantage of Eq. (4.54) over Eq. (4.52) is that it can incorporate anisotropic surface roughness both through altered $\boldsymbol{k}$ dependence of the individual $\mathsf{R}_{\boldsymbol{k}}$, but it can also affect each component of the energy density flux vector independently, which is impossible by altering the reflectivity.

4.3 Extracting anisotropy from diffusion

In the previous section we obtained the anisotropic diffusion tensor in terms of a transport mean free path vector and an energy velocity, which were both vector quantities. In isotropic media the angle dependence is integrated out, and the transport mean free path and energy velocity reduce to scalars. In this section we want to partition the diffusion tensor in an isotropic diffusion constant and an anisotropy tensor.

In isotropic media the isotropic diffusion tensor D_i is expressed in an isotropic transport mean free path l_i and an isotropic energy velocity v_i (which we do not expect to be confused with the earlier specified phase velocity of the incident non-scattered wave, which was also v_i). These isotropic transport quantities are defined by [68],

$$l_{\mathrm{i}\omega} \equiv \tau_\omega\left\langle v_\mathrm{p}(\boldsymbol{e}_{\boldsymbol{k}})\right\rangle_{\boldsymbol{e}_{\boldsymbol{k}}} \tag{4.55a}$$

$$v_{\mathrm{i}\omega} \equiv \frac{{c_\mathrm{i}}^2}{\left[1+\delta_\omega\right]\left\langle v_\mathrm{p}(\boldsymbol{e}_{\boldsymbol{k}})\right\rangle_{\boldsymbol{e}_{\boldsymbol{k}}}} \tag{4.55b}$$

$$D_{\mathrm{i}\omega} \equiv \frac{1}{3}l_{\mathrm{i}\omega}v_{\mathrm{i}\omega}, \tag{4.55c}$$

which are all scalar quantities, and τ is a transport mean free time [50]. Note that when we use a homogeneous and isotropic dispersion relation with unit anisotropy tensor $\mathsf{A} = 1$ then $\langle v_\mathrm{p} \rangle = \mathsf{c}_\mathrm{i}$, and our result for the anisotropic diffusion tensor (3.11) reduces to $\mathsf{D}_\mathrm{i} = D_\mathrm{i} 1$.

We can express the anisotropic diffusion tensor D, (4.48a)

in terms of the isotropic diffusion tensor D_i by extracting the time scale τ from the transport time scale tensor t. We find

$$\mathsf{D}_\omega \quad = \quad D_{\mathrm{i}\omega} \frac{\mathsf{t}_\omega}{\tau_\omega} \cdot \mathsf{A}, \tag{4.56}$$

where the anisotropy tensor is related to the anisotropy in the dielectric by $\mathsf{A} \equiv 3\varepsilon^{-1}/\mathrm{Tr}\left(\varepsilon^{-1}\right)$, (2.6a). We can express (4.56) in terms of an angular averaged momentum transfer cross section tensor s, which, is defined by $n\mathsf{s} \equiv (\mathsf{c}_\mathrm{i}\mathsf{t})^{-1}$, so then

$$\mathsf{D}_\omega \quad = \quad D_{\mathrm{i}\omega} \left(\frac{\mathsf{s}_\omega}{\frac{1}{3}\mathrm{Tr}[\mathsf{s}_\omega]} \right)^{-1} \cdot \frac{\varepsilon^{-1}}{\frac{1}{3}\mathrm{Tr}[\varepsilon^{-1}]}. \tag{4.57}$$

We see that the anisotropy in the momentum transfer cross section must be inversely proportional to $\mathsf{s} \propto \varepsilon^{-1}$ in order to exactly cancel the anisotropy ε of the host medium. From (4.57) we conclude that any problem with isotropic homogeneous permeability μ and isotropic homogeneous permittivity ε to which local anisotropic dielectric scatterers are added can be replaced by a problem with anisotropic dielectric host and isotropic magnetic scatterers. Also any problem which appears to be a combination of anisotropic scatterers and anisotropic host can be replaced by a problem in which only the host is anisotropic.

4.4 Propagators for the diffuse energy density

In this section we calculate Green functions for the diffuse energy density in a semi-infinite medium and in a slab geometry. Together with the Green functions for the wave amplitudes coupling in and out of a medium, the Green function for the energy density is a required ingredient for the calculation of the bistatic coefficients, which describe the reflection and transmission properties of disordered media. Moreover, given the Green function for the diffuse energy density, the solution to a problem with an arbitrary source inside the disordered medium can easily be calculated, as it is just an integral over the Green function.

In order to calculate reflection and transmission properties of multiple scattering media, we require solutions to the diffusion equation,

$$\frac{\partial \mathscr{H}_\omega(\boldsymbol{x},t)}{\partial t} - \boldsymbol{\nabla}\cdot \mathsf{D}_\omega \cdot \boldsymbol{\nabla}\mathscr{H}_\omega(\boldsymbol{x},t) \quad = \quad s_\omega(\boldsymbol{x},t). \tag{4.58}$$

In illumination experiments the source s is a part of the incoming energy which has scattered once. In the rest of this section we will suppress the ω dependencies, for reasons of legibility of the formulas to come. It is understood that all newly introduced quantities depend on ω.

We need to solve the diffusion equation for an arbitrary source, because we do not specify a specific scatterer yet. Therefore we require the Green function defined by

$$\frac{\partial G_{\mathscr{H}}(\boldsymbol{x},t,\boldsymbol{x}_0,t_0)}{\partial t} - \boldsymbol{\nabla}\cdot \mathsf{D}\cdot\boldsymbol{\nabla} G_{\mathscr{H}}(\boldsymbol{x},t,\boldsymbol{x}_0,t_0) \quad = \quad \delta^3(\boldsymbol{x}-\boldsymbol{x}_0)\delta(t-t_0). \tag{4.59}$$

We impose boundary conditions to find the solutions for specific geometries. In the next subsections we solve for semi-infinite media and slab geometries.

4.4.a Diffusive Green functions for semi-infinite media

We consider a semi-infinite disordered anisotropic medium. The boundary is at $z=0$, the disorder at $z>0$, and the inward pointing unit normal is $\boldsymbol{n}_\perp = \boldsymbol{e}_z$. The diffusion equation is supplied with a boundary condition at $z=0$, and an initial condition at $t=0$,

$$\mathscr{H}(\boldsymbol{x},t) \quad = \quad \boldsymbol{C}\cdot\boldsymbol{\nabla}\mathscr{H}(\boldsymbol{x},t), \tag{4.60a}$$

$$\mathscr{H}(\boldsymbol{x},t_0) \quad = \quad C_0(\boldsymbol{x}). \tag{4.60b}$$

Here $\boldsymbol{C}$ is a shorthand for the quantity in boundary condition (4.49), and $C_0(\boldsymbol{x})$ is some initial distribution of diffuse energy density. In the absence of internal reflections, $\mathsf{R}=0$, we take $\boldsymbol{C} = 2\boldsymbol{l}(\boldsymbol{n}_\perp)/3$ and recover boundary condition (4.46). If we do want to incorporate internal reflections we must take the more complicated vector from the modified boundary condition (4.49). Furthermore, for any source at finite depth the energy density must achieve a finite value when $z\to\infty$.

For $t\neq t_0$ and $\boldsymbol{x}\neq\boldsymbol{x}_0$, we can separate time and space coordinates, and we write $\mathscr{H}_\omega(\boldsymbol{x},t) = h_\omega(\boldsymbol{x})h_\omega(t)$, such that

$$\frac{1}{h(t)}\frac{\partial h(t)}{\partial t} \quad = \quad \frac{1}{h(\boldsymbol{x})}\boldsymbol{\nabla}\cdot\mathsf{D}\cdot\boldsymbol{\nabla}h(\boldsymbol{x}) \quad \equiv \quad -\mathrm{C}_1. \tag{4.61}$$

For stationary diffusion $C_1=0$, otherwise $\mathrm{C}_1>0$. The solution for the dynamic part $h(t)$ is almost trivial, it is an exponential decay $h(t) = \exp\left[-\mathrm{C}_1(t-t_0)\right]$.

We will now proceed with the calculation of the stationary Green function $G_{\mathscr{H}}(\boldsymbol{x}, \boldsymbol{x}_0)$, which is related to $h(\boldsymbol{x})$.

Due to the translational symmetry parallel to the interface, momentum is conserved in those directions, and it is convenient to transform the parallel coordinates to Fourier space. We end up with a function which depends only on a single $\boldsymbol{q}_\parallel$, which is the Fourier transform of $\boldsymbol{x}_\parallel - \boldsymbol{x}_{0\parallel}$. It is convenient to introduce

$$b_1(\boldsymbol{q}_\parallel, \boldsymbol{n}_\perp) \equiv \sqrt{\frac{\boldsymbol{q}_\parallel \cdot \mathsf{D} \cdot \boldsymbol{q}_\parallel}{\boldsymbol{n}_\perp \cdot \mathsf{D} \cdot \boldsymbol{n}_\perp} - {b_2}^2(\boldsymbol{q}_\parallel, \boldsymbol{n}_\perp) + \mathrm{C}_1}, \tag{4.62a}$$

$$b_2(\boldsymbol{q}_\parallel, \boldsymbol{n}_\perp) \equiv -\frac{\boldsymbol{q}_\parallel \cdot \mathsf{D} \cdot \boldsymbol{n}_\perp}{\boldsymbol{n}_\perp \cdot \mathsf{D} \cdot \boldsymbol{n}_\perp}. \tag{4.62b}$$

When an axis of the anisotropy is perpendicular to the boundary or when $\mathsf{D} = D1$, then $b_2 = 0$. With the parallel coordinates Fourier transformed away we have a one dimensional second order differential equation for $h(\boldsymbol{z})$. Our b_1 and b_2 can be used to create the eigenvalues of the second order partial differential equation, $-\mathrm{i}b_2 \pm b_1$. In contrast to the isotropic diffusion equation where $b_2 = 0$, our eigenvalues have an imaginary part. In Eq. (4.62a) we have a subtraction of different ratios of diffusion tensor components, and we can wonder if the subtraction can become negative, thus leading to a complex b_1. We do not need to worry about the constant C_1, because it satisfies $\mathrm{C}_1 \geq 0$, being zero only for stationary diffusion. The diffusion tensor D is symmetric, its trace is invariant, and therefore there exists no anisotropy in which $\boldsymbol{q}_\parallel \cdot \mathsf{D} \cdot \boldsymbol{q}_\parallel$ approaches zero more rapidly than $(\boldsymbol{q}_\parallel \cdot \mathsf{D} \cdot \boldsymbol{n}_\perp)^2$, not even when we shrink one direction to zero and another to infinity while keeping the trace fixed. Therefore both b_1 and b_2 are always real valued.

The Fourier transformation of the $\boldsymbol{x}_\parallel$ components also affects boundary condition (4.60a), which becomes

$$\mathscr{H}(\boldsymbol{q}_\parallel, 0, t) = \frac{\boldsymbol{C} \cdot \boldsymbol{n}_\perp}{1 + \mathrm{i}\boldsymbol{q}_\parallel \cdot \boldsymbol{C}} \frac{\partial \mathscr{H}(\boldsymbol{q}_\parallel, 0, t)}{\partial z}, \tag{4.63a}$$

$$\equiv \frac{\mathrm{C}_\perp}{1 + \mathrm{i}\mathrm{C}_\parallel(\boldsymbol{q}_\parallel)} \frac{\partial \mathscr{H}}{\partial z}(\boldsymbol{q}_\parallel, 0, t). \tag{4.63b}$$

If the initial energy density is homogeneously distributed in the parallel directions, then there is nothing to break the translational symmetry along the interface and $C_\parallel(\boldsymbol{q}_\parallel) = 0$. In the absence of internal reflections we end up with a single component of the mean free path, $\boldsymbol{C} \cdot \boldsymbol{n}_\perp = 2l_\perp(\boldsymbol{n}_\perp)/3$.

We start with the solution for a situation which is stationary, and is completely homogeneous parallel to the interface. Although equations of the form $\partial^2 f(z)/\partial z^2 = 0$ are elementary, the Green for this problem is a required result

if we want to calculate the escape function, which we will do in section 4.5.a. In the stationary limit, $C_1 = 0$, and the homogeneity along the interface implies $\boldsymbol{q}_\parallel = \boldsymbol{0}$. Using the Heaviside unit step function $\theta(z)$, which is 0 for $z < 0$ and 1 for $z > 0$, and 1/2 at $z = 0$, the solution for the Green function at $\boldsymbol{q}_\parallel = \boldsymbol{0}$ is

$$G_{\mathscr{H}}(\boldsymbol{0}, z, z_0) = \frac{z_0 + C_\perp}{D_{zz}}\theta(z - z_0) + \frac{z + C_\perp}{D_{zz}}\theta(z_0 - z). \tag{4.64}$$

This Green function satisfies reciprocity, $G_{\mathscr{H}}(\boldsymbol{0}, z, z_0) = G_{\mathscr{H}}(\boldsymbol{0}, z_0, z)$ and is valid for both z and z_0 greater than 0.

It is well known that the Green function is a very general solution which can be used to calculate solutions for a given source. As illustration, we will now give an example of a solution for a particular source. In stationary illumination experiments we often have the energy density flux $\boldsymbol{n}_\perp \cdot \boldsymbol{v}(\boldsymbol{n}_\perp)\mathscr{H}_0$ of a plane wave impinging perpendicular to the surface as the source. This energy density travels at energy velocity $\boldsymbol{v}$, which inside the anisotropic disordered medium is not directed along $\boldsymbol{n}_\perp$, unless a principal axis of the anisotropy is along $\boldsymbol{n}_\perp$. Inside the disordered medium the flux of the plane wave decays exponentially with the extinction mean free path in agreement with the Bouguer-Lambert-Beer Law. Therefore in each illuminated area A we have for the the probability density $\exp(-z/|\boldsymbol{l}_e(\boldsymbol{n}_\perp)|)/(|\boldsymbol{l}_e(\boldsymbol{n}_\perp)| \int_A \mathrm{d}^2 x_\parallel)$ to find flux $\boldsymbol{n}_\perp \cdot \boldsymbol{v}(\boldsymbol{n}_\perp)\mathscr{H}_0$. Thus the source s in Eq. (4.58) for the diffuse energy density is

$$s(\boldsymbol{x}_\parallel, z) = \boldsymbol{n}_\perp \cdot \boldsymbol{v}(\boldsymbol{n}_\perp)\mathscr{H}_0 \frac{\mathrm{e}^{-\frac{z}{|\boldsymbol{l}_e(\boldsymbol{n}_\perp)|}}}{|\boldsymbol{l}_e(\boldsymbol{n}_\perp)| \int_A \mathrm{d}^2 x_\parallel}. \tag{4.65}$$

Here we assume that the real part of the refractive index of the homogeneous and inhomogeneous are index matched, otherwise there is a transmission tensor sandwiched between $\boldsymbol{n}_\perp$ and $\boldsymbol{v}(\boldsymbol{n}_\perp)$.

Solving for $\mathscr{H}$ is straightforward using source (4.65) and Green function (4.64). We keep the illuminated area $\int_A \mathrm{d}^2 x_\parallel$ finite and take this area to infinity at the end of the integration, i.e.

$$\frac{\mathscr{H}(\boldsymbol{0}, z)}{\mathscr{H}_0} = \lim_{A\to\infty} \int_A \mathrm{d}^2 x_\parallel \int_0^\infty \mathrm{d}z_0 G_{\mathscr{H}}(\boldsymbol{0}, z, z_0) \frac{s(\boldsymbol{x}_\parallel, z_0)}{\mathscr{H}_0} \tag{4.66a}$$

$$= 2 + \frac{3|\boldsymbol{l}_e(\boldsymbol{n}_\perp)|}{\boldsymbol{l}(\boldsymbol{n}_\perp) \cdot \boldsymbol{n}_\perp} \left(1 - \mathrm{e}^{-\frac{z}{|\boldsymbol{l}_e(\boldsymbol{n}_\perp)|}}\right). \tag{4.66b}$$

The constant 2 originates from the integration of extrapolation length $C_\perp = 2\boldsymbol{l}(\boldsymbol{n}_\perp) \cdot \boldsymbol{n}_\perp/3$ over the exponential. We also used $D_{zz} = \boldsymbol{n}_\perp \cdot \boldsymbol{v}(\boldsymbol{n}_\perp)\boldsymbol{l}(\boldsymbol{n}_\perp) \cdot \boldsymbol{n}_\perp/3$. In Fig. 4.4.a we illustrate the extrapolation length $C_\perp$, and the effective source depth $|\boldsymbol{l}_e|$. The incoming plane wave decays with the extinction mean free

path. In some texts the extinction mean free path is replaced by the transport mean free path. This latter situation is depicted in Fig. 4.4.b and we see that the effective source depth is the transport mean free $|l|$ in that case. We plotted the result for a transport mean free path which is longer than the extinction mean free path, and we also see in Fig. 4.4.b that then more diffuse energy density is predicted than in 4.4.a. We can also see that for shorter transport mean free path the predicted energy density is lower when we let the incoming plane wave decay with the transport mean free path. However, the incoming plane wave always decays with the extinction mean free path, and replacing the extinction mean free path by the transport mean free path, as in Fig. 4.4.b is an error.

Solution (4.66b) is very useful for problems homogeneous along the interface, but this symmetry is often broken because the source is not homogeneous along the interface, e.g. when we focus a laser on or in a sample. Moreover when we want to use the diffusive propagator to to calculate the enhanced backscattering cone, we require the the diffusive propagator at $\boldsymbol{q}_\parallel \neq \boldsymbol{0}$ to obtain the shape of the cone. Although in the experiment itself the impinging intensity can be considered planar, in the calculation of the cone shape the source is scattered light from two plane waves traveling in different directions.

For $\boldsymbol{q}_\parallel \neq \boldsymbol{0}$ the calculation of the Green function is much more involved, the methods for this calculation can be found in the literature, such as in [6, 9, 104]. We obtain for an anisotropic disordered semi-infinite medium with boundary at $z = 0$ for $\boldsymbol{q}_\parallel \neq \boldsymbol{0}$ the result

$$\begin{aligned} G_{\mathscr{H}\, z>z_0}(\boldsymbol{q}_\parallel, z, z_0) \quad = \quad & \frac{\mathrm{e}^{-\mathrm{i}(z-z_0)b_2}}{2D_{zz}b_1} \\ & \times\Big\{\mathrm{e}^{-(z-z_0)b_1} - \mathrm{e}^{-(z+z_0)b_1} \\ & \quad + \frac{2b_1\mathrm{C}_\perp\left[1+b_1\mathrm{C}_\perp - 2\mathrm{i}b_1\left(\mathrm{C}_\parallel + b_2\mathrm{C}_\perp\right)\right]}{1+\mathrm{C}_\parallel^2 + 2\left(b_1+b_2\mathrm{C}_\parallel\right)\mathrm{C}_\perp + \left(b_1^2+b_2^2\right)\mathrm{C}_\perp^2}\mathrm{e}^{-(z+z_0)b_1}\Big\}, \end{aligned} \tag{4.67a}$$

$$\begin{aligned} G_{\mathscr{H}\, z<z_0}(\boldsymbol{q}_\parallel, z, z_0) \quad = \quad & \frac{\mathrm{e}^{-\mathrm{i}(z-z_0)b_2}}{2D_{zz}b_1} \\ & \times\Big\{\mathrm{e}^{-(z_0-z)b_1} - \mathrm{e}^{-(z+z_0)b_1} \\ & \quad + \frac{2b_1\mathrm{C}_\perp\left[1+b_1\mathrm{C}_\perp - 2\mathrm{i}b_1\left(\mathrm{C}_\parallel + b_2\mathrm{C}_\perp\right)\right]}{1+\mathrm{C}_\parallel^2 + 2\left(b_1+b_2\mathrm{C}_\parallel\right)\mathrm{C}_\perp + \left(b_1^2+b_2^2\right)\mathrm{C}_\perp^2}\mathrm{e}^{-(z+z_0)b_1}\Big\}. \end{aligned} \tag{4.67b}$$

The above Green functions for $z > z_0$ and $z < z_0$ have an imaginary part and it is not obvious if these Green functions combined satisfy the reciprocity sym-

metry $G_{\mathscr{H}}(\boldsymbol{q}_\parallel, z, z_0) = G_{\mathscr{H}}(-\boldsymbol{q}_\parallel, z_0, z)$. However $b_2(\boldsymbol{q}_\parallel) = -b_2(-\boldsymbol{q}_\parallel)$ and also $\mathrm{C}_\parallel(\boldsymbol{q}_\parallel) = -\mathrm{C}_\parallel(-\boldsymbol{q}_\parallel)$ switch sign. Moreover using the definition of the transport mean free path (4.45), we can write $\mathrm{D}\cdot\boldsymbol{n}_\perp = \boldsymbol{n}_\perp\cdot\boldsymbol{v}(\boldsymbol{n}_\perp)\boldsymbol{l}(\boldsymbol{n}_\perp)/3$, and it is easy to show that boundary conditions (4.46) or (4.49) lead to $\mathrm{C}_\parallel = -b_2\mathrm{C}_\perp$, and therefore that reciprocity holds. In media with a principal axis of the anisotropy perpendicular to the boundary, both $\mathrm{C}_\parallel$ and b_2 vanish by themselves.

Both our boundary condition without internal reflection as the one with internal reflections have the property that $\mathrm{C}_\parallel = -b_2\mathrm{C}_\perp$. When we eliminate $\mathrm{C}_\parallel$ in favor of b_2 and $\mathrm{C}_\perp$, and we obtain a single equation

$$G_{\mathscr{H}}(\boldsymbol{q}_\parallel, z, z_0) \quad = \quad \frac{\mathrm{e}^{-\mathrm{i}(z-z_0)b_2}}{2D_{zz}b_1}\left\{\mathrm{e}^{-(z-z_0)b_1} - \frac{1-b_1\mathrm{C}_\perp}{1+b_1\mathrm{C}_\perp}\mathrm{e}^{-(z+z_0)b_1}\right\}. \tag{4.68}$$

It is clear that this equation satisfies reciprocity. Due to the fact that the eigenvalues of the anisotropic diffusion equation had an imaginary part, also our Green function has an imaginary part. In anisotropic media the product $b_1\mathrm{C}_\perp$ is, in the absence of internal reflections

$$b_1(\boldsymbol{q}_\parallel)\mathrm{C}_\perp \quad = \quad \frac{2}{3}|\boldsymbol{q}_\parallel|\boldsymbol{n}_\perp\cdot\boldsymbol{l}(\boldsymbol{n}_\perp)\sqrt{\frac{\boldsymbol{e}_\parallel\cdot\boldsymbol{v}(\boldsymbol{e}_\parallel)\boldsymbol{l}(\boldsymbol{e}_\parallel)\cdot\boldsymbol{e}_\parallel}{\boldsymbol{n}_\perp\cdot\boldsymbol{v}(\boldsymbol{n}_\perp)\boldsymbol{l}(\boldsymbol{n}_\perp)\cdot\boldsymbol{n}_\perp} - \left(\frac{\boldsymbol{l}(\boldsymbol{n}_\perp)\cdot\boldsymbol{e}_\parallel}{\boldsymbol{l}(\boldsymbol{n}_\perp)\cdot\boldsymbol{n}_\perp}\right)^2 + \mathrm{C}_1}. \tag{4.69}$$

Apart from the ratio of transport mean free path, we also see a ratio of energy velocities. If the transport cross section tensor is isotropic, then we can replace the ratio energy velocities by a ratio of transport mean free path.

A final indication of the correctness of Eqs. (4.67) and (4.68) is the stationary isotropic limit. In this limit $\mathrm{C}_\parallel = 0$, $b_2 = 0$, $\mathrm{D} = vl1/3$, $b_1 = |\boldsymbol{q}_\parallel|$, and, in the absence of internal reflections, $\mathrm{C}_\perp = 2l/3$. Thus equations (4.67) reduce to the well known result for isotropic media, [101]

$$G_{\mathscr{H}}(\boldsymbol{q}_\parallel, z, z_0) \quad = \quad \frac{3}{2vl|\boldsymbol{q}_\parallel|}\left\{\mathrm{e}^{-|z-z_0||\boldsymbol{q}_\parallel|} - \frac{1-\frac{2l}{3}|\boldsymbol{q}_\parallel|}{1+\frac{2l}{3}|\boldsymbol{q}_\parallel|}\mathrm{e}^{-(z+z_0)|\boldsymbol{q}_\parallel|}\right\}. \tag{4.70}$$

We use equation (4.68) in the calculation of the enhanced backscattering cone for anisotropic disordered semi-infinite media.

4.4.b Diffusive Green function for a slab

When we want to calculate the bistatic cross section for the transmission of radiance through a slab of disordered material, a calculation we will do in section 4.6, then we require the diffusive Green function for a slab. In slab geometries we have an additional boundary at $z = L$ which we must take into

account. The boundary condition at L is similar to the boundary condition (4.60a) at $z = 0$. The inward pointing normal to the interface at $z = L$ differs by a sign with respect to the inward pointing normal of the interface at $z = 0$. Therefore we have boundary condition

$$\mathscr{H}(\boldsymbol{x},t) = -\boldsymbol{C}\cdot\boldsymbol{\nabla}\mathscr{H}(\boldsymbol{x},t), \tag{4.71a}$$

$$\mathscr{H}(\boldsymbol{q}_\parallel,L,t) = \frac{-\mathrm{C}_\perp}{1-\mathrm{i}\mathrm{C}_\parallel(\boldsymbol{q}_\parallel)}\frac{\partial\mathscr{H}(\boldsymbol{q}_\parallel,L,t)}{\partial z}. \tag{4.71b}$$

Again it is useful to calculate the solution for $\boldsymbol{q}_\parallel = \boldsymbol{0}$ first, and employing the extra boundary condition (4.71) we obtain

$$\begin{aligned} G_{\mathscr{H}}(\boldsymbol{0},z,z_0) = {} & \frac{(L-z+\mathrm{C}_\perp)(z_0+\mathrm{C}_\perp)}{D_{zz}(L+2\mathrm{C}_\perp)}\theta(z-z_0) \\ & +\frac{(z+\mathrm{C}_\perp)(L-z_0+\mathrm{C}_\perp)}{D_{zz}(L+2\mathrm{C}_\perp)}\theta(z_0-z). \end{aligned} \tag{4.72}$$

When we take $L\to\infty$, we recover the Green function for the semi-infinite medium. Green function (4.72) gives rise to the well known tent shape for the light emerging from a source plane somewhere inside the slab. In Fig. 4.5 we plot this tent shape and compare it with the solution given source (4.65), and observe only notable differences near the maxima of both curves. Using this source, we find in the absence of internal reflections

$$\begin{aligned} \frac{\mathscr{H}(\boldsymbol{0},z)}{\mathscr{H}_0} = {} & 2+\frac{3|\boldsymbol{l}_\mathrm{e}(\boldsymbol{n}_\perp)|}{\boldsymbol{l}(\boldsymbol{n}_\perp)\cdot\boldsymbol{n}_\perp}\left(1-\mathrm{e}^{-\frac{z}{|\boldsymbol{l}_\mathrm{e}(\boldsymbol{n}_\perp)|}}\right) \\ & -\frac{2|\boldsymbol{l}_\mathrm{e}(\boldsymbol{n}_\perp)|+\left(\frac{2}{3}\boldsymbol{l}(\boldsymbol{n}_\perp)\cdot\boldsymbol{n}_\perp-|\boldsymbol{l}_\mathrm{e}(\boldsymbol{n}_\perp)|\right)\left(1+\mathrm{e}^{-\frac{L}{|\boldsymbol{l}_\mathrm{e}(\boldsymbol{n}_\perp)|}}\right)}{L+\frac{4}{3}\boldsymbol{l}(\boldsymbol{n}_\perp)\cdot\boldsymbol{n}_\perp} \\ & \times\left(2+\frac{3z}{\boldsymbol{l}(\boldsymbol{n}_\perp)\cdot\boldsymbol{n}_\perp}\right). \end{aligned} \tag{4.73}$$

The first two terms are exactly the solution for the semi-infinite medium, the third term is a correction of order z with negative sign. It simply means that at the second boundary energy is transmitted to infinity, which is shown in Fig. 4.5.

Also for slabs we can not expect that the $\boldsymbol{q}_\parallel = \boldsymbol{0}$ solution suffices for any given problem. We again use Green function methods from [6, 9, 104] to calculate the propagator for $\boldsymbol{q}_\parallel \neq \boldsymbol{0}$. A lengthy calculation for a slab of thickness

L and boundaries at $z=0$ and $z=L$ leads to the result

$$
\begin{aligned}
G_{\mathscr{H}\,z>z_0}(\boldsymbol{q}_\parallel,z,z_0) \;=\; & \\
& \frac{[\cosh(b_1L)]^{-1}\,\mathrm{e}^{-\mathrm{i}(z-z_0)b_2}}{2D_{zz}b_1\left\{2b_1\mathrm{C}_\perp+\left[1+\mathrm{C}_\parallel^2+2b_2\mathrm{C}_\parallel\mathrm{C}_\perp+\left(b_1^2+b_2^2\right)\mathrm{C}_\perp^2\right]\tanh(b_1L)\right\}} \\
& \times\Big\{\left[1+\mathrm{C}_\parallel^2+2b_2\mathrm{C}_\parallel\mathrm{C}_\perp+\left(b_1^2+b_2^2\right)\mathrm{C}_\perp^2\right]\cosh(b_1L-b_1z+b_1z_0) \\
& \quad-\left[1+\mathrm{C}_\parallel^2+2b_2\mathrm{C}_\parallel\mathrm{C}_\perp-\left(b_1^2-b_2^2\right)\mathrm{C}_\perp^2\right]\cosh(b_1L-b_1z-b_1z_0) \\
& \quad+2b_1\mathrm{C}_\perp\sinh(b_1L-b_1z+b_1z_0) \\
& \quad-2\mathrm{i}b_1\mathrm{C}_\perp\left(\mathrm{C}_\parallel+b_2\mathrm{C}_\perp\right)\sinh(b_1L-b_1z-b_1z_0)\Big\}, \qquad (4.74a)
\end{aligned}
$$

$$
\begin{aligned}
G_{\mathscr{H}\,z<z_0}(\boldsymbol{q}_\parallel,z,z_0) \;=\; & \\
& \frac{[\cosh(b_1L)]^{-1}\,\mathrm{e}^{-\mathrm{i}(z-z_0)b_2}}{2D_{zz}b_1\left\{2b_1\mathrm{C}_\perp+\left[1+\mathrm{C}_\parallel^2+2b_2\mathrm{C}_\parallel\mathrm{C}_\perp+\left(b_1^2+b_2^2\right)\mathrm{C}_\perp^2\right]\tanh(b_1L)\right\}} \\
& \times\Big\{\left[1+\mathrm{C}_\parallel^2+2b_2\mathrm{C}_\parallel\mathrm{C}_\perp+\left(b_1^2+b_2^2\right)\mathrm{C}_\perp^2\right]\cosh(b_1L+b_1z-b_1z_0) \\
& \quad-\left[1+\mathrm{C}_\parallel^2+2b_2\mathrm{C}_\parallel\mathrm{C}_\perp-\left(b_1^2-b_2^2\right)\mathrm{C}_\perp^2\right]\cosh(b_1L-b_1z-b_1z_0) \\
& \quad+2b_1\mathrm{C}_\perp\sinh(b_1L+b_1z-b_1z_0) \\
& \quad-2\mathrm{i}b_1\mathrm{C}_\perp\left(\mathrm{C}_\parallel+b_2\mathrm{C}_\perp\right)\sinh(b_1L-b_1z-b_1z_0)\Big\}. \qquad (4.74b)
\end{aligned}
$$

The reciprocity symmetry $G_{\mathscr{H}}(\boldsymbol{q}_\parallel,z,z_0)=G_{\mathscr{H}}(-\boldsymbol{q}_\parallel,z_0,z)$ can be verified by the same method as for (4.67).

Our boundary conditions again give rise to the simplification $\mathrm{C}_\parallel=-b_2\mathrm{C}_\perp$, and much simpler equations are recovered for the slab,

$$
\begin{aligned}
G_{\mathscr{H}\,z>z_0}(\boldsymbol{q}_\parallel,z,z_0) \;=\; & \frac{\mathrm{e}^{-\mathrm{i}(z-z_0)b_2}}{2D_{zz}b_1\left\{2b_1\mathrm{C}_\perp\cosh(b_1L)+\left[1+b_1^2\mathrm{C}_\perp^2\right]\sinh(b_1L)\right\}} \\
& \times\Big\{\left[1+b_1^2\mathrm{C}_\perp^2\right]\cosh(b_1L-b_1z+b_1z_0) \\
& \quad+2b_1\mathrm{C}_\perp\sinh(b_1L-b_1z+b_1z_0) \\
& \quad-\left[1-b_1^2\mathrm{C}_\perp^2\right]\cosh(b_1L-b_1z-b_1z_0)\Big\}, \qquad (4.75a)
\end{aligned}
$$

$$
\begin{aligned}
G_{\mathscr{H}\,z<z_0}(\boldsymbol{q}_\parallel,z,z_0) \;=\; & \frac{\mathrm{e}^{-\mathrm{i}(z-z_0)b_2}}{2D_{zz}b_1\left\{2b_1\mathrm{C}_\perp\cosh(b_1L)+\left[1+b_1^2\mathrm{C}_\perp^2\right]\sinh(b_1L)\right\}} \\
& \times\Big\{\left[1+b_1^2\mathrm{C}_\perp^2\right]\cosh(b_1L+b_1z-b_1z_0) \\
& \quad+2b_1\mathrm{C}_\perp\sinh(b_1L+b_1z-b_1z_0) \\
& \quad-\left[1-b_1^2\mathrm{C}_\perp^2\right]\cosh(b_1L-b_1z-b_1z_0)\Big\}. \qquad (4.75b)
\end{aligned}
$$

This final Green function is what we need to calculate the enhanced backscattering cone for disordered slabs of arbitrary anisotropy.

4.5 Escape and reflection from semi-infinite media

Optically thick media can be modeled very well by a semi-infinite medium geometry. The main advantage of considering a semi-infinite medium is that there is only a single planar interface. Thus the theory is not complicated by reflections from the back side of the medium, or other parts of the boundary which could occur were the boundary concave or convex. Already in (isotropic) media thicker than two transport mean free path [8] we can use the diffusion approximation, while keeping the error with solutions to the radiative transfer equation very small.

There are two key observables for disordered semi-infinite media, the escape function, which describes the redistribution of light over angles by the disorder, and the bistatic coefficient, which is quite similar to a scattering cross section. In this section we will consider two situations. In the first situation we place a source infinitely deep inside an anisotropic disordered semi-infinite medium. The anisotropic disordered medium will redistribute the radiance over all possible angles, and we will calculate the angular distribution of escaping radiance. This probability distribution is known as either the escape or as the injection function, because the reciprocal problem yields the same result. The second type of problem is an illumination experiment. We will calculate the reflection function or bistatic cross section for single scattering, diffuse multiple scattering and for the enhanced backscattering cone for anisotropic disordered semi-infinite media.

4.5.a Escape function

The disordered media we consider consist of elastic scatterers, and are therefore called white media. It is well known that most white surfaces, such as a layer of (non glossy) white paint, show diffuse reflection of light, following Lambert's law [54, 98]. Lambert's law states that the surface brightness of a white surface is isotropic, independent of the illumination direction. This law implies that the reflected light is unpolarized, even if the incident light was polarized. When an energy density flux per frequency band $\boldsymbol{S}_\omega$ impinges on an area element $\mathrm{d}^2 x_\parallel$ with normal vector $\boldsymbol{n}_\perp$, it receives the amount of energy $|\boldsymbol{S}_\omega|\mathrm{d}^2 x_\parallel$, and reflects an amount of energy $|\boldsymbol{S}_\omega|\boldsymbol{e}_{\boldsymbol{k}}\cdot\boldsymbol{n}_\perp \mathrm{d}^2 x_\parallel/\pi$ in direction $\boldsymbol{e}_{\boldsymbol{k}}$. The inner product $\boldsymbol{e}_{\boldsymbol{k}}\cdot\boldsymbol{n}_\perp$ is the reason why Lambert's law is also known as Lambert's cosine law. When radiance emerging from a surface satisfies Lambert's law one speaks of diffuse reflection or diffuse emission. Instead of a rough surface, we consider a smooth surface with disorder behind it. This bulk disorder also causes diffuse reflection or diffuse emission of light, but does not exactly follow Lambert's law, but bears a close resemblance to it. The

diffuse emission of bulk disorder is described by the escape function [75].

To determine the escape function we place a source of radiation at infinite optical depth in a semi-infinite multiple scattering medium, such as depicted in Fig 4.3. The source must be placed at infinite depth, otherwise not all radiance escaping the medium is diffuse. We detect the radiance in the far field, i.e. far away from the slab. The unit normal to the interface pointing into the disordered medium is $\boldsymbol{n}_\perp$. In the process of multiple scattering, the radiance from the source is redistributed over angles, this probability distribution is

$$K(\boldsymbol{x}) \quad \equiv \quad \frac{|\boldsymbol{x}|^2 \langle\langle|\psi(\boldsymbol{x})|^2\rangle\rangle}{N_{\boldsymbol{n}_\perp} \int \mathrm{d}^2 x_\parallel}. \tag{4.76}$$

The quantity $\langle\langle|\psi(\boldsymbol{x})|^2\rangle\rangle$ is the ensemble averaged product of wave amplitudes, $\int \mathrm{d}^2 x_\parallel$ is the area of observation, and $N_{\boldsymbol{n}_\perp}$ is some normalization constant. In isotropic media this distribution of radiance over escape angles is always a Lambertian distribution [75, 105],

$$K_\mathrm{i}(\theta) \quad = \quad \cos\theta \left[1 + \frac{3}{2}\cos\theta\right]. \tag{4.77}$$

Here $\cos\theta = -\boldsymbol{n}_\perp \cdot \boldsymbol{e}_{\boldsymbol{x}}$. Equation (4.77) is not equal to Lambert's law for diffuse reflection, in which only the first term appears. The difference arises from the fact that the light escaping a disordered medium still has to travel a certain distance from its last scattering event to the interface. This distance to the interface becomes longer for larger angle θ, and along the way the radiance decays with $1/(l\cos\theta)$, and is the isotropic limit of the factor which we also observe in the Green function for propagation amplitude across an interface Eq. (4.25). The Lambertian distribution is considered to be universal for disordered media, and often also applied to anisotropic media.

When there is an index mismatch, then internal reflections can be incorporated by

$$K_\mathrm{i}(\theta) \quad = \quad [1 - R(\cos\theta_\mathrm{i})]\cos\theta \left[\frac{1+R_\omega}{1-R_\omega} + \frac{3}{2}\cos\theta_\mathrm{i}\right]. \tag{4.78}$$

Note that one reflectivity and one cosine depend on θ_i, the angle inside the sample, and accounts for refraction at the interface [105].

To calculate the escape function we need three quantities. First we require the diffuse wave energy density. Second a type of scatterer $\sigma_{\mathrm{e}\omega}(\boldsymbol{e}_{\boldsymbol{k}}) = \sigma_{\mathrm{e}\omega}$ and scatterer density n to generate the disorder, and third the amplitude propagator to couple out of the medium after the final scattering event. The boundary of the semi-infinite medium is at $z = 0$, and the inward pointing unit normal is $\boldsymbol{n}_\perp = \boldsymbol{e}_z$.

Performing the integrations over the illuminated surface area and over the Bethe-Salpeter irreducible vertex or differential scattering cross section in Eq. 4.76, we find end up with

$$K(\boldsymbol{x},\boldsymbol{n}_\perp) \quad = \quad 4\pi \mathrm{c_i}\sqrt{\det \mathsf{A}}|\boldsymbol{x}|^2 \int_0^\infty \mathrm{d}z_1 G^*_{\mathrm{b}\omega}(\boldsymbol{x},z_1) G_{\mathrm{b}\omega}(\boldsymbol{x},z_1) \frac{n\sigma_{\mathrm{e}\omega}}{N_{\boldsymbol{n}_\perp}} \frac{\mathscr{H}_\omega(z_1)}{1+\delta_\omega}. \tag{4.79}$$

Here $\mathscr{H}_\omega(z_1)/(1+\delta_\omega)$ is the radiative diffuse energy density coming from the source plane at infinite optical depth,and $G_{\mathrm{b}\omega}(\boldsymbol{x},z_1) = G_{\mathrm{b}\omega}(\boldsymbol{x},z_1,0)$ is the amplitude Green function for $\boldsymbol{x}$ far away from the interface, as defined in Eq. (4.25). The $\sqrt{\det \mathsf{A}}$ is the result of the integral over the Bethe-Salpeter irreducible vertex. In the absence of internal reflections the diffuse energy density is obtained from Eq. (4.64) in the by taking the coordinate z_0 of the planar source to infinity,

$$\mathrm{c_i} n\sigma_{\mathrm{e}\omega} \frac{\mathscr{H}_\omega(z_1)}{1+\delta_\omega} \quad = \quad 3\mathrm{C} \frac{z_1 + \frac{2}{3}\boldsymbol{l}_\omega(\boldsymbol{n}_\perp)\cdot\boldsymbol{n}_\perp}{\boldsymbol{l}_{\mathrm{e}\omega}(\boldsymbol{n}_\perp)\cdot\boldsymbol{n}_\perp \boldsymbol{l}_\omega(\boldsymbol{n}_\perp)\cdot\boldsymbol{n}_\perp}. \tag{4.80}$$

The constant C governs the strength of the source radiance at infinite depth.

The normal to the wave surface at $\boldsymbol{n}_\varphi(\boldsymbol{x})$ will appear many times as argument to a function, so for brevity we write in this section $\boldsymbol{e}_{\boldsymbol{k}} = \boldsymbol{n}_\varphi(\boldsymbol{x})$. For the product of amplitude Green functions we use Eq. (4.25),

$$|\boldsymbol{x}|^2 G^*_{\mathrm{b}\omega}(\boldsymbol{x},\boldsymbol{x}_1) G_{\mathrm{b}\omega}(\boldsymbol{x},z_1) \quad = \quad \left(\frac{\mathrm{B}^>}{\mathrm{B}^<}\right)^2 \frac{|\boldsymbol{v}_{\mathrm{g}}(\boldsymbol{e}_{\boldsymbol{k}})|^2}{(4\pi \mathrm{c_i}\sqrt{\det \mathsf{A}})^2} \exp\left[\frac{-z_1}{|\boldsymbol{l}_{\mathrm{e}\omega}(\boldsymbol{n}_\perp)|\, u(\boldsymbol{e}_{\boldsymbol{k}},\boldsymbol{n}_\perp)}\right]. \tag{4.81}$$

The function u is the generalization to anisotropic media of the angle with the outward normal to the surface defined by $\cos\theta \equiv -\boldsymbol{e}_{\boldsymbol{k}}\cdot\boldsymbol{n}_\perp$.

When we absorb all constants in $N_{\boldsymbol{n}_\perp}$, we find for the semi-infinite medium the probability to escape in direction $\boldsymbol{e}_{\boldsymbol{k}}$, or the escape function

$$K(\boldsymbol{e}_{\boldsymbol{k}},\boldsymbol{n}_\perp) \quad = \quad \frac{3}{2N_{\boldsymbol{n}_\perp}} \left|\frac{\boldsymbol{v}_{\mathrm{g}}(\boldsymbol{e}_{\boldsymbol{k}})}{\mathrm{c_i}}\right|^2 u(\boldsymbol{e}_{\boldsymbol{k}},\boldsymbol{n}_\perp)\left[\,\tau_{\mathrm{e}}(\boldsymbol{n}_\perp) + u(\boldsymbol{e}_{\boldsymbol{k}},\boldsymbol{n}_\perp)\,\right]. \tag{4.82}$$

Here $N_{\boldsymbol{n}_\perp}$ is defined by $\langle K(\boldsymbol{e}_{\boldsymbol{k}},\boldsymbol{n}_\perp)\rangle_{\boldsymbol{e}_{\boldsymbol{k}}} \equiv 1$ with $\boldsymbol{e}_{\boldsymbol{k}}$ limited to all outgoing flux components, $\boldsymbol{n}_\perp\cdot\boldsymbol{v}_{\mathrm{g}}(\boldsymbol{e}_{\boldsymbol{k}}) \le 0$, and τ_{e} is the extrapolation ratio

$$\tau_{\mathrm{e}}(\boldsymbol{n}_\perp) \quad \equiv \quad \frac{2\boldsymbol{l}_\omega(\boldsymbol{n}_\perp)\cdot\boldsymbol{n}_\perp}{3|\boldsymbol{l}_{\mathrm{e}\omega}(\boldsymbol{n}_\perp)|}. \tag{4.83}$$

For isotropic scatterers in the absence of internal reflections the extrapolation ratio is $\tau_{\mathrm{e}} = 2/3$ and $|\boldsymbol{v}_{\mathrm{g}}/\mathrm{c_i}|^2$=1.

We can incorporate internal reflections by when we take Eq. (4.64) with $3C_\perp = 2\boldsymbol{l}_\omega(\boldsymbol{n}_\perp)\cdot\boldsymbol{n}_\perp \boldsymbol{n}_\perp\cdot(1+\mathsf{R}_\omega)\cdot\boldsymbol{v}_\omega(\boldsymbol{n}_\perp)/\boldsymbol{n}_\perp\cdot(1-\mathsf{R}_\omega)\cdot\boldsymbol{v}_\omega(\boldsymbol{n}_\perp)$ instead of $3C_\perp = 2\boldsymbol{l}_\omega(\boldsymbol{n}_\perp)\cdot\boldsymbol{n}_\perp$. We can include the internal reflections in the extrapolation ratio, which becomes

$$\tau_{\mathrm{e}}(\boldsymbol{n}_\perp) \equiv \frac{2\boldsymbol{l}_\omega(\boldsymbol{n}_\perp)\cdot\boldsymbol{n}_\perp}{3|\boldsymbol{l}_{\mathrm{e}\omega}(\boldsymbol{n}_\perp)|}\frac{\boldsymbol{n}_\perp\cdot(1+\mathsf{R}_\omega)\cdot\boldsymbol{v}_\omega(\boldsymbol{n}_\perp)}{\boldsymbol{n}_\perp\cdot(1-\mathsf{R}_\omega)\cdot\boldsymbol{v}_\omega(\boldsymbol{n}_\perp)}. \tag{4.84}$$

The escape function which incorporates internal reflections is also given by Eq. (4.82) provided we use extrapolation ratio (4.84).

In isotropic random media the escape function is universal, independent of the phase function of the scatterers [75]. We calculate the escape function in anisotropic media for realistic values of the anisotropic permittivity and isotropic scatterers, and we see unexpected behavior, see Figs. 4.6 and 4.7, where we set $\mathsf{R}_\omega = 0$ or equivalently $R_\omega = 0$. Anisotropic media can not satisfy requirement $R_\omega = 0$ for all angles. If the director is perpendicular to the output surface we observe a bell shaped curve, which resembles the isotropic result. When we tilt the director with respect to the boundary surface normal, the bell shape disappears, which is related to the fact that the transport length has its minimum where $|\boldsymbol{v}_{\mathrm{g}}|$ and $|\boldsymbol{v}|$ are minimal. The energy density current is deflected in the direction perpendicular to the surface normal. We see that it is only possible to perfectly index match the anisotropic medium with isotropic scatterers to the outside anisotropic world if the anisotropy axes are parallel or perpendicular to the boundary.

4.5.b Reflection from a disordered medium

Instead of a source at infinite depth, we will now illuminate the anisotropic disordered medium with a plane wave, and calculate how much of the light is reflected. The reflection function for the disordered medium is the limit of the N particle cluster differential scattering cross section per geometric cross section of the cluster $A = \int \mathrm{d}^2 x_\parallel$, when we take both $N \to \infty$ and $A \to \infty$ at constant particle number density n. The bistatic coefficient γ is defined by

$$|t_{\mathrm{F}}(\boldsymbol{k})|^2 \cos\theta_{\mathrm{i}}\gamma(\boldsymbol{\kappa}_{\mathrm{i}}, \boldsymbol{x}_{\mathrm{o}}, \boldsymbol{n}_\perp) \equiv \frac{|\boldsymbol{x}|^2\langle\langle|\psi(\boldsymbol{x})|^2\rangle\rangle}{|\psi_0|^2\int \mathrm{d}^2 x_\parallel}. \tag{4.85}$$

Here we extracted the effect of internal reflections, $\boldsymbol{\kappa}_{\mathrm{i}}$ is the wave vector of the incoming plane wave, and $\cos\theta_{\mathrm{i}} = \boldsymbol{e}_{\mathrm{i}}\cdot\boldsymbol{n}_\perp$ is the projection of the illuminated area on the incoming wave vector direction.

In the bistatic coefficient three contributions can be identified, the single scattered contribution, the diffuse multiple scattered contribution, and an interference contribution which gives rise to the enhanced backscattering cone,

$$\gamma(\boldsymbol{\kappa}_{\mathrm{i}}, \boldsymbol{x}_{\mathrm{o}}, \boldsymbol{n}_\perp) = \gamma_{\mathrm{s}}(\boldsymbol{\kappa}_{\mathrm{i}}, \boldsymbol{x}_{\mathrm{o}}, \boldsymbol{n}_\perp) + \gamma_{\mathrm{d}}(\boldsymbol{\kappa}_{\mathrm{i}}, \boldsymbol{x}_{\mathrm{o}}, \boldsymbol{n}_\perp) + \gamma_{\mathrm{c}}(\boldsymbol{\kappa}_{\mathrm{i}}, \boldsymbol{x}_{\mathrm{o}}, \boldsymbol{n}_\perp). \tag{4.86}$$

These three contributions we will discuss next.

Single scattering

We calculate the bistatic coefficient for the single scattered light. As for the escape function, we need to evaluate a product of amplitudes. This time the radiance of an incoming plane wave is the source. Moreover, the reflection function depends on both an incoming and a scattered direction, which are $\boldsymbol{e}_\mathrm{i}$ and $\boldsymbol{e}_\mathrm{s}$ respectively. Thus the quantity we must evaluate is,

$$\cos\theta_\mathrm{i}\gamma_\mathrm{s}(\boldsymbol{\kappa}_\mathrm{i},\boldsymbol{x}_\mathrm{o},\boldsymbol{n}_\perp) = \frac{4\pi\sqrt{\det \mathsf{A}}|\boldsymbol{x}|^2}{|t_\mathrm{F}(\boldsymbol{k})|^2|\psi_0|^2}\int_0^\infty \mathrm{d}z_1 \left|G_{\mathrm{b}\omega}(\boldsymbol{x},z_1)\right|^2 n\sigma_{\mathrm{e}\omega}|\psi_{\boldsymbol{\kappa}_\mathrm{i}}(z_1)|^2. \tag{4.87}$$

The incoming radiance is similar to the outgoing radiance in Eq. (4.81). When we send in a plane wave of intensity $|\psi_0|^2$, then the transmitted radiance is obtained from Eqs. (4.16) and (4.39b)

$$|\psi_{\boldsymbol{\kappa}_\mathrm{i}}(z_1)|^2 = |t_\mathrm{F}(\boldsymbol{k})|^2|\psi_0|^2\exp\left[\frac{z_1}{|\boldsymbol{l}_{\mathrm{e}\omega}(\boldsymbol{n}_\perp)|u(\boldsymbol{e}_\mathrm{i},\boldsymbol{n}_\perp)}\right]. \tag{4.88}$$

We define for future convenience a transformation of variables

$$2v(\boldsymbol{e}_\mathrm{i},\boldsymbol{e}_\mathrm{o},\boldsymbol{n}_\perp) \equiv \frac{1}{u(\boldsymbol{e}_\mathrm{o},\boldsymbol{n}_\perp)} - \frac{1}{u(\boldsymbol{e}_\mathrm{i},\boldsymbol{n}_\perp)}, \tag{4.89a}$$

$$2w(\boldsymbol{e}_\mathrm{i},\boldsymbol{e}_\mathrm{o},\boldsymbol{n}_\perp) \equiv \frac{1}{u(\boldsymbol{e}_\mathrm{o},\boldsymbol{n}_\perp)} + \frac{1}{u(\boldsymbol{e}_\mathrm{i},\boldsymbol{n}_\perp)}. \tag{4.89b}$$

In the bistatic coefficient for reflection we have $v > 0$ because $1/u_\mathrm{i} < 0$ and $1/u_\mathrm{o} > 0$. We can not guarantee that $w > 0$, but for reflection we do have the inequalities $v + w > 0$ and $v - w > 0$. We obtain the single scattering bistatic coefficient for the semi-infinite medium

$$\begin{aligned}\cos\theta_\mathrm{i}\gamma_\mathrm{s}(\boldsymbol{e}_\mathrm{i},\boldsymbol{e}_\mathrm{o},\boldsymbol{n}_\perp) = {} & \frac{1}{4\pi\sqrt{\det \mathsf{A}}}\left(\frac{\mathrm{B}^>}{\mathrm{B}^<}\right)^2 \frac{v_\mathrm{p}(\boldsymbol{n}_\perp)}{v_\mathrm{i}(\boldsymbol{n}_\perp)}\frac{|\boldsymbol{l}_{\mathrm{e}\omega}(\boldsymbol{n}_\perp)|}{\boldsymbol{l}_{\mathrm{e}\omega}(\boldsymbol{n}_\perp)\cdot\boldsymbol{n}_\perp} \\ & \times\left|\frac{\boldsymbol{v}_\mathrm{g}(\boldsymbol{e}_\mathrm{o})}{\mathrm{c}_\mathrm{i}}\right|^2 \frac{1}{2v(\boldsymbol{e}_\mathrm{i},\boldsymbol{e}_\mathrm{o},\boldsymbol{n}_\perp)}.\end{aligned} \tag{4.90}$$

Here v_i is the phase velocity in the isotropic homogeneous medium. We plotted the bistatic coefficient for single scattered reflection from anisotropic disordered semi-infinite medium as a function of the angle θ defined by $\cos\theta \equiv -\boldsymbol{n}_\perp\cdot\boldsymbol{e}_\mathrm{o}$ and compared it with the isotropic result in Fig. 4.8.

Diffuse multiple scattering

The bistatic coefficient for diffuse multiple scattered light in a semi-infinite medium has similarities with the one for single scattered light. Coupling in and out of the disordered medium is the same, but in between those events light propagates diffusely through the medium. We need to calculate

$$\begin{aligned}\cos\theta_{\mathrm{i}}\gamma_{\mathrm{d}}(\boldsymbol{\kappa}_{\mathrm{i}},\boldsymbol{x}_{\mathrm{o}},\boldsymbol{n}_{\perp}) &= \frac{(4\pi n\sigma_{\mathrm{e}\omega}\sqrt{\det \mathsf{A}}|\boldsymbol{x}|)^2}{|t_{\mathrm{F}}(\boldsymbol{k})|^2|\psi_0|^2} \\ &\quad\times\int_0^\infty \mathrm{d}z_2\int_0^\infty \mathrm{d}z_1\left|G_{\mathrm{b}\omega}(\boldsymbol{x},z_2)\right|^2\frac{G_{\mathscr{H}}(z_2,z_1)}{1+\delta_\omega}|\psi_{\boldsymbol{\kappa}_{\mathrm{i}}}(z_1)|^2.\end{aligned} \tag{4.91}$$

The Green function for the diffuse energy density in the semi-infinite medium is

$$G_{\mathscr{H}}(z_2<z_1) = \mathscr{H}_\omega(z_2) \tag{4.92a}$$

$$G_{\mathscr{H}}(z_2>z_1) = \mathscr{H}_\omega(z_1) \tag{4.92b}$$

In terms of the variables defined in Eqs. (4.89) we derive the bistatic coefficient for diffuse multiple scattering,

$$\cos\theta_{\mathrm{i}}\gamma_{\mathrm{d}}(\boldsymbol{e}_{\mathrm{i}},\boldsymbol{e}_{\mathrm{o}},\boldsymbol{n}_{\perp}) = \frac{3C_{\boldsymbol{n}_\perp}\left|v_{\mathrm{g}}(\boldsymbol{e}_{\mathrm{o}})\right|^2[1+2v(\boldsymbol{e}_{\mathrm{i}},\boldsymbol{e}_{\mathrm{o}},\boldsymbol{n}_{\perp})\tau_{\mathrm{e}}(\boldsymbol{n}_{\perp})]}{2v(\boldsymbol{e}_{\mathrm{i}},\boldsymbol{e}_{\mathrm{o}},\boldsymbol{n}_{\perp})\mathrm{c_i}^2\left[v^2(\boldsymbol{e}_{\mathrm{i}},\boldsymbol{e}_{\mathrm{o}},\boldsymbol{n}_{\perp})-w^2(\boldsymbol{e}_{\mathrm{i}},\boldsymbol{e}_{\mathrm{o}},\boldsymbol{n}_{\perp})\right]}. \tag{4.93}$$

Here the constant $C_{\boldsymbol{n}_\perp}$ is given by

$$C_{\boldsymbol{n}_\perp} = \left(\frac{\mathrm{B}^>}{\mathrm{B}^<}\right)^2\left(\frac{v_{\mathrm{p}}(\boldsymbol{n}_\perp)}{v_{\mathrm{i}}(\boldsymbol{n}_\perp)}\right)^2\frac{|\boldsymbol{l}_{\mathrm{e}\omega}(\boldsymbol{n}_\perp)|^3}{\boldsymbol{l}_\omega(\boldsymbol{n}_\perp)\cdot\boldsymbol{n}_\perp(\boldsymbol{l}_{\mathrm{e}\omega}(\boldsymbol{n}_\perp)\cdot\boldsymbol{n}_\perp)^2}. \tag{4.94}$$

In isotropic media in the absence of internal reflections we have $3C_{\boldsymbol{n}_\perp}/2 = 1/\tau_{\mathrm{e}}(\boldsymbol{n}_\perp)$. We plotted the bistatic coefficient for multiple scattered reflected radiance from anisotropic disordered semi-infinite medium as a function of the angle θ defined by $\cos\theta \equiv -\boldsymbol{n}_\perp\cdot\boldsymbol{e}_{\mathrm{o}}$ and compared it with the isotropic result in Fig. 4.10.

Enhanced backscattering

The bistatic coefficient of the cone is obtained from the bistatic coefficient for diffuse multiple scattered light by taking the reciprocal of one of the amplitude

paths. We then have

$$\begin{aligned}\cos\theta_{\rm i}\gamma_{\rm c}(\boldsymbol{\kappa}_{\rm i},\boldsymbol{x}_{\rm o},\boldsymbol{n}_\perp) &= \frac{(4\pi n\sigma_{{\rm e}\omega}\sqrt{\det \mathsf{A}}|\boldsymbol{x}|)^2}{|t_{\rm F}(\boldsymbol{k})|^2|\psi_0|^2} \\ &\quad\times\int_0^\infty {\rm d}z_2\int_0^\infty {\rm d}z_1\Big\{G^*_{{\rm b}\omega}(\boldsymbol{x},z_1)G_{{\rm b}\omega}(\boldsymbol{x},z_2) \\ &\qquad\times\frac{G_{\mathscr{H}}(\boldsymbol{q}_\parallel,z_2,z_1)}{1+\delta_\omega}\psi^*_{\boldsymbol{\kappa}_{\rm i}}(z_2)\psi_{\boldsymbol{\kappa}_{\rm i}}(z_1)\Big\}.\end{aligned} \tag{4.95}$$

Here $\boldsymbol{q}_\parallel=\boldsymbol{k}_{{\rm i}\parallel}+\boldsymbol{k}_{{\rm o}\parallel}$. This time also the imaginary parts of the exponents survive, and therefore, to obtain a relatively simple expression it is convenient to work with

$$\tilde v(\boldsymbol{e}_{\rm i},\boldsymbol{e}_{\rm o},\boldsymbol{n}_\perp) \equiv \frac{\omega|\boldsymbol{l}_{{\rm e}\omega}(\boldsymbol{n}_\perp)|}{|\boldsymbol{v}_{\rm g}(\boldsymbol{n}_\perp)|}\left[\tilde u(\boldsymbol{e}_{\rm o},\boldsymbol{n}_\perp)-\tilde u(\boldsymbol{e}_{\rm i},\boldsymbol{n}_\perp)\right], \tag{4.96a}$$

$$\tilde w(\boldsymbol{e}_{\rm i},\boldsymbol{e}_{\rm o},\boldsymbol{n}_\perp) \equiv \frac{\omega|\boldsymbol{l}_{{\rm e}\omega}(\boldsymbol{n}_\perp)|}{|\boldsymbol{v}_{\rm g}(\boldsymbol{n}_\perp)|}\left[\tilde u(\boldsymbol{e}_{\rm o},\boldsymbol{n}_\perp)+\tilde u(\boldsymbol{e}_{\rm i},\boldsymbol{n}_\perp)\right], \tag{4.96b}$$

$$\beta_1(\boldsymbol{q}_\parallel,\boldsymbol{n}_\perp) \equiv b_1(\boldsymbol{q}_\parallel,\boldsymbol{n}_\perp)|\boldsymbol{l}_{{\rm e}\omega}(\boldsymbol{n}_\perp)|, \tag{4.96c}$$

$$\beta_2(\boldsymbol{q}_\parallel,\boldsymbol{n}_\perp) \equiv b_2(\boldsymbol{q}_\parallel,\boldsymbol{n}_\perp)|\boldsymbol{l}_{{\rm e}\omega}(\boldsymbol{n}_\perp)|. \tag{4.96d}$$

The quantities b_1 and b_2 are related to anisotropic diffusion, and were defined in Eqs. (4.62).

Upon performing the integrations we find the result

$$\cos\theta_{\rm i}\gamma_{\rm c}(\boldsymbol{\kappa}_{\rm i},\boldsymbol{x}_{\rm o},\boldsymbol{n}_\perp) = \frac{\left|\frac{\boldsymbol{v}_{\rm g}(\boldsymbol{e}_{\rm o})}{c_{\rm i}}\right|^2\frac{3C_{\boldsymbol{n}_\perp}}{2\nu(\boldsymbol{e}_{\rm i},\boldsymbol{e}_{\rm o},\boldsymbol{n}_\perp)}\left[1+\frac{2\nu(\boldsymbol{e}_{\rm i},\boldsymbol{e}_{\rm o},\boldsymbol{n}_\perp)\tau_{\rm e}(\boldsymbol{n}_\perp)}{1+\beta_1(\boldsymbol{q}_\parallel,\boldsymbol{n}_\perp)\tau_{\rm e}(\boldsymbol{n}_\perp)}\right]}{[\nu(\boldsymbol{e}_{\rm i},\boldsymbol{e}_{\rm o},\boldsymbol{n}_\perp)+\beta_1(\boldsymbol{q}_\parallel,\boldsymbol{n}_\perp)]^2+[\tilde w(\boldsymbol{e}_{\rm i},\boldsymbol{e}_{\rm o},\boldsymbol{n}_\perp)+\beta_2(\boldsymbol{q}_\parallel,\boldsymbol{n}_\perp)]^2}. \tag{4.97}$$

Here the constant $C_{\boldsymbol{n}_\perp}$ is again given by (4.94). At exact backscattering, i.e. $\boldsymbol{e}_{\rm i}=-\boldsymbol{e}_{\rm o}$, we have $\beta_1=0$, $\beta_2=0$, $w=0$, and $\tilde w=0$, so there $\gamma_{\rm d}=\gamma_{\rm c}$, which is why the maximal enhancement is two.

In Fig 4.10 the cone is plotted as a function of θ, here $-\boldsymbol{e}_{\rm o}\cdot\boldsymbol{n}_\perp=\cos\theta$. In isotropic media it is well known that the enhanced backscattering cone is cusped, and the derivative with respect to θ has a discontinuity at $\theta=0$. We consider

an incoming plane wave with $\cos\theta_i = 1$ and expand (4.97) around $\theta = 0$,

$$\begin{aligned}\frac{2{c_i}^2\gamma_c(\boldsymbol{n}_\perp,\theta,\boldsymbol{e}_{o\parallel})}{3|\boldsymbol{v}_g(\boldsymbol{n}_\perp)|^2 C_{\boldsymbol{n}_\perp}} \approx\ & 1+2\tau_e(\boldsymbol{n}_\perp)+2\beta_1(\boldsymbol{e}_{o\parallel},\boldsymbol{n}_\perp)\,[1+\tau_e(\boldsymbol{n}_\perp)]^2\,|\theta| \\ & +4\frac{\boldsymbol{v}_g(\boldsymbol{n}_\perp)}{|\boldsymbol{v}_g(\boldsymbol{n}_\perp)|}\cdot\left[1-\frac{\boldsymbol{v}_g(\boldsymbol{n}_\perp)\boldsymbol{n}_\perp}{v_p(\boldsymbol{n}_\perp)}\right] \\ & \times\frac{\boldsymbol{v}_g(\boldsymbol{e}_{o\parallel})}{|\boldsymbol{v}_g(\boldsymbol{n}_\perp)|}\frac{v_p(\boldsymbol{e}_{o\parallel})}{v_p(\boldsymbol{n}_\perp)}\,[1+2\tau_e(\boldsymbol{n}_\perp)]\,|\theta|. \end{aligned} \tag{4.98}$$

We see that also in anisotropic media the derivative with respect to θ is discontinuous at $\theta = 0$. The first term in Eq. (4.98) is the size of the cone at $\theta = 0$, and the only difference with isotropic media is that it depends on the orientation of the boundary with respect to the principal axes of the anisotropic medium. The second term in (4.98)is a generalization of another term that is also present for isotropic media, where $\beta_1(\boldsymbol{q}_\parallel) = |\boldsymbol{q}_\parallel||\mathrm{l}_e|$. If the anisotropy is perpendicular to the boundary, $\beta_1/|\boldsymbol{l}_e|$ can be obtained from the isotropic medium by scaling $\boldsymbol{q}_\parallel$ according to $\tilde{\boldsymbol{q}}_\parallel = \mathsf{D}^{1/2}\cdot\boldsymbol{q}_\parallel/\sqrt{\boldsymbol{n}_\perp\cdot\mathsf{D}\cdot\boldsymbol{n}_\perp}$. Note that to obtain β_1 we should also scale $|\boldsymbol{l}_\perp|$ and take its value along the $\boldsymbol{n}_\perp$ direction, which is easily overlooked. In media with anisotropy at an angle with the boundary, β_1 can not be obtained by a scaling, because we have an additional term,

$$\beta_1(\boldsymbol{e}_{o\parallel},\boldsymbol{n}_\perp) = \frac{\omega}{v_i}|\boldsymbol{l}_e(\boldsymbol{n}_\perp)|\sqrt{\frac{\boldsymbol{e}_{o\parallel}\cdot\boldsymbol{v}(\boldsymbol{e}_{o\parallel})\boldsymbol{l}(\boldsymbol{e}_{o\parallel})\cdot\boldsymbol{e}_{o\parallel}}{\boldsymbol{n}_\perp\cdot\boldsymbol{v}(\boldsymbol{n}_\perp)\boldsymbol{l}(\boldsymbol{n}_\perp)\cdot\boldsymbol{n}_\perp}-\left(\frac{\boldsymbol{l}(\boldsymbol{n}_\perp)\cdot\boldsymbol{e}_{o\parallel}}{\boldsymbol{l}(\boldsymbol{n}_\perp)\cdot\boldsymbol{n}_\perp}\right)^2}. \tag{4.99}$$

The second term in (4.99) can not be obtained be scaling the isotropic result. The third term in the expansion of the cone (4.98) originates from $|\boldsymbol{v}_g(\boldsymbol{e}_o)|$, and is not present for isotropic media. Also in anisotropic media with a principal axis of the anisotropy perpendicular to the surface, this term vanishes, and the shape of the cone is fully determined by β_1.

4.6 Reflection from and Transmission through a Slab

In slab geometries we can not only measure reflection from the slab, but also transmission through the slab. The bistatic coefficient for reflection will decrease, as some light will be transmitted. We will calculate the bistatic coefficients for both reflection and transmission.

We define the optical thickness of the slab by

$$\mathscr{L} \equiv \frac{L}{|\boldsymbol{l}_{e\omega}(\boldsymbol{n}_\perp)|}. \tag{4.100}$$

In order to keep the equations for the slab of a reasonable size, we introduce the factors

$$f_1(\boldsymbol{e}_\mathrm{i},\boldsymbol{e}_\mathrm{o},\boldsymbol{n}_\perp) \equiv \left[\nu(\boldsymbol{e}_\mathrm{i},\boldsymbol{e}_\mathrm{o},\boldsymbol{n}_\perp)+\beta_1(\boldsymbol{q}_\parallel,\boldsymbol{n}_\perp)\right]^2+\left[\tilde{w}(\boldsymbol{e}_\mathrm{i},\boldsymbol{e}_\mathrm{o},\boldsymbol{n}_\perp)+\beta_2(\boldsymbol{q}_\parallel,\boldsymbol{n}_\perp)\right]^2, \tag{4.101a}$$

$$f_2(\boldsymbol{e}_\mathrm{i},\boldsymbol{e}_\mathrm{o},\boldsymbol{n}_\perp) \equiv \left[\nu(\boldsymbol{e}_\mathrm{i},\boldsymbol{e}_\mathrm{o},\boldsymbol{n}_\perp)-\beta_1(\boldsymbol{q}_\parallel,\boldsymbol{n}_\perp)\right]^2+\left[\tilde{w}(\boldsymbol{e}_\mathrm{i},\boldsymbol{e}_\mathrm{o},\boldsymbol{n}_\perp)+\beta_2(\boldsymbol{q}_\parallel,\boldsymbol{n}_\perp)\right]^2, \tag{4.101b}$$

$$\begin{aligned} f_3(\boldsymbol{e}_\mathrm{i},\boldsymbol{e}_\mathrm{o},\boldsymbol{n}_\perp) \equiv\ & 2\beta_1(\boldsymbol{q}_\parallel,\boldsymbol{n}_\perp)\tau_\mathrm{e}(\boldsymbol{n}_\perp)\cosh\left(\mathscr{L}\beta_1(\boldsymbol{q}_\parallel,\boldsymbol{n}_\perp)\right) \\ & +\left[1+\beta_1^2(\boldsymbol{q}_\parallel,\boldsymbol{n}_\perp)\tau_\mathrm{e}^2(\boldsymbol{n}_\perp)\right]\sinh\left(\mathscr{L}\beta_1(\boldsymbol{q}_\parallel,\boldsymbol{n}_\perp)\right). \end{aligned} \tag{4.101c}$$

Using the above abbreviations we will present in the next subsections the results for the bistatic coefficients in reflection and transmission.

4.6.a Bistatic coefficients for reflection

The procedure for calculating the bistatic coefficient for reflection from a slab is analogous to the calculation for semi-infinite media, only now we use the Green function for the slab in stead of the one for the semi-infinite medium The bistatic coefficients for reflection from a slab of optical thickness $\mathscr{L}$ are

$$\cos\theta_\mathrm{i}\gamma_\mathrm{s}(\boldsymbol{e}_\mathrm{i},\boldsymbol{e}_\mathrm{o},\boldsymbol{n}_\perp) = \frac{1}{4\pi\sqrt{\det\mathsf{A}}}\frac{|\boldsymbol{l}_{\mathrm{e}\omega}(\boldsymbol{n}_\perp)|}{\boldsymbol{l}_{\mathrm{e}\omega}(\boldsymbol{n}_\perp)\cdot\boldsymbol{n}_\perp}\left|\frac{\boldsymbol{v}_\mathrm{g}(\boldsymbol{e}_\mathrm{o})}{c_\mathrm{i}}\right|^2\frac{1-\mathrm{e}^{-2\mathscr{L}\nu(\boldsymbol{e}_\mathrm{i},\boldsymbol{e}_\mathrm{o},\boldsymbol{n}_\perp)}}{2\nu(\boldsymbol{e}_\mathrm{i},\boldsymbol{e}_\mathrm{o},\boldsymbol{n}_\perp)}, \tag{4.102a}$$

$$\begin{aligned} \cos\theta_\mathrm{i}\gamma_\mathrm{d}(\boldsymbol{e}_\mathrm{i},\boldsymbol{e}_\mathrm{o},\boldsymbol{n}_\perp) = & \left|\frac{\boldsymbol{v}_\mathrm{g}(\boldsymbol{e}_\mathrm{o})}{c_\mathrm{i}}\right|^2\frac{3C_{\boldsymbol{n}_\perp}\mathrm{e}^{-\mathscr{L}\nu}}{2\nu(\nu^2-w^2)^2(\mathscr{L}+2\tau_\mathrm{e})} \\ & \times\Big\{8\nu w\tau_\mathrm{e}\sinh(\mathscr{L}w) \\ & +2\left[(\mathscr{L}-2\tau_\mathrm{e})\nu^2-(\mathscr{L}+2\tau_\mathrm{e})w^2\right]\sinh(\mathscr{L}\nu) \\ & +4\nu\left[1-\tau_\mathrm{e}(\mathscr{L}+\tau_\mathrm{e})\left(\nu^2-w^2\right)\right]\cosh(\mathscr{L}\nu) \\ & -4\nu\left[1-\tau_\mathrm{e}^2(\nu^2-w^2)\right]\cosh(\mathscr{L}w)\Big\}, \end{aligned} \tag{4.102b}$$

$$\begin{aligned} \cos\theta_\mathrm{i}\gamma_\mathrm{c}(\boldsymbol{e}_\mathrm{i},\boldsymbol{e}_\mathrm{o},\boldsymbol{n}_\perp) = & \left|\frac{\boldsymbol{v}_\mathrm{g}(\boldsymbol{e}_\mathrm{o})}{c_\mathrm{i}}\right|^2\frac{3C_{\boldsymbol{n}_\perp}\mathrm{e}^{-\mathscr{L}\nu}}{2\nu f_1 f_2 f_3} \\ & \times\Big\{2f_2(\nu+\beta_1)\tau_\mathrm{e}\sinh\left(\mathscr{L}\nu+\mathscr{L}\beta_1\right) \\ & -2f_1(\nu-\beta_1)\tau_\mathrm{e}\sinh\left(\mathscr{L}\nu-\mathscr{L}\beta_1\right) \\ & +f_2\left[1+\left(2\nu\tau_\mathrm{e}+\beta_1\tau_\mathrm{e}\right)\beta_1\tau_\mathrm{e}\right]\cosh\left(\mathscr{L}\nu+\mathscr{L}\beta_1\right) \\ & -f_1\left[1-\left(2\nu\tau_\mathrm{e}-\beta_1\tau_\mathrm{e}\right)\beta_1\tau_\mathrm{e}\right]\cosh\left(\mathscr{L}\nu-\mathscr{L}\beta_1\right) \\ & +4\nu\beta_1\tau_\mathrm{e}^2\left\{1-\left[\nu^2+(\tilde{w}+\beta_2)^2\right]\tau_\mathrm{e}^2\right\}\cos\left(\mathscr{L}\tilde{w}+\mathscr{L}\beta_2\right) \\ & -8\nu\beta_1(\tilde{w}+\beta_2)\tau_\mathrm{e}\sin\left(\mathscr{L}\tilde{w}+\mathscr{L}\beta_2\right)\Big\}. \end{aligned} \tag{4.102c}$$

When we take the limit $\mathscr{L} \to \infty$ we recover the semi-infinite medium result. In Figs. 4.11, 4.12, and 4.13 these bistatic cross sections are plotted.

4.6.b Bistatic coefficients for transmission

Slabs also have a bistatic coefficient for transmission of radiance. In transmission, after the final scattering event, the radiance couples out with

$$\begin{aligned} G_{\mathrm{b}\omega}(\boldsymbol{x}, \boldsymbol{x}_0 - L\boldsymbol{n}_\perp, t) \quad \equiv \quad & \frac{\left|\boldsymbol{v}_{\mathrm{g}}(\boldsymbol{n}_\phi(\boldsymbol{x}))\right|}{\mathrm{c_i}\sqrt{\det \mathsf{A}}} \frac{\exp\left\{\mathrm{i}\frac{\omega}{\mathrm{c_i}}[\phi_\omega(\boldsymbol{x}) - \mathrm{c_i}\, t]\right\}}{4\pi|\boldsymbol{x}|} \\ & \times \exp\left\{\mathrm{i}\boldsymbol{k}_\parallel \cdot \boldsymbol{x}_0 + \mathrm{i}\frac{\omega \tilde{u}_\omega(\boldsymbol{e}_{\boldsymbol{k}}, \boldsymbol{n}_\perp)(z_0 - L)}{|\boldsymbol{v}_{\mathrm{g}}(\boldsymbol{n}_\perp)|}\right. \\ & \left. - \frac{z_0 - L}{2|\boldsymbol{l}_{\mathrm{e}\omega}(\boldsymbol{n}_\perp)|\, u_\omega(\boldsymbol{e}_{\boldsymbol{k}}, \boldsymbol{n}_\perp)}\right\}. \end{aligned} \tag{4.103}$$

Here $\tilde{u}(\boldsymbol{e}_{\mathrm{o}}, \boldsymbol{n}_\perp)$ and $u(\boldsymbol{e}_{\mathrm{o}}, \boldsymbol{n}_\perp)$ are both negative, being defined as the generalization of $\cos\theta = -\boldsymbol{e}_{\boldsymbol{k}} \cdot \boldsymbol{n}_\perp$. Then $w < 0$, as well as $v + w < 0$ and $w - v < 0$.

The bistatic coefficients for transmission through anisotropic slabs are

$$\cos\theta_{\mathrm{i}} \gamma_{\mathrm{s}}(\boldsymbol{e}_{\mathrm{i}}, \boldsymbol{e}_{\mathrm{o}}, \boldsymbol{n}_\perp) = \frac{\mathrm{e}^{\frac{\mathscr{L}}{u(\boldsymbol{e}_{\mathrm{o}}, \boldsymbol{n}_\perp)}}}{4\pi\sqrt{\det \mathsf{A}}} \frac{|\boldsymbol{l}_{\mathrm{e}\omega}(\boldsymbol{n}_\perp)|}{\boldsymbol{l}_{\mathrm{e}\omega}(\boldsymbol{n}_\perp) \cdot \boldsymbol{n}_\perp} \left|\frac{\boldsymbol{v}_{\mathrm{g}}(\boldsymbol{e}_{\mathrm{o}})}{\mathrm{c_i}}\right|^2 \frac{1 - \mathrm{e}^{-2\mathscr{L} v(\boldsymbol{e}_{\mathrm{i}}, \boldsymbol{e}_{\mathrm{o}}, \boldsymbol{n}_\perp)}}{2v(\boldsymbol{e}_{\mathrm{i}}, \boldsymbol{e}_{\mathrm{o}}, \boldsymbol{n}_\perp)}, \tag{4.104a}$$

$$\begin{aligned} \cos\theta_{\mathrm{i}} \gamma_{\mathrm{d}}(\boldsymbol{e}_{\mathrm{i}}, \boldsymbol{e}_{\mathrm{o}}, \boldsymbol{n}_\perp) = & \left|\frac{\boldsymbol{v}_{\mathrm{g}}(\boldsymbol{e}_{\mathrm{o}})}{\mathrm{c_i}}\right|^2 \frac{3C_{\boldsymbol{n}_\perp} \mathrm{e}^{\frac{\mathscr{L}}{u(\boldsymbol{e}_{\mathrm{i}}, \boldsymbol{n}_\perp)}}}{2v(v^2 - w^2)^2(\mathscr{L} + 2\tau_{\mathrm{e}})} \\ & \times \Big\{ 8vw\tau_{\mathrm{e}} \sinh(\mathscr{L} w) \\ & + 2\left[(\mathscr{L} - 2\tau_{\mathrm{e}})\, v^2 - (\mathscr{L} + 2\tau_{\mathrm{e}})\, w^2\right] \sinh(\mathscr{L} v) \\ & + 4v\left[1 - \tau_{\mathrm{e}}(\mathscr{L} + \tau_{\mathrm{e}})\left(v^2 - w^2\right)\right] \cosh(\mathscr{L} v) \\ & - 4v\left[1 - \tau_{\mathrm{e}}^2 (v^2 - w^2)\right] \cosh(\mathscr{L} w) \Big\}, \end{aligned} \tag{4.104b}$$

$$\begin{aligned} \cos\theta_{\mathrm{i}} \gamma_{\mathrm{c}}(\boldsymbol{e}_{\mathrm{i}}, \boldsymbol{e}_{\mathrm{o}}, \boldsymbol{n}_\perp) = & \left|\frac{\boldsymbol{v}_{\mathrm{g}}(\boldsymbol{e}_{\mathrm{o}})}{\mathrm{c_i}}\right|^2 \frac{3C_{\boldsymbol{n}_\perp} \mathrm{e}^{\frac{\mathscr{L}}{u(\boldsymbol{e}_{\mathrm{i}}, \boldsymbol{n}_\perp)}}}{2v f_1 f_2 f_3} \\ & \times \Big\{ 2f_2(v + \beta_1)\tau_{\mathrm{e}} \sinh\left(\mathscr{L} v + \mathscr{L}\beta_1\right) \\ & - 2f_1(v - \beta_1)\tau_{\mathrm{e}} \sinh\left(\mathscr{L} v - \mathscr{L}\beta_1\right) \\ & + f_2\left[1 + \left(2v\tau_{\mathrm{e}} + \beta_1\tau_{\mathrm{e}}\right)\beta_1\tau_{\mathrm{e}}\right] \cosh\left(\mathscr{L} v + \mathscr{L}\beta_1\right) \\ & - f_1\left[1 - \left(2v\tau_{\mathrm{e}} - \beta_1\tau_{\mathrm{e}}\right)\beta_1\tau_{\mathrm{e}}\right] \cosh\left(\mathscr{L} v - \mathscr{L}\beta_1\right) \\ & + 4v\beta_1\tau_{\mathrm{e}}^2\left\{1 - \left[v^2 + (\tilde{w} + \beta_2)^2\right]\tau_{\mathrm{e}}^2\right\} \cos\left(\mathscr{L}\tilde{w} + \mathscr{L}\beta_2\right) \\ & - 8v\beta_1(\tilde{w} + \beta_2)\tau_{\mathrm{e}} \sin\left(\mathscr{L}\tilde{w} + \mathscr{L}\beta_2\right) \Big\}. \end{aligned} \tag{4.104c}$$

The bistatic coefficients for transmission differ by an exponential extinction factor from the bistatic coefficients for reflection. This difference is explained by the Bouguer-Lambert-Beer law for light propagating a distance L through disordered media.

The bistatic coefficient for diffuse transmission (4.104b) reduces for thick slabs to a product of escape functions, or rather an injection function times an escape function. In the thick slab limit the angular resolved transmission is

$$T(\boldsymbol{e}_{\rm i},\boldsymbol{e}_{\rm o},\boldsymbol{n}_\perp) \quad = \quad \frac{4}{3}\frac{l_\perp(\boldsymbol{n}_\perp)K(\boldsymbol{e}_{\rm i})K(\boldsymbol{e}_{\rm o})}{L+\frac{4}{3}l_\perp(\boldsymbol{n}_\perp)}. \tag{4.105}$$

Here we have redefined both u such that they are positive. We see a product of escape functions, which makes physical sense because the first is the injection function, and the second the escape function. Slabs of many mean free path thick are effectively infinite, and the incoming direction is totally scrambled.

The total transmission or all channel in all channel out transmission is easily obtained by using the fact that the escape functions are normalized to unity,

$$T(\boldsymbol{e}_{\rm i},\boldsymbol{e}_{\rm o},\boldsymbol{n}_\perp) \quad = \quad \frac{4}{3}\frac{l_\perp(\boldsymbol{n}_\perp)}{L+\frac{4}{3}l_\perp(\boldsymbol{n}_\perp)}. \tag{4.106}$$

The component of the transport mean free path perpendicular to the surface governs the amount of transmitted light.

4.7 Conclusion

We have studied the effect of boundaries on propagation of light through disordered media, and collected all the ingredients required to calculate reflection and transmission properties of anisotropic disordered media.

The mapping of the electromagnetic energy density and flux on the energy density and flux of a scalar model allows us to map the boundary conditions on the electromagnetic fields, which follow from the Maxwell equations in material media, onto the scalar model. The Fresnel reflection and transmission coefficients were derived for anisotropic media. It is possible to identify polarization in the scalar model, and it predicts Brewster angles at the correct locations for isotropic media. Usually scalar models can not predict the Brewster angle because the scalar field and its derivative normal to the boundary are taken to be continuous, as for Schrödinger waves. When the medium becomes anisotropic the Brewster angle can shift in location by tens of degrees.

The propagator for the amplitude traveling from the disordered medium to the homogeneous medium was calculated in the far field limit.

For the energy density flux we established the reflectivity and transmissivity, which also show the Brewster angle for parallel polarized light. Using continuity of the flux component perpendicular to the interface, we established the transport mean free path and energy velocity. These quantities turned out to be vectors, and we split up the diffusion constant using these vectors. We incorporated internal reflections due to anisotropic index mismatch, and related the reflectivity and transmissivity, angle and polarization averaged, to the reflectivity and transmissivity of individual plane waves. We did the same for reflection and transmission tensors, which allow us to incorporate additional anisotropy due to surface roughness into the boundary conditions.

For semi-infinite media and slab geometries we calculated the Green functions, and the solutions for plane waves. Having collected all the ingredients for coupling light in and out of the medium and diffuse propagation, we calculated the key observable for anisotropic disordered media, the escape function which describes how diffusion redistributes the radiance over angles. Instead of the Lambertian distribution, which is the distribution found for isotropic diffusion of light, we found additional structure in the distribution over angles, even leading to two maxima for certain anisotropic media. In addition we were able to calculate the bistatic coefficients for anisotropic disordered semi-infinite media and slabs. The bistatic coefficients were separated into one for single scattering, one for diffusion and one for the interference effect known as enhanced backscattering. The bistatic coefficient for single scattering and diffusion clearly reveal the anisotropy in the escape function. In the bistatic coefficient for enhanced backscattering we see that the enhanced backscattering cone becomes narrower or broader, depending on the anisotropy in the components of the transport mean free path vector.

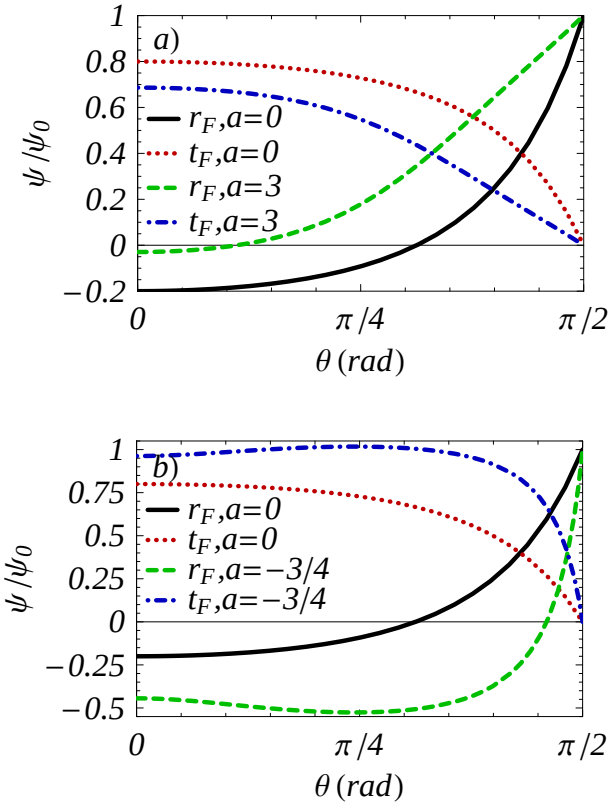

Figure 4.1 (color online).
Some examples of the Fresnel reflection and transmission coefficients r_{F} *and* t_{F} *for plane waves polarized parallel to the plane of incidence are plotted as a function of* $\cos\theta = -\boldsymbol{e_k}\cdot\boldsymbol{e}_z$. *The interface is between air and a uniaxial medium with dielectric anisotropy,* $\varepsilon_{xx} = \varepsilon_{yy} = (1+a)\varepsilon_{zz}$, *and compared to the air-glass (*$a = 0$*) interface (solid and dotted), possibly the best known example in the literature. In* a*) the anisotropy parameter is* $a = 3$, *and in* b*) it is* $a = -3/4$. *Negative values imply a phase difference between the reflected and transmitted wave, and we observe a vanishing of the reflected amplitude at the Brewster angle, whose position shifts due to the anisotropy. The curves are for homogeneous media.*

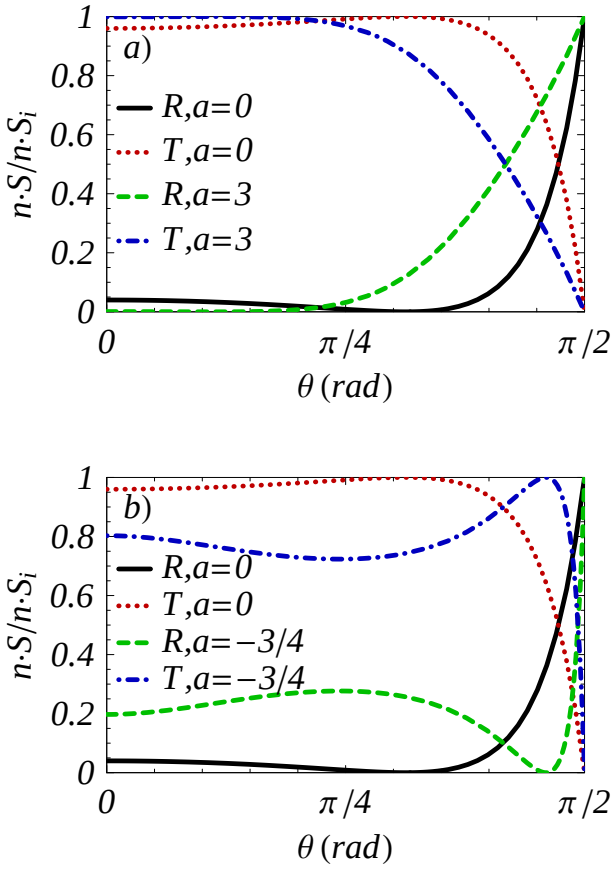

Figure 4.2 (color online).
Some examples of the reflectivity and transmissivity R and T for plane waves polarized parallel to the plane of incidence are plotted as a function of $\cos\theta = -\boldsymbol{e_k}\cdot\boldsymbol{e}_z$. *The interface is between air and a uniaxial medium with dielectric anisotropy,* $\varepsilon_{xx} = \varepsilon_{yy} = (1+a)\varepsilon_{zz}$, *and compared to the air-glass* ($a = 0$) *interface (solid and dotted), possibly the best known example in the literature. In a) the anisotropy parameter is* $a = 3$, *and in b) it is* $a = -3/4$. *We observe a vanishing of the reflectivity at the Brewster angle, whose position shifts due to the anisotropy. The curves are for homogeneous media.*

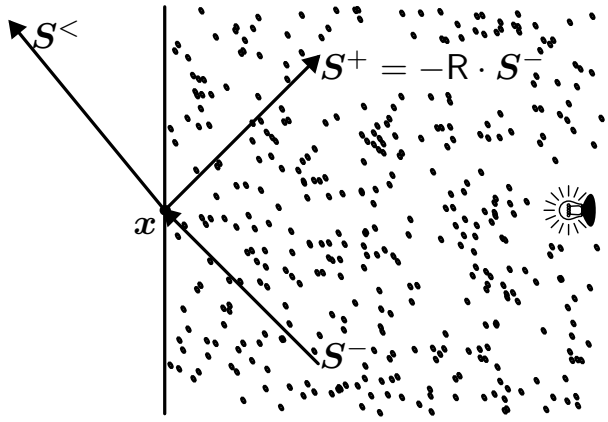

Figure 4.3.
The phenomenological picture behind the boundary condition of the (multiple scattered) radiance or diffuse energy density. Deep inside the medium is some light source, here depicted by the light bulb. Close to the boundary at $\boldsymbol{x}$ we consider the flux components $\boldsymbol{S}^-$ traveling outward, and $\boldsymbol{S}^+$ traveling inward. Some part $\boldsymbol{S}^<$ is refracted at the interface and escapes to $z \to -\infty$, another part $\mathsf{R} \cdot \boldsymbol{S}^-$ is reflected back into the medium. Only the flux component perpendicular to the interface is continuous. If there are no sources outside the medium, and in the absence of internal reflection, i.e. $\mathsf{R} = 0$, there will be no flux contributions coming in from the outside, which is expressed by $\boldsymbol{S}^+(\boldsymbol{x}, t) = \boldsymbol{0}$.

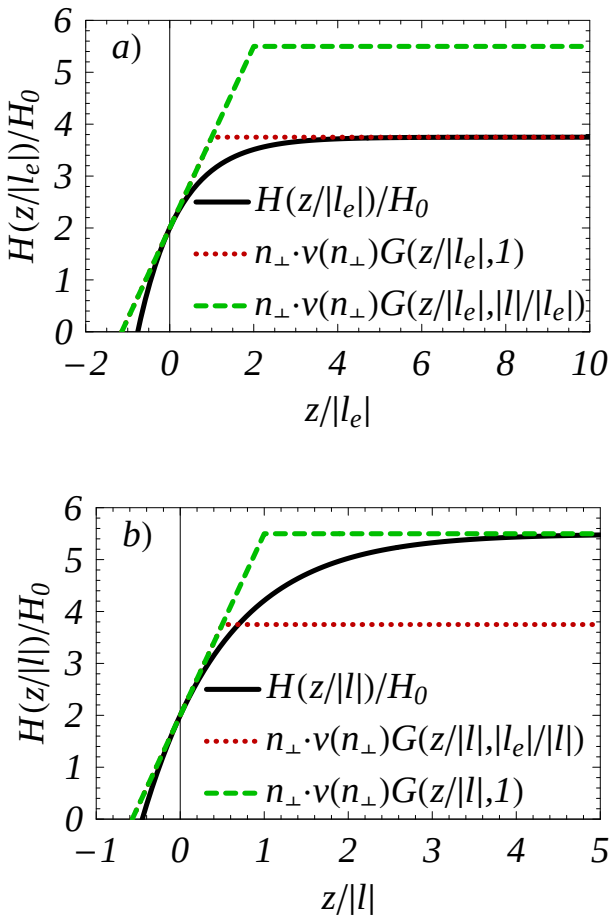

Figure 4.4 (color online).
In a) the exact result (solid) for the diffuse energy density, generated by an incoming plane wave in an anisotropic disordered semi-infinite medium, is compared to two approximations. A planar source placed at a depth of one extinction mean free path $z = |\boldsymbol{l}_e|$ (dotted) approximates the exact result very well. A planar source at a depth of a transport mean free path $z = |\boldsymbol{l}|$ (dashed) can strongly deviate from the exact result. In b) the incoming plane wave decays with the transport mean free path $|\boldsymbol{l}|$ (solid). A planar source at $z = |\boldsymbol{l}|$ (dashed) is a good approximation. The planar source at $z = |\boldsymbol{l}_e|$ seems to deviate. The plot is for a realistic uniaxial medium with the optical axis at an angle of $\pi/4$ radians with the interface, and the permittivity along the optical axis four times smaller than along the other two axes. The extrapolation length is in both figures $2\boldsymbol{e}_z \cdot \boldsymbol{l}(\boldsymbol{e}_z)/3$. a) is the correct picture.

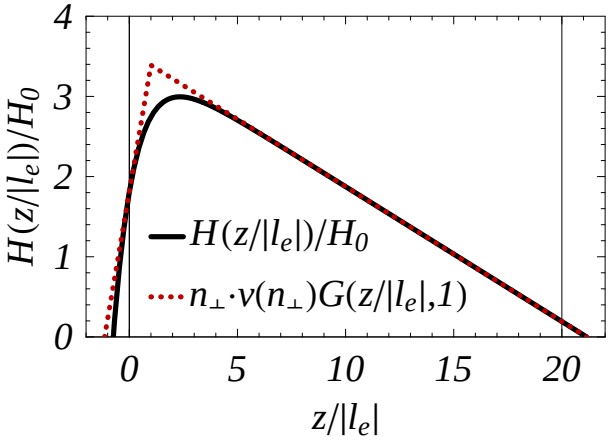

Figure 4.5 (color online).
The exact solution (solid) for the diffuse energy density resulting from an incoming plane wave is plotted. We compare the exact solution to the diffuse energy density resulting from a planar source at a depth of one extinction mean free path and observe very good agreement. The permittivity has one axis four times smaller than the other two axes, and the optical axis is at at an angle of $\pi/4$ radians with the interface.

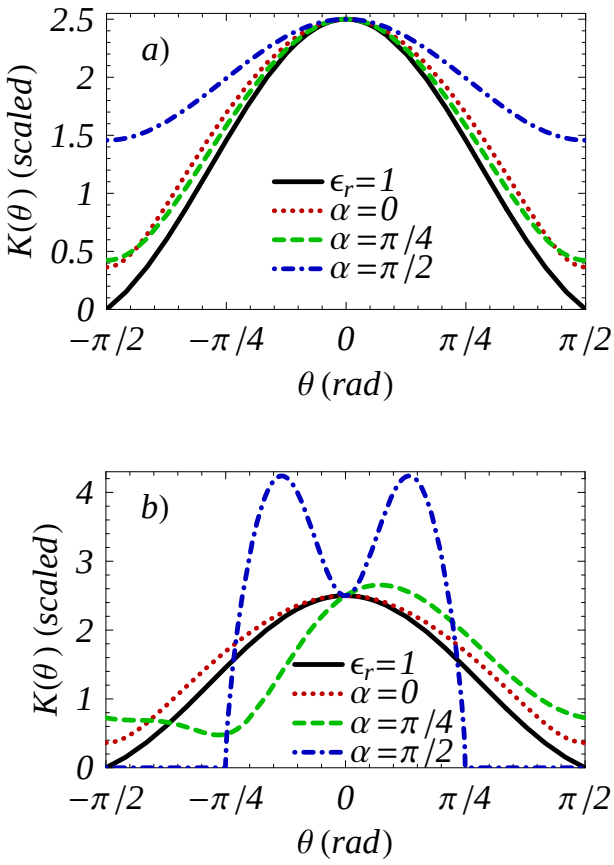

Figure 4.6 (color online).
Examples of escape functions for anisotropic disordered media compared to the Lambertian escape function $K_{\varepsilon_r=1}$ (solid) for isotropic media. Scale factor $a \equiv 2\pi K_{\varepsilon_r=1}(0)/K_{\varepsilon_r}(0)$ and makes all $\theta = 0$ values coincide. The angle θ of wave vector $\boldsymbol{e_k}$ and inward pointing surface normal $\boldsymbol{n}_\perp$ is defined by $\cos\theta \equiv -\boldsymbol{e_k}\cdot\boldsymbol{n}_\perp$. The anisotropic medium is semi-infinite and uniaxial. We plotted several orientations $\cos\alpha \equiv \boldsymbol{d}\cdot\boldsymbol{n}_\perp$ of optical axis $\boldsymbol{d}$ with respect to the inward pointing normal to the interface $\boldsymbol{n}$. The principal axes of the dielectric tensor are related by $\varepsilon_{11} = \varepsilon_{22} = \varepsilon_{33}/4$ and the escaping radiance is observed in vacuum, and we tried to index match. In (a) the wave vector is in the plane with normal $\boldsymbol{n}_\perp \times (\boldsymbol{d}\times\boldsymbol{n}_\perp)$, and we see a deformed bell shape. In (b) in the plane with normal $\boldsymbol{d}\times\boldsymbol{n}_\perp$. We see an anisotropic bell shape for $\alpha = \pi/2$. When $\alpha = \pi/4$ perfect index matching is impossible and we get internal reflection for $\theta > \pi/4$. When $\alpha = 0$ we see two maxima, with symmetry around $\boldsymbol{d}$. We see total internal reflections and a strong deformation of the isotropic bell shape.

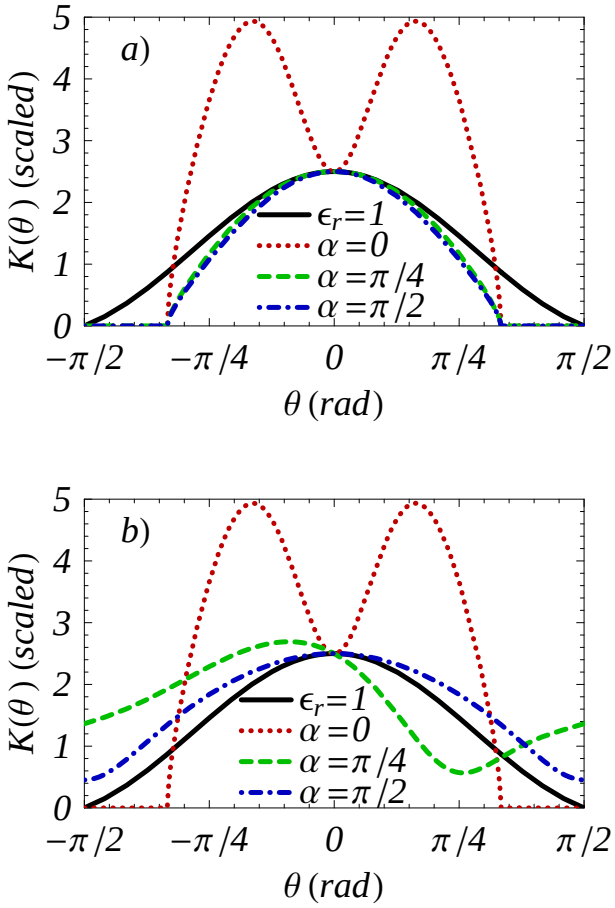

Figure 4.7 (color online).
Examples of escape functions for anisotropic disordered media compared to the Lambertian escape function $K_{\varepsilon_r=1}$ (solid) for isotropic media. Scale factor $a \equiv 2\pi K_{\varepsilon_r=1}(0)/K_{\varepsilon_r}(0)$ and makes all $\theta = 0$ values coincide. The angle θ of wave vector $\boldsymbol{e_k}$ and inward pointing surface normal $\boldsymbol{n}_\perp$ is defined by $\cos\theta \equiv -\boldsymbol{e_k}\cdot\boldsymbol{n}_\perp$. The anisotropic medium is semi-infinite and uniaxial. We plotted several orientations $\cos\alpha \equiv \boldsymbol{d}\cdot\boldsymbol{n}_\perp$ of optical axis $\boldsymbol{d}$ with respect to the inward pointing normal to the interface $\boldsymbol{n}$. The principal axes of the dielectric tensor are related by $\varepsilon_{11} = \varepsilon_{22} = 4\varepsilon_{33}$ and the escaping radiance is observed in vacuum, and we tried to index match. In (a) the wave vector is in the plane with normal $\boldsymbol{n}_\perp \times (\boldsymbol{d} \times \boldsymbol{n}_\perp)$. Index matching is impossible for $\theta > 7\pi/20$, and in addition we see two maxima when $\alpha \to 0$. In (b) in the plane with normal $\boldsymbol{d} \times \boldsymbol{n}_\perp$. For $\alpha = 0$ we observe again the two maxima and index mismatch. When $\alpha = \pi/4$ the maxima shift and decrease in magnitude and if $\alpha = \pi/2$ we see a strongly deformed bell shape.

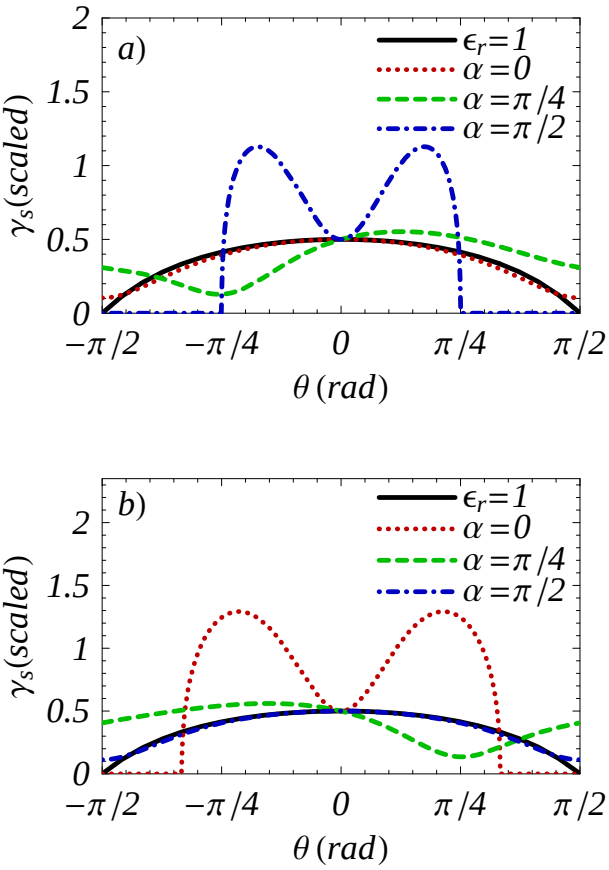

Figure 4.8 (color online).
Examples of single scattering bistatic coefficients for disordered uniaxial semi-infinite media are plotted, and compared to the result for isotropic media (solid). Scale factor $a \equiv \gamma_{s_{\varepsilon_r=1}}(0)/\gamma_{s_{\varepsilon_r}}(0)$ *makes all* $\theta = 0$ *values coincide. The optical axis* $\boldsymbol{d}$ *is at angle* $\cos\alpha = \boldsymbol{d}\cdot\boldsymbol{n}_\perp$ *with the normal to the interface* $\boldsymbol{n}_\perp$*. The wave vector is in the plane with normal* $\boldsymbol{d}\times\boldsymbol{n}_\perp$*. In a) the dielectric is on principal axes given by* $\varepsilon_{11} = \varepsilon_{22} = \varepsilon_{33}/4$*, and in b) the dielectric is on principal axes given by* $\varepsilon_{11} = \varepsilon_{22} = 4\varepsilon_{33}$*. We used the phase function of point scatterers.*

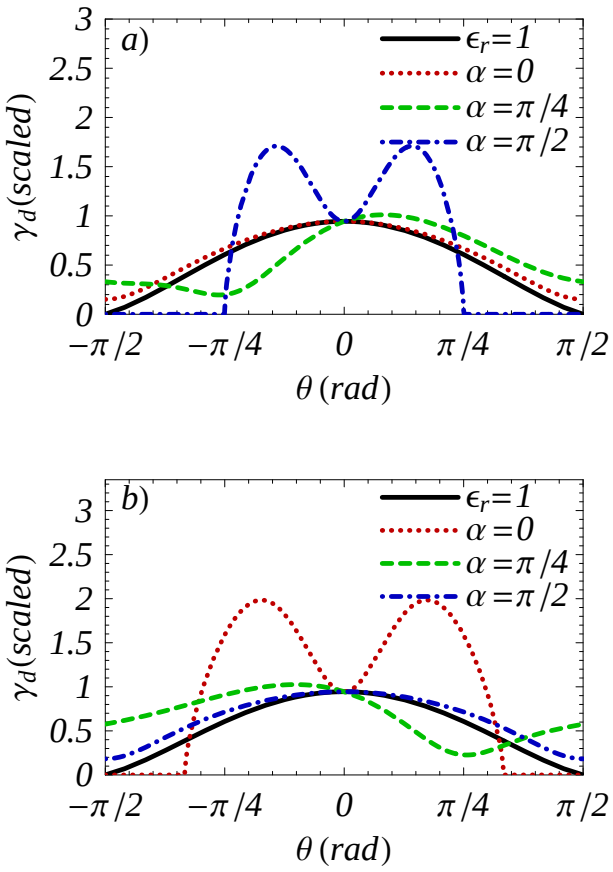

Figure 4.9 (color online).
Examples of the diffuse multiple scattering bistatic coefficients for disordered uniaxial semi-infinite media are plotted, and compared to the result for isotropic media (solid). Scale factor $a \equiv \gamma_{s_{\varepsilon_r=1}}(0)/\gamma_{s_{\varepsilon_r}}(0)$ *makes all* $\theta = 0$ *values coincide. The optical axis* $\boldsymbol{d}$ *is at angle* $\cos\alpha = \boldsymbol{d}\cdot\boldsymbol{n}_\perp$ *with the normal to the interface* $\boldsymbol{n}_\perp$*. The wave vector is in the plane with normal* $\boldsymbol{d}\times\boldsymbol{n}_\perp$*. In a) the dielectric is on principal axes given by* $\varepsilon_{11} = \varepsilon_{22} = \varepsilon_{33}/4$*, and in b) the dielectric is on principal axes given by* $\varepsilon_{11} = \varepsilon_{22} = 4\varepsilon_{33}$*. We used the phase function of point scatterers.*

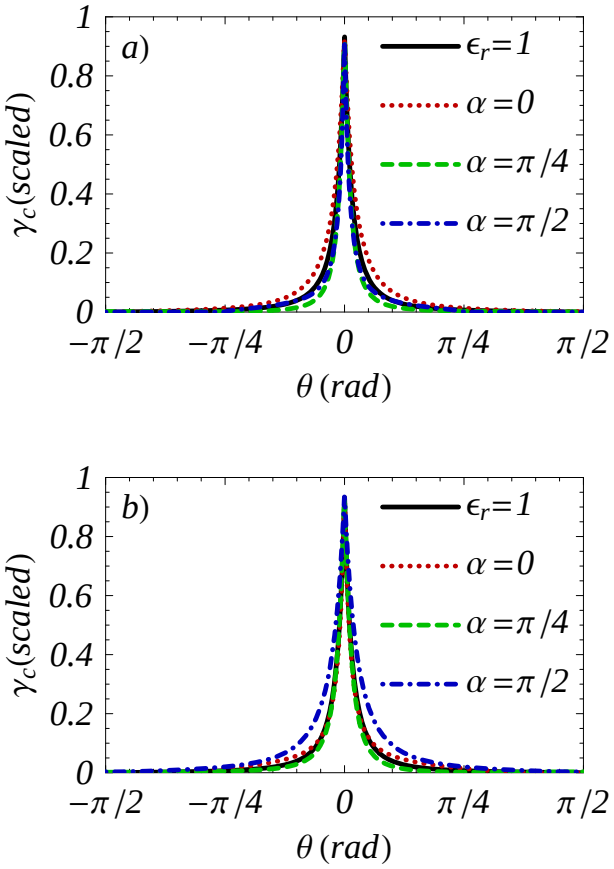

Figure 4.10 (color online).
Examples of the enhanced backscattering cone for disordered uniaxial semi-infinite media are plotted, and compared to the result for isotropic media (solid). Scale factor $a \equiv \gamma_{s_{\varepsilon_r=1}}(0)/\gamma_{s_{\varepsilon_r}}(0)$ *makes all* $\theta = 0$ *values coincide. The optical axis* $\boldsymbol{d}$ *is at angle* $\cos\alpha = \boldsymbol{d}\cdot\boldsymbol{n}_\perp$ *with the normal to the interface* $\boldsymbol{n}_\perp$*. The wave vector is in the plane with normal* $\boldsymbol{d}\times\boldsymbol{n}_\perp$*. In a) the dielectric is on principal axes given by* $\varepsilon_{11} = \varepsilon_{22} = \varepsilon_{33}/4$*, and in b) the dielectric is on principal axes given by* $\varepsilon_{11} = \varepsilon_{22} = 4\varepsilon_{33}$*. We used the phase function of point scatterers.*

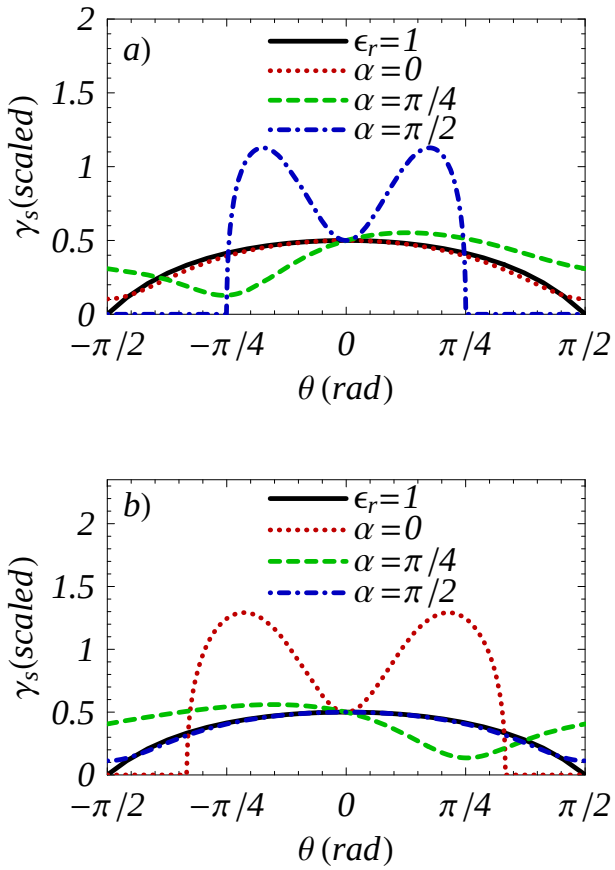

Figure 4.11 (color online).
Examples of single scattering bistatic coefficients for disordered uniaxial slabs are plotted, and compared to the result for isotropic media (solid). Scale factor $a \equiv \gamma_{s_{\varepsilon_r=1}}(0)/\gamma_{s_{\varepsilon_r}}(0)$ *makes all* $\theta = 0$ *values coincide. The optical axis* $\boldsymbol{d}$ *is at angle* $\cos\alpha = \boldsymbol{d}\cdot\boldsymbol{n}_\perp$ *with the normal to the interface* $\boldsymbol{n}_\perp$*. The wave vector is in the plane with normal* $\boldsymbol{d}\times\boldsymbol{n}_\perp$*. In a) the dielectric is on principal axes given by* $\varepsilon_{11} = \varepsilon_{22} = \varepsilon_{33}/4$*, and in b) the dielectric is on principal axes given by* $\varepsilon_{11} = \varepsilon_{22} = 4\varepsilon_{33}$*. We used the phase function of point scatterers. We used the phase function of point scatterers.*

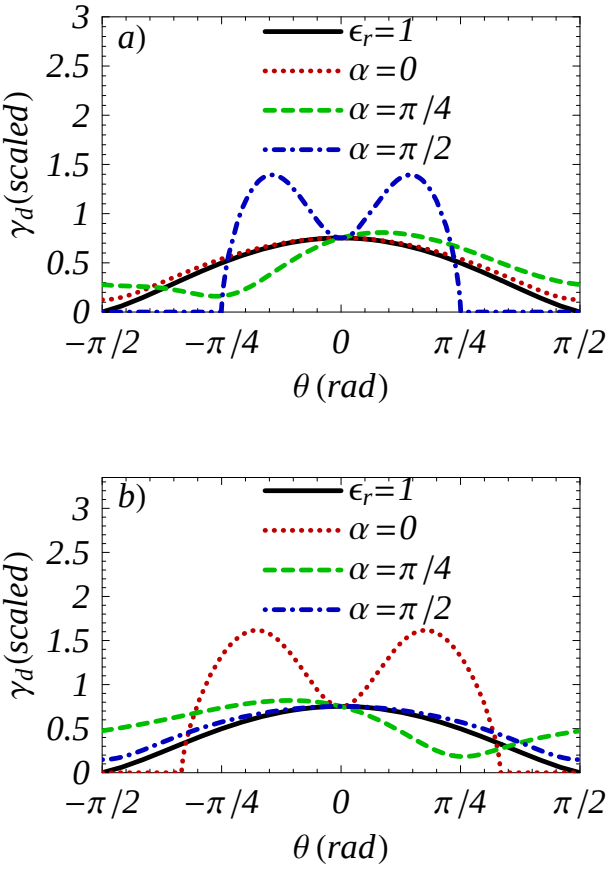

Figure 4.12 (color online).
Examples of the diffuse multiple scattering bistatic coefficients for disordered uniaxial slabs are plotted, and compared to the result for isotropic media (solid). Scale factor $a \equiv \gamma_{s\varepsilon_r=1}(0)/\gamma_{s\varepsilon_r}(0)$ *makes all* $\theta = 0$ *values coincide. The optical axis* $\boldsymbol{d}$ *is at angle* $\cos\alpha = \boldsymbol{d}\cdot\boldsymbol{n}_\perp$ *with the normal to the interface* $\boldsymbol{n}_\perp$*. The wave vector is in the plane with normal* $\boldsymbol{d}\times\boldsymbol{n}_\perp$*. In a) the dielectric is on principal axes given by* $\varepsilon_{11} = \varepsilon_{22} = \varepsilon_{33}/4$*, and in b) the dielectric is on principal axes given by* $\varepsilon_{11} = \varepsilon_{22} = 4\varepsilon_{33}$*. We used the phase function of point scatterers.*

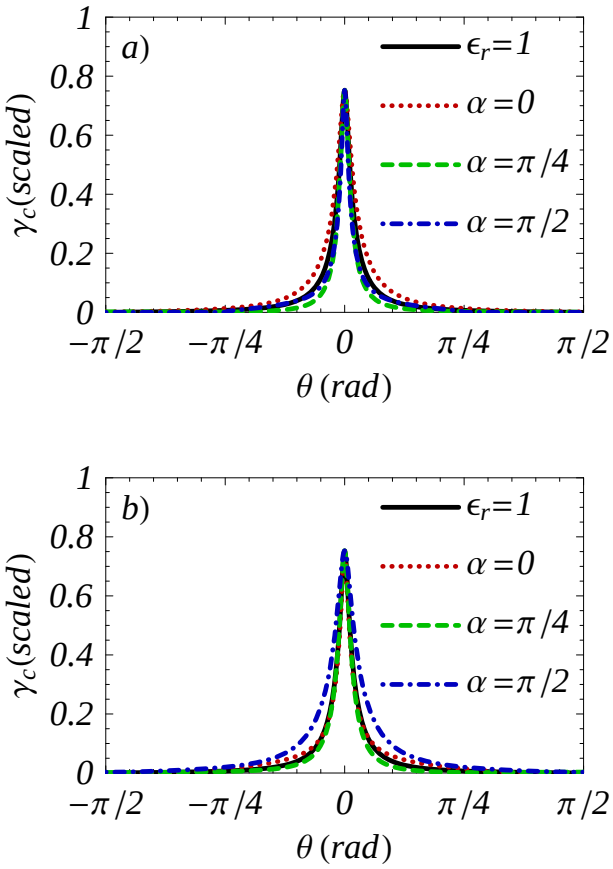

Figure 4.13 (color online).
Examples of the enhanced backscattering cone for disordered uniaxial slabs are plotted, and compared to the result for isotropic media (solid). Scale factor $a \equiv \gamma_{s_{\varepsilon_r=1}}(0)/\gamma_{s_{\varepsilon_r}}(0)$ *makes all* $\theta = 0$ *values coincide. The optical axis* $\boldsymbol{d}$ *is at angle* $\cos\alpha = \boldsymbol{d}\cdot\boldsymbol{n}_\perp$ *with the normal to the interface* $\boldsymbol{n}_\perp$*. The wave vector is in the plane with normal* $\boldsymbol{d}\times\boldsymbol{n}_\perp$*. In a) the dielectric is on principal axes given by* $\varepsilon_{11} = \varepsilon_{22} = \varepsilon_{33}/4$*, and in b) the dielectric is on principal axes given by* $\varepsilon_{11} = \varepsilon_{22} = 4\varepsilon_{33}$*. We used the phase function of point scatterers.*

Chapter 5

Conclusion

The conclusions of this thesis are summarized.

We presented a scalar wave model for electromagnetic waves in anisotropic disordered dielectric media. Our scalar model for light can predict a number of measurable quantities of both homogeneous and disordered anisotropic media, such as the Fresnel reflection and transmission coefficients, the Brewster angle, the reflectivity and transmissivity, the escape function, the bistatic coefficients, the cone of enhanced backscattering, the extinction, scattering and transport mean free path, the energy velocity and the diffusion tensor. In the isotropic limit our scalar model for light reduces to the results known from the literature. Not only can we use this model to describe media with an isotropic magnetic permeability and an anisotropic dielectric permittivity, but we can switch the interpretations of the electric and magnetic fields and describe media which have an anisotropic magnetic permeability and an isotropic permittivity.

In order to calculate the values of the measurable quantities, we need some information about the anisotropic disordered medium. The required ingredients for are the average permittivity, the average permeability, the differential scattering cross section of the typical scatterer in the medium, and the density of the scatterers. We presented calculations for semi-infinite medium and slab geometries, but the boundary conditions we used are also applicable to more complicated geometries.

The scalar model gives rise to an anisotropic radiative transfer equation. If one of the principal components of the dielectric tensor is smaller than the other two components, the radiative transfer equation tends to steer the radiance into the plane perpendicular to the axis with smaller dielectric constant. If on the other hand one of the components is larger than the others, the anisotropic radiative transfer equation tends to waveguide the light along a single direction. We presented an outline for a numerical simulation of this equation.

In uniaxial media the ordinary wave satisfies an isotropic dispersion relation whereas the extraordinary waves satisfy an anisotropic dispersion relation. Our scalar model can describe both waves, but not at the same time.

For an accurate characterization of anisotropic disordered media we require the angle and polarization averaged reflectivity and transmissivity, the transport mean free path, and the energy velocity. We related the angle and polarization averaged reflectivity and transmissivity to the reflectivity and the transmissivity of the plane waves, which we in turn related to the Fresnel reflection and transmission coefficients. Measurements of the Fresnel coefficients for plane wave amplitude can provide us the angle and polarization averaged reflectivity and transmissivity. The transport mean free path vector can be established from transmission experiments for the three principal axes of the anisotropy. Time resolved transmission experiments for the three principal axes of the anisotropy give us the energy velocity.

The location of the transition to Anderson localization shifts in anisotropic media, such that the transition occurs at longer scattering mean free path. We like to speculate about the possibility to design disordered anisotropic media where all becomes easier.

Appendix A

Derivation of the Ward identity

The Ward identity is a fundamental relation between the Dyson self energy and the Bethe-Salpeter irreducible vertex. In this technical derivation of the Ward identity for scalar waves we follow the appendix in [89], but we consider anisotropic media and are more explicit.

We define the wave equation matrix elements $K_\omega(\boldsymbol{x}_0,\boldsymbol{x})$ and $L_\omega(\boldsymbol{x}_0,\boldsymbol{x})$ by

$$K_\omega(\boldsymbol{x}_0,\boldsymbol{x}) \equiv \delta^3(\boldsymbol{x}_0-\boldsymbol{x})[\boldsymbol{\nabla}\cdot\mathsf{A}\cdot\boldsymbol{\nabla}+\frac{\omega^2}{{c_i}^2}], \tag{A.1}$$

$$L_\omega(\boldsymbol{x}_0,\boldsymbol{x}) \equiv K_\omega(\boldsymbol{x}_0,\boldsymbol{x})-V_\omega(\boldsymbol{x}_0,\boldsymbol{x}), \tag{A.2}$$

where the scattering potential $V_\omega(\boldsymbol{x}_0,\boldsymbol{x})$ has been defined in Eq. (2.9), and we note that we can write

$$V_\omega(\boldsymbol{x}_0,\boldsymbol{x}) = -f_\omega\tilde{V}(\boldsymbol{x}_0)\delta^3(\boldsymbol{x}_0-\boldsymbol{x}), \tag{A.3}$$

and furthermore note that $f_\omega = {f^*}_\omega$ and $\tilde{V}(\boldsymbol{x}_0)=\tilde{V}^*(\boldsymbol{x}_0)$. It is useful to define a $\tilde{K}$ and $\tilde{L}$ by

$$K_\omega(\boldsymbol{x}_0,\boldsymbol{x}) \equiv \delta^3(\boldsymbol{x}_0-\boldsymbol{x})\tilde{K}_\omega(\boldsymbol{x}), \tag{A.4}$$

$$L_\omega(\boldsymbol{x}_0,\boldsymbol{x}) \equiv \delta^3(\boldsymbol{x}_0-\boldsymbol{x})\tilde{L}_\omega(\boldsymbol{x}). \tag{A.5}$$

We calculate the auxiliary result

$$f_{\omega_-}\tilde{L}^*_{\omega_+}(\boldsymbol{x})-f_{\omega_+}\tilde{L}_{\omega_-}(\boldsymbol{x}) = f_{\omega_-}\tilde{K}^*_{\omega_+}(\boldsymbol{x})-f_{\omega_+}\tilde{K}_{\omega_-}(\boldsymbol{x}), \tag{A.6}$$

and we have by definition

$$\delta^3(\boldsymbol{x}_1-\boldsymbol{x}_2)G_\omega(\boldsymbol{x}_3,\boldsymbol{x}_4) = \tilde{L}^*_\omega(\boldsymbol{x}_1)G^*_\omega(\boldsymbol{x}_1,\boldsymbol{x}_2)G_\omega(\boldsymbol{x}_3,\boldsymbol{x}_4), \tag{A.7}$$

Thus we obtain

$$\delta^3(\boldsymbol{x}-\boldsymbol{x}_1)f_{\omega_-}G_{\omega_-}(\boldsymbol{x},\boldsymbol{x}_2)-f_{\omega_+}G^*_{\omega_+}(\boldsymbol{x},\boldsymbol{x}_1)\delta^3(\boldsymbol{x}-\boldsymbol{x}_2) = [f_{\omega_-}\tilde{K}^*_{\omega_+}(\boldsymbol{x})-f_{\omega_+}\tilde{K}_{\omega_-}(\boldsymbol{x})]G^*_{\omega_+}(\boldsymbol{x},\boldsymbol{x}_1)G_{\omega_-}(\boldsymbol{x},\boldsymbol{x}_2). \tag{A.8}$$

This equation is now ensemble averaged, and Fourier transformed with respect to all coordinates, the functions of $\boldsymbol{x}$ and $\boldsymbol{x}_1$ to $\boldsymbol{p}_+$ and $\tilde{\boldsymbol{p}}_+$ respectively, and the functions of $\boldsymbol{x}$ and $\boldsymbol{x}_2$ to $\boldsymbol{p}_-$ and $\tilde{\boldsymbol{p}}_-$ respectively, with $\boldsymbol{p}_\pm = \boldsymbol{p} \pm \boldsymbol{P}/2$ and $\tilde{\boldsymbol{p}}_\pm = \tilde{\boldsymbol{p}} \pm \tilde{\boldsymbol{P}}/2$. The coordinate $\boldsymbol{x}$ appeared twice, which means that $\boldsymbol{P}$ is integrated out automatically. Furthermore we integrate over $\tilde{\boldsymbol{p}}$, we use (2.39a) to identify $\Phi_\omega(\boldsymbol{p}, \tilde{\boldsymbol{p}}, \tilde{\boldsymbol{P}}, \tilde{\Omega})$, and replace $\tilde{\boldsymbol{P}}$ by $\boldsymbol{P}$ and $\tilde{\Omega}$ by Ω

$$f_{\omega_-} G_{\omega_-}(\boldsymbol{p}_-) - f_{\omega_+} G^*_{\omega_+}(\boldsymbol{p}_+) = \int \frac{\mathrm{d}^3\tilde{p}}{(2\pi)^3} \Phi_\omega(\boldsymbol{p}, \tilde{\boldsymbol{p}}, \boldsymbol{P}, \Omega) \times [f_{\omega_-} \tilde{K}^*_{\omega_+}(\tilde{\boldsymbol{p}}_+) - f_{\omega_+} \tilde{K}_{\omega_-}(\tilde{\boldsymbol{p}}_-)], \tag{A.9}$$

so in $\tilde{\boldsymbol{p}}_\pm$ we have $\boldsymbol{P}$, not $\tilde{\boldsymbol{P}}$. We divide (A.9) by $G^*_{\omega_+}(\boldsymbol{p}_+) G_{\omega_-}(\boldsymbol{p}_-)$, and use the Dyson equation (2.29) and the Bethe-Salpeter equation (2.38) for Φ to obtain

$$f_{\omega_-} \Sigma^*_{\omega_+}(\boldsymbol{p}_+) - f_{\omega_+} \Sigma_{\omega_-}(\boldsymbol{p}_-) = \int \frac{\mathrm{d}^3\tilde{p}}{(2\pi)^3} U_\omega\left(\boldsymbol{p}, \tilde{\boldsymbol{p}}, \boldsymbol{P}, \Omega\right) \times \left[f_{\omega_+} G^*_{\omega_+}\left(\tilde{\boldsymbol{p}}_+\right) - f_{\omega_-} G_{\omega_-}\left(\tilde{\boldsymbol{p}}_-\right)\right]. \tag{A.10}$$

If we define $\delta_\omega(\boldsymbol{p}, \boldsymbol{P}, \Omega)$ by

$$\begin{aligned} \delta_\omega(\boldsymbol{p}, \boldsymbol{P}, \Omega) \equiv & -2\frac{\Sigma^*_{\omega_+}(\boldsymbol{p}_+) + \Sigma_{\omega_-}(\boldsymbol{p}_-)}{f_{\omega_+} + f_{\omega_-}} \\ & -2\int \frac{\mathrm{d}^3\tilde{p}}{(2\pi)^3} U_\omega\left(\boldsymbol{p}, \tilde{\boldsymbol{p}}, \boldsymbol{P}, \Omega\right) \frac{G^*_{\omega_+}\left(\tilde{\boldsymbol{p}}_+\right) + G_{\omega_-}\left(\tilde{\boldsymbol{p}}_-\right)}{f_{\omega_+} + f_{\omega_-}}, \end{aligned} \tag{A.11}$$

then, using $f_\omega = \omega^2/{c_i}^2$, the Ward identity for classical scalar waves in anisotropic media can be written as

$$\int \frac{\mathrm{d}^3 p}{(2\pi)^3} \gamma_\omega\left(\boldsymbol{p}, \boldsymbol{p}_0, \boldsymbol{P}, \Omega\right) = -\mathrm{i}\Omega \delta_\omega\left(\boldsymbol{p}_0, \boldsymbol{P}, \Omega\right), \tag{A.12}$$

with γ defined by (2.43d), representing extinction and scattering, and δ related to scattering delay. Our result is similar to results in the literature [68, 89, 90]. However in order to obtain a radiative transfer equation we need the result also per solid angle element, hence we define a differential δ by

$$\int \frac{\mathrm{d}p}{(2\pi)^3} p^2 \gamma_\omega\left(\boldsymbol{p}, \boldsymbol{p}_0, \boldsymbol{P}, \Omega\right) = -\mathrm{i}\Omega \frac{\mathrm{d}\delta_\omega\left(\boldsymbol{e}_{\boldsymbol{p}}, \boldsymbol{p}_0, \boldsymbol{P}, \Omega\right)}{\mathrm{d}^2 e_{\boldsymbol{p}}}. \tag{A.13}$$

When in the definition (A.11) of $\delta_\omega(\boldsymbol{p}, \boldsymbol{P}, \Omega)$ we first take the limit $\lim_{\boldsymbol{P}\to\boldsymbol{0}}$ and then $\lim_{\boldsymbol{\Omega}\to 0}$ then we obtain

$$\delta_\omega(\boldsymbol{p}, \boldsymbol{0}, 0) = -\frac{\partial \mathrm{Re}[\Sigma_\omega(\boldsymbol{p})]}{\partial f_\omega} - \int \frac{\mathrm{d}^3\tilde{p}}{(2\pi)^3} \frac{\partial}{\partial f_\omega} \left\{U_\omega(\boldsymbol{p}, \tilde{\boldsymbol{p}}, \boldsymbol{0}, 0) \mathrm{Re}[G_\omega(\tilde{\boldsymbol{p}})]\right\}, \tag{A.14}$$

which, using again $f_\omega = \omega^2/{c_i}^2$, looks the same as usual, but is nonetheless a generalization of a result found in [68], to anisotropic host media. The scattering potential we defined in (2.9) has $\boldsymbol{P} = 0$, and therefore there is no additional nonlocal term proportional to $\boldsymbol{P}$ in (A.12).

Appendix B

Linear response theory

In section 3.3 we derived an anisotropic diffusion equation from the anisotropic radiative transfer equation using a multipole expansion for the radiance. In section 3.6 we added interference corrections to the diffusion equation starting from a Green-Kubo type formula generalized to accommodate anisotropic media. In this section we give the foundation for the self consistent expansion of the radiance (3.6), and we will generalize the Green-Kubo formula to anisotropic media.

In order to obtain the anisotropic diffusion solution to the Bethe-Salpeter equation, we do not necessarily need to derive the anisotropic radiative transfer equation first. Instead, we can consider the diffusive pole of the Bethe-Salpeter equation and find the related eigenfunction. The diffusive pole is the most relevant pole of the Bethe-Salpeter equation when Ω and $\boldsymbol{P}$ are small with respect to transport mean free time and transport mean free path respectively. Therefore we make an expansion in the parameters Ω and $\boldsymbol{P}$. A similar approach to ours has been considered by [89].

Starting with the generalized Boltzmann equation (2.44) which we multiply by $\boldsymbol{P}\cdot\boldsymbol{P}$, and write $\tilde{\Psi}_\omega \equiv \boldsymbol{P}\cdot\boldsymbol{P}\Psi_\omega$, so $\tilde{\Psi}_\omega$ has no pole, nor is there a source term for $\boldsymbol{P}\to 0$,

$$\left[\mathrm{i}\Omega - \frac{{c_\mathrm{i}}^2}{\omega}\boldsymbol{p}\cdot\mathsf{A}\cdot\mathrm{i}\boldsymbol{P}\right]\tilde{\Psi}_\omega\left(\boldsymbol{p},\boldsymbol{P},\Omega\right) = \boldsymbol{P}\cdot\boldsymbol{P}\frac{\xi_\omega\left(\boldsymbol{e}_{\boldsymbol{k}},\boldsymbol{x},t\right)}{\left|\boldsymbol{v}_\mathrm{g}\left(\boldsymbol{e}_{\boldsymbol{k}}\right)\right|} + \int\frac{\mathrm{d}^3p_0}{(2\pi)^3}\gamma_\omega\left(\boldsymbol{p},\boldsymbol{p}_0,\boldsymbol{P},\Omega\right)\tilde{\Psi}_\omega\left(\boldsymbol{p}_0,\boldsymbol{P},\Omega\right). \tag{B.1}$$

Here the term γ describes scattering and extinction and is given by

$$\gamma_\omega\left(\boldsymbol{p},\boldsymbol{p}_0,\boldsymbol{P},\Omega\right) \equiv \frac{\mathrm{c_i}^2}{\omega}\Delta\Sigma_\omega\left(\boldsymbol{p},\boldsymbol{P},\Omega\right)(2\pi)^3\delta^3\left(\boldsymbol{p}-\boldsymbol{p}_0\right) - \frac{\mathrm{c_i}^2}{\omega}\Delta G_\omega\left(\boldsymbol{p},\boldsymbol{P},\Omega\right)U_\omega\left(\boldsymbol{p},\boldsymbol{p}_0,\boldsymbol{P},\Omega\right), \tag{B.2a}$$

$$\Delta G_\omega\left(\boldsymbol{p},\boldsymbol{P},\Omega\right) \equiv \frac{G_{\omega_-}\left(\boldsymbol{p}_-\right)-G^*_{\omega_+}\left(\boldsymbol{p}_+\right)}{2\mathrm{i}}, \tag{B.2b}$$

$$\Delta\Sigma_\omega\left(\boldsymbol{p},\boldsymbol{P},\Omega\right) \equiv \frac{\Sigma_{\omega_-}\left(\boldsymbol{p}_-\right)-\Sigma^*_{\omega_+}\left(\boldsymbol{p}_+\right)}{2\mathrm{i}}. \tag{B.2c}$$

We will look at the eigenvalues and eigenfunctions of equation (B.1). The radiance per frequency band, I_ω is related to Ψ by

$$I_\omega\left(\boldsymbol{e}_{\boldsymbol{p}},\boldsymbol{P},\Omega\right) \equiv \frac{\omega^2}{\mathrm{c_i}^2}\int\frac{\mathrm{d}p}{(2\pi)^3}p^2\frac{|\mathrm{c_i}^2\mathsf{A}\cdot\boldsymbol{p}|}{\omega}\Psi_\omega\left(\boldsymbol{p},\boldsymbol{P},\Omega\right). \tag{B.3}$$

The relations for energy density and energy density flux, (3.3a) and (3.3b) give rise to a continuity equation (3.4), therefore we know that for $\boldsymbol{P}=\boldsymbol{0}$ we have an eigenvalue proportional to Ω, and for$\Omega=0$ we have an eigenvalue proportional to $|\boldsymbol{P}|^2$. It is very hard to find the exact eigenfunctions up to all orders, so we will start in the situation with $\Omega=0$ and $\boldsymbol{P}=\boldsymbol{0}$, where we expect a diffusive pole if we expand to Ω and $\boldsymbol{P}$. In this appendix we will consider only the eigenfunction related to the diffusive pole, and start from the transport quantity Φ introduced in section 3.5,

$$\Phi_\omega(\boldsymbol{p},\boldsymbol{p}_0,\boldsymbol{P},\Omega) = \frac{\Psi^*_{0\omega}(\boldsymbol{p}_0,\boldsymbol{P},\Omega)\Psi_{0\omega}(\boldsymbol{p},\boldsymbol{P},\Omega)}{\mathrm{i}\Omega-\mathrm{i}\boldsymbol{P}\cdot\mathsf{D}_\omega\cdot\mathrm{i}\boldsymbol{P}}. \tag{B.4}$$

From (B.1), it follows that eigenfunction $\Psi_{0\omega}(\boldsymbol{p},\boldsymbol{0},0)$ satisfies

$$0 = \int\frac{\mathrm{d}^3p_0}{(2\pi)^3}\gamma_\omega\left(\boldsymbol{p},\boldsymbol{p}_0,\boldsymbol{0},0\right)\Psi_{0\omega}\left(\boldsymbol{p}_0,\boldsymbol{0},0\right). \tag{B.5}$$

Using the Ward identity (A.12) for $\Omega=0$ and $\boldsymbol{P}=\boldsymbol{0}$, we find the eigenfunction, it is

$$\Psi_{0\omega}(\boldsymbol{p},\boldsymbol{0},0) = M_{0\omega}\mathrm{Im}[G_\omega(\boldsymbol{p})] \tag{B.6}$$

where M_0 is a normalization constant, we define

$$M_{0\omega} \equiv \lim_{\Omega\to0}\lim_{\boldsymbol{P}\to\boldsymbol{0}}\int\frac{\mathrm{d}^3p}{(2\pi)^3}\frac{\Psi^*_{0\omega}(\boldsymbol{p},\boldsymbol{P},\Omega)\Psi_{0\omega}(\boldsymbol{p},\boldsymbol{P},\Omega)}{\Delta G_\omega(\boldsymbol{p},\boldsymbol{P},\Omega)}, \tag{B.7}$$

and using (B.6) we have $1/M_{0\omega}=\int\mathrm{d}^3p/(2\pi)^3\mathrm{Im}[G_\omega(\boldsymbol{p})]$.

We expand equation (B.1) for eigenfunction $\Psi_{0\omega}(\boldsymbol{p},\boldsymbol{P},\Omega)$ around $\Omega=0$ and $\boldsymbol{P}=\boldsymbol{0}$ to first order,

$$\begin{aligned}
0 \;=\; & \left[\mathrm{i}\Omega-\frac{{c_\mathrm{i}}^2}{\omega}\boldsymbol{p}\cdot\mathsf{A}\cdot\mathrm{i}\boldsymbol{P}\right]\Psi_{0\omega}\left(\boldsymbol{p},\boldsymbol{0},0\right)\\
& -\int\frac{\mathrm{d}^3p_0}{(2\pi)^3}\gamma_\omega\left(\boldsymbol{p},\boldsymbol{p}_0,\boldsymbol{0},0\right)\Psi_{0\omega}\left(\boldsymbol{p}_0,\boldsymbol{0},0\right)\\
& -\Omega\int\frac{\mathrm{d}^3p_0}{(2\pi)^3}\left.\frac{\partial\gamma_\omega\left(\boldsymbol{p},\boldsymbol{p}_0,\boldsymbol{P},\Omega\right)\Psi_{0\omega}\left(\boldsymbol{p}_0,\boldsymbol{P},\Omega\right)}{\partial\Omega}\right|_{\substack{\Omega=0\\\boldsymbol{P}=\boldsymbol{0}}}\\
& -\boldsymbol{P}\cdot\int\frac{\mathrm{d}^3p_0}{(2\pi)^3}\left.\frac{\partial\gamma_\omega\left(\boldsymbol{p},\boldsymbol{p}_0,\boldsymbol{P},\Omega\right)\Psi_{0\omega}\left(\boldsymbol{p}_0,\boldsymbol{P},\Omega\right)}{\partial\boldsymbol{P}}\right|_{\substack{\Omega=0\\\boldsymbol{P}=\boldsymbol{0}}}\\
& +\mathrm{O}(\Omega^2,\Omega\boldsymbol{P},\boldsymbol{P}\boldsymbol{P}).
\end{aligned}\tag{B.8}$$

In equation (B.8) we collect the parts proportional to 1, Ω, and $\boldsymbol{P}$, and we can treat them as independent equations. The equation for order 1 is already satisfied. Using the Ward identity and

$$\left.\frac{\partial\Delta G_\omega(\boldsymbol{p},\boldsymbol{P},\Omega)}{\partial\Omega}\right|_{\substack{\Omega=0\\\boldsymbol{P}=\boldsymbol{0}}} = \frac{\mathrm{i}}{2}\frac{\partial\mathrm{Re}[G_\omega(\boldsymbol{p})]}{\partial\omega},\tag{B.9a}$$

$$\left.\frac{\partial\Delta G_\omega(\boldsymbol{p},\boldsymbol{P},\Omega)}{\partial\boldsymbol{P}}\right|_{\substack{\Omega=0\\\boldsymbol{P}=\boldsymbol{0}}} = \frac{\mathrm{i}}{2}\frac{\partial\mathrm{Re}[G_\omega(\boldsymbol{p})]}{\partial\boldsymbol{p}},\tag{B.9b}$$

we find similar results for the leading corrections to $\gamma_\omega(\boldsymbol{p},\tilde{\boldsymbol{p}},\boldsymbol{0},0)$,

$$\begin{aligned}
\int\frac{\mathrm{d}^3p_0}{(2\pi)^3}\left.\frac{\partial\gamma_\omega\left(\boldsymbol{p},\boldsymbol{p}_0,\boldsymbol{P},\Omega\right)}{\partial\Omega}\right|_{\substack{\Omega=0\\\boldsymbol{P}=\boldsymbol{0}}}\Psi_{0\omega}\left(\boldsymbol{p}_0,\boldsymbol{0},0\right) \;=\;&\\
-\mathrm{i}\Psi_{0\omega}(\boldsymbol{p},\boldsymbol{0},0)\delta_\omega(\boldsymbol{p},\boldsymbol{0},0) - M_{0\omega}\int\frac{\mathrm{d}^3p_0}{(2\pi)^3}\gamma_\omega\left(\boldsymbol{p},\boldsymbol{p}_0,\boldsymbol{0},0\right)\frac{\mathrm{i}}{2}\frac{\partial\mathrm{Re}[G_\omega(\boldsymbol{p}_0)]}{\partial\omega},&
\end{aligned}\tag{B.10a}$$

$$\begin{aligned}
\int\frac{\mathrm{d}^3p_0}{(2\pi)^3}\left.\frac{\partial\gamma_\omega\left(\boldsymbol{p},\boldsymbol{p}_0,\boldsymbol{P},\Omega\right)}{\partial\boldsymbol{P}}\right|_{\substack{\Omega=0\\\boldsymbol{P}=\boldsymbol{0}}}\Psi_{0\omega}\left(\boldsymbol{p}_0,\boldsymbol{0},0\right) \;=\;&\\
-M_{0\omega}\int\frac{\mathrm{d}^3p_0}{(2\pi)^3}\gamma_\omega\left(\boldsymbol{p},\boldsymbol{p}_0,\boldsymbol{0},0\right)\frac{\mathrm{i}}{2}\frac{\partial\mathrm{Re}[G_\omega(\boldsymbol{p}_0)]}{\partial\boldsymbol{p}_0}.&
\end{aligned}\tag{B.10b}$$

We obtain the order Ω correction to the eigenvalue by using completeness of the set of eigenfunctions $\{\Psi_{n\omega}(\boldsymbol{p},\boldsymbol{P},\Omega)\}$ at $\boldsymbol{P}=\boldsymbol{0}$ and $\Omega=0$. We only have

energy conservation, and there is only a single eigenfunction in the set, which is Ψ_0, thus $\Psi_{0\omega}^*(\boldsymbol{p},\boldsymbol{0},0)\Psi_{0\omega}(\tilde{\boldsymbol{p}},\boldsymbol{0},0) = (2\pi)^3\delta^3(\boldsymbol{p}-\tilde{\boldsymbol{p}})\Psi_{0\omega}(\tilde{\boldsymbol{p}},\boldsymbol{0},0)$. We define

$$\delta_\omega \equiv \int \frac{\mathrm{d}^3p}{(2\pi)^3}\delta_\omega(\boldsymbol{p},\boldsymbol{0},0)\Psi_{0\omega}^*(\boldsymbol{p},\boldsymbol{0},0), \tag{B.11}$$

which leads to the eigenvalue correct to order Ω,

$$\mathrm{i}\Omega\left[1+\delta_\omega(\boldsymbol{p},\boldsymbol{0},0)\right]\Psi_{0\omega}(\boldsymbol{p},\boldsymbol{0},0) = \mathrm{i}\Omega\left[1+\delta_\omega\right]\Psi_{0\omega}(\boldsymbol{p},\boldsymbol{0},0), \tag{B.12a}$$

and the order Ω correction to the eigenfunction is

$$\left.\frac{\partial\Psi_{0\omega}(\boldsymbol{p},\boldsymbol{P},\Omega)}{\partial\Omega}\right|_{\substack{\Omega=0\\ \boldsymbol{P}=\boldsymbol{0}}} = M_{0\omega}\frac{\mathrm{i}}{2}\frac{\partial\mathrm{Re}[G_\omega(\boldsymbol{p})]}{\partial\omega}. \tag{B.12b}$$

The correction linear in $\boldsymbol{P}$ is more difficult, we use (B.10b) to obtain the equation for the order $\boldsymbol{P}$ corrections,

$$\begin{aligned} 0 = {} & \left[-\frac{{c_i}^2}{\omega}\boldsymbol{p}\cdot\mathsf{A}\cdot\mathrm{i}\boldsymbol{P}\right]\Psi_{0\omega}(\boldsymbol{p},\boldsymbol{0},0) \\ & +\boldsymbol{P}\cdot M_{0\omega}\int\frac{\mathrm{d}^3p_0}{(2\pi)^3}\gamma_\omega(\boldsymbol{p},\boldsymbol{p}_0,\boldsymbol{0},0)\frac{\mathrm{i}}{2}\frac{\partial\mathrm{Re}[G_\omega(\boldsymbol{p}_0)]}{\partial\boldsymbol{p}_0} \\ & -\boldsymbol{P}\cdot\int\frac{\mathrm{d}^3p_0}{(2\pi)^3}\gamma_\omega(\boldsymbol{p},\boldsymbol{p}_0,\boldsymbol{0},0)\left.\frac{\partial\Psi_{0\omega}(\boldsymbol{p}_0,\boldsymbol{P},\Omega)}{\partial\boldsymbol{P}}\right|_{\substack{\Omega=0\\ \boldsymbol{P}=\boldsymbol{0}}}. \end{aligned} \tag{B.13}$$

In Eq. (B.13) the correction to the eigenfunction linear in $\boldsymbol{P}$ is integrated together with γ. We can consider an auxiliary function of which Ψ_0 is the result when we integrate it together with γ. We introduce the auxiliary vector function $\boldsymbol{\Psi}_\mathrm{a}$ by

$$\boldsymbol{\Psi}_{\mathrm{a}\omega}(\boldsymbol{p},\boldsymbol{P},\Omega) \equiv \frac{\omega}{{c_i}^2}\int\frac{\mathrm{d}^3p_0}{(2\pi)^3}\Phi_\omega(\boldsymbol{p},\boldsymbol{p}_0,\boldsymbol{P},\Omega)\boldsymbol{p}_0. \tag{B.14}$$

The Boltzmann transport equation for $\boldsymbol{\Psi}_\mathrm{a}$, at lowest order yields the result

$$\Psi_{0\omega}(\boldsymbol{p},\boldsymbol{0},0)\boldsymbol{p} = M_{0\omega}\int\frac{\mathrm{d}^3p_0}{(2\pi)^3}\gamma_\omega(\boldsymbol{p},\boldsymbol{p}_0,\boldsymbol{0},0)\boldsymbol{\Psi}_{\mathrm{a}\omega}(\boldsymbol{p}_0,\boldsymbol{0},0). \tag{B.15}$$

We use $\Psi_{0\omega}(\boldsymbol{p},\boldsymbol{P},\Omega) = \Psi_{0\omega}(\boldsymbol{p},\boldsymbol{P},\Omega)\boldsymbol{w}(\boldsymbol{P})\cdot\boldsymbol{p}/\boldsymbol{w}(\boldsymbol{P})\cdot\boldsymbol{p}$ with $\boldsymbol{w}(\boldsymbol{P}) = {c_i}^2\boldsymbol{P}\cdot\mathsf{A}/\omega$, and we identify the correction to the eigenfunction up to order $\boldsymbol{P}$ to be

$$\boldsymbol{P}\cdot\left.\frac{\partial\Psi_{0\omega}(\boldsymbol{p},\boldsymbol{P},\Omega)}{\partial\boldsymbol{P}}\right|_{\substack{\Omega=0\\ \boldsymbol{P}=\boldsymbol{0}}} \equiv -M_{0\omega}\frac{{c_i}^2}{\omega}\mathrm{i}\boldsymbol{P}\cdot\mathsf{A}\cdot\left[\boldsymbol{\Psi}_{\mathrm{a}\omega}(\boldsymbol{p},\boldsymbol{0},0)-\boldsymbol{p}\frac{\partial\mathrm{Re}[G_\omega(\boldsymbol{p})]}{\partial(\frac{{c_i}^2}{\omega}\boldsymbol{p}\cdot\mathsf{A}\cdot\boldsymbol{p})}\right]. \tag{B.16}$$

We used that for any function F we can write

$$\frac{\partial F(\boldsymbol{p})}{\partial \boldsymbol{p}} = 2\mathsf{A}\cdot\boldsymbol{p}\frac{\partial F(\boldsymbol{p})}{\partial \boldsymbol{p}\cdot\mathsf{A}\cdot\boldsymbol{p}}, \tag{B.17}$$

for $\mathsf{A} = \mathsf{A}^{\mathrm{T}}$. Equation (B.16) is a generalization of formula (21) in [89], which would have been obtained had we identified $\boldsymbol{w} = \mathsf{A}\cdot\boldsymbol{p}$ and isotropic media ($\mathsf{A} = 1$).

The vector quantity $\boldsymbol{\Psi}_{\mathrm{a}}$ only appears in inner products with the vector $\mathrm{c_i}^2\boldsymbol{P}\cdot\mathsf{A}/\omega$. To simplify calculations we introduce a scalar function Γ by $\mathrm{c_i}^2\boldsymbol{P}\cdot\mathsf{A}\cdot\boldsymbol{\Psi}_{\mathrm{a}\omega}(\boldsymbol{p},\boldsymbol{0},0)/\omega \equiv |G_\omega(\boldsymbol{p})|^2\Gamma_\omega(\boldsymbol{p},\boldsymbol{P})$. Just like $\boldsymbol{\Psi}_{\mathrm{a}}$, also Γ satisfies a generalized Boltzmann equation, which is

$$\Gamma_\omega(\boldsymbol{p},\boldsymbol{P}) = \boldsymbol{P}\cdot\frac{\mathrm{c_i}^2}{\omega}\mathsf{A}\cdot\boldsymbol{p} + \int\frac{\mathrm{d}^3p_0}{(2\pi)^3}U_\omega(\boldsymbol{p},\boldsymbol{p}_0,\boldsymbol{0},0)|G_\omega(\boldsymbol{p}_0)|^2\Gamma(\boldsymbol{p}_0,\boldsymbol{P}). \tag{B.18}$$

When we insert our $\Omega,\boldsymbol{P}$ expansion of the eigenvectors into the generalized Boltzmann equation, we see that the term of order $\boldsymbol{P}\boldsymbol{P}$ divided by $1+\delta_\omega$ determines diffusion. The diffusion tensor is

$$\mathrm{i}\boldsymbol{P}\cdot\mathsf{D}_\omega\cdot\mathrm{i}\boldsymbol{P} \equiv -M_{0\omega}\int\frac{\mathrm{d}^3p}{(2\pi)^3}\frac{[\mathrm{i}\boldsymbol{P}\cdot\frac{\mathrm{c_i}^2}{\omega}\mathsf{A}\cdot\boldsymbol{p}]^2}{1+\delta_\omega}\Big[\frac{|G_\omega(\boldsymbol{p})|^2\Gamma_\omega(\boldsymbol{p},\boldsymbol{P})}{\frac{\mathrm{c_i}^2}{\omega}\boldsymbol{P}\cdot\mathsf{A}\cdot\boldsymbol{p}} - \frac{\partial\mathrm{Re}[G_\omega(\boldsymbol{p})]}{\partial(\frac{\mathrm{c_i}^2}{\omega}\boldsymbol{p}\cdot\mathsf{A}\cdot\boldsymbol{p})}\Big]. \tag{B.19}$$

Eq. (B.19) is a generalization to anisotropic media of the equation known as the Green-Kubo formula for the diffusion tensor [89]. The derivative of the real part of the Green function removes the UV catastrophe of the first term.

Our generalization (B.19) of the Green-Kubo formula justifies our expansion of Ψ in terms of the self consistent energy density $\mathscr{H}$ and self consistent energy density flux $\boldsymbol{S}$, (3.3a) and (3.3b). When we replace $\mathrm{Im}[G]$ by $\mathrm{Im}[g]$, i.e. when we take the dispersion relation without scattering effects, (2.7), then we can neglect the derivatives of $\mathrm{Re}[G]$, and the eigenfunction expansion we found becomes the multipole expansion containing only the monopole and dipole terms

$$\frac{\omega^2}{\mathrm{c_i}^2}\Psi_\omega(\boldsymbol{p},\boldsymbol{P},\Omega) = M_\omega\mathrm{Im}[g_\omega(\boldsymbol{p})]\left[\frac{\mathscr{H}_\omega(\boldsymbol{P},\Omega)}{1+\delta_\omega} + \frac{3\boldsymbol{p}\cdot\boldsymbol{S}_\omega(\boldsymbol{P},\Omega)}{\boldsymbol{p}\cdot\boldsymbol{v}_{\mathrm{g}}(\boldsymbol{p})}\right]. \tag{B.20}$$

Here we have set $\boldsymbol{v}_{\mathrm{g}}(\boldsymbol{p}) = \mathrm{c_i}^2/\omega\mathsf{A}\cdot\boldsymbol{p}$, and the relations (3.3a) and (3.3b) of Ψ with energy density and flux yield $1/M_\omega = \int\mathrm{d}^3p/(2\pi)^3\mathrm{Im}[g_\omega(\boldsymbol{p})]$. Equation (B.20) justifies our starting point (3.6) to obtain (3.11). The interpretation of $\mathrm{Im}[g]$ is that of the spectral density of the radiative states. Finally we note that the diffusion tensor (B.19) coincides in this limit with (3.11).

Bibliography

[1] J. Heiskala, I. Nissilä, T. Neuvonen, S. Järvenpää, and E. Somersalo, *Modelling anisotropic light propagation in a realistic model of the human head*, Appl. Opt. **44**, 2049 (2005).

[2] O. Dudko and G. H. Weiss, *Estimation of anisotropic optical parameters of tissue in a slab geometry*, Biophys. J. **88**, 3205 (2005).

[3] A. Kienle, C. Wetzel, A. Bassi, D. Comelli, P. Taroni, and A. Pifferi, *Determination of the optical properties of anisotropic biological media using an isotropic diffusion model*, J. Biomed. Opt. **12**, 014026 (2007).

[4] J. Heiskala, T. Neuvonen, P. E. Grant, and I. Nissilä, *Significance of tissue anisotropy in optical tomography of the infant brain*, Appl. Opt. **46**, 1633 (2007).

[5] C. Baravian, F. Caton, J. Dillet, G. Toussaint, and P. Flaud, *Incoherent light transport in an anisotropic random medium: A probe of human erythrocyte aggregation and deformation*, Phys. Rev. E **76**, 011409 (2007).

[6] P. M. Morse and H. Feshbach, *Methods of theoretical physics* (McGraw–Hill, New York, 1953), Vol. I and II.

[7] S. Chandrasekhar, *Radiative transfer* (Dover Publications Inc., New York, 1960).

[8] M. B. van der Mark, *Propagation of light in disordered media: A search for anderson localization*, Ph. d. thesis, Universiteit van Amsterdam, Natuurkundig Laboratorium der Universiteit van Amsterdam, Valckenierstraat 65, 1018XE Amsterdam, The Netherlands, 1990.

[9] H. S. Carslaw and J. C. Jaeger, *Conduction of heat in solids*, 2nd ed. (Oxford University Press, Oxford, 1959).

[10] J. Hammersley and D. C. Handscomb, *Monte Carlo methods* (Chapman and Hall, London, 1979).

[11] M. H. Kalos and P. A. Whitlock, *Monte Carlo methods* (John Wiley & Sons, New York, 1986), Vol. 1: Basics.

[12] K. Ren, G. Bal, and A. H. Hielscher, *Transport- and diffusion-based optical tomography in small domains: a comparative study*, Appl. Opt. **46**, 6669 (2007).

[13] E. Yablonovitch, *Inhibited spontaneous emission in solid-state physics and electronics*, Phys. Rev. Lett. **58**, 2059 (1987).

[14] S. John, *Strong localization of photons in certain disordered dielectric superlattices*, Phys. Rev. Lett. **58**, 2486 (1987).

[15] A. F. Koenderink and W. L. Vos, *Light exiting from real photonic band gap crystals is diffuse and strongly directional*, Phys. Rev. Lett. **91**, 213902 (2003).

[16] F. A. Koenderink, *Emission and transport of light in photonic crystals*, Ph. d. thesis, Universiteit Twente, Universiteit Twente, Faculteit Technische Natuurwetenschappen, Gebouw Hogekamp, Postbus 217, 7500AE Enschede, 2003.

[17] A. F. Koenderink and W. L. Vos, *Optical properties of real photonic crystals: anomalous diffuse transmission*, J. Opt. Soc. Am. B **22**, 1075 (2005).

[18] R. Rengarajan, D. Mittleman, C. Rich, and V. Colvin, *Effect of disorder on the optical properties of colloidal crystals*, Phys. Rev. E **71**, 016615 (2005).

[19] S. Noda, K. Tomoda, N. Yamamoto, and A. Chutinan, *Full Three-Dimensional Photonic Bandgap Crystals at Near-Infrared Wavelengths*, Science **289**, 604 (2000).

[20] Y. A. Vlasov, X.-Z. Bo, J. C. Sturm, and D. J. Norris, *On-chip natural assembly of silicon photonic bandgap crystals*, Nature **414**, 289 (2001).

[21] V. M. Apalkov, M. E. Raikh, and B. Shapiro, *Incomplete photonic band gap as inferred from the speckle pattern of scattered light waves*, Phys. Rev. Lett. **92**, 253902 (2004).

[22] L. Tsang and A. Ishimaru, *Backscattering enhancement of random discrete scatterers*, J. Opt. Soc. Am. A **1**, 836 (1984).

[23] L. Tsang and A. Ishimaru, *Theory of backscattering enhancement of random discrete isotropic scatterers based on the summation of all ladder and cyclical terms*, J. Opt. Soc. Am. A **2**, 1331 (1985).

[24] L. Tsang and A. Ishimaru, *Radiative wave and cyclical transfer equations for dense nontenuous media*, J. Opt. Soc. Am. A **2**, 2187 (1985).

[25] M. P. V. van Albada and A. Lagendijk, *Observation of weak localization of light in a random medium*, Phys. Rev. Lett. **55**, 2692 (1985).

[26] P.-E. Wolf and G. Maret, *Weak localization and coherent backscattering of photons in disordered media*, Phys. Rev. Lett. **55**, 2696 (1985).

[27] B. P. J. Bret and A. Lagendijk, *Anisotropic enhanced backscattering induced by anisotropic diffusion*, Phys. Rev. E **70**, 036601 (2004).

[28] R. Sapienza, S. Mujumdar, C. Cheung, A. G. Yodh, and D. Wiersma, *Anisotropic weak localization of light*, Phys. Rev. Lett. **92**, 033903 (2004).

[29] B. P. J. Bret, *Multiple light scattering in porous gallium phosphide*, Ph. d. thesis, Universiteit Twente, Universiteit Twente, Faculteit Technische Natuurwetenschappen, Gebouw Hogekamp, Postbus 217, 7500AE Enschede, 2005.

[30] P. W. Anderson, *Absence of diffusion in certain random lattices*, Phys. Rev. **109**, 1492 (1958).

[31] S. John, *Electromagnetic absorption in a disordered medium near a photon mobility edge*, Phys. Rev. Lett. **53**, 2169 (1984).

[32] T. R. Kirkpatrick, *Localization of acoustic waves*, Phys. Rev. B **31**, 5746 (1985).

[33] H. De Raedt, A. Lagendijk, and P. de Vries, *Transverse localization of light*, Phys. Rev. Lett. **62**, 47 (1989).

[34] D. S. Wiersma, P. Bartolini, A. Lagendijk, and R. Righini, *Localization of light in a disordered medium*, Nature **390**, 671 (1999).

[35] T. Schwartz, G. Bartal, S. Fishman, and M. Segev, *Transport and anderson localization in disordered two-dimensional photonic lattices*, Nature **446**, 52 (2007).

[36] S. K. Cheung and Z. Q. Zhang, *Scaling behavior of classical wave transport in mesoscopic media at the localization transition*, Phys. Rev. B **72**, 235102 (2005).

[37] R. L. Weaver, *Transport and localization amongst coupled substructures*, Phys. Rev. E **73**, 036610 (2006).

[38] S. E. Skipetrov and B. A. van Tiggelen, *Dynamics of anderson localization in open 3d media*, Phys. Rev. Lett. **96**, 043902 (2006).

[39] M. Störzer, P. Gross, C. M. Aegerter, and G. Maret, *Observation of the critical regime near anderson localization of light*, Phys. Rev. Lett. **96**, 063904 (2006).

[40] C. M. Aegerter, M. Störzer, S. Fiebig, W. Bührer, and G. Maret, *Observation of anderson localization of light in three dimensions*, J. Opt. Soc. Am. A **24**, A23 (2007).

[41] J. H. Page, H. Hu, S. Skipetrov, and B. A. van Tiggelen, *Ultrasonic investigation of phonon localization in a disordered three-dimensional mesoglass*, J. Phys: Conf. Ser. **92**, 012129 (2007).

[42] G. Samelsohn and V. Freilikher, *Localization of classical waves in weakly scattering two-dimensional media with anisotropic disorder*, Phys. Rev. E **70**, 046612 (2004).

[43] A. Small and D. Pine, *Delocalization of classical waves in highly anisotropic random media*, Phys. Rev. E **75**, 016617 (2007).

[44] G. Labeyrie, F. de Tomasi, J.-C. Bernard, C. A. Müller, C. Miniatura, and R. Kaiser, *Coherent backscattering of light by cold atoms*, Phys. Rev. Lett. **83**, 5266 (1999).

[45] R. C. Kuhn, C. Miniatura, D. Delande, O. Sigwarth, and C. A. Müller, *Localization of matter waves in two-dimensional disordered optical potentials*, Phys. Rev. Lett. **95**, 250403 (2005).

[46] U. Gavish and Y. Castin, *Matter-wave localization in disordered cold atom lattices*, Phys. Rev. Lett. **95**, 020401 (2005).

[47] P. Massignan and Y. Castin, *Three-dimensional strong localization of matter waves by scattering from atoms in a lattice with a confinement-induced resonance*, Phys. Rev. A **74**, 013616 (2006).

[48] J. Billy, V. Josse, Z. Zuo, A. Bernard, B. Hambrecht, P. Lugan, D. Clément, L. Sanchez-Palencia, P. Bouyer, and A. Aspect, *Direct observation of anderson localization of matter waves in a controlled disorder*, Nature **453**, 891 (2008).

[49] G. Roati, C. D'Errico, L. Fallani, F. M., C. Fort, M. Zaccanti, G. Modugno, and M. Inguscio, *Anderson localization of a non-interacting boseŰeinstein condensate*, Nature **453**, 895 (2008).

[50] B. C. Kaas, B. A. van Tiggelen, and A. Lagendijk, *Anisotropy and interference in wave transport: An analytic theory*, Phys. Rev. Lett. **100**, 123902 (2008).

[51] A. A. Asatryan, L. C. Botten, M. A. Byrne, V. D. Freilikher, S. A. Gredeskul, I. V. Shadrivov, R. C. McPhedran, and Y. S. Kivshar, *Suppression of anderson localization in disordered metamaterials*, Phys. Rev. Lett. **99**, 193902 (2007).

[52] Y. Lahini, A. Avidan, F. Pozzi, M. Sorel, R. Morandotti, D. N. Christodoulides, and Y. Silberberg, *Anderson localization and nonlinearity in one-dimensional disordered photonic lattices*, Phys. Rev. Lett. **100**, 013906 (2008).

[53] J. D. Jackson, *Classical electrodynamics*, 3rd ed. (Wiley, New York, 1999).

[54] M. Born and E. Wolf, *Principles of optics*, seventh ed. (Cambridge University Press, Cambridge, 2003).

[55] C. H. R. Huygens, *Traité de la lumière* (van der Aa, Leiden, 1690).

[56] B. J. Hoenders and H. A. Ferwerda, *Identification of the radiative and nonradiative parts of a wave field*, Phys. Rev. Lett. **87**, 060401 (2001).

[57] M. Fernández Guasti, *Complementary fields conservation equation derived from the scalar wave equation*, J. Phys. A: Math. Gen. **37**, 4107 (2004).

[58] D. J. Thouless, *Maximum metallic resistance in thin wires*, Phys. Rev. Lett. **39**, 1167 (1977).

[59] D. Vollhardt and P. Wölfle, *Anderson localization in $d \leq 2$ dimensions: A self-consistent diagrammatic theory*, Phys. Rev. Lett. **45**, 842 (1980).

[60] D. Vollhardt and P. Wölfle, *Scaling equations from a self-consistent theory of anderson localization*, Phys. Rev. Lett. **48**, 699 (1982).

[61] E. N. Economou, C. M. Soukoulis, and A. D. Zdetsis, *Localized states in disordered systems as bound states in potential wells*, Phys. Rev. B **30**, 1686 (1984).

[62] P. Wölfle and R. N. Bhatt, *Electron localization in anisotropic systems*, Phys. Rev. B **30**, 3542 (1984).

[63] M. J. Stephen, *Temporal fluctuations in wave propagation in random media*, Phys. Rev. B **37**, 1 (1988).

[64] F. C. MacKintosh and S. John, *Diffusing-wave spectroscopy and multiple scattering of light in correlated random media*, Phys. Rev. B **40**, 2383 (1989).

[65] H. S. Green and E. Wolf, *A scalar representation of electromagnetic fields*, Proc. Phys. Soc. A **66**, 1129 (1953).

[66] E. Wolf, *A scalar representation of electromagnetic fields: II*, Proc. Phys. Soc. **74**, 269 (1959).

[67] P. Roman, *A scalar representation of electromagnetic fields: III*, Proc. Phys. Soc. **74**, 281 (1959).

[68] A. Lagendijk and B. A. van Tiggelen, *Resonant multiple scattering of light*, Phys. Rep. **270**, 143 (1996).

[69] D. A. Boas, J. Culver, J. J. Stott, and A. K. Dunn, *Three dimensional monte carlo code for photon migration through complex heterogeneous media including the adult human head*, Opt. Express **10**, 159 (2002).

[70] H. K. Roy, Y. Kim, Y. Liu, R. K. Wali, M. Goldberg, V. Turzhitsky, J. Horwitz, and V. Backman, *Risk stratification of colon carcinogenesis through enhanced backscattering spectroscopy analysis of the uninvolved colonic mucosa*, Clin. Cancer Res. **12**, 961 (2006).

[71] H. Subramanian, P. Pradhan, Y. L. Kim, Y. Liu, X. Li, and V. Backman, *Modeling low-coherence enhanced backscattering using monte carlo simulation*, Appl. Opt. **45**, 6292 (2006).

[72] R. Snieder, A. Gret, H. Douma, and J. Scales, *Coda Wave Interferometry for Estimating Nonlinear Behavior in Seismic Velocity*, Science **295**, 2253 (2002).

[73] J. A. Scales and M. Batzle, *Millimeter wave analysis of the dielectric properties of oil shales*, Appl. Phys. Lett. **89**, 024102 (2006).

[74] E. Larose, J. de Rosny, L. Margerin, D. Anache, P. Gouedard, M. Campillo, and B. van Tiggelen, *Observation of multiple scattering of khz vibrations in a concrete structure and application to monitoring weak changes*, Phys. Rev. E **73**, 016609 (2006).

[75] H. C. van de Hulst, *Multiple light scattering* (Academic, New York, 1980), Vol. 1 and 2.

[76] P. M. Johnson, B. P. J. Bret, J. Gómez Rivas, J. J. Kelly, and A. Lagendijk, *Anisotropic diffusion of light in a strongly scattering material*, Phys. Rev. Lett. **89**, 243901:1 (2002).

[77] L. Margerin, *Attenuation, transport, and diffusion of scalar waves in textured random media*, Tectonophysics **416**, 229 (2006).

[78] H. Weimer, M. Michel, J. Gemmer, and G. Mahler, *Transport in anisotropic model systems analyzed by a correlated projection superoperator technique*, Phys. Rev. E **77**, 011118 (2008).

[79] L. Dagdug, G. H. Weiss, and A. H. Gandjbakche, *Effects of anisotropic optical properties on photon migration in structured tissues*, Phys. Med. Biol **48**, 1361 (2003).

[80] J. Heino, S. Arridge, J. Sikora, and E. Somersalo, *Anisotropic effects in higly scattering media*, Phys. Rev. E **68**, 031908 (2003).

[81] T. Binzoni, C. Courvoisier, R. Giust, G. Tribillon, T. Gharbi, J. C. Hebden, T. S. Leung, and D. T. Delpy, *Anisotropic photon migration in human skeletal muscle*, Phys. Med. Biol. **51**, N79 (2006).

[82] A. Kienle, R. Michels, and R. Hibst, *Magnification– a new look at a long–known optical property of dentin*, J. Dent. Res. **85**, 955 (2006).

[83] A. Heiderich, R. Maynard, and B. van Tiggelen, *Monte-carlo simulations for light propagation in nematic liquid crystals*, J. Physique II (France) **7**, 765 (1997).

[84] M. P. van Albada and A. Lagendijk, *Vector character of light in weak localization: Spatial anisotropy in coherent backscattering from a random medium*, Phys. Rev. B **36**, 2353 (1987).

[85] R. Newton, *Scattering theory of waves and particles*, 2nd ed. (Dover Publications Inc., Mineola, New York, 2002).

[86] P. de Vries, D. V. van Coevorden, and A. Lagendijk, *Point scatterers for classical waves*, Rev. Mod. Phys. **70**, 447 (1998).

[87] G. D. Mahan, *Many–particle physics*, 3rd ed. (Kluwer Academic / Plenum Publishers, New York, 2000).

[88] D. Vollhardt and P. Wölfle, *Diagrammatic, self-consistent treatment of the anderson localization problem in $d \leq 2$ dimensions*, Phys. Rev. B **22**, 4666 (1980).

[89] Y. N. Barabanenkov and V. D. Ozrin, *Asymptotic solution of the bethe–salpeter equation and the green–kubo formula for the diffusion constant for wave propagation in random media*, Phys. Lett. A **154**, 38 (1991).

[90] P. Sheng, *Introduction to wave scattering, localization and mesoscopic phenomena* (Academic Press, New York, 1995).

[91] A. A. Abrikosov, *Anderson localization in strongly anisotropic metals*, Phys. Rev. B **50**, 1415 (1994).

[92] A. Ishimaru, *Wave propagation and scattering in random media* (Academic Press, New York, 1978), Vol. I.

[93] B. van Tiggelen and H. Stark, *Nematic liquid crystals as a new challenge for radiative transfer*, Rev. Mod. Phys. **72**, 1017 (2000).

[94] O. L. Muskens, S. L. Diedenhofen, M. H. M. van Weert, M. T. Borgström, E. P. A. M. Bakkers, and J. Gómes Rivas, *Epitaxial growth of aligned semiconductor nanowire metamaterials for photonic applications*, Adv. Func. Mater. **18**, 1039 (2008).

[95] M. J. Stephen, *Rayleigh scattering and weak localization*, Phys. Rev. Lett. **56**, 1809 (1986).

[96] B. A. van Tiggelen, A. Lagendijk, A. Tip, and G. F. Reiter, *Effect of resonant scattering on localization of waves*, Europhys. Lett. **15**, 535 (1991).

[97] G. Strangi, S. Ferjani, V. Barna, A. D. Luca, C. Versace, N. Scaramuzza, and R. Bartolino, *Random lasing and weak localization of light indye-doped nematic liquid crystals*, Opt. Express **14**, 7737 (2006).

[98] H. C. van de Hulst, *Light scattering by small particles* (Dover, Mineola N.Y., 1981).

[99] E. N. Economou, in *Green's functions in quantum physics*, Vol. 7 of *Solid-State Sciences*, edited by P. Fulde (Springer-Verlag, Berlin, 1979).

[100] M. C. W. van Rossum and T. M. Nieuwenhuizen, *Multiple scattering of classical waves: microscopy, mesoscopy, and diffusion*, Rev. Mod. Phys. **71**, 313 (1999).

[101] A. Lagendijk, R. Vreeker, and P. de Vries, *Influence of internal reflection on diffusive transport in strongly scattering media*, Phys. Lett. A **136**, 81 (1989).

[102] J. Zhu, D. Pine, and D. Weitz, *Internal reflection of diffusive light in random media*, Phys. Rev. A **44**, 3948 (1991).

[103] M. Vera and D. Durian, *Angular distribution of diffusely transmitted light*, Phys. Rev. E **53**, 3215 (1996).

[104] G. B. Arfken and H. J. Weber, *Mathematical methods for physicists*, sixth ed. (Elsevier Academic Press, New York, 2005).

[105] D. J. Durian, *Influence of boundary reflection and refraction on diffusive photon transport*, Phys. Rev. E **50**, 857 (1994).

Index